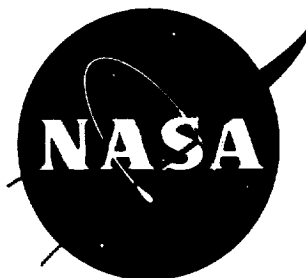NASA CR-

159 455

Computer-Aided Analysis and Design of the Shape Rolling

Process for Producing Turbine Engine Airfoils

G. D. Lahoti, N. Akgerman, and T. Altan

December, 1978

BATTELLE

Columbus Laboratories

505 King Avenue
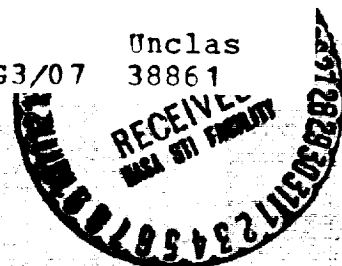
Columbus, Ohio 43201
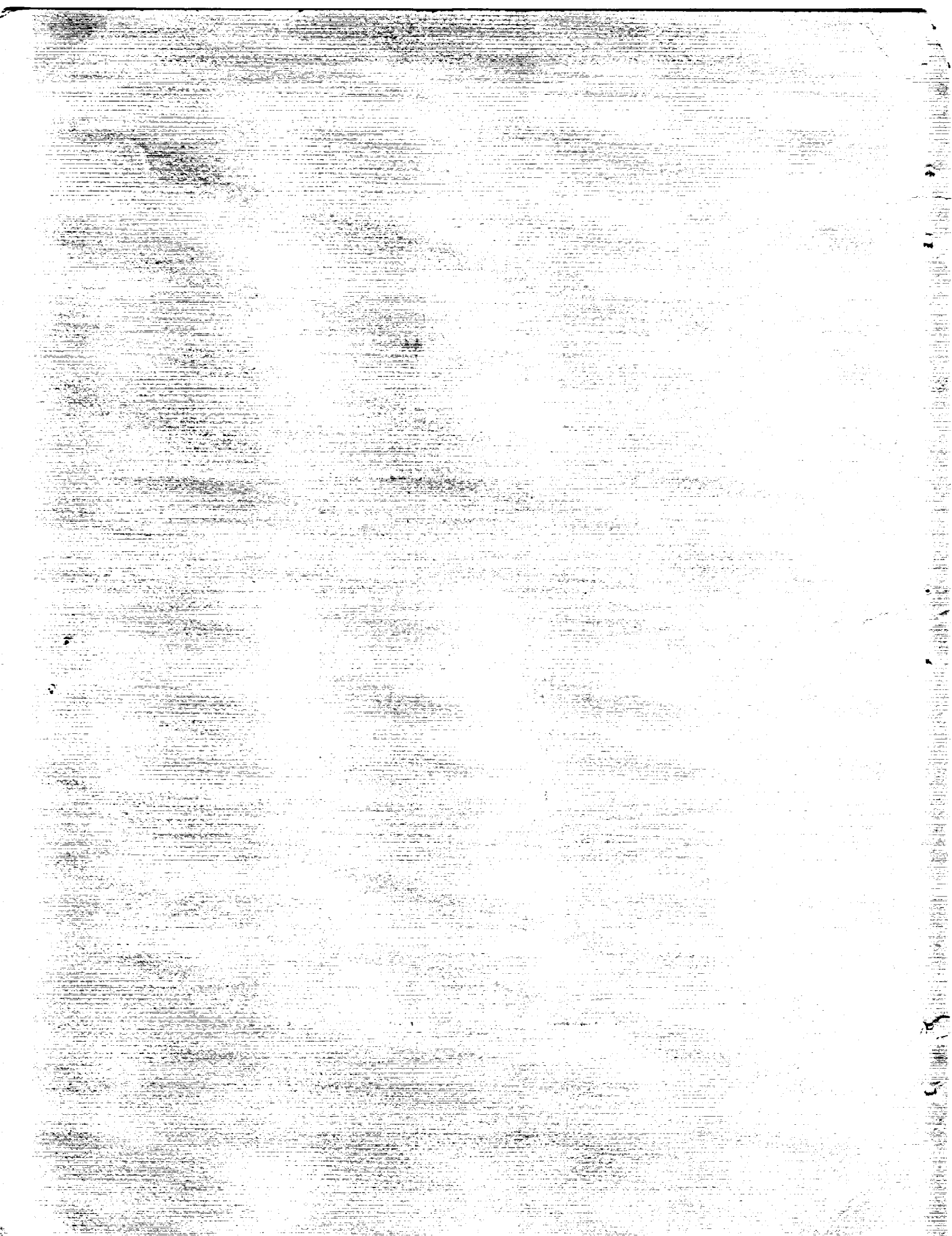
prepared for

NATIONAL AERONAUTICS AND SPACE ADMINISTRATION

NASA Lewis Research Center

Contract NAS 3-20380

Final Report

1. Report No. NASA CR-159**155**	2. Government Accession No.	3. Recipient's Catalog No.
4. Title and Subtitle Computer-Aided Analysis and Design of the Shape-Rolling Process for Producing Turbine Engine Airfoils		5. Report Date December, 1978
		6. Performing Organization Code
7. Author(s) G. D. Lahoti, N. Akgerman and T. Altan		8. Performing Organization Report No.
		10. Work Unit No.
9. Performing Organization Name and Address BATTELLE Columbus Laboratories 505 King Avenue Columbus, Ohio 43201		11. Contract or Grant No. NAS3-20380
		13. Type of Report and Period Covered Contractor Report/Final October 1, 1976 to June 30, '78
12. Sponsoring Agency Name and Address National Aeronautics & Space Administration Washington, D.C. 20546		14. Sponsoring Agency Code

15. Supplementary Notes
   Project Manager: Dr. John D. Whittenberger, Materials & Structures Division
   NASA-Lewis Research Center, Cleveland, Ohio 44135

16. Abstract

The purpose of this program was to develop and verify a computer-aided method for roll pass design in rolling of airfoil shapes used in turbine engines. Mild steel (AISI 1018) was selected as model cold-rolling material and Ti-6Al-4V and Inconel 718 were selected as typical hot-rolling and cold-rolling alloys, respectively. The flow stress and workability of these alloys were characterized and friction factor at the roll/workpiece interface was determined at their respective working conditions by conducting ring tests.

Computer-aided mathematical models for predicting metal flow and stresses, and for simulating the shape-rolling process were developed. These models utilize the upper-bound and the slab methods of analysis, and are capable of predicting the lateral spread, roll-separating force, roll torque, and local stresses, strains and strain rates. This computer-aided design (CAD) system is also capable of simulating the actual rolling process, and thereby designing the roll-pass schedule in rolling of an airfoil or a similar shape.

The predictions of metal flow and stresses made by the CAD system were compared with the results of cold and hot rolling experiments using mild steel plates. The correlation between the theory and the experiments was very good for practical purposes. The CAD system was then evaluated by comparing predictions with the results of cold (mild steel) and hot-isothermal (Ti-6Al-4V) rolling of an airfoil shape. The predicted and the measured values were in good agreement in both the cases.

Finally, a cost-benefit study of applying computer-aided techniques to metal deformation processes was conducted. The results of this study indicated that substantial cost savings can be achieved by the use of computer-aided techniques, especially when the lot size of production is relatively small, and when the process development requires large amount of trial and error and experimentation.

17. Key Words (Suggested by Author(s)) Rolling of Airfoil Shapes Metal Flow Analysis Roll-Pass Design Flow Stress-Friction-Workability Hot-Isothermal Rolling	18. Distribution Statement Unclassified - Unlimited		
19. Security Classif. (of this report) Unclassified	20. Security Classif. (of this page) Unclassified	21. No. of Pages 250	22. Price*

FOREWORD

This Final Report on "Computer-Aided Analysis and Design of the Shape-Rolling Process for Producing Turbine Engine Airfoils" is prepared for NASA Lewis Research Center and covers the work performed under Contract No. NAS3-20380, with Battelle's Columbus Laboratories, from October 1, 1976, to June 30, 1978. The Technical Monitor for this program was Dr. J. Whittenberger, Materials Application Branch, NASA Lewis Research Center, Cleveland, Ohio 44135.

This program was conducted at Battelle in the Metalworking Section, with Mr. T. G. Byrer as Section Manager. Drs. G. D. Lahoti and N. Akgerman were the principal investigators of the program and, at Battelle, the work was technically directed by Dr. T. Altan, Senior Research Leader. Other members of Battelle staff were consulted, as necessary. The experimental work under this program has been recorded in Battelle's Laboratory Record Book No. 33670.

The metallographic studies on as-received and as-rolled materials were conducted at NASA-Lewis Research Center by Dr. J. Whittenberger.

SUMMARY

The purpose of this program was to develop and verify a method for computer-aided analysis and design of the shape rolling process with emphasis on turbine engine airfoil geometries. In this report, the state of the technology on shape rolling process is briefly reviewed. Three representative alloys (AISI 1018 Steel, INCO 718, Ti-6Al-4V) were selected for the purpose of experimental evaluation and their basic deformation characteristics were determined under expected processing conditions.

A computer-aided design (CAD) system for (a) predicting metal flow and stresses, and (b) for simulating and designing the shape rolling process was developed. This CAD system utilizes information on material flow stress, interface friction and workability as inputs. The various capabilities of the CAD system for shape rolling, developed under this program, are:

- Analysis of Metal Flow: A method for predicting the metal flow in rolling of airfoil shapes was developed. The analysis utilizes a modular upper-bound method. A computer program named SHPROL was developed based on this analysis. This program is capable of predicting lateral spread, elongation, boundaries of the deformation zone, location of the neutral plane and the roll torque.

- Analysis of Stresses: A method for predicting the stresses, roll separating force and roll torque in rolling of airfoil shapes was developed. The slab method of analysis was used and a computer program named ROLPAS was developed based on this analysis. ROLPAS also offers graphic display capabilities, for interactive design.

- Process Simulation and Roll Pass Design: The program ROLPAS was also designed to facilitate its use as a tool for simulation of the shape rolling process and for actual designing of roll pass schedule. The system lets the user perform many different operations on the data base via a light pen from a menu on the Cathode Ray Terminal screen. In the end, a summary of the results is displayed.

The validity of the computerized models were evaluated by (a) conducting plate and airfoil shape rolling experiments in laboratory at room temperature and under hot-isothermal conditions and (b) comparing the experimental results with computer predictions. For rolling of plates, the predictions of metal flow (lateral spread) and stresses (roll separating force and roll torque) were in very good agreement with the experiments. Predictions of metal flow for initial passes of shape rolling of an airfoil shape were satisfactory but not very accurate. However, the models were found to be capable of (a) predicting metal flow and stresses well in the later passes of shape rolling, and (b) designing of roll pass schedule in rolling of airfoil or similar shapes from rectangular stock. Thus, the CAD system is considered to be valid for practical engineering purposes and can be utilized by companies for roll pass design and analysis for plates as well as airfoil and similar shapes. The CAD system was also used satisfactorily to evaluate the shape rolling process for an airfoil shape which is currently being produced commercially.

Finally, a systematic procedure for analyzing the cost-benefits of applying computer-aided techniques to metal-forming processes was developed. This procedure was applied to evaluate cost-benefits of applying computer-aided techniques to shape extrusion, forging of airfoil shapes and shape rolling of airfoil shapes. The results of these cost-benefit analyses indicated that substantial cost savings can be achieved by applying computer aided techniques to design and planning of metal forming processes. The computer techniques are most beneficial when (a) the development of a metal forming process, to produce a specific part, requires extensive trial and error and experimentation and (b) the lot sizes for production are relatively small. The advantages of the computer techniques are apparent mainly in (a) savings in material, (b) die or tool design and manufacture and (c) reduction in process development costs. In addition, reductions in lead times can also be achieved in most cases.

TABLE OF CONTENTS

INTRODUCTION

Metalforming is, in general, an experienced-based technology. The know-how and skill required in this field is usually developed through many years of experience. As a result, development of new or improved metalforming processes is largely a trial-and-error procedure relying heavily on past experience as a guide. Recently modern theoretical and experimental techniques and computer methods have been developed to solve complex engineering problems. These techniques when applied to metalforming, can expand the capabilities of metalforming and reduce the amount of costly tryout procedures required in process development.

Rolling of shapes is one of the least understood metal-deformation processes. A round or round-cornered square bar is rolled in several passes into a nonsymmetric shape, such as L, U, T, I, H, or an airfoil. During each pass, the bar elongates as well as spreads. Thus, a very complex three-dimensional metal flow takes place. The spread is usually only a small fraction of the elongation. However, the ratio between spread and elongation varies at each pass with reduction, roll-shape configuration, bar material and temperature, friction between the rolls and the bar, roll speed, roll diameter, and roll surface finish. The factors influencing the process of rolling a shape are so intermixed and complex that roll and roll-pass design have been, until now, a purely empirical, intuitive, and experience-based art. Through decades of experience, roll-pass designs have been developed for most commonly used shapes from conventional materials. However, when novel processes, such as the high-temperature rolling process, and relatively new materials, such as titanium and nickel alloys, are used, the empirical rules do not directly apply. Process development through experimentation becomes very time consuming and expensive. Consequently, it is necessary to develop objective and quantitative engineering methods for roll-pass design. Since, in shape rolling, there are large numbers of process variables involved, and since the complex metal flow is difficult to analyze, the use of computer techniques as an engineering tool becomes extremely attractive and practical.

OUTLINE OF PROGRAM

The purpose of this program was to develop and verify a method for computer-aided analysis of the shape-rolling process with emphasis on turbine-engine airfoil geometries. Computerized models were developed to analyze the mechanics of metal deformation during rolling of complex geometries, such as airfoils, and to predict the roll-pass design requirements. Evaluation of the models was accomplished by conducting laboratory rolling experiments of an airfoil shape using the predictions of the computer models. In addition, the computerized models were applied to one commercial airfoil shape-rolling process that is currently in production. A comparison of experimental results with predicted values was made along with corrections to the models, as required, to improve predictibility. Finally, the cost-benefits of applying computer-aided analyses to shape rolling and to two other metalforming processes were determined.

The technical program was divided into four tasks and is shown schematically by a flow chart in Figure 1. Task I included determination of the basic deformation characteristics of the alloys used in this investigation. Task II was the major part of this program and included development of the computerized models of the shape rolling process. Laboratory and commercial evaluations of the process were accomplished in Task III, and cost-benefits of applying computer-aided analyses to metalforming processes was covered under Task IV.

This is the Final Report and the work accomplished includes the following:

(a) Determination of the flow stress, friction and workability data for selected alloys

(b) Development of a computer-aided design (CAD) system for deformation mechanics and for roll-pass design in rolling of airfoil shapes.

(c) Evaluation of the CAD system with plate-rolling experiments.

(d) Evaluation of the CAD system with airfoil-rolling experiments.

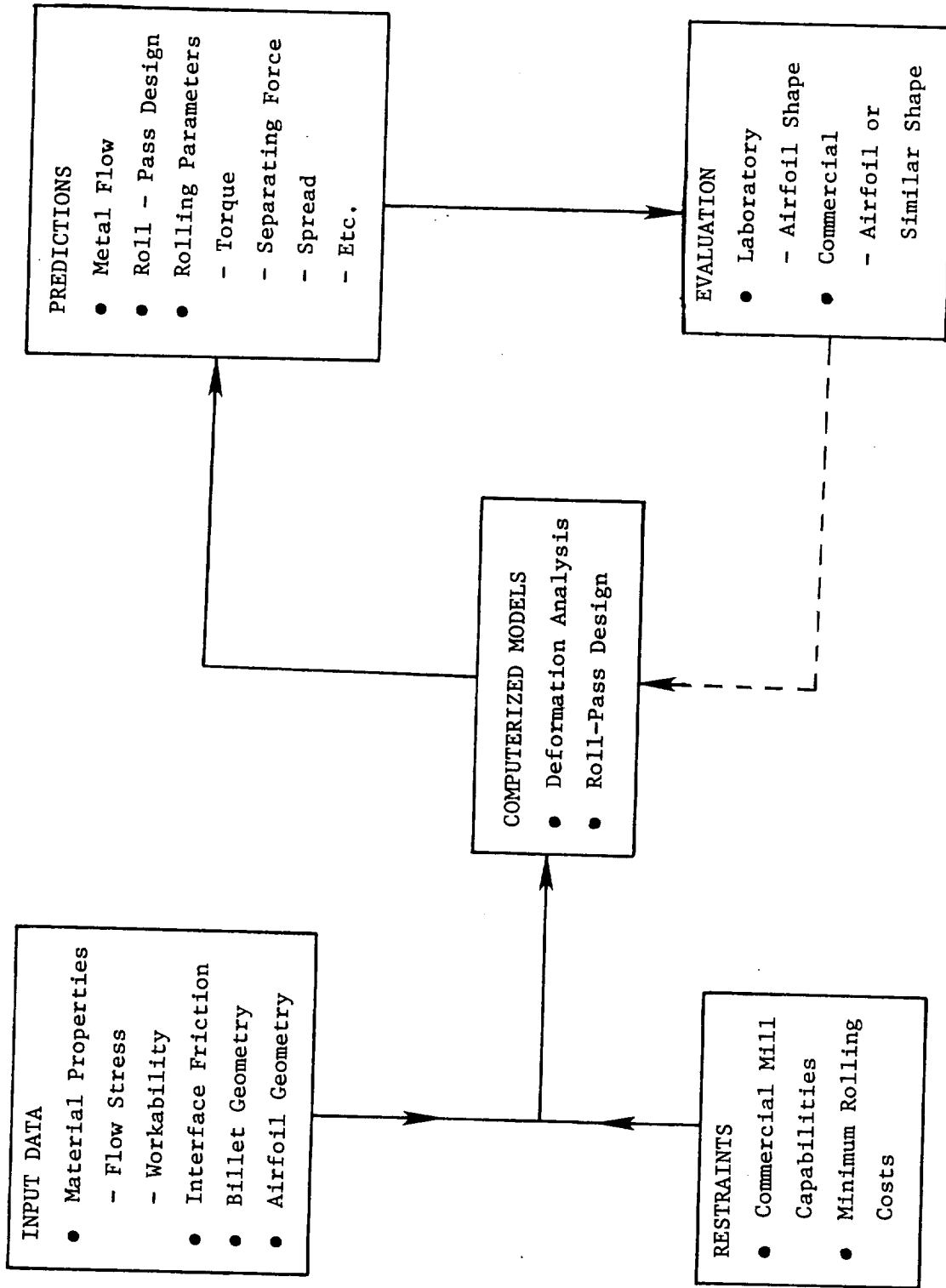(e) Evaluation of the CAD system with a commercial shape-rolling process for airfoils in current production.

FIGURE 1. OUTLINE OF THE PROGRAM ON COMPUTER-AIDED ANALYSIS AND DESIGN OF THE SHAPE ROLLING PROCESS FOR PRODUCING TURBINE ENGINE AIRFOILS

(f) Cost-benefit analysis of applying the CAD system to shape
     rolling of airfoils and two other metalworking processes.

BACKGROUND ON SHAPE ROLLING

Shape rolling is a relatively old and well-known process and the
expenditures involved in establishing a shape-rolling installation are in
the order of several million dollars. The costs of designing and manufac-
turing of rolls for a given shape are very high. Despite these factors,
however, there are very little useful, quantitative engineering data on
shape rolling available in the published literature[1-3]. A relatively
recent book, published in East Germany, summarizes the advances made in
roll-pass design in the Eastern and Western rolling industry and research
laboratories[4]. Although several empirical engineering methods are
available for estimating the roll-separating force and the roll torque in
shape rolling, it appears that no quantitative engineering method of analy-
zing the complex three-dimensional deformation and of roll-pass design exists.

Metal Flow in Shape Rolling. In terms of complexity of metal flow,
the shape-rolling process can be classified in the following three categories:

(a) Uniform Reduction of Cross Section: This type of
     deformation occurs in rolling of thick plates.
     The material elongates in the longitudinal direc-
     tion and spreads in the transverse direction while
     it is compressed uniformly in the thickness direc-
     tion. This is illustrated schematically in Figure 2a.

(b) Moderately Nonuniform Reduction of Cross Section:
     Rolling of an oval shape or an airfoil section from
     a rectangular cross section, as shown in Figure 2b,
     can be considered in this category. Here, the
     reduction in the thickness direction is nonuniform.
     However, the metal elongates and spreads laterally
     outwards in a manner similar to that in rolling of
     plates.

(c) <u>Highly Nonuniform Reduction of Cross Section</u>: In
this type of deformation, the reduction is highly
nonuniform in thickness direction, and part of the
cross section is reduced in height while other parts
may be extruded, as shown in Figure 2c. This results
in both inward and outward flow of metal in the
lateral direction and a flow perpendicular to the
plane of rolling. In addition, the metal flows in
the longitudinal direction.

The lateral metal flow, briefly discussed above, must be quantitatively
evaluated for each location within the deformation zone between the rolls. The
deformation zone is limited with the entrance, where an already prerolled shape
enters the rolls, and the exit, where the rolled shape leaves the rolls. A
method for investigating the metal flow in shape rolling is illustrated in
Figure 3[5]. The deformation zone is cross sectioned with several planes, 1
through 5, (1 is at entrance, 5 is at exit). The roll position and the defor-
mation of the incoming billet are investigated at each of these planes. Thus,
a more detailed analysis of metal flow and an improved method for designing
the configuration of the rolls is possible. It is evident that this technique
can be drastically improved and made extremely efficient by using a computer.
The computer, then, would allow to take a very large number of cross-sectional
planes and would automatically draft the configurations of the rolls and of the
billet at each cross section.

<u>Roll-Pass Design</u>. For a given material and final cross-sectional
shape, there is no unique method of roll-pass design. For example, Figure 4
illustrates schematically five different methods of pass design for a steel
angle with equal legs[6]. Similar illustrations are given in Figure 5 for a
steel angle with unequal legs.

In roll-pass design for shapes, the most difficult problem is due to
the fact that the cross section of a shape is not deformed uniformly. This is
illustrated in Figure 6 for a relatively simple shape. The reductions in height
are not equal for the Zones A and B of the shape, seen in Figure 6a. Consequent-
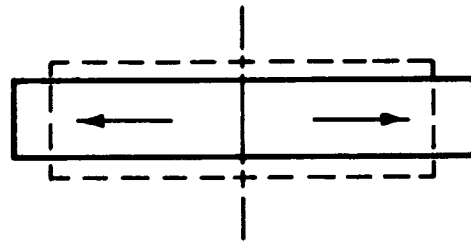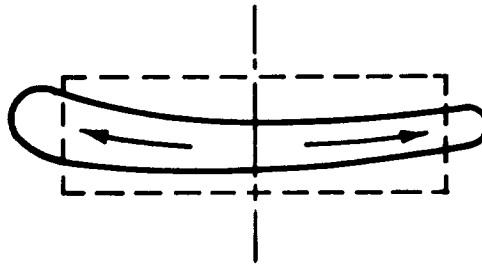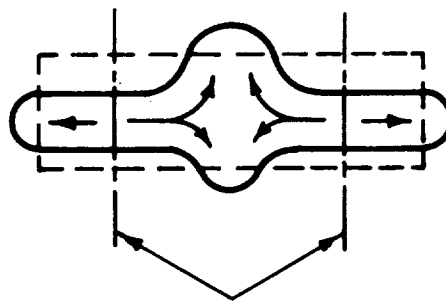
FIGURE 2. THREE TYPES OF METAL FLOW IN ROLLING OF SHAPES

FIGURE 3. ANALYSIS OF A ROLL PASS USED IN ROLLING RAILS[5]
(Sketches 1 through 5 illustrate the stock, broken lines and the roll, full lines at various positions of the deformation zone)

FIGURE 4. SCHEMATIC OF FIVE DIFFERENT ROLL-PASS[6] DESIGNS FOR AN ANGLE SHAPE FROM STEEL
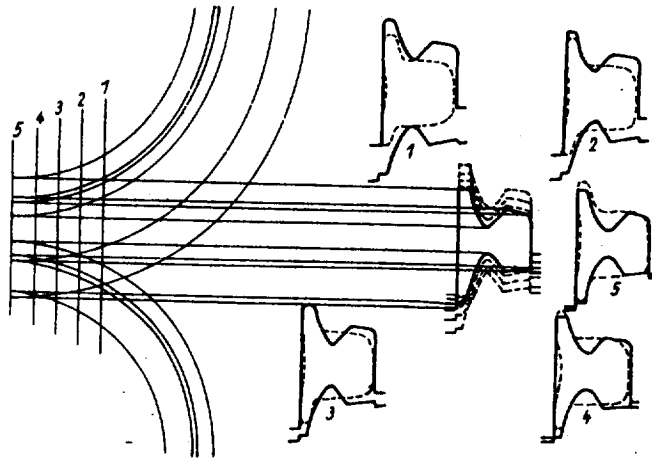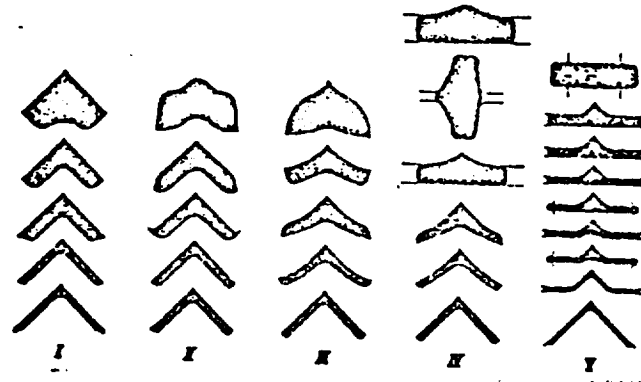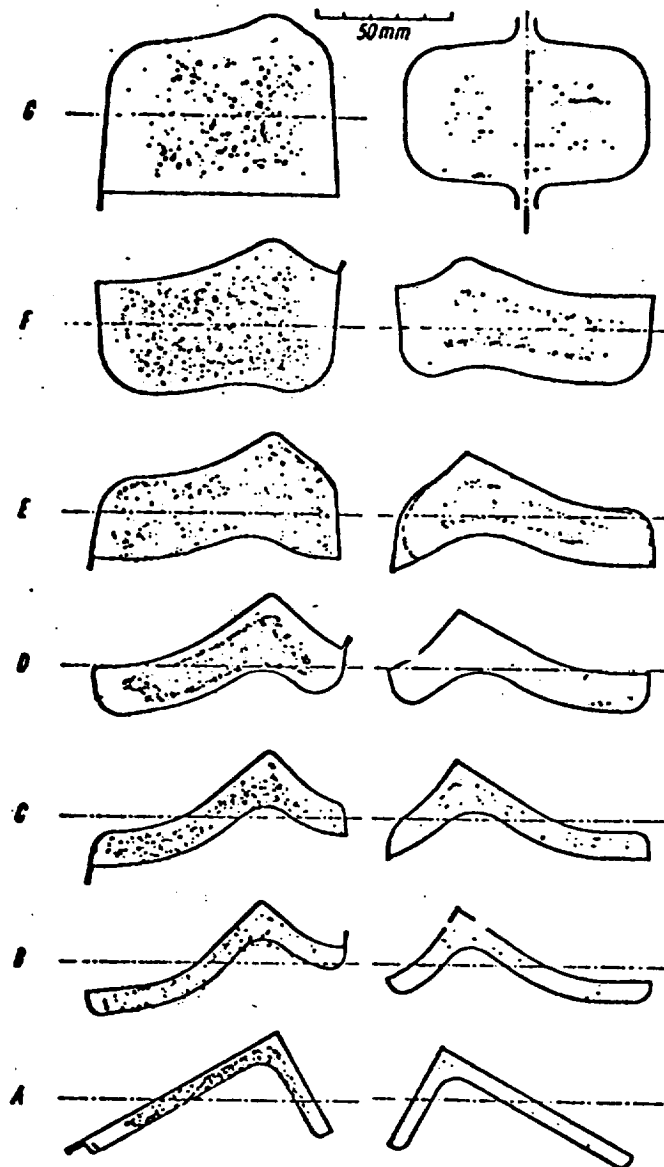

FIGURE 5. SCHEMATIC OF TWO DIFFERENT ROLL-PASS DESIGNS FOR A STEEL ANGLE WITH UNEQUAL LEGS[7]
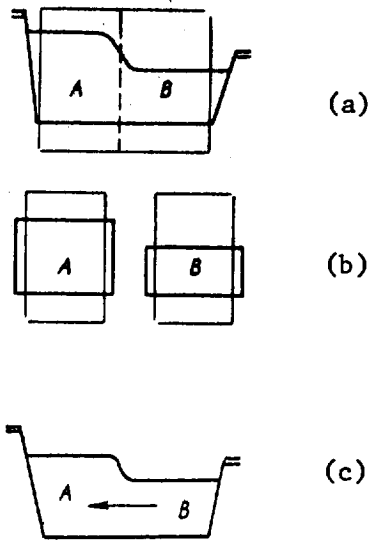
FIGURE 6. NONUNIFORM DEFORMATION IN ROLLING OF A SHAPE

ly, if these two Zones, A and B, were completely independent from each other, Figure 6b, the Zone B would elongate much longer than the Zone A. However, both zones are connected and as part of rolled shape, they must have equal elongation at the exit from the rolls. Therefore, during rolling, metal must flow from Zone B into Zone A so that a uniform elongation of the overall cross section is obtained[7-9]. This lateral flow is also influenced by the temperature differences which exist in the cross section because of varying material thickness and heat flow.

In establishing the number of passes and the shape of the rolls for each pass, the following factors must be considered:

(1) The Characteristics of the Available Installation: These include: (a) diameters and lengths of the rolls, (b) bar dimensions, (c) distance between roll stands, (d) distance from last stand to the shear, and (e) tolerances which are required and which can be maintained.

(2) Reduction per Pass: The reduction per pass must be adjusted so that (a) the installation is utilized at a maximum capacity, (b) the roll stands must not be overloaded, and (c) the wear of the rolls must be minimized. The maximum value of the reduction per pass is limited by (a) the excessive lateral metal flow which results in edge cracking, (b) the power and load capacity of the roll stand, (c) the requirement for the rolls to bite in the incoming bar, (d) roll wear, and (e) tolerance requirements.

DETERMINATION OF FLOW STRESS, WORKABILITY AND FRICTION FACTOR

The two basic material characteristics that greatly influence the rolling process are the flow stress and the workability of the material being rolled. The flow stress represents the resistance of a material to plastic deformation, and the workability represents its ability to deform without

failure, regardless of the magnitude of the local stress and strain rate required for deformation. In rolling of airfoil shapes, relatively moderate strains and strain rates are encountered in the deforming material. Consequently, the response of the alloys of interest must be determined in the practical range of temperatures, strains, and strain rates. Another important variable to be characterized is the friction factor (ratio of frictional shear stress to shear flow stress) at the tool-material interface.

Flow Stress and Its Determination. For a given metal, the flow stress is most commonly obtained by conducting the uniform compression tests without barreling[10]. In this test, a well-lubricated, short cylindrical specimen, machined from the material under study, is compressed between a pair of hardened flat parallel platens. At hot-working temperatures, the test is conducted in a fixture, as shown in Figure 7. The flow stress of a material is influenced by the conditions of the deformation process, mainly the temperature of deformation (θ), the degree of deformation or the strain (ε) and the rate of deformation or the strain rate ($\dot{\varepsilon}$). Therefore, the uniform compression tests must be conducted at the temperature and the strain-rate conditions that exist in the practical deformation process, under consideration. The degree of deformation, or the strain, is generally defined in terms of logarithmic (true) strain ε. In uniform upset test, the strain ε is given as below:

$$\varepsilon = \ln\left[\frac{h_o}{h}\right] , \tag{1}$$

where h_o = initial sample height

h = instantaneous sample height

The strain rate $\dot{\varepsilon}$ is the derivation of strain ε with respect to time or:

$$\dot{\varepsilon} = \frac{d\varepsilon}{dt} = \frac{dh}{hdt} = \frac{V}{h} , \tag{2}$$

where V = instantaneous compression speed

In all metalworking operations, except in uniform compression, ε and $\dot{\varepsilon}$ values vary within the deforming material. Consequently, in using strains and strain rates in practical rolling operations, average values must be employed.
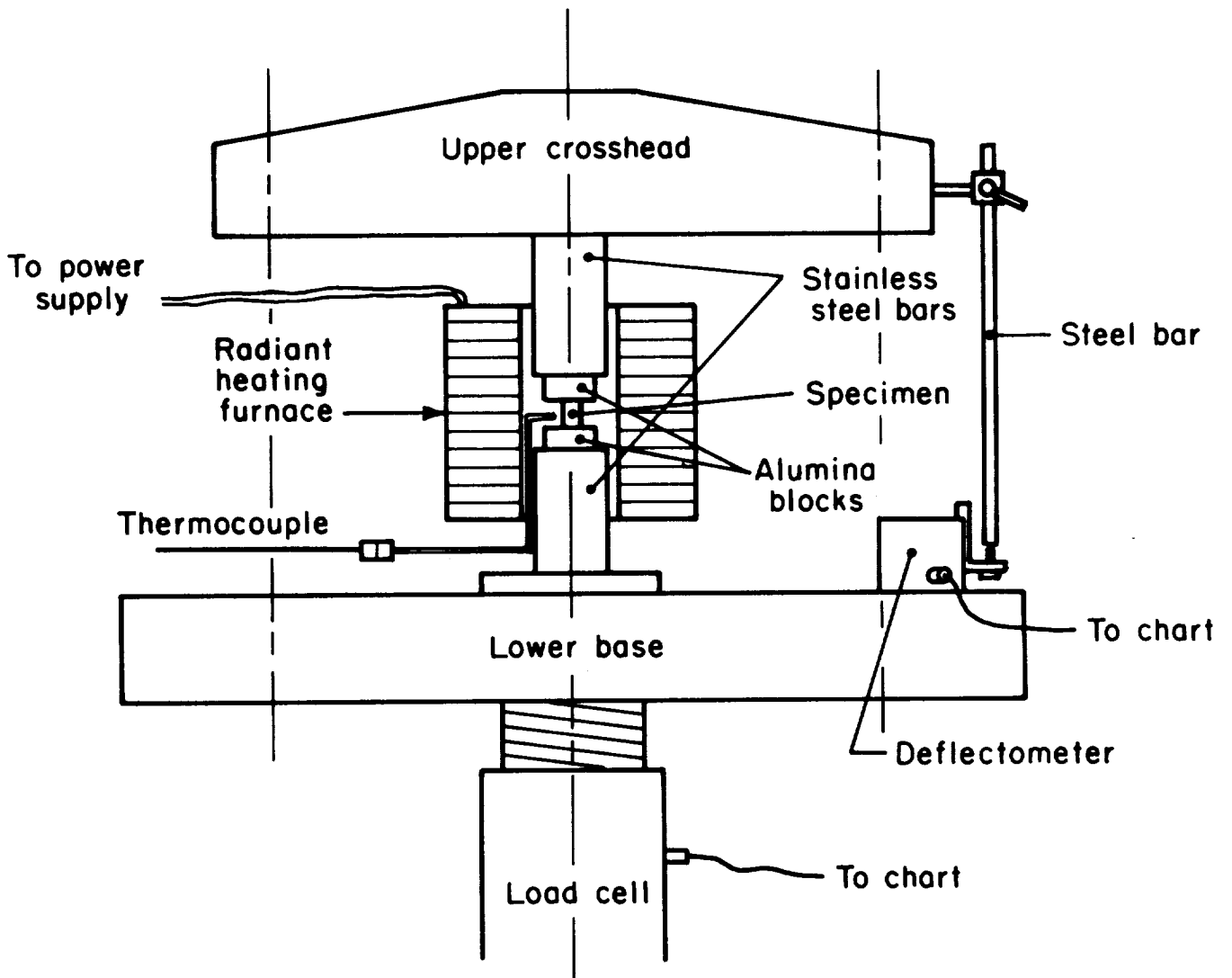
FIGURE 7. EXPERIMENTAL SET UP ON A UNIVERSAL TESTING
MACHINE FOR DETERMINATION OF FLOW STRESS

Workability and Its Determination. Workability of a metal represents its ability to deform without failure, regardless of the magnitude of the local stress and strain rate required for deformation. The nonuniform compression test and the torsion test are two of the most commonly used methods for evaluating workability of metals and alloys[11]. Although there is no general agreement as to which test gives the best result, it was decided to measure workability using the nonuniform compression test, since the stresses in compression of cylinders and rolling of shapes are primarily compressive in nature. In these tests, a cylindrical specimen is compressed under two flat platens without any lubrication. The workability of the material is measured in terms of percent reduction in height to visible fracture on the specimen surface.

Friction Factor and Its Determination with the Ring Test. Friction at the tool-workpiece interface is another important process variable which needs characterization in order to be used in making predictions from analytical models. For this purpose, the friction factor associated with the actual rolling conditions is determined by using the well-established Ring Test[12]. The ring test consists of compressing a flat ring-shaped specimen to a known reduction, Figure 8. The change in internal and external diameters of the forged ring is very much dependent upon the friction at the tool-specimen interface. The internal diameter of the ring is reduced if the interface friction is large; increased if friction is low. Thus, the change in the internal diameter represents a simple method for evaluating interface friction.
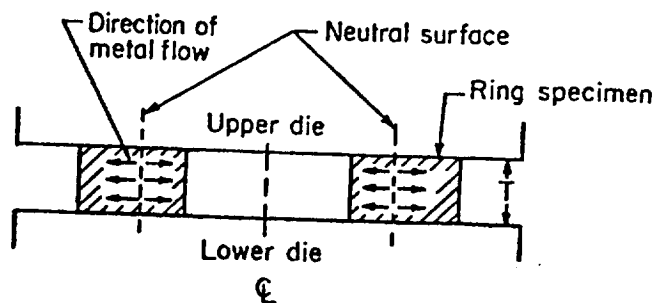

FIGURE 8. METAL FLOW IN RING COMPRESSION TEST

In hot forming, as die temperatures usually are lower than billet temperatures, die chilling results. This effect influences the frictional conditions, and it is included in the measurement of the friction factor by using the ring test at hot-forging temperatures. Die chilling, however, also influences the temperature of the deforming billet and, consequently, its flow stress. It is, therefore, difficult to estimate the actual flow stress, $\bar{\sigma}$, and the friction factor, f, (or the shear factor, m) under practical rolling conditions. If these two values are known, shear stress, τ, is given by:

$$\tau = \bar{\sigma} \; \frac{m}{\sqrt{3}} = \bar{\sigma} \; f \quad . \tag{3}$$

To obtain the magnitude of the friction, the internal diameter of the compressed ring must be compared with the values predicted by using various friction factors, f, or shear factors, m. For this purpose, the upper-bound analysis and the associated computer program were developed earlier at Battelle were available for use[12]. The computer program mathematically simulates the ring-compression process for given shear factors, m, by including the bulging of the free surfaces. Thus, ring dimensions for various reductions in height and shear factors (m) can be determined. This is the conventional way of representing theoretical calibration curves used in evaluating friction with the ring test.

In determining the value of the shear factor (m) for a given experimental condition, the measured dimensions (reduction in height and variation in internal diameter) are placed on the appropriate calibration figure. From the position of that point with respect to theoretical curves given for various m's, the value of the shear factor (m), which existed in the experiment, is obtained.

MATERIAL DEFORMATION STUDIES

Materials

In this program, mild steel (AISI 1018) was selected as model cold rolling material and Ti-6Al-4V alloy was selected as a typical hot-working material. INCONEL 718 (INCO 718) was selected as a material currently being used in cold rolling of airfoil sections. The nominal composition of these materials is given in Table I.

In order to determine the flow stress, workability and friction factor under actual processing conditions uniform compression and ring compression tests were used. Initially all the three materials were ordered in round bar stock. The mild steel bars were cold drawn and the Ti-6AL-4V and INCO 718 bars were hot finished, rough ground and solution treated. The specimens for uniform compression tests were machined from 17.7 mm diameter bar stock, whereas the ring specimens were machined from 19.05 mm diameter bar stock. All the specimens were cut in the longitudinal direction and, except for Ti-6Al-4V specimens, were annealed at appropriate temperatures and shot blasted prior to testing.

Later, Ti-6Al-4V alloy was also ordered in sheet material of 2.327 mm (0.131 in.) thickness. The sheet material was hot rolled, annealed and cleaned. The sheet material was ordered in sufficient quantity such that the specimens for hot-isothermal rolling experiments under Task II could also be machined from the same stock.

Flow Stress

In the present work, specimens were machined to a nominal diameter of 12.7 mm (0.500 inch), a nominal height of 19.1 mm (0.750 inch), and the sharp corners were broken. Mild steel and INCO 718 specimens were cleaned with acetone and placed on teflon sheets in between hardened steel platens (R_c 65). The test conditions are summarized in Table II. The details of experiments are included in Appendix A.

TABLE I. NOMINAL COMPOSITION OF THE ALLOYS USED IN THE PRESENT PROGRAM

AISI 1018 Steel

C	0.15 - 0.20	Mn	0.60 - 0.90
P,max	0.040	S,max	0.050
Fe	Balance		

Ti-6Al-4V Alloy

Al	5.5 - 6.75	V	3.5 - 4.5
Fe	0.30	O	0.20
C	0.10	N	0.05
H	0.0125	Ti	Balance

INCONEL 718 Alloy*

Cr	18.28	Fe	17.70
Al	0.65	Ti	1.03
Mo	3.07	Cu	0.17
Cb + Ta	5.15	C	0.04
Mn	0.15	Si	0.17
Cu	0.04	S	0.003
P	0.013	B	0.002
Ni	Balance (53.43)		

Ti-6Al-4V Alloy (Sheet Material)*

Al	5.8	V	3.8
Fe	0.14	O	0.135
C	0.03	N	0.013
H	75 ppm	Ti	Balance

* As supplied by the vendor

TABLE II. UNIFORM COMPRESSION TEST CONDITIONS

MATERIAL	CONDITION	TEST TEMP.	TEST MACHINE	CROSSHEAD SP.	LUBRICANT
AISI 1018	Annealed at 1600 F for 1 hr Furnace Cooled	Room Temperature	Baldwin Capacity 60.000 (lb)	0.02 inch/min	Teflon Sheet 0.010 inch
INCO 718	Annealed at 1800 F for 1 hr Air Cooled	Room Temperature	Baldwin Capacity 100.000 (lb)	0.02 inch/min	Teflon Sheet 0.010 inch
TI-6Aℓ-4V	As Received	1700 F	Baldwin Capacity 60.000 (lb)	1 inch/min	Window Glass

NOTES: 1) Nominal dimensions of all samples were 0.500-inch diameter x 0.750-inch high.

2) During the tests that were conducted at room temperature, the lubricant (teflon sheet) was renewed at every 10 percent reduction.

The AISI 1015 tests were conducted in a Baldwin universal testing machine of 267 kN (60,000 lb) capacity. More load was required for INCO 718; hence, a 445 kN (100,000 lb) capacity machine was used. The teflon sheets were replaced at every 10% reduction in order to ensure adequate lubrication and prevent bulging. Three specimens of each material were tested and the load-displacement curve was recorded.

The Ti-6Al-4V (bar stock) tests were conducted under isothermal conditions at 927 C (1700 F) using powdered window glass as lubricant. Ti-6Al-4V was tested at 927 C as it is a typical hot-working temperature for this alloy. The experimental fixturing is illustrated in Figure 7. A spiral groove was machined at the ends of each specimen to enhance lubricant retainment and ensure uniform compression conditions. Three specimens were tested and the load-displacement curve was recorded. From the load-displacement curves, the necessary calculations to obtain the flow stress versus strain curves, given in Figures 9 through 11 were made using a simple computer program.

The microstructure of Ti-6Al-4V compression test specimens was examined at the NASA-Lewis Research Center. Sections perpendicular to the applied stress (cross section) and parallel to the applied stress (longitudinal section) were mounted, polished, and etched (2 parts HCl, 1 part HF) for the as-received material and the six isothermally compressed specimens. In addition, a piece of as-received alloy, which was subjected to a heat treatment (placed in furnace at approximately 677 C (1250 F); slowly heated to 927 C (1700 F) over 2 hr; held for a few minutes at 927 C (1700 F); air cooled) designed to simulate the thermal portion of the compression test cycle was also examined.

The microstructure of as-received alloy is shown in Figure 12. The structure consists of large alpha grains surrounded by small beta and alpha grains. This microstructure is similar in appearance to that shown in Figure 2724 of the Metals Handbook, Vol. 7 (Reference 14) and is the result of a fabrication schedule involving work above the beta transus temperature followed by significant amounts of work in the two phase (alpha plus beta) temperature range. The microstructure of the heat-treated material is shown in Figure 13. It consists of primary alpha
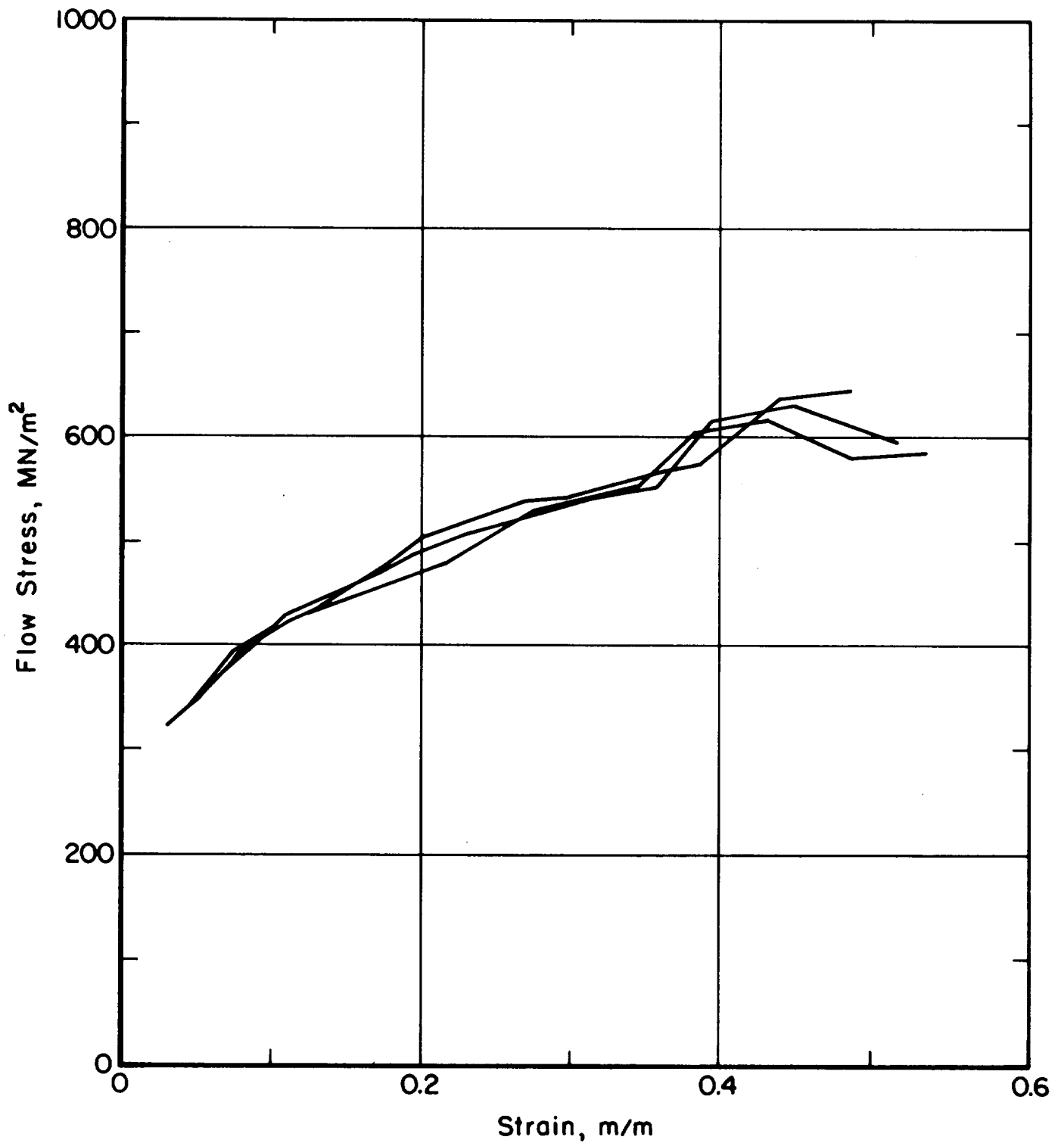
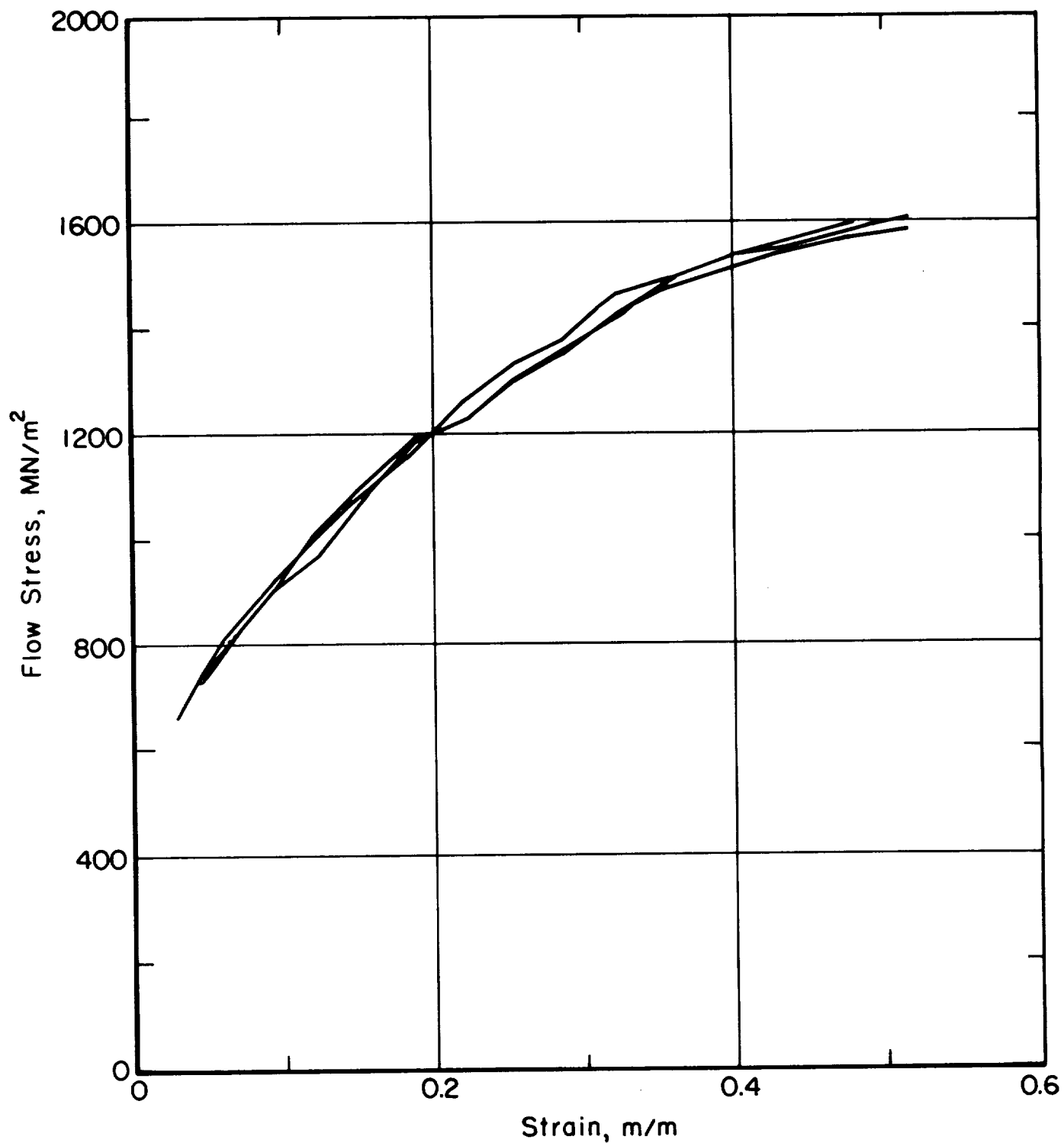FIGURE 9. UNIFORM COMPRESSION TEST RESULTS FOR FLOW STRESS OF AISI 1018 AT ROOM TEMPERATURE

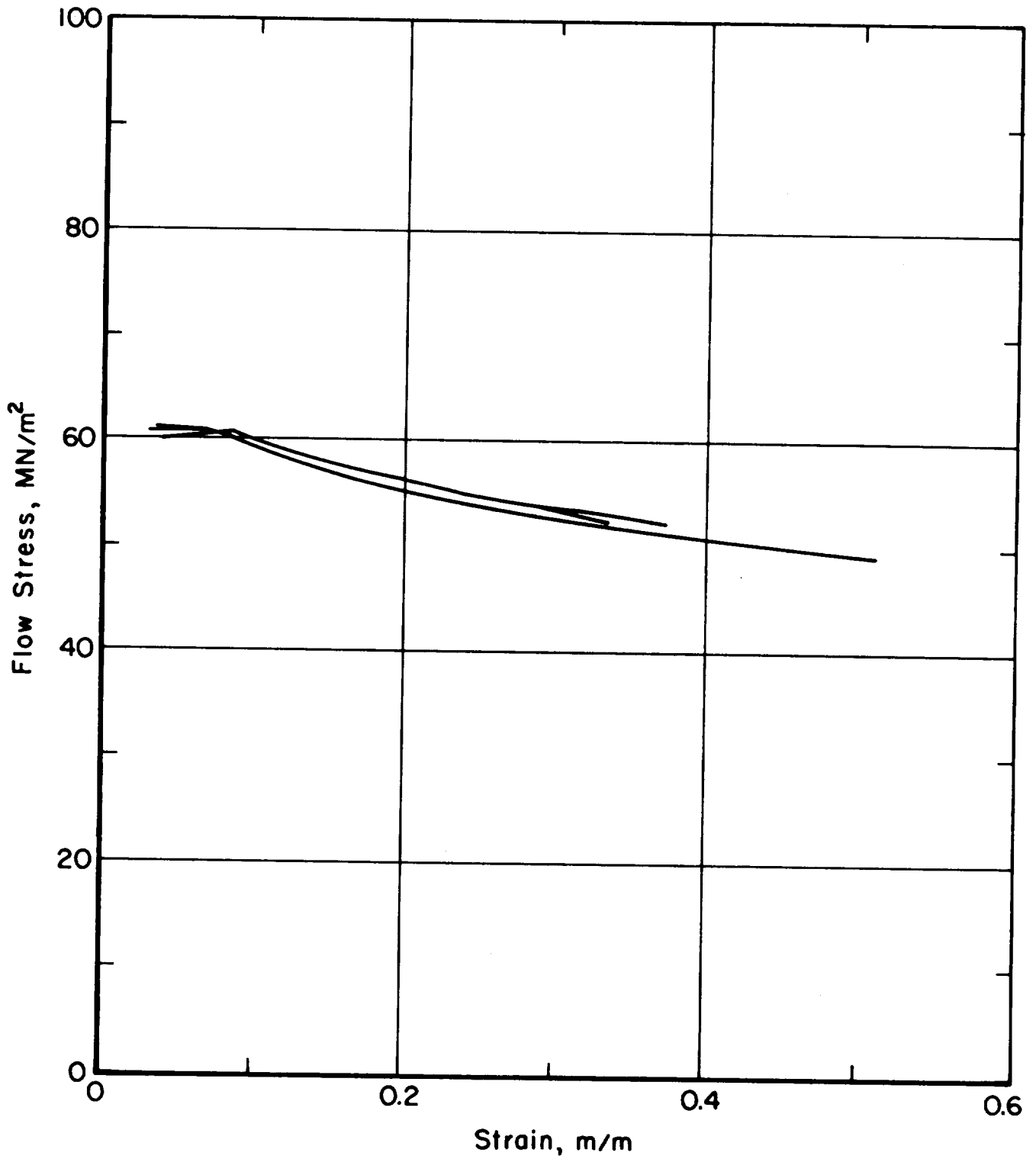FIGURE 10. UNIFORM COMPRESSION TEST RESULTS FOR FLOW STRESS OF INCO 718 AT ROOM TEMPERATURE

FIGURE 11. UNIFORM COMPRESSION TEST RESULTS FOR FLOW STRESS OF Ti-6Aℓ-4V (BAR STOCK) AT 927 C (1700 F)

(large alpha grains present before heat treatment, see the longitudinal section of Figure 12), acicular alpha, and intergranular beta. This microstructure is similar to that shown in Figures 2713 and 2714 of the Metals Handbook, Vol. 7 (Reference 14). Comparison of Figures 12 and 13 indicates that heat treatment is tending to form on equiaxed microstructure about 10μm in diameter; however, definite signs (primary alpha) of the as-received microstructure remain.

In general, the microstructures of the tested samples (6 samples with true strain ranging from -0.37 to -0.71) are identical and consist of equiaxed alpha grains about 4μm in diameter and intergranular beta (very small distinct particles), as shown in Figure 14. The microstructure is somewhat similar to those in Figures 2712 and 2719 of the Metals Handbook, Vol. 7 (Reference 14). Comparison of the microstructures of the tested specimens to the heat-treated specimen (Figure 13) indicates that working has fully developed a small equiaxed grain structure which is apparently not significantly affected by the work levels investigated in this study (true strains ranging from -0.37 to -0.71). Attempting to correlate the observed microstructure with mechanical behavior, it appears that some critical amount of work (approximately 10%, see Figure 11) must be introduced in order to start recrystallization. Once started, recrystallization is a dynamic process with the observed grain size remaining essentially constant over strain range investigated. This observation agrees with Luton and Sellars[15] who indicated that the dynamic recrystallized grain size is function of the flow stress.
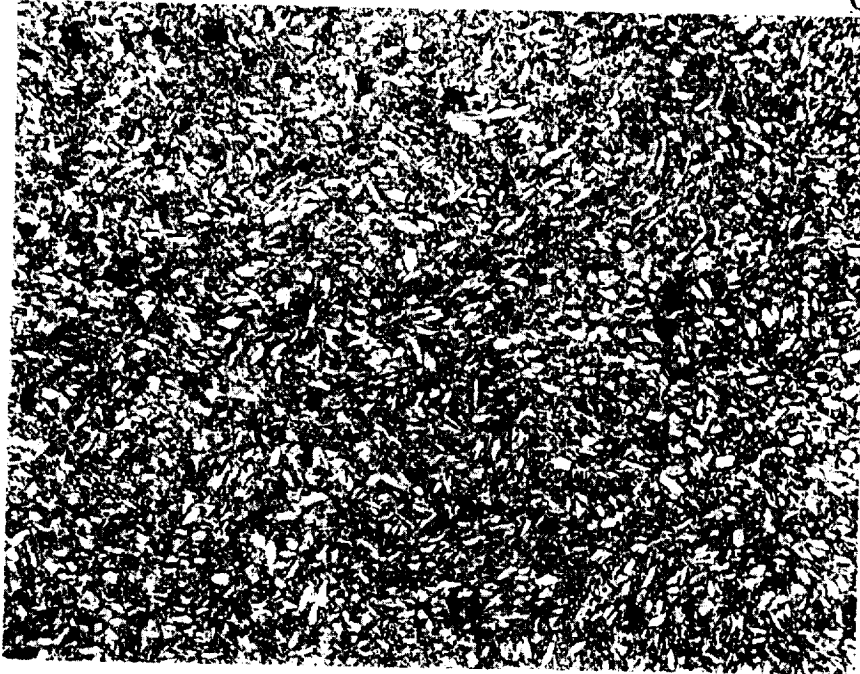
As-Received Cross Section

Bar Axis

100 μm
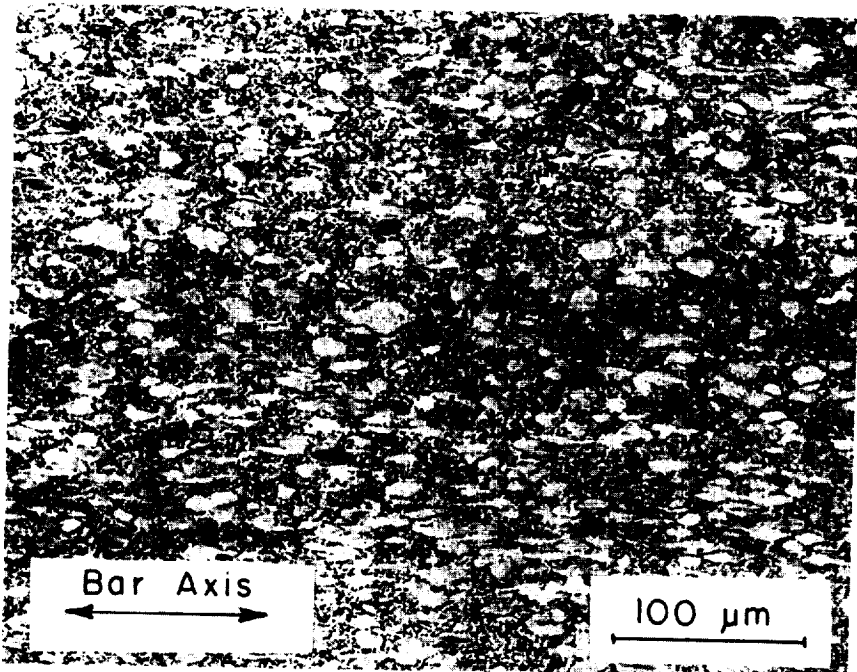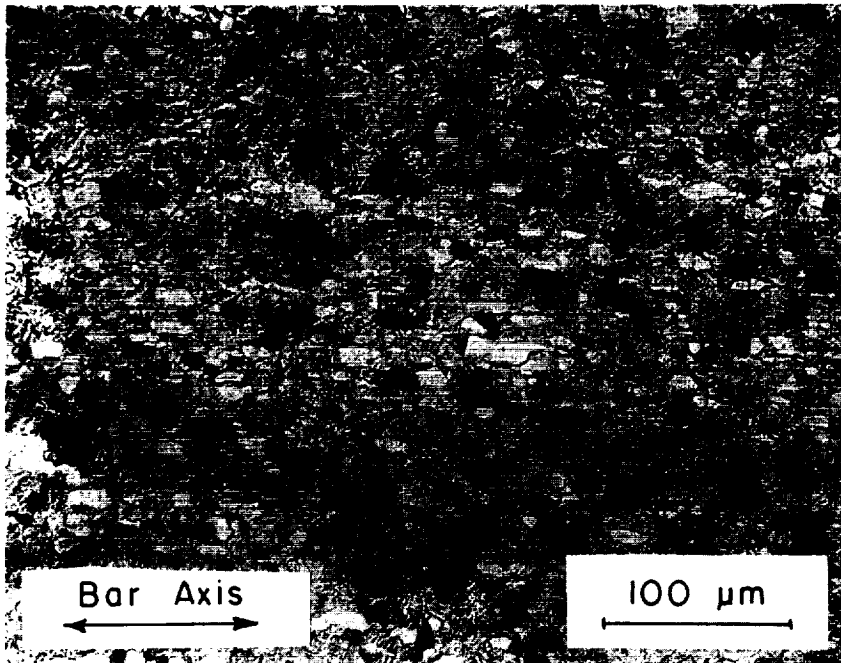
As-Received Longitudinal

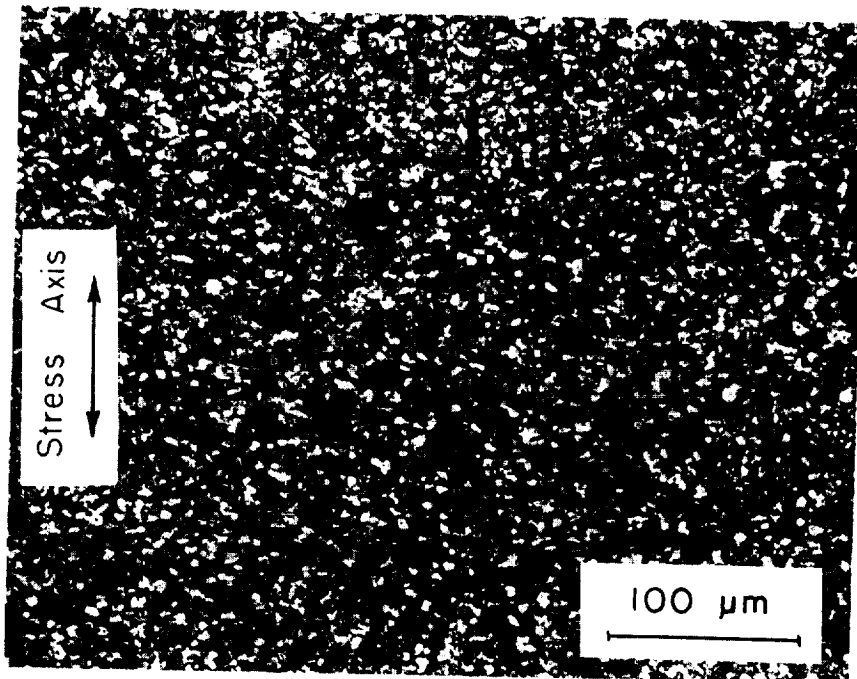FIGURE 12.   PHOTOMICROGRAPHS OF AS-RECEIVED Ti-6Al-4V
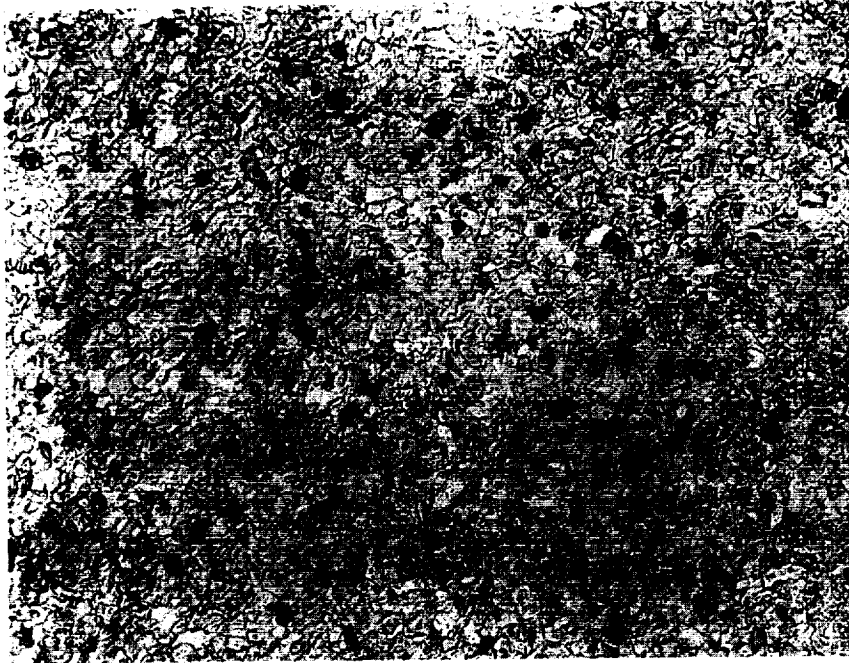
Heat Treated Cross Section

Heat Treated Longitudinal

FIGURE 13.   PHOTOMICROGRAPHS OF HEAT-TREATED Ti-6Al-4V
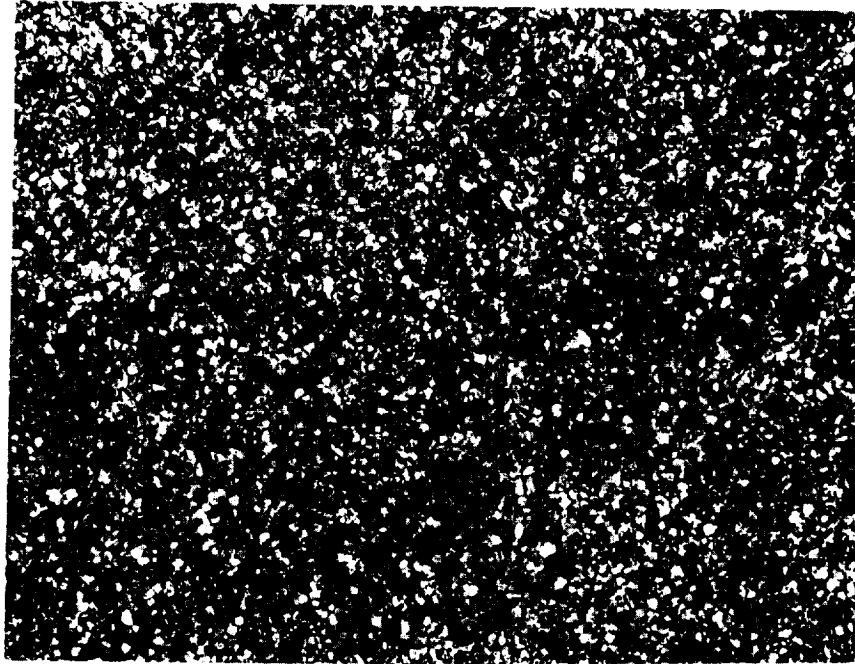
Specimen 1 Cross Section

Specimen 1 Longitudinal

FIGURE 14.   PHOTOMICROGRAPHS OF TEST SPECIMEN AFTER COMPRESSION TEST
($\varepsilon = -0.56$, t = .428, t_o = 0.75, ε = ln t/t_o)

Flow Stress of Ti-6Al-4V Sheet Material. In a recent study on hot-isothermal rolling of titanium strips[16], it was found that the flow stress data obtained from the uniform compression tests (using specimens machined from bar stock) were not valid for strip material under similar processing conditions. The possible reasons for the difference between the flow stress of sheet and bar material from Ti-6Al-4V alloy under similar processing conditions are believed to be the texture in the sheet material and the microstructural and lot-to-lot variations between the bar and the sheet material. Therefore, in order to determine the flow stress of Ti-6Al-4V sheet material to be rolled under hot-isothermal conditions, uniform compression tests were conducted using specimens made from a stack of sheet material. Six specimens, as shown in Figure 15, were fabricated from 3.3 mm (0.130-inch) thick, Ti-6Al-4V sheet in the as-received condition. The rolling direction was marked in ink on the surface of the sheet before shearing the material into 19 mm (3/4-inch) squares. Six squares were stacked and held compressively in a lathe and turned to 12.7 mm (0.5-inch) diameter. One flat surface of the two end pieces of each cylinder was machined so as to have 0.13 mm (0.005-inch) deep V-groove in a spiral pattern. The rolling direction of the material was identified on each disk by a small indentation on the outer diameter. The diameter of the disk at that point corresponds to the rolling direction of the material. Prior to final assembly, the flat surface of each disk was lightly rubbed on 180 grit sand paper in three different stroke direction approximately 120° apart to remove surface film, burrs, and to slightly abrade the surface. The disks were then cleaned with acetone, assembled in a stacked position in a V-block and clamped firmly in position for welding. A disk with the spiral surface exposed capped either end of each fabricated cylinder. Each cylinder was TIG welded under argon with four beads, 90" apart, parallel to the axis of the cylinder on the OD surface.
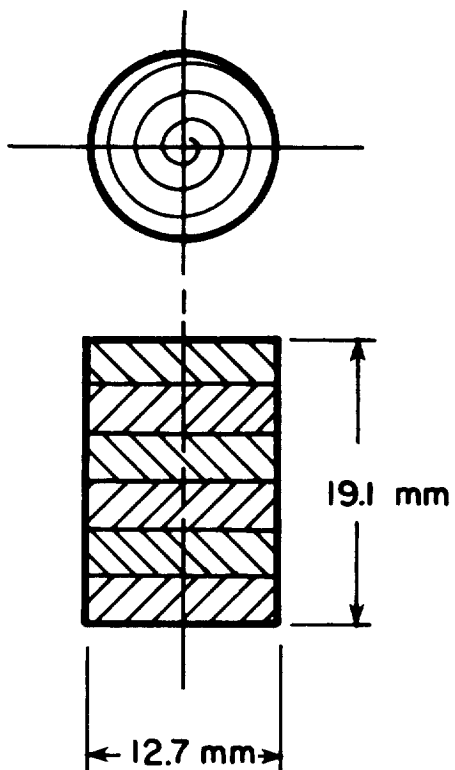
FIGURE 15.   UNIFORM COMPRESSION TEST SPECIMEN

The tests were conducted on Battelle's 500-ton mechanical press. The flywheel was slowed down to 33 rpm in order to achieve strain rates ranging between 6 to 8 per second. The specimens were heated in an insulted container that also held the platens, as shown in Figure 16. The container was constructed from Inconel alloy 601 (60.5 Ni - 23 Cr - 14.1 Fe - 1.35 Al) which was selected for its excellent resistance to oxidation at high temperature. The platens were cemented titanium carbide (Kentanium K162B supplied by Kennametal, Inc.) which was selected on the basis of its excellent strength and hardness at high temperature.

For the uniform compression tests, the cylinders were first lubricated at room temperature by dipping them in a slurry of glass in isopropyl alcohol and allowed to dry. They were then placed in the furnace next to the protective container and heated to the forging temperature. Approximately 15 minutes prior to each test, the sample was placed on the lower anvil of the container, and the top anvil was inserted. The entire assembly was then returned to the furnace and reheated to the forging temperature. While the glass-slurry coating on the sample minimized oxidation, it was inadequate to provide sufficient lubrication during the upset test. Therefore, additional powdered glass was sprinkled on the bottom anvil and on the top of the specimen, after placing it into the container. This technique worked well and allowed uniform upsetting of the cylindrical samples.

The specimens were deformed inside the fixture and the load-displacement data were recorded on a visicorder. The flow stress versus strain and strain rate versus strain curves, as shown in Figures 17 and 18, were reduced from the load-displacement information by using a simple computer program developed earlier at Battelle.
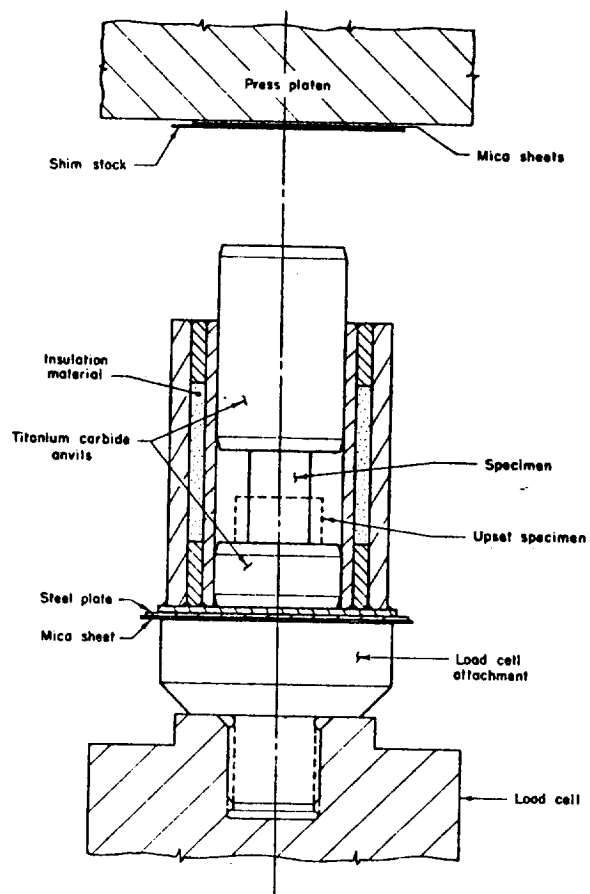
FIGURE 16. PRESS SETUP AND FIXTURE USED IN HEATING AND
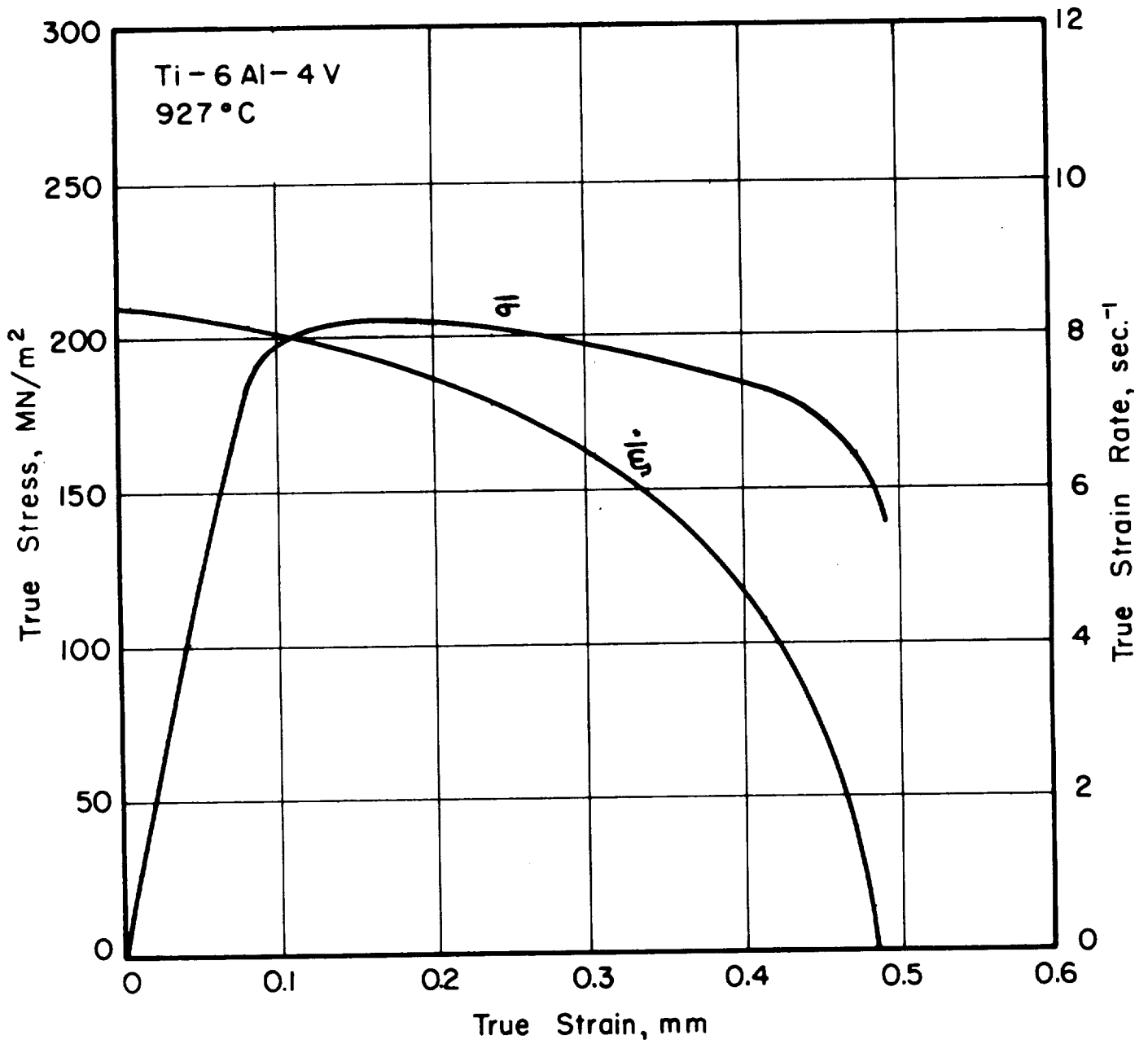ISOTHERMAL COMPRESSION OF CYLINDERS AND RINGS

FIGURE 17. FLOW STRESS AND STRAIN RATE VERSUS STRAIN
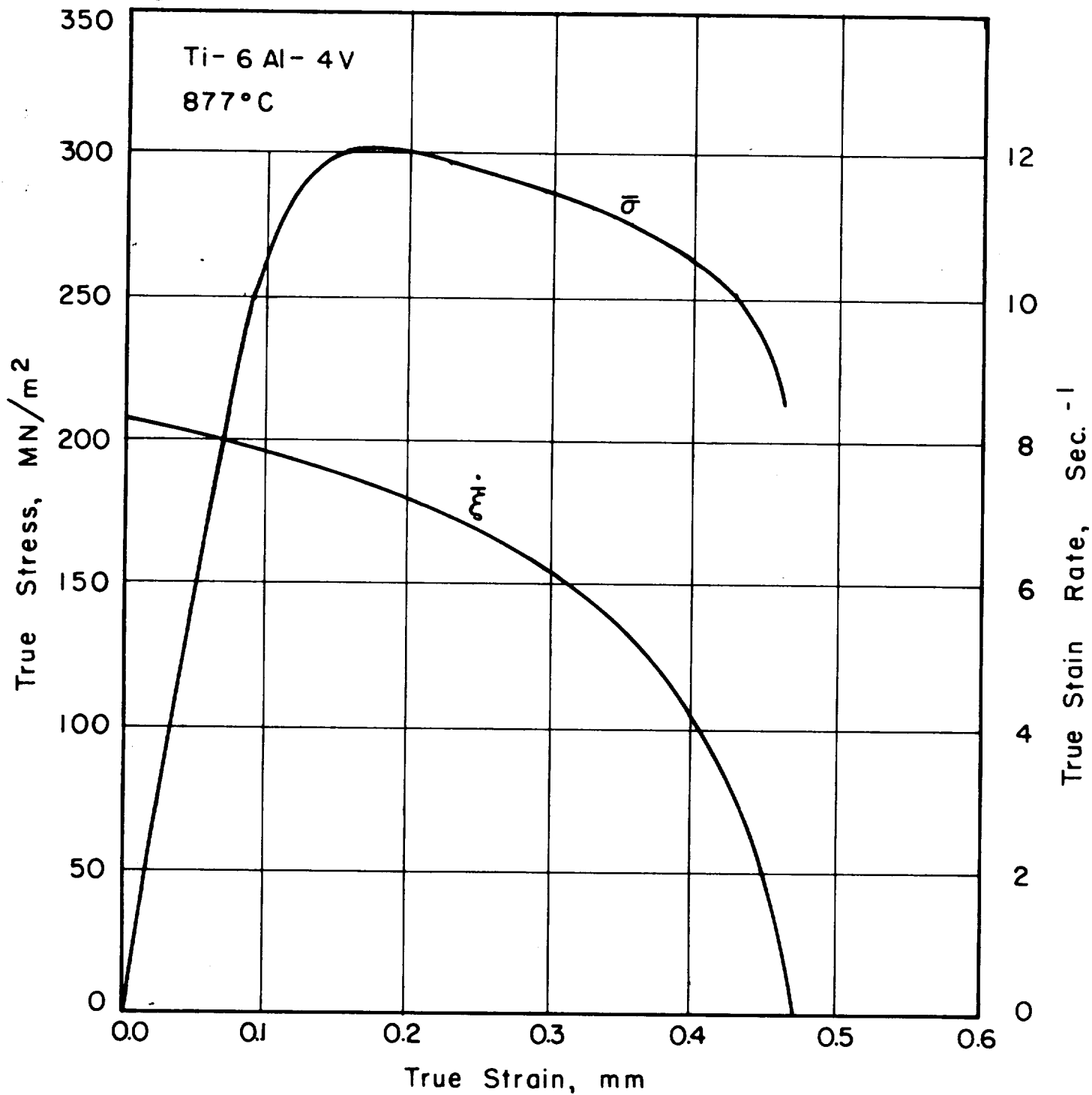FOR Ti-6Al-4V (SHEET STOCK) AT 927 C

FIGURE 18. FLOW STRESS AND STRAIN RATE VERSUS STRAIN
FOR Ti-6Al-4V (SHEET STOCK) AT 877 C

The microstructure of as received Ti-6Al-4V alloy sheet and the microstructure of the compression test specimens were examined at the NASA-Lewis Research Center. All the samples were mounted, polished and etched with a dilute acid mixture (1 part H_2O to 1 part of the following: 33 cc H_2O, 33cc acetic acid, 33cc HNO_3, and 1 cc HF).

The microsturcture of the as-received Ti-6Al-4V strip is presented in Figure 19. It consists of "large" cigar-shaped alpha grains (elongated in the rolling direction) surrounded by "small" alpha and beta grains. A few stringers of alpha grains elongated in the long transverse direction were seen halfway through the sheet thickness.

Figures 20 and 21 contain the metallography of a Ti-6Al-4V hot compression test specimen composed of six pieces of sheet stock which were tack welded. Basically, except for the tack welded regions, the micro-structure of each piece of sheet was almost identical to the as-received material. Away from the tack welded regions, the individual sheets were not welded as seen in Figure 21. The lack of welding between the sheets even after approximately 40 percent reduction is somewhat surprizing. How-ever, the oxidation during heating of the specimens may have been sufficient to prevent pressure welding of the sheets. Furthermore, the microstructure of the tack welded region is perhaps much stronger at 927 C (1700 F) than the microstructure of the as-received sheet.[17] Therefore, the flow stress measured with this test specimen might be on the high side due to four tack welds.

Workability

Workability tests were conducted for AISI 1018 and INCO 718 at room temperature. 17.2 mm (0.5-inch) diameter, 19.1 mm (0.750-inch) long nonlubricated cylindrical specimens were compressed in a universal testing machine until cracks appeared. AISI 1018 specimens were compressed 70 per-cent without any cracks, at which point the test was stopped. INCO 718 specimens showed classical 45 degree cracks at approximately 56 percent ± 2 percent reduction consistently. Figure 22 shows an INCO 718 specimen which cracked at 56 percent reduction in height and an uncracked AISI 1018 steel specimen which was compressed to 70 percent reduction in height.
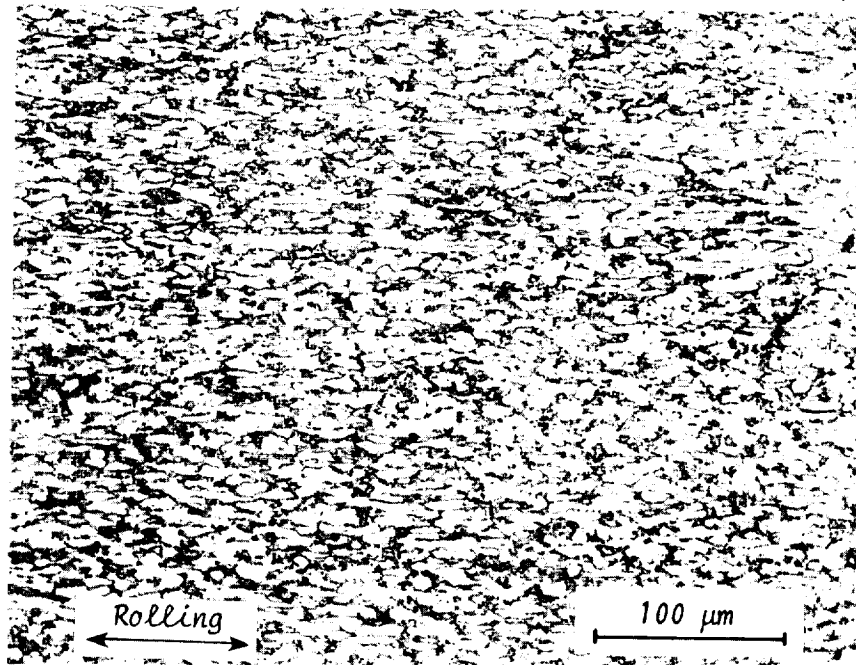
(a) Rolling Direction
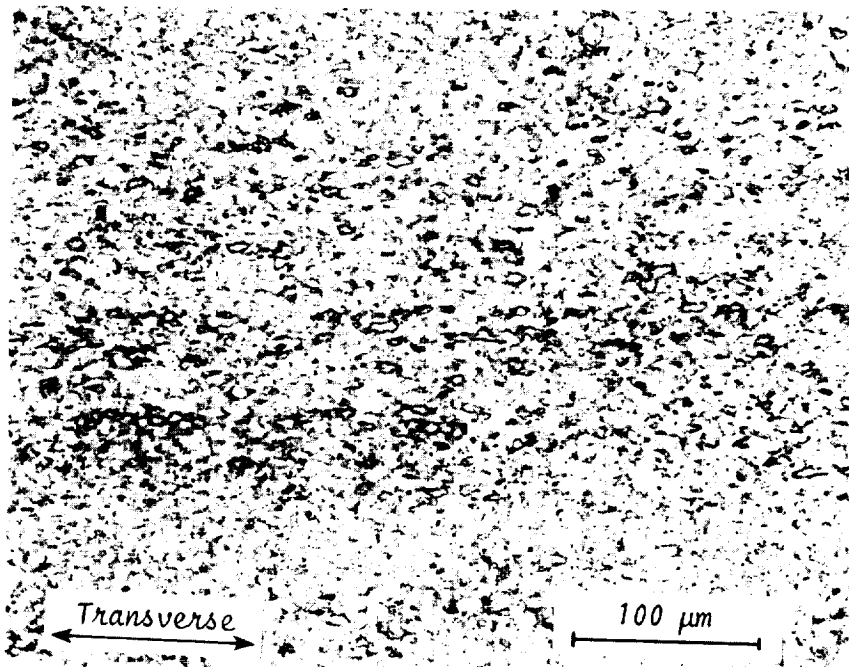
(b) Long Transverse

FIGURE 19. MICROSTRUCTURE OF THE AS-RECEIVED Ti-6Al-4V SHEET METAL
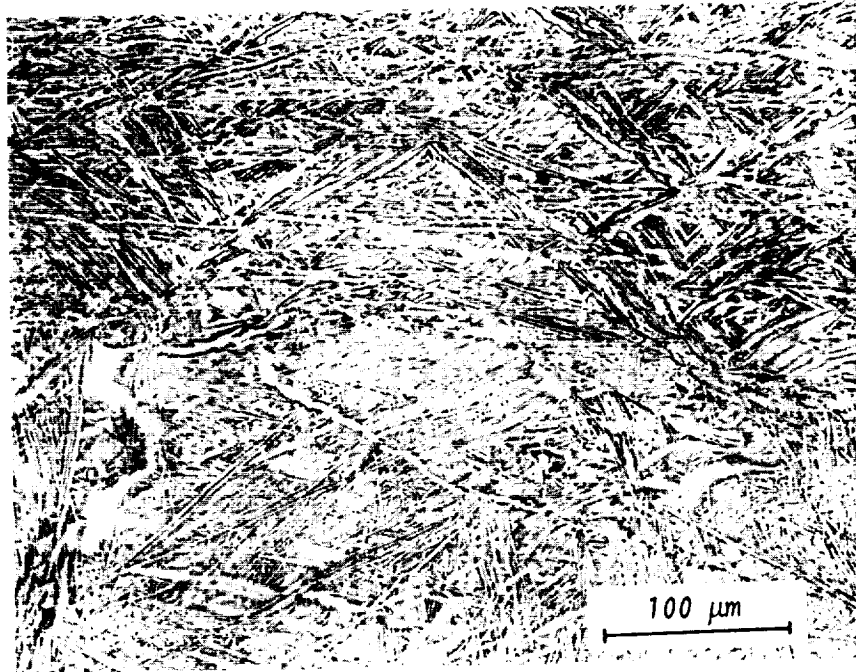
(a) At the Surface of the Specimen Along the Tack Weld Region
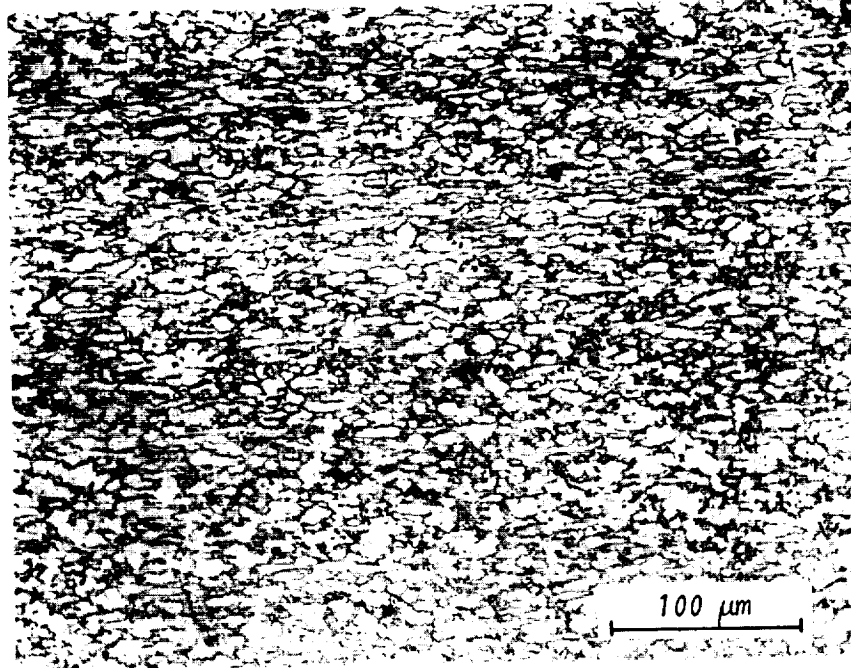
(b) At the Surface of the Specimen Away from Tack Weld

FIGURE 20. MICROSTRUCTURE OF A LAMENA IN A COMPRESSION TEST SPECIMEN
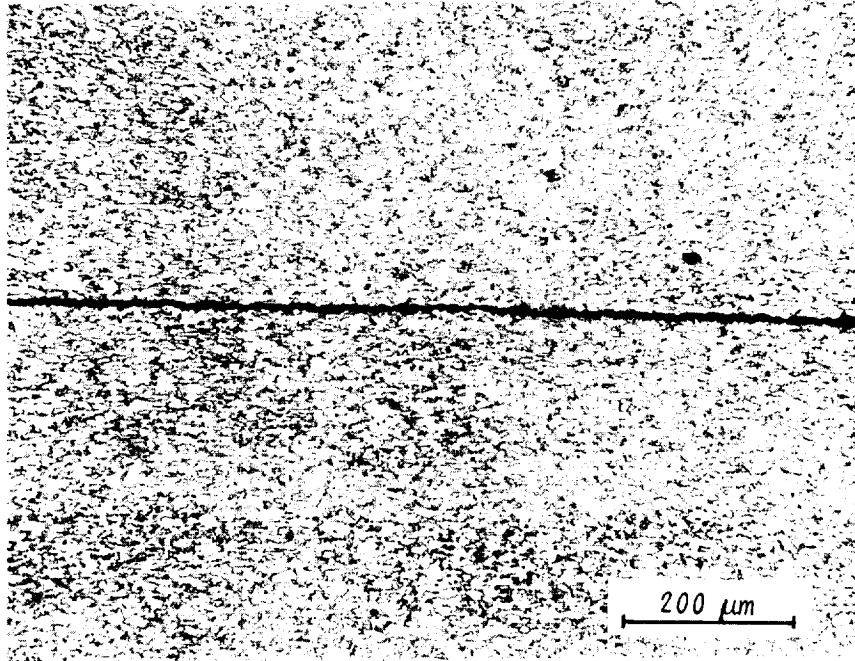
(a)
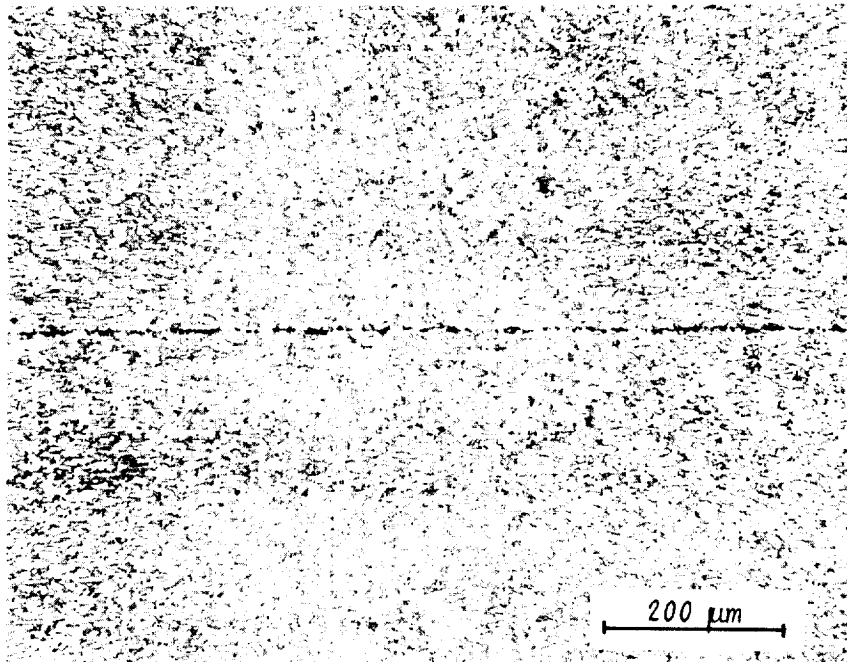
(b)

FIGURE 21.   MICROSTRUCTURE OF COMPRESSION TEST SPECIMEN AT THE INTERFACE OF TWO SHEETS

(a)   (b)

FIGURE 22. DEFORMED SAMPLES FROM NONUNIFORM COMPRESSION TESTS FOR
DETERMINING WORKABILITY: (a) INCO 718 Specimen after 56
Percent Reduction, (b) AISI 1018 Steel Specimen after 70
Percent Reduction

Non-uniform compression tests were also conducted in order to
determine workability of Ti-6Al-4V alloy under hot isothermal rolling con-
ditions. 12.7 mm diameter x 19.0 mm long specimens were machined from a
12.7 mm (0.500-inch) diameter as-received bar. The test fixture shown in
Figure 16 was also used in these tests. The unlubricated specimens were
heated to 927 C (1700 F) inside the clean fixture and compressed to various
reductions in height (up to 70 percent) on Battelle's 500-ton mechanical
press with flywheel running at 33 rpm. Since no cracks were observed in
any of the specimens, the workability is not considered to be a limiting
factor in hot isothermal rolling of Ti-6Al-4V shapes.

Friction Factor

In the present work, ring tests with AISI 1018 and INCO 718 were
conducted at room temperature using essentially the same experimental set
up as that used for uniform compression and workability tests. Ring speci-
mens were machined to have 19.1 mm (0.750-inch) OD x 9.52 mm (0.375-inch)
ID x 6.35 mm (0.250-inch) height. Rings were upset between flat hardened
platens to approximately 15, 30 and 40 percent reduction in height. In
order to approximate the friction conditions, which are present during
cold shape rolling in practice, the rings were dipped into a drawing lubri-
cant (Turco Draw 300) prior to upsetting.

ORIGINAL PAGE IS
OF POOR QUALITY

Figure 23 shows AISI 1018 steel rings before and after deforma-
tion. Ring tests were conducted using Ti-6Al-4V alloy specimens in order
to determine the friction factor at the roll-workpiece interface under hot-
isothermal rolling conditions. Again, ring specimens with 19 mm OD x 8.5
mm ID x 6.35 mm height were machined from a 19.1 mm (0.75-inch) diameter
as-received bar. The specimens were heated and compressed inside the fix-
ture shown in Figure 16. The press flywheel speed was kept at 33 rpm. Sev-
eral ring specimens were compressed to various reductions in height (up to
44 percent).

After the tests, the dimensions of the rings were measured. The
friction shear factor m was determined from the variation of the internal
ring diameter by using the theoretical calibration curves given in Figure 24.
The results show that the friction factor m is approximately 0.3 for INCO
718, 0.25 for AISI 1018 under cold rolling conditions and 0.8 for Ti-6Al-4V
under hot-isothermal rolling conditions.

FIGURE 23. AISI 1018 RINGS BEFORE AND AFTER DEFORMATION
(Left to Right: Reduction in Height 0, 20,
30 and 40 Percent, Respectively)
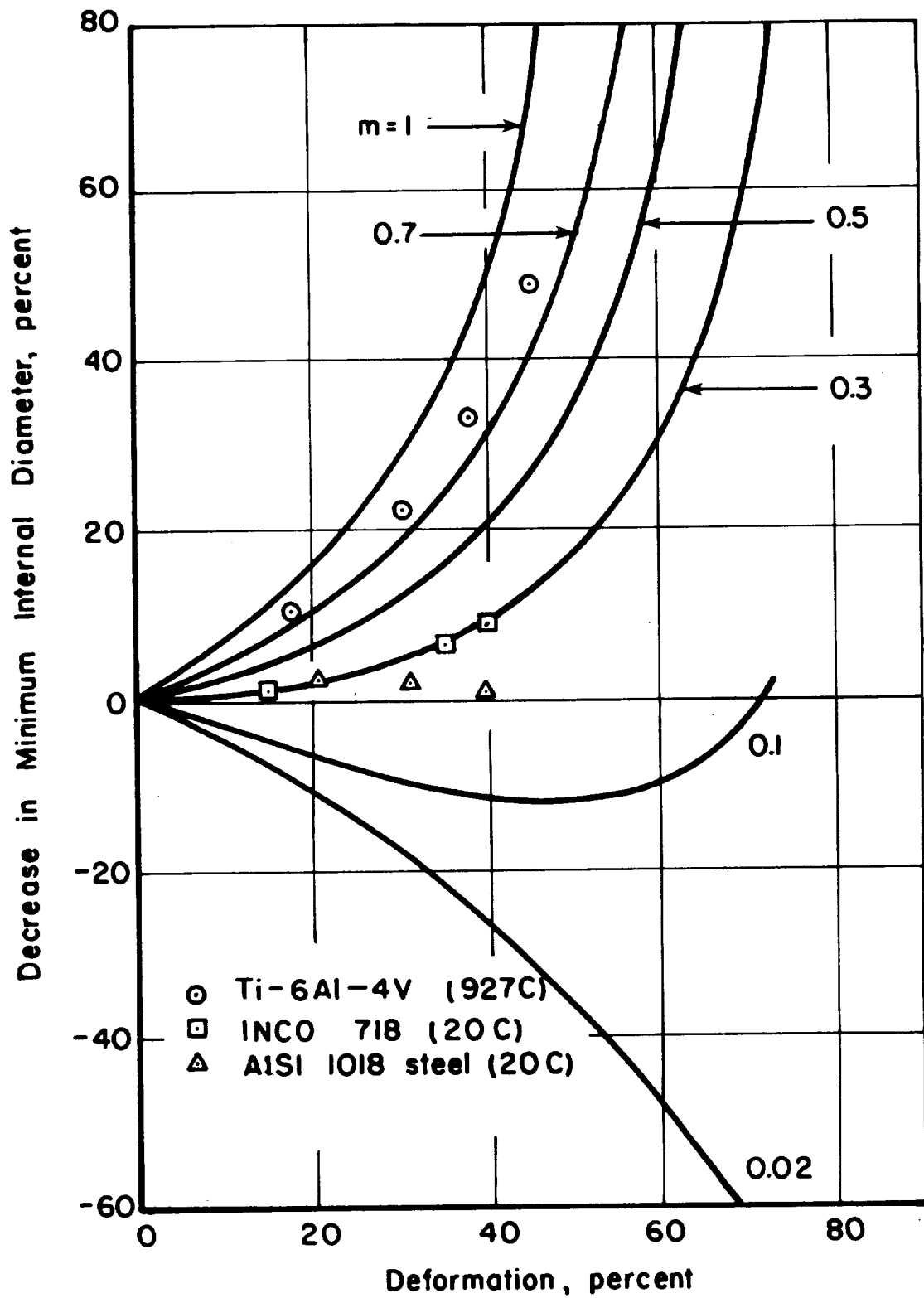
FIGURE 24. CALIBRATION CURVES AND EXPERIMENTAL POINTS FOR
DETERMINING FRICTION FACTOR FROM UPSETTING OF
6:3:2 RINGS

ANALYSIS AND PREDICTION OF METAL FLOW

In rolling of shapes, the material elongates in the rolling direction as well as it spreads in the transverse direction. Thus, an analysis of deformation in rolling of airfoil shapes includes not only the determination of roll torque and the location of the neutral plane, but also the determination of spread in the transverse direction. The purpose of the present analysis is to determine the distribution of metal flow during rolling of a bar with an initial arbitrary section through a pair of rolls with airfoil-like contours. Based on this analysis, a computer program named SHPROL was coded to simulate the metal flow in rolling of airfoil shapes. The details of the analysis are included in Appendix B. The description of the computer program SHPROL, together with instructions for preparing input to the program and a list of all the important variable names, is included in Appendix C.

The present analysis employs the upper-bound type theory to predict the distribution of metal within the deformation zone between the rolls. One essential feature of applying the upper-bound technique to the present uncontained steady-state metal flow problem is to find a kinematically admissible velocity field (which satisfies the volume constancy and the velocity boundary conditions) which retains the shape of the deformation zone. It is usually very difficult to find an admissible velocity field for problems involving general configurations even under nonsteady-state conditions. The conditions of steady-state makes the problem of determining an admissible velocity field even more difficult. Therefore, a modular approach, somewhat similar to the finite-element method, is developed here and the following simplifying assumptions are made in performing the present analysis:

(1) An airfoil shape can be considered as an aggregate of slabs, as shown in Figure 25.

(2) Plane sections perpendicular to the rolling direction
remain plane during rolling. Thus, the axial velocity
(i.e., velocity in rolling x-direction) at any section
perpendicular to the rolling direction is uniform over
the cross section.

(3) The velocity components in the transverse y, and the
thickness z directions are functions of x and linear
in y and z coordinates, respectively (see Figure 25).

The above assumptions correspond approximately to actual metal flow
conditions and have been shown to yield good predictions of metal flow in
rolling of plates.

Approach. The method used in solving the present problem is somewhat
similar to the finite-element method in the sense that the deformation zone is
divided into quadrilateral elements on the x-y plane, as shown in Figure 25. The
divisions in the transverse (y-) direction are made such that the velocities
normal to the dividing lines are zero. Thus, these lines represent streamlines
of metal flow. However, a finite number of velocity discontinuities occur
across the planes perpendicular to x-y plane and passing through these stream-
lines. The divisions along the longitudinal (x) direction, lines T_i-T_i, are
made arbitrarily. Similarly, a finite number of velocity discontinuities occur
across the y-z planes passing through these transverse lines, T_i-T_i, dividing
the deformation zone.

It is assumed that the top and bottom surfaces of each element can be
approximated by tapered planes, and the cross section of each element by a
rectangle, as shown in Figure 25, where the area under a rectangle with broken
lines is equal to the area of the original element. With this assumption, it is
possible to treat each element as a plate for which it is possible to derive a
kinematically admissible velocity field.

Velocity Field. The kinematically admissible velocity in the deformation
zone for an element i is then given by:

Upper roll

Billet

Lower roll

Product

z

y

o

x

Deformation zone

$Y = W_1(X)$

Ti

Entrance section

Exit section

Ti

$Y = W_2(X)$

y

o

x

x_n

Neutral surface
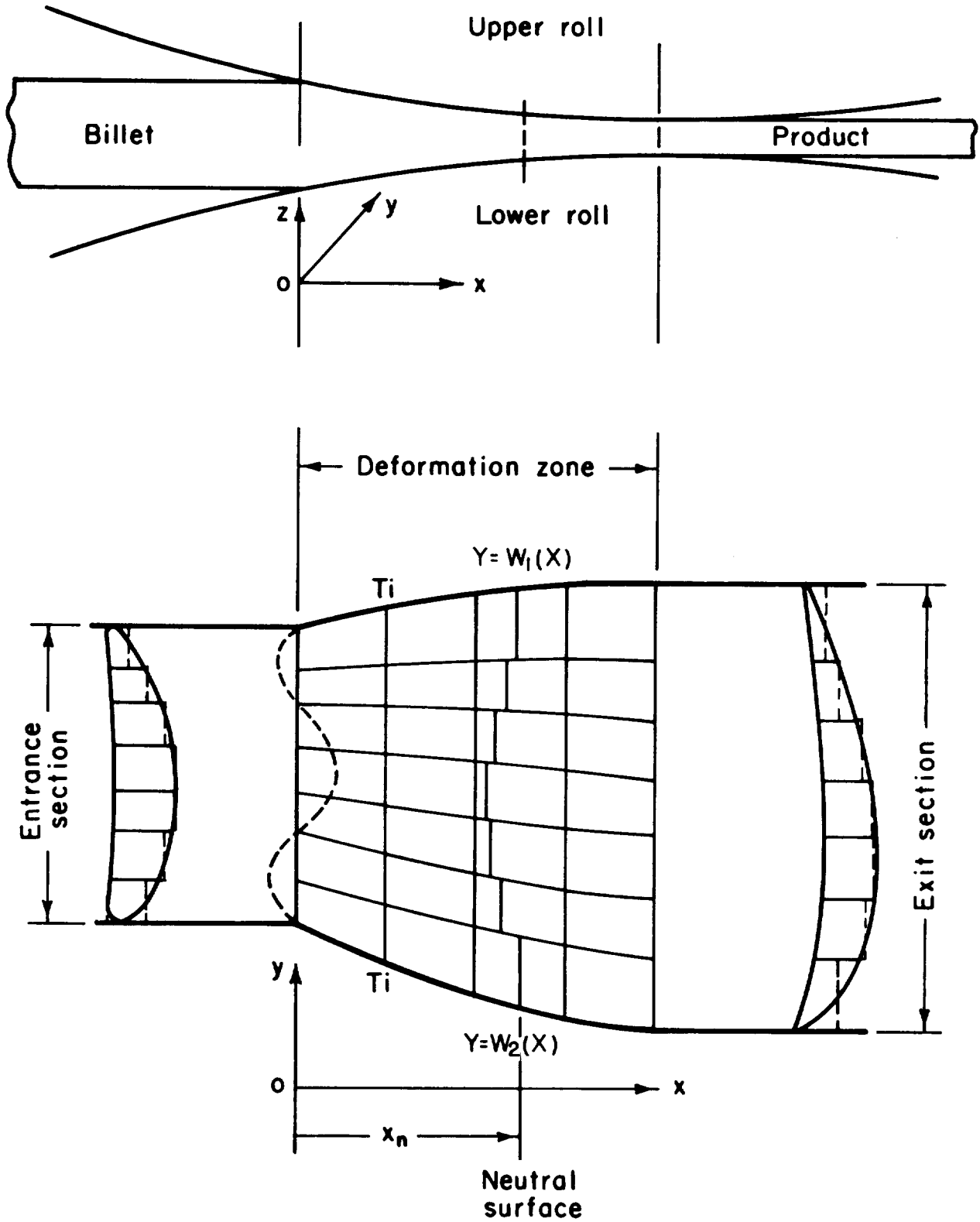
FIGURE 25.   CONFIGURATION OF DEFORMATION ZONE IN ROLLING OF AIRFOIL SHAPES

$$V_x = U \, v_x = U \, \frac{A_1(x_o)}{A_1(x)}$$

$$V_y = U \, v_y = U \, v_x \, \frac{f_1' \, (y - Y)}{f_1 - Y} \tag{4}$$

$$V_z = U \, v_z = U \, v_x \, \frac{h_1' \, (z - Z)}{h_1 - Z} \quad .$$

where V_x, V_y, V_z are the velocity components in the x, y, z directions, respectively. U is the velocity of incoming strip and $A_1(x)$ is the area of cross section of the element at x. f, h, y and z are given in Figure 26 and the prime denotes a derivative with respect to x. In Figure 26 (ζ, ξ, η) is the local coordinate system of an element.

The components of the strain-rate field can be derived from Equations (4). If $\dot{\epsilon}_x$, $\dot{\epsilon}_y$, and $\dot{\epsilon}_z$ represent the normal strain-rate components and $\dot{\gamma}_{xy}$ and $\dot{\gamma}_{xz}$ are the shear strain rates, then

$$\dot{\epsilon}_y = U \, \frac{\partial v_x}{\partial x} \quad , \quad \dot{\epsilon}_y = U \, \frac{\partial v_y}{\partial y} \quad , \quad \dot{\epsilon}_z = U \, \frac{\partial v_z}{\partial z} \quad ,$$

$$\tag{5}$$

$$\dot{\gamma}_{xy} = U \left(\frac{\partial v_x}{\partial y} + \frac{\partial v_y}{\partial x} \right) \quad , \quad \text{and} \quad \dot{\gamma}_{xz} = U \left(\frac{\partial v_x}{\partial z} + \frac{\partial v_z}{\partial x} \right)$$

Total Energy Rate. The total energy rate of the process consists of the energy rate of plastic deformation, energy rate associated with velocity discontinuities and the energy rate to overcome the frictional restraint.

The energy rate of plastic deformation, $\dot{E}_p$, for an element is given as follows:
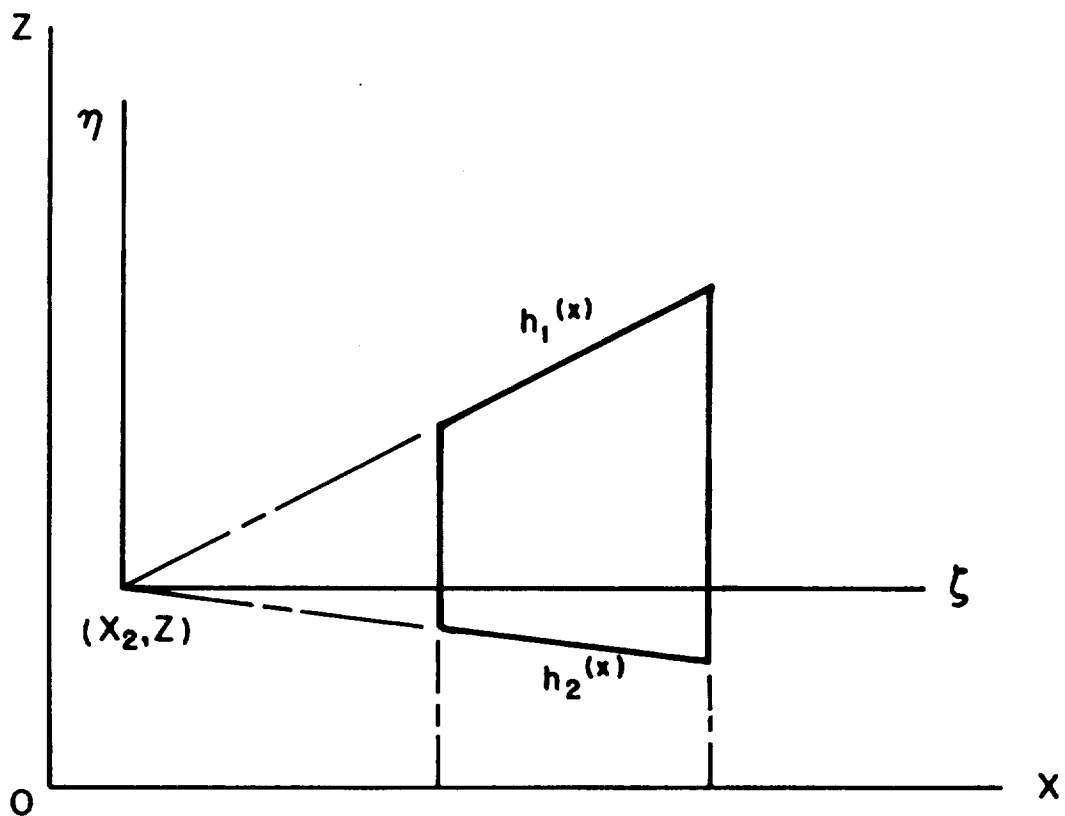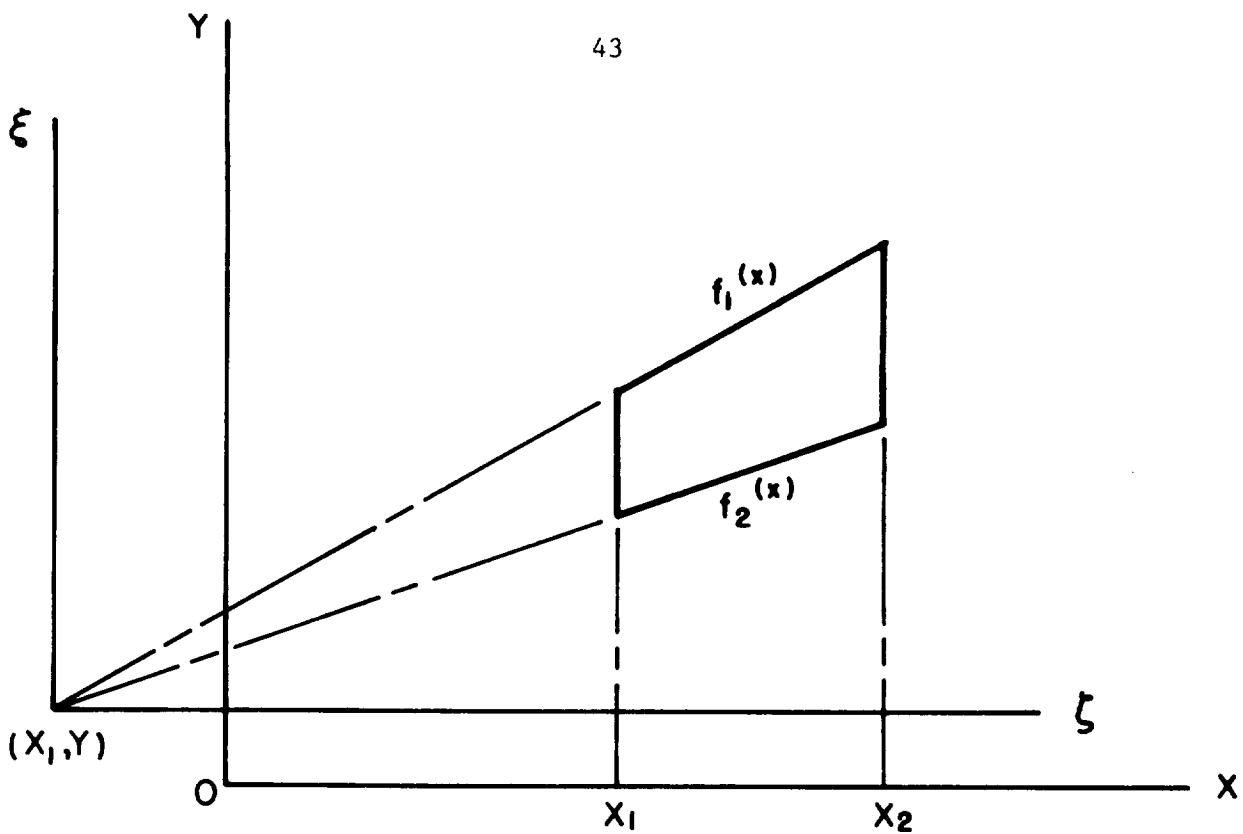
FIGURE 26. CONFIGURATION OF AN ELEMENT IN THE x-y AND x-z PLANES

$$\dot{E}_p = \int_V \bar{\sigma}\, \dot{\bar{\epsilon}}\, dV \quad , \tag{6}$$

where $\bar{\sigma}$ is the flow stress of the deforming material, V is the volume of the element, and $\dot{\bar{\epsilon}}$ is the effective strain rate given by:

$$\dot{\bar{\epsilon}} = \frac{2}{3}\sqrt{(\dot{\epsilon}_x^2 + \dot{\epsilon}_y^2 + \dot{\epsilon}_z^2 + \frac{1}{2}\dot{\gamma}_{xy}^2 + \frac{1}{2}\dot{\gamma}_{xz}^2)} \quad .$$

The energy rates associated with velocity discontinuities are due to shearing along the planes of velocity jumps. Across the transverse sections, velocity discontinuities can occur along the y- and the z- directions. Velocity discontinuities across the longitudinal sections can occur along the longitudinal direction and the z-direction. The energy rate due to velocity discontinuity along a section with area of cross section A is given as:

$$\dot{E}_d = \frac{\bar{\sigma}}{\sqrt{3}} \int_A \left| \Delta V \right| dA \quad , \tag{7}$$

where ΔV is the velocity jump across the area A.

Energy is dissipated in overcoming the friction at the roll-workpiece interface. If ΔU is the velocity differential at the roll-workpiece interface with surface area S, the energy dissipation due to friction, $\dot{E}_f$, is given as below.

$$\dot{E}_f = \frac{m\,\bar{\sigma}}{\sqrt{3}} \int_S \left| \Delta U \right| dS \quad , \tag{8}$$

where m ($0 \leq m \leq 1$) is the friction shear factor at the interface.

The total energy dissipation rate, $\dot{E}$, is the sum of the deformation energy rate, the energy rates due to velocity discontinuities and the friction energy rate. The detailed derivations of each term can be found in Appendix B. $\dot{E}$ is a function of unknown spread profiles w_1 and w_2 (see Figure 25) and the location

of the neutral plane x_n. The unknown coefficients of w_1 and w_2 and x_n are determined by minimizing the total energy rate. The minimization of $\dot{E}$ with respect to unknown parameters is done by numerical techniques. In order to keep the number of unknown variables to a niminum, the curves $y = w_1(x)$ and $y = w_2(x)$ are considered as a third order polynomials, each with two unknowns. The location of the neutral plane, $x = x_n$, is an additional unknown. Thus, a total of five independent variables, which are determined by minimization of the total energy rate, are sufficient for the formulation of the problem.

Computer Program. Based on the above modular upper-bound analysis, a system of computer programs, named SHPROL, was developed to predict metal flow in rolling of airfoil shapes. SHPROL is coded in FORTRAN IV and requires approximately 60,000 octal words of memory space in a CDC Cyber 70 computer. The properties of the material being deformed are provided through a subroutine named MATERL. A detailed description of SHPROL is given in Appendix C.

All the input data to the computer programs SHPROL are transferred through READ statements. This includes variables defining the number of elements in the deformation zone, shape and location of the preform section, shape and location of the upper and lower roll profiles, angular velocities of rolls, friction factor at the roll-workpiece interface, temperature of workpiece, and some controlling variables for selecting proper options. A detailed description of these variables will be given in the input preparation. The flow stress of the deforming material, as a function of strain, strain rate and temperature, is furnished through a subroutine named MATERL, and it needs to be inserted in the program deck for the material under consideration.

The output from the program prints coordinates of the grid points, spread profiles as functions of axial distance (in rolling direction) from roll entry, the total energy dissipation rate and its various components, the location of the neutral plane, the extension rate as a function of axial distance, and the strain, strain rate and flow stress distribution in the deforming material. The output corresponds to a minimum total energy rate, which is minimized by a simplex method with respect to various unknown parameters. At the end of the execution, the output from the minimization routine is written on TAPE7. If further calculations are required, for example, to reduce the error of minimization, the contents of TAPE7 are read into TAPE8 and calculations are restarted from the point where they were left rather than from the beginning.

The computer program SHPROL was used to study the metal flow in finish rolling of GE's H-369 airfoil shape, which is used for stationary vanes in Stage 4 of the F-101 engine. The inlet strip shape was taken as the actual vane shape, except that its thickness was approximately 15 percent larger than the desired vane thickness. The rolling simulation was carried out using flow properties of mild steel, which was selected as a model material in the present investigation. Figure 27 schematically shows the results predicted by SHPROL.
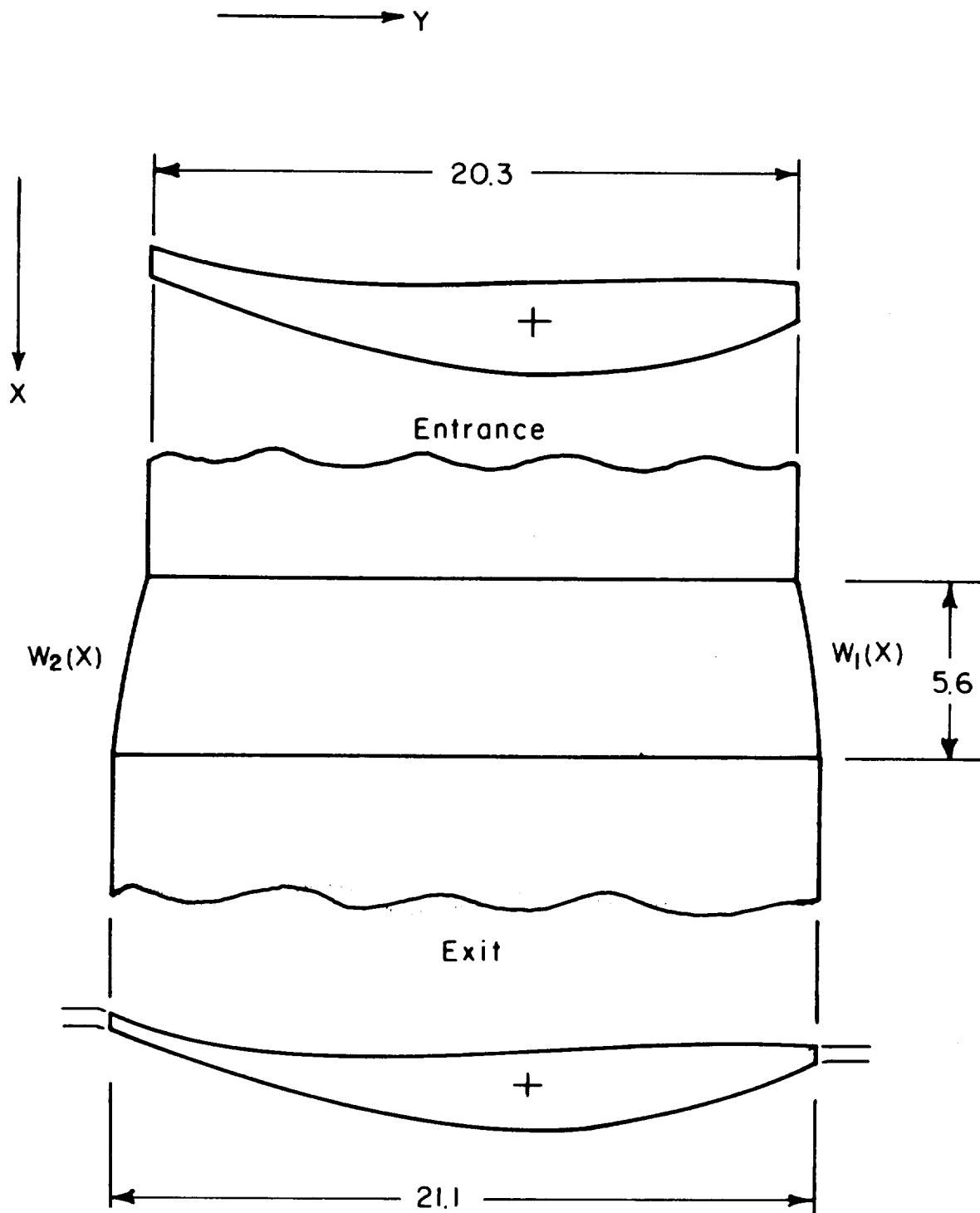
FIGURE 27. ROLLING OF GE'S H-369 AIRFOIL FROM MILD STEEL USING 203.2 mm ROLLS (AVG REDUCTION = 15.75 PERCENT, TORQUE = 1053 JOULES $w_1(x) = 0.4 + 0.027 \ x - 0.061 \ x^2$; $w_2(x) = -0.4 - 0.082 \ x + 0.184 \ x^2$)

MODELING FOR LOAD AND STRESS ANALYSIS

The mathematical modeling of the shape rolling process for airfoil like geometries was implemented as a simulation. The deformation zone is divided into N_y sections in the direction of rolling. The preform is input to the first section, the output of which is input to section two, etc. Thus a step by step simulation is performed to obtain the stress distribution on the zone of deformation. The deformation zone geometry, percent elongation and reduction and other pertinent process parameters are calculated. This simulation has been implemented in computer program ROLPAS; which, is described in detail in Appendix D.

The simulation technique uses "Slab Method" for stress analysis, which is described later in this section. The pattern recognition and geometry handling that is inherent in a simulation is described in Appendix E. The following steps summarize the simulation technique:

1. The material cross section at J-1'st step is input to the J'th step. The deformation zones are determined.

2. Stress analysis calculates the pressure distribution and determines the neutral surfaces.

3. Cross sectional area is distributed as a function of percent elongation and the position of the neutral surfaces.

4. J is incremented and control returns to step 1, if J is not the exit section.

The computer program, ROLPAS, is capable of calculating the roll-separating forces, stress distribution and roll torque for most airfoil-like shapes. It can process rounds, slabs, diamonds, airfoils, but not T, H, U or other such shapes with a protrusion.

Description of Slab Method. The slab method, sometimes called "elementary theory" in European literature is an approximate method for analyzing plastic deformation problems and was originally applied by Siebel[18] to various forming processes.

When applying the slab method, the following are usually assumed:

(a) The material is isotropic and incompressible.

(b) Elastic deflections are negligible.

(c) Inertial forces are negligible.

(d) Plane surfaces in the material remain plane.

(e) Flow stress $\bar{\sigma}$, is constant in the deformation zone studied.

(f) The shear stress due to friction is expressed as $\tau = f\bar{\sigma}$, where f = friction factor.

(g) Material flows according to von Mises' flow rule, i.e., for plane-strain deformation: $\sigma_z - \sigma_x = -\dfrac{2}{\sqrt{3}}\bar{\sigma}$;

for axisymmetric deformation: $\sigma_z - \sigma_r = -\bar{\sigma}$.

The notation is described in Figure 28.

In light of the above assumptions, the equations for plane strain upsetting under inclined platens are derived for a deformation element using elementary stress analysis techniques.

The stress distribution is given by:

$$\sigma_z = \frac{K_2}{K_1} \ln \left(\frac{h_e}{h_b + K_1 x}\right) + \sigma_{ze}$$

where $K_1 = \tan \alpha + \tan \beta$

$$K_2 = \frac{2K_1\bar{\sigma}}{\sqrt{3}} + f\bar{\sigma} \, (2 + \tan^2\alpha + \tan^2\beta)$$

Description of the Computer Program ROLPAS. The ROLPAS system was developed on a PDP-11/40 minicomputer using RT-11 operating system. In order to run ROLPAS with no (or minor) modifications, the following hardware and software components are required:
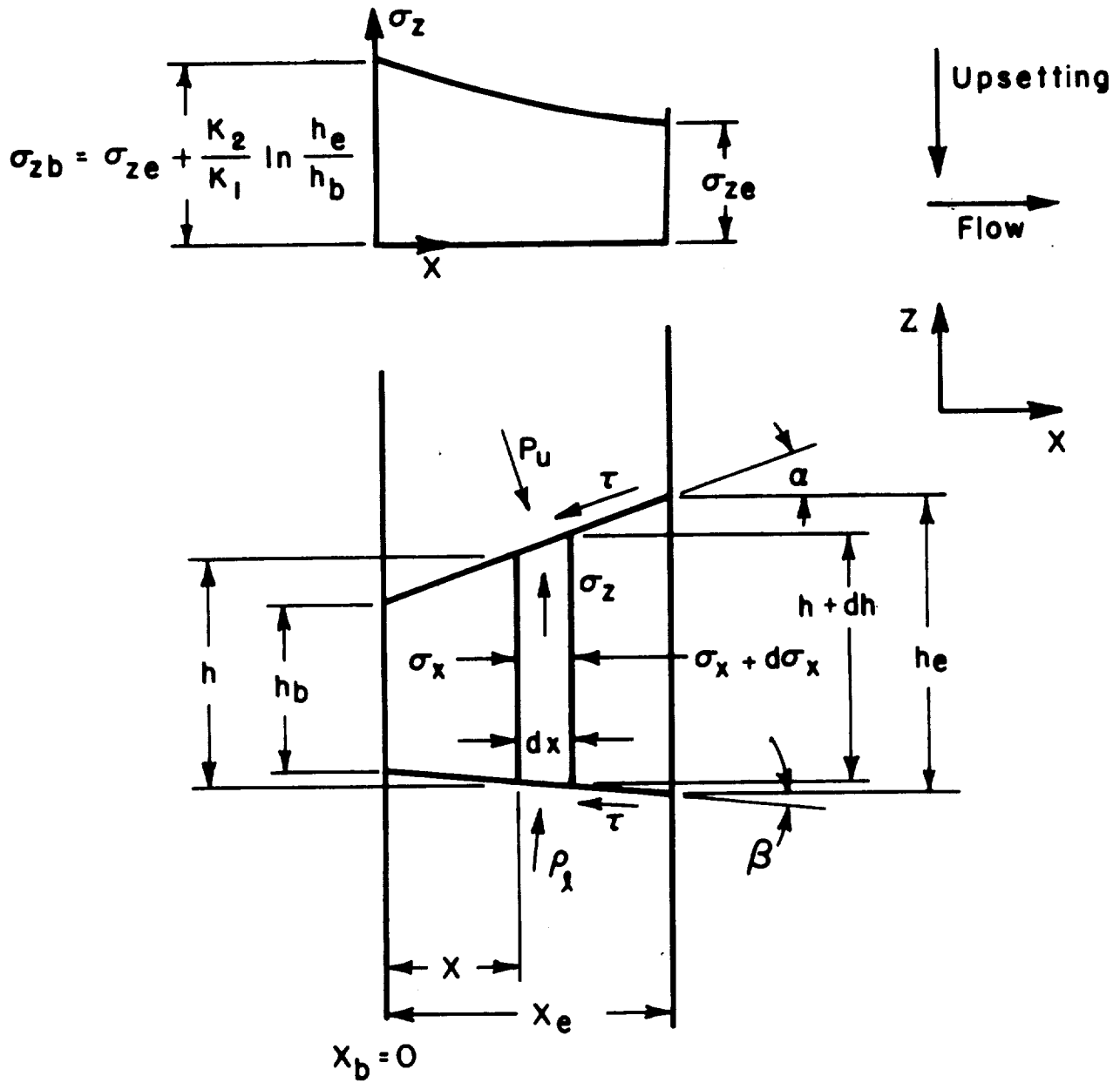
FIGURE 28. STRESSES IN PLANE-STRAIN UPSETTING BETWEEN INCLINED PLATES AND WITH UNIT DEPTHS (Divergent outward flow)

(1) A PDP-11 series computer (except LSI-11) with a minimum of 28K words of memory operating under RT-11.

(2) A random access external storage device such as a disk cartridge drive or a dual floppy disk drive.

(3) A computer terminal (keyboard/printer) such as a teletype or DEC writer.

(4) VT-11 display processor with a graphics CRT and light pen.

(5) An x-y plotter interfaced to the PDP-11. Needed only if hard copies of the CRT graphics is desired.

ROLPAS was coded as an highly interactive program. Most man-machine interaction is achieved by use of the light pen and the extensive interactive capabilities of the display processor. When running ROLPAS, a menu of "operations" are displayed on the left side of the screen. Since ROLPAS is coded as a series of mathematical operations on the data base, this mode of interaction is a natural. At present, the following operations are defined:

- Data Input: Read part geometry from data file.
- Check Input: Display the input geometry for visual checkout.
- Add Flash: Add flash to one or both sides of the input shape.
- Position Preform: Change the position of the preform with respect to the rolls. The user is allowed to move the preform anywhere on the screen with the light pen with respect to the rolls.
- Check Roll-Bite: Checks for roll-bite condition.
- Move the Rolls: Move the rolls up or down, thus opening or closing the exit cross section. Used for simulating different passes with the same rolls.
- Change Parameters: Can be called any time to change system parameters.

- Simulate Rolling: Simulates the rolling process, displaying
  each step as it steps from input to exit. The first step
  of the simulation of rolling an arbitrary preform through
  airfoil rolls is shown in Figure 29. Note that the input
  shape is preserved where it is not deforming. Figure 30
  shows the last step of the simulation as the product exits
  from the rolls.

- Display Stress: Displays the stress distribution calculated
  during simulation. The display is a three-dimensional
  representation. Figure 31 shows the stress distribution
  obtained while rolling the preform of Figure 29. The shape
  of the contact zone and the spread pattern can also be
  ascertained from this display.

- Display Percent Elongation: Displays the distribution of
  elongation from entrance to exit along the exit cross
  section.

- Summarize Results: Provide an up-to-date summary of the
  results.

At all times, only those operations that are logically allowable are
displayed on the menu. This prevents execution of illogical sequences of
operations by the user.

During simulation of rolling a shape, ROLPAS determines the geometry
of the actual contact zone, a plan view of which is shown in Figure 32.
Simulation starts at the entrance to the rolls and proceeds to the exit. At
each step, one cross section parallel to the zx plane is processed. The geometry
of the material at j-1'st section is input to the j'th roll section. Stress
distribution is calculated and the material is deformed according to the stresses
and the elongation criteria. At the completion of simulation from entrance to
exit, a stress analysis is performed along the streamlines of Figure 32. At
each mode of the mesh, the lower of the two σ_z values is accepted as the actual
stress. The stress surface is integrated to obtain the roll-separating force
and the roll torque.

UPPER ROLL

PREFORM

LOWER ROLL
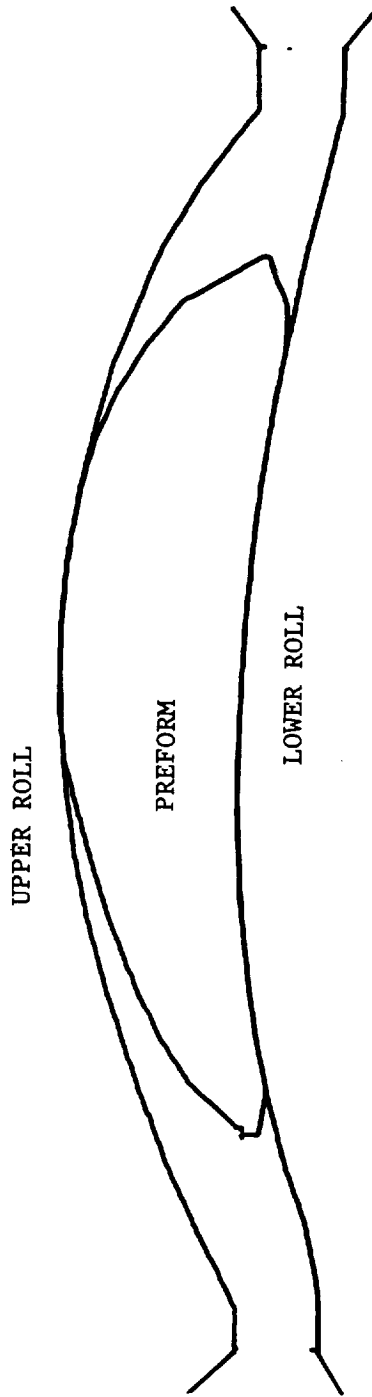
FIGURE 29. DEFORMATION OF A PREFORM AS IT ENTERS AIRFOIL SHAPED ROLLS. THE STRESS OUTLINE IS LABELED AS STEP 1 IN FIGURE 31.

FLASH

FLASH

UPPER ROLL

MATERIAL

LOWER ROLL
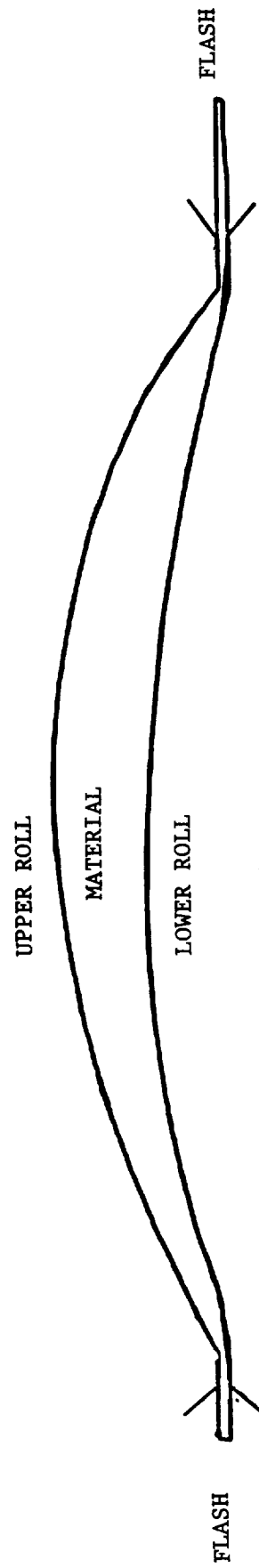
FIGURE 30. ROLLED AIRFOIL AS IT EXITS THE ROLLS. THE CALCULATED STRESS DISTRIBUTION IS DISPLAYED AT STEP 15 OF FIGURE 31.
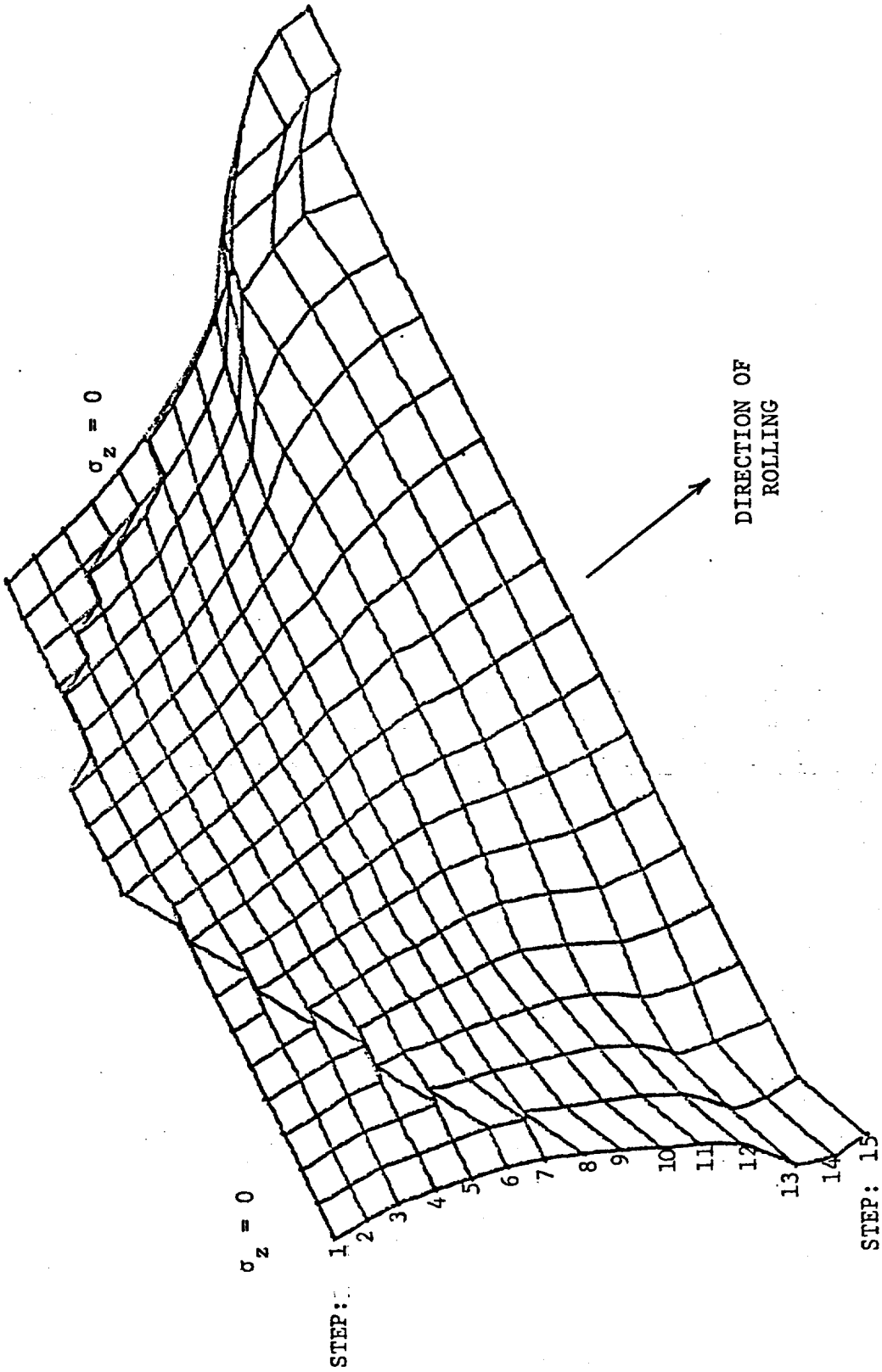
FIGURE 31. THREE DIMENSIONAL REPRESENTATION OF THE CALCULATED STRESS (σ_z) SURFACE FOR ROLLING OF THE SHAPE ILLUSTRATED IN FIGURE 32.
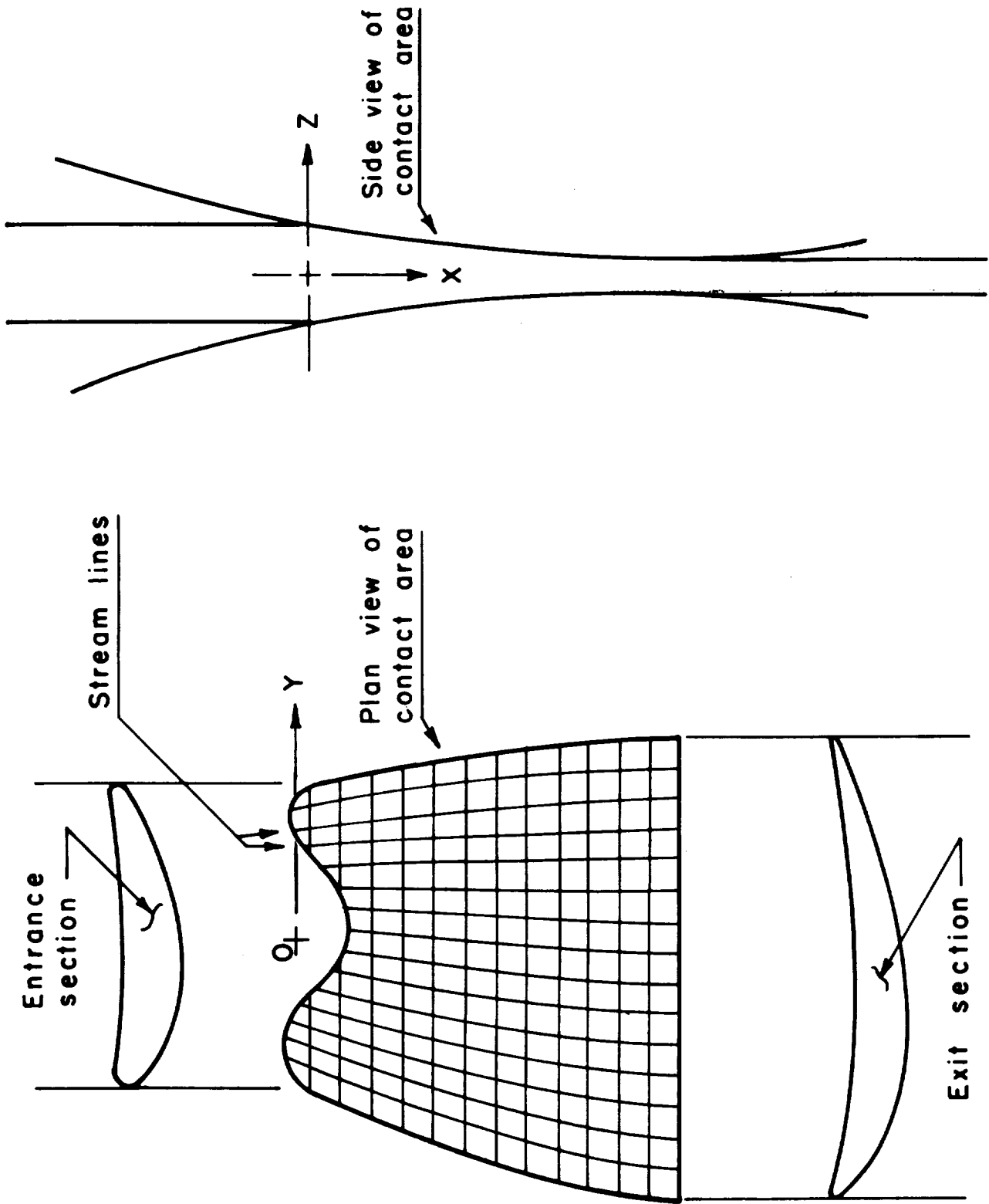
FIGURE 32. PLAN AND SIDE VIEWS OF THEORETICAL CONTACT AREA OF ROLLS AND MATERIAL DURING ROLLING OF AIRFOILS

ROLPAS is intended to be a tool for use in the design of roll passes. To this end, the user, at his option, can simulate various designs and observe the shape produced. He can try different roll separations for the same preform. Using the percent elongation and percent reduction displays, he can make design decisions on how to modify his preform.

As discussed in the following sections, the results from ROLPAS have compared favorably with experimental observations on rolling of slabs.

EXPERIMENTAL EVALUATION OF COMPUTER MODELS

Experimental evaluation of the model for metal flow analysis and the model for load and stress analysis was carried out in two phases. Under the first phase, it was planned to evaluate these models by using the existing experimental data on rolling of plates. However, the available experimental data on plate rolling are not described adequately in the literature, and were found insufficient for a complete evaluation of the models developed under this project. Therefore, a set of plate-rolling trials, both cold and hot, under controlled conditions, were undertaken. Under the second phase, it was planned to experimentally evaluate the validity of the computerized models of shape rolling and roll-pass design by conducting laboratory experiments to roll an airfoil shape at room temperature from mild steel and under hot-isothermal conditions from Ti-6Al-4V alloy. In addition, it was planned to evaluate the computerized models with at least one commercial airfoil (or a similar shape) rolling process that is currently in production.

Plate-Rolling Experiments

One-inch thick mild steel (AISI 1018) steel plates were selected in widths of 1, 2, 3 and 4 inches, in order to have width-to-thickness ratios of 1, 2, 3 and 4, respectively. Nine-inch long rolling specimens were cut from each size, and were annealed, shot blasted and cleaned. Half of each size of specimens were cold rolled and the other half were hot rolled at 1000 C on an instrumented two-high rolling mill with 16-inch diameter x 24-inch long rolls. Specimens for hot rolling were heated in an electric furnace. No

lubricant was used under both cold and hot-rolling conditions. The cold specimens were rolled to a maximum of 25 percent reduction in height, per pass, in increments of 5 percent reduction in height. The hot specimens were rolled to a maximum of 50 percent reduction in height in a single pass, in steps of 10 percent reduction in height. During each rolling trial, the roll-separating force and the roll rpm were recorded on a brush recorder. The current (in ampere) and the voltage (in volt) across the mill motor were also recorded under idle and load conditions on a separate brush recorder. This information, together with roll rpm, was needed to approximately estimate the roll torque. The average height and width of each specimen before and after rolling were recorded.

Predictions of the roll-separating force and roll torque for cold rolling of plates were made by using the computer program ROLPAS. The friction and flow stress data for mild steel were taken from Task I results of this program. Theoretically predicted values of roll-separating force and roll torque, together with the experimental results, are shown in Figures 33 and 34. The agreement between theory and experiment appears to be very good.

Predictions of the lateral spread and roll torque for cold rolling of plates were made by using the computer program SHPROL. Again, the flow st ss and the friction data were taken from Task I results. As seen in Figure , which shows lateral spread in plate rolling against reduction in height for various width/height ratios of the plates, the agreement between theory and experiment is good at small reductions in height. At large reductions in height, the experimentally measured values of lateral spread are always higher than the theoretically predicted values. This is mainly due to the fact that, at large reductions, the rolls did not bite freely into the plates and a certain amount of axial push was required to accomplish the rolling. Figure 36 shows total roll torque against reduction in height for various width to height ratios of the plate. The agreement between the predictions and the measurements is reasonably good, except at large reductions for reasons described above.
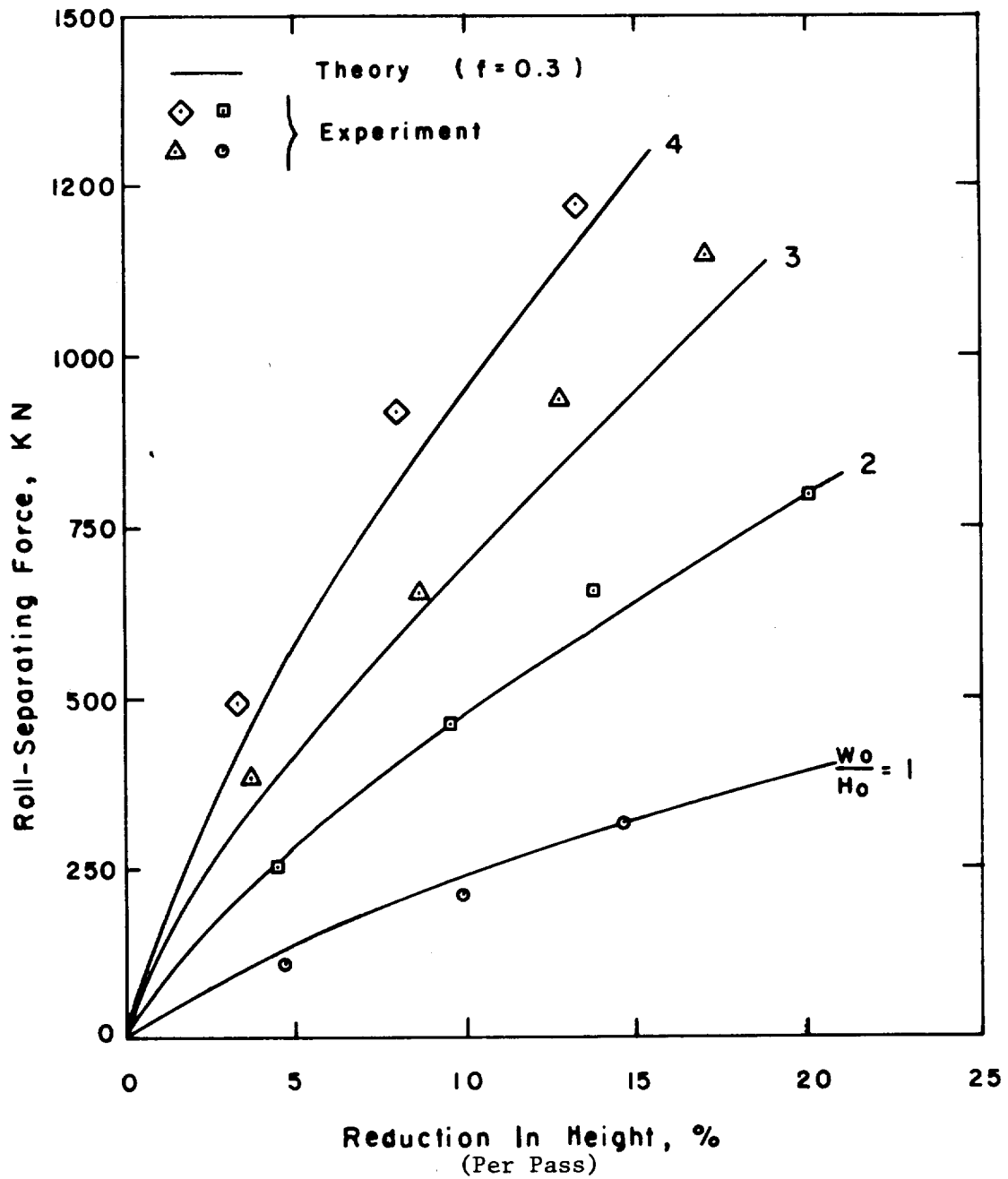
FIGURE 33. THEORETICALLY PREDICTED AND EXPERIMENTALLY MEASURED
ROLL-SEPARATING FORCE FOR ROOM TEMPERATURE ROLLING
OF 1-INCH THICK MILD STEEL PLATES OF VARIOUS ASPECT
RATIOS W_o/H_o (Width/Thickness)
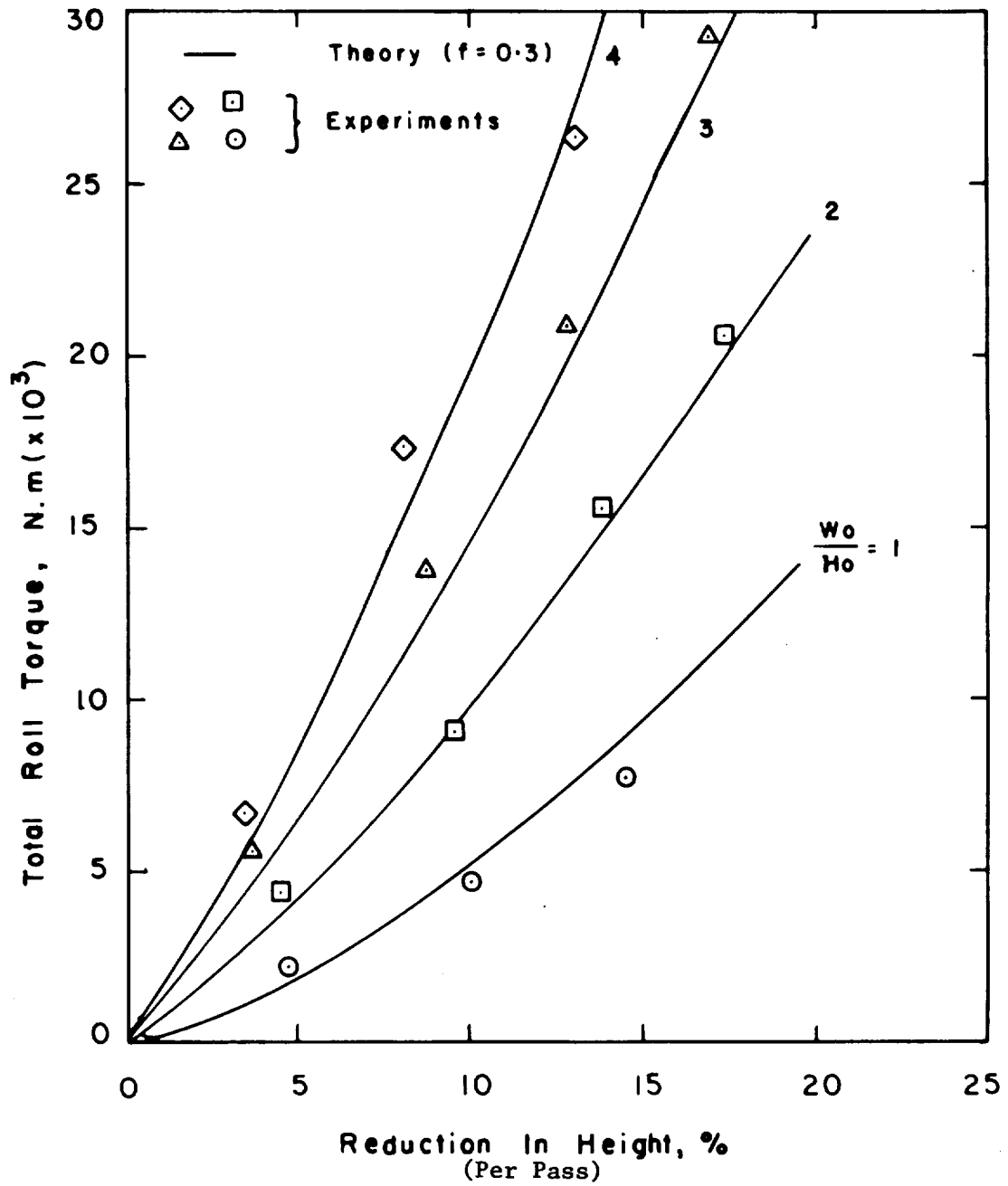
FIGURE 34. THEORETICALLY PREDICTED AND EXPERIMENTALLY MEASURED
ROLL TORQUE FOR ROOM TEMPERATURE ROLLING OF 1-INCH
THICK MILD STEEL PLATES FOR VARIOUS WIDTH TO
THICKNESS RATIOS (W_o/H_o)

FIGURE 35. THEORETICALLY PREDICTED AND EXPERIMENTALLY MEASURED
LATERAL SPREAD IN COLD ROLLING OF MILD STEEL PLATES
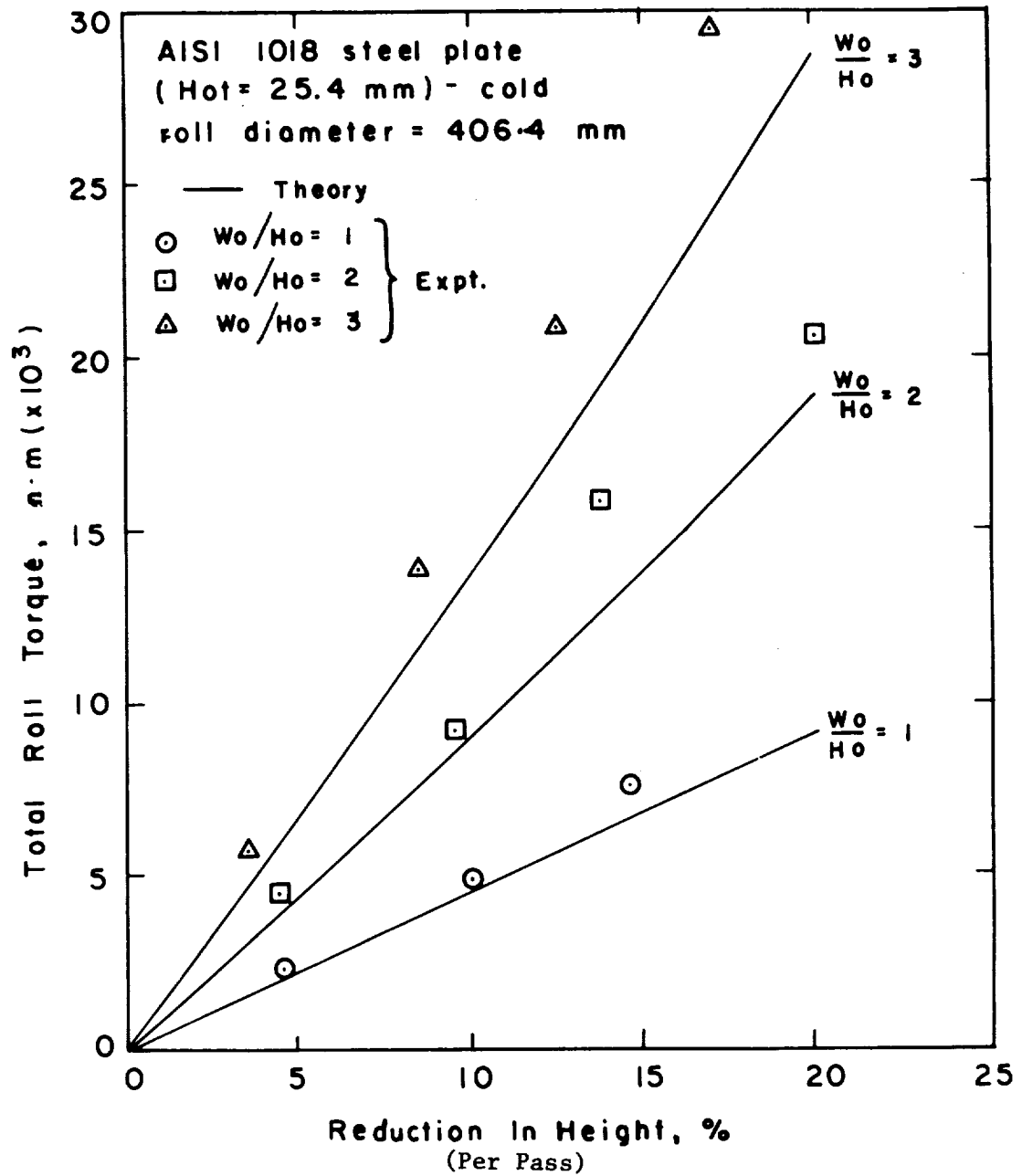
FIGURE 36. THEORETICALLY PREDICTED AND EXPERIMENTALLY MEASURED ROLL
TORQUE IN COLD ROLLING OF MILD STEEL PLATES

A similar evaluation of the computer programs SHPROL and ROLPAS was conducted under hot rolling conditions. The flow stress versus strain relationship for mild steel (AISI 1018) and the friction factor m under hot rolling conditions were determined by conducting ring compression tests. The friction factor, m, was estimated to be approximately 0.75 and the flow stress versus strain at 1000 C is given in Figure 37.

Theoretically predicted values of the roll-separating force, made by using the computer program ROLPAS, are given in Figure 38, together with the experimental results. The agreement between the predictions and the measured values is very good for all three aspect ratios (Wo/Ho) of the initial plate specimens.

Predictions of the lateral spread and the torque were made using the computer program SHPROL. In Figure 39, lateral spread is plotted against reduction in height for various initial width to initial height ratios. The predictions are in reasonable agreement at low values of reduction in height (below 15 percent). At large reductions in height, the measured values of spread is much higher than the predicted values. This can be attributed to mainly the axial push required to make the rolls bite into the incoming plate. Higher values of friction under actual rolling conditions, as compared to the conditions in the ring test, may also be responsible for this discrepancy. In any case, these large reductions in height are less significant under actual production situations, where reductions in height of 10-20 percent per pass are commonly used. Figure 40 shows the theoretically predicted and experimentally measured roll torques for hot rolling of mild steel plates for various width to height ratios. As in the case of roll-separating force, the experimental results are in excellent agreement with predictions. Thus, it is believed that the models are sufficiently accurate for all practical purposes.
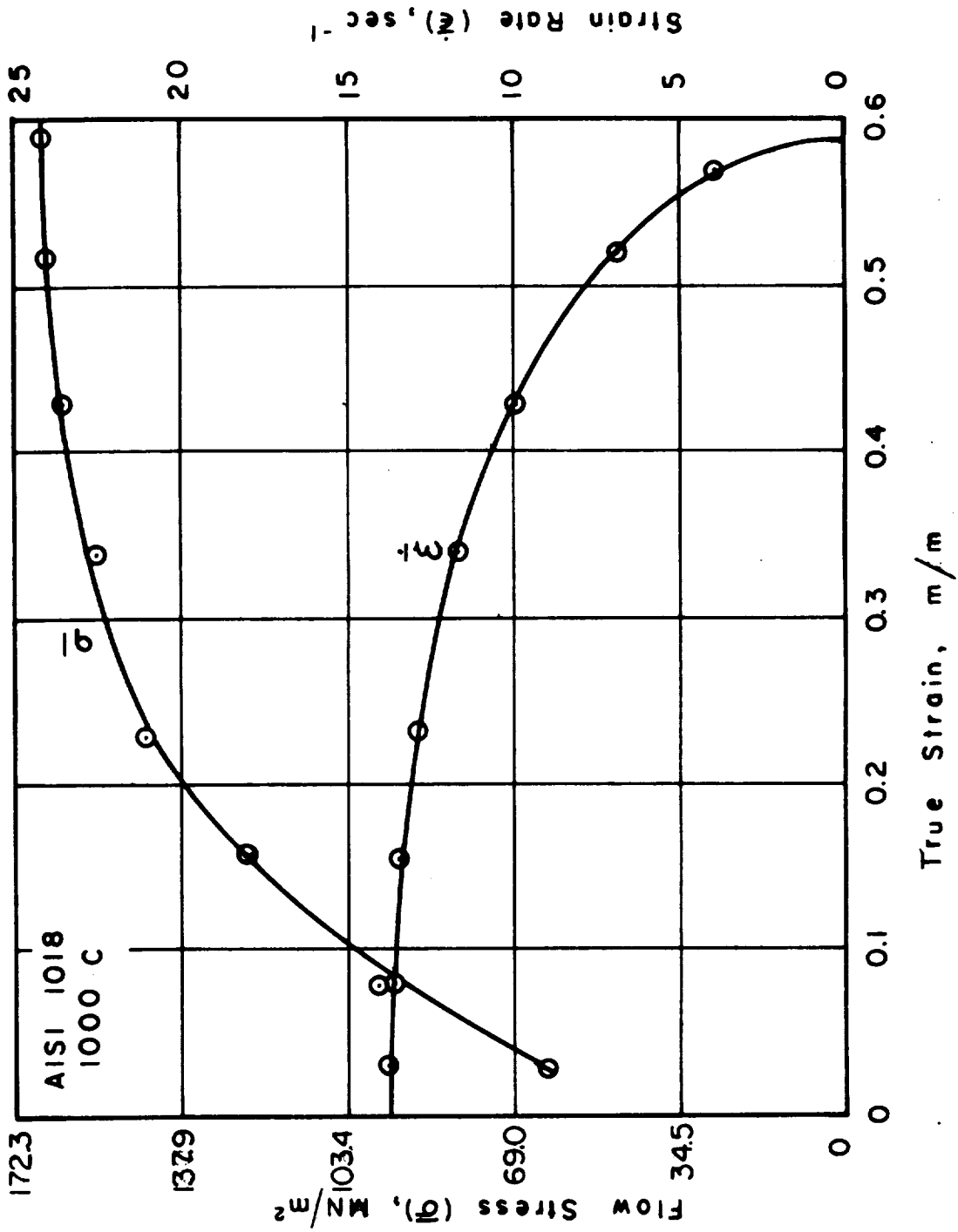
FIGURE 37. FLOW STRESS AND STRAIN RATE VERSUS STRAIN FOR AISI 1018 STEEL AT 1000 C
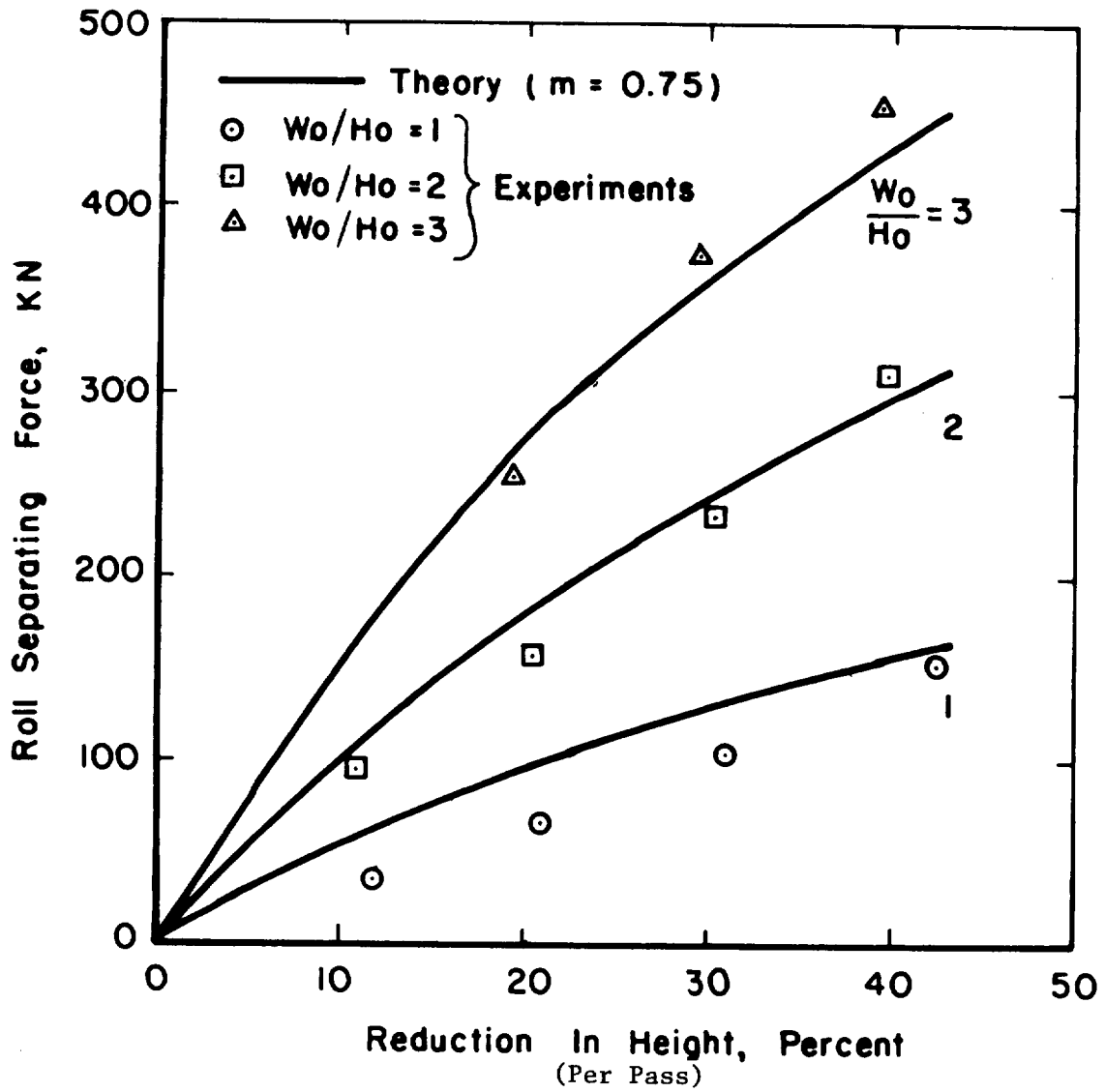
FIGURE 38. THEORETICALLY PREDICTED AND EXPERIMENTALLY MEASURED
ROLL SEPARATING FORCE IN HOT ROLLING OF MILD STEEL
PLATES OF VARIOUS ASPECT RATIOS Wo/Ho (Width/Thickness)
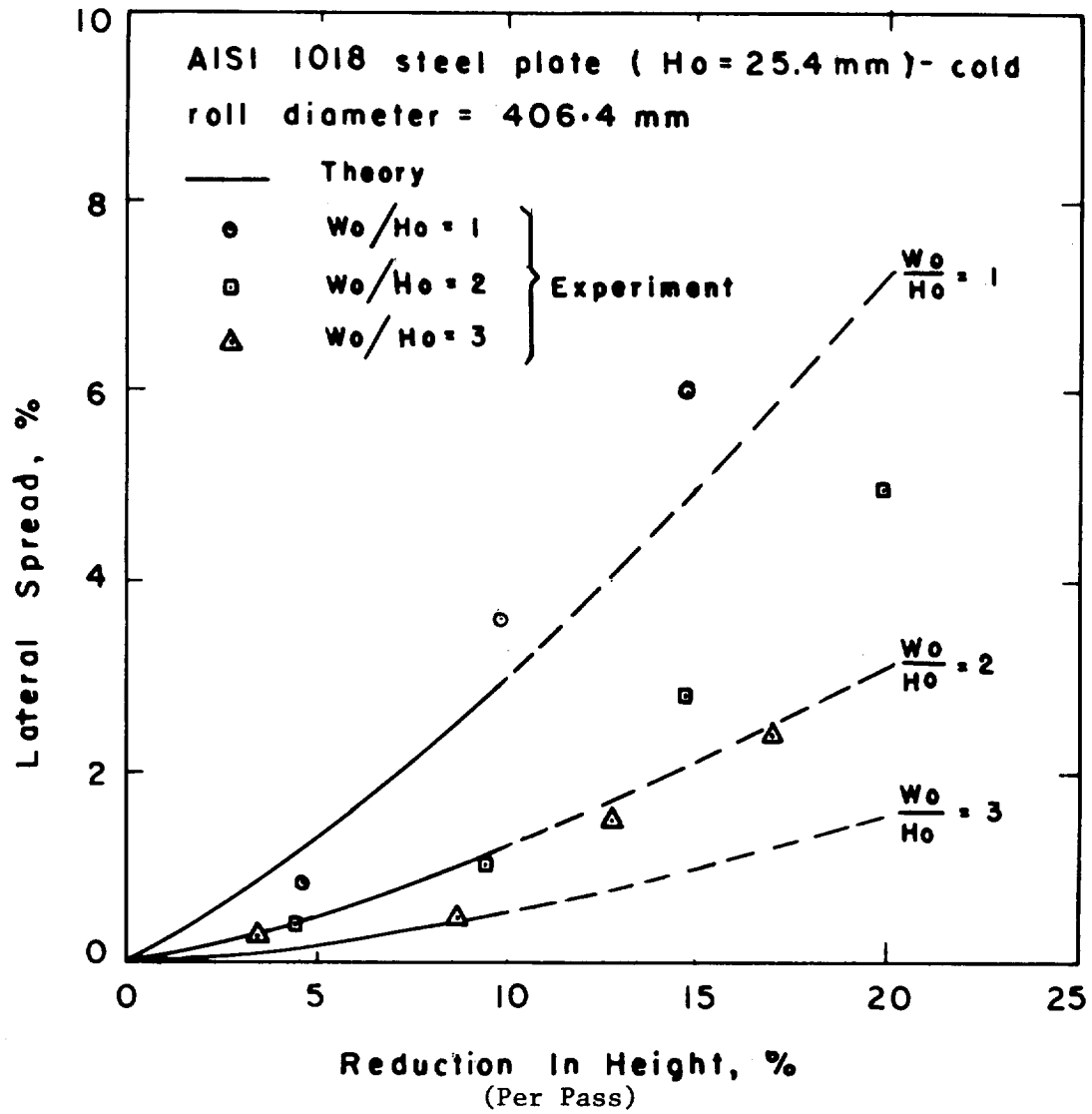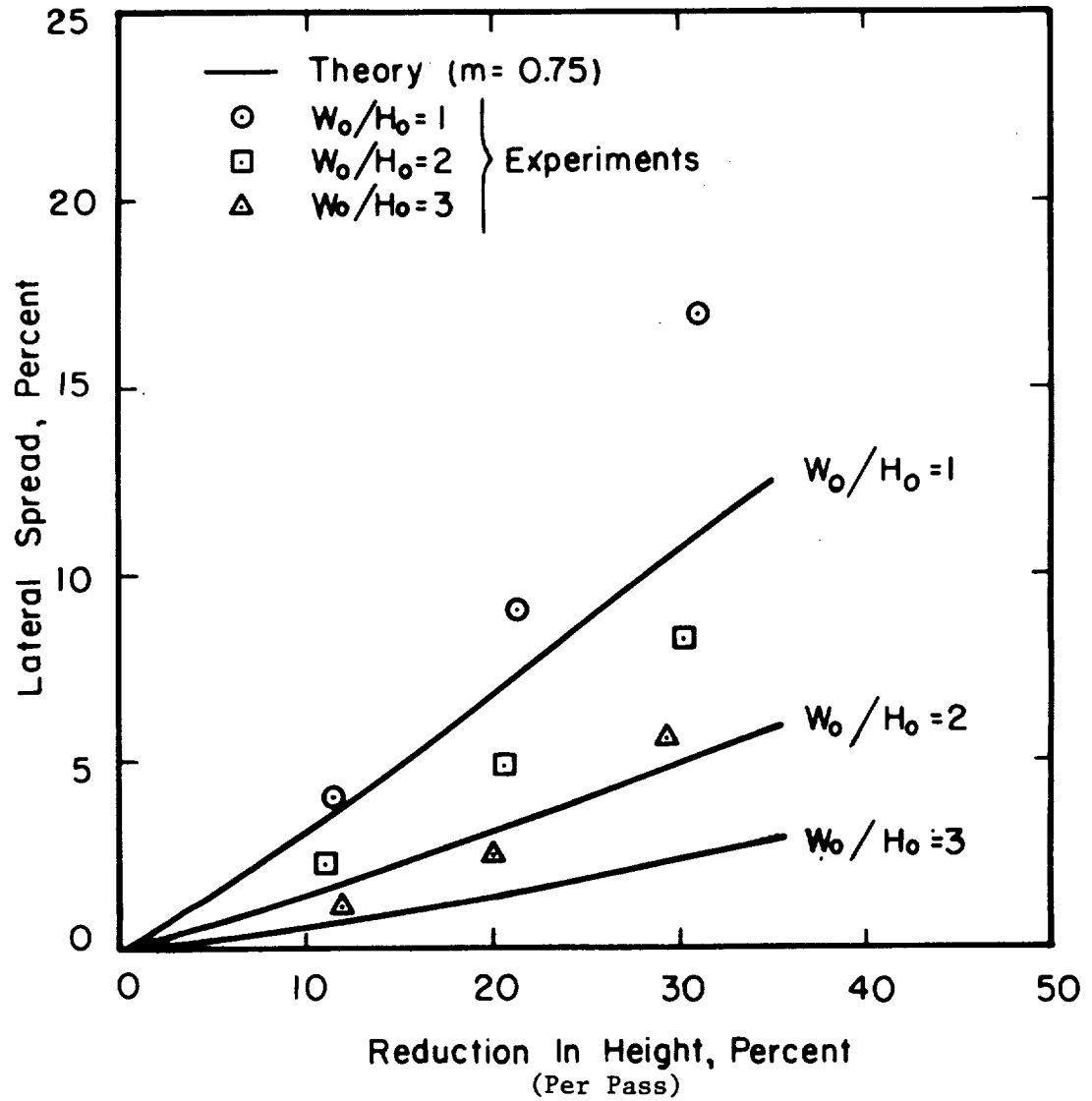
FIGURE 39. THEORETICALLY PREDICTED AND EXPERIMENTALLY MEASURED LATERAL
SPREAD IN HOT ROLLING OF MILD STEEL PLATES OF VARIOUS
ASPECT RATIOS W_o/H_o (Width/Thickness)
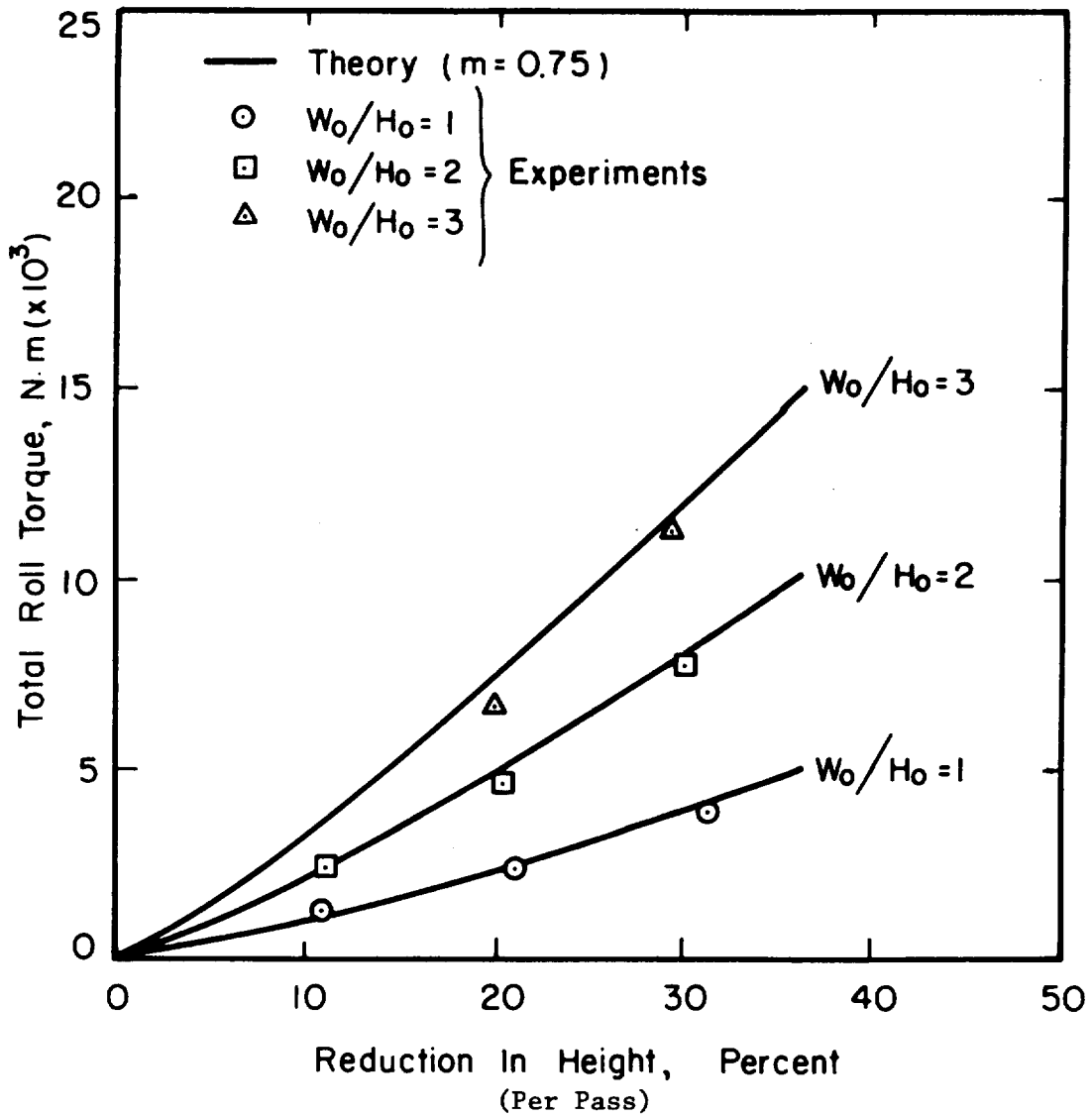
FIGURE 40. THEORETICALLY PREDICTED AND EXPERIMENTALLY MEASURED ROLL
TORQUE IN HOT ROLLING OF MILD STEEL PLATES OF VARIOUS
ASPECT RATIOS W_o/H_o (Width/Thickness)

Shape Rolling Experiments

In order to evaluate the computerized models of shape rolling and roll-pass design, laboratory experiments for rolling an airfoil shape were conducted. For this purpose, a turbine engine vane (General Electric, Evandale, vane for Stator, State 4, Drawing No. 9064M84), as shown in Figure 41, was selected for both cold and hot rolling. At room temperature, this shape was rolled from mild steel, (AISI 1018), which was selected as a model material, strips of rectangular cross section. At hot working temperature, this shape was rolled from rectangular strips of Ti-6Al-4V alloy under near-isothermal conditions.

Equipment and Tooling

The laboratory experiments were conducted on Battelle's two-high rolling mill with 0.203 m (8-inch) diameter x 0.305 m (12 inch) wide rolls, as shown in Figure 42. The mill drive is through a 37.3 kW (50 hp), 230 V, dc variable speed motor, and the roll surface speed can be varied from 0.33 to 1.02 m/sec (65 to 200 fpm). The gap between the rolls can be adjusted with hand operated screws. The mill is equipped with two load cells to measure the roll-separating force on each side of the mill. The load cells are jacketed with copper tubing through which water can be circulated to avoid any variations in the load cell temperature. The load cells were calibrated and hooked to a two-channel continuous-chart pen recorded to record the load on each side of the mill. The mill rpm can be measured easily with the aid of a stop watch.

The roll construction is of composite nature to provide both cold and hot-isothermal rolling, as shown in Figure 43. The rolls consist of tool steel (H13) arbors A, sleeves B with airfoil shape, spacer sleeves C, and a pair of lock nuts D. The tool steel arbors were gun drilled to let water flow through in order to cool the journals and the interior of the rolls during hot-isothermal rolling and were machined to fit the mill drive and the sleeves and lock nut. They were then heat treated to R_c 50-52, and ground finished on the mating surfaces.
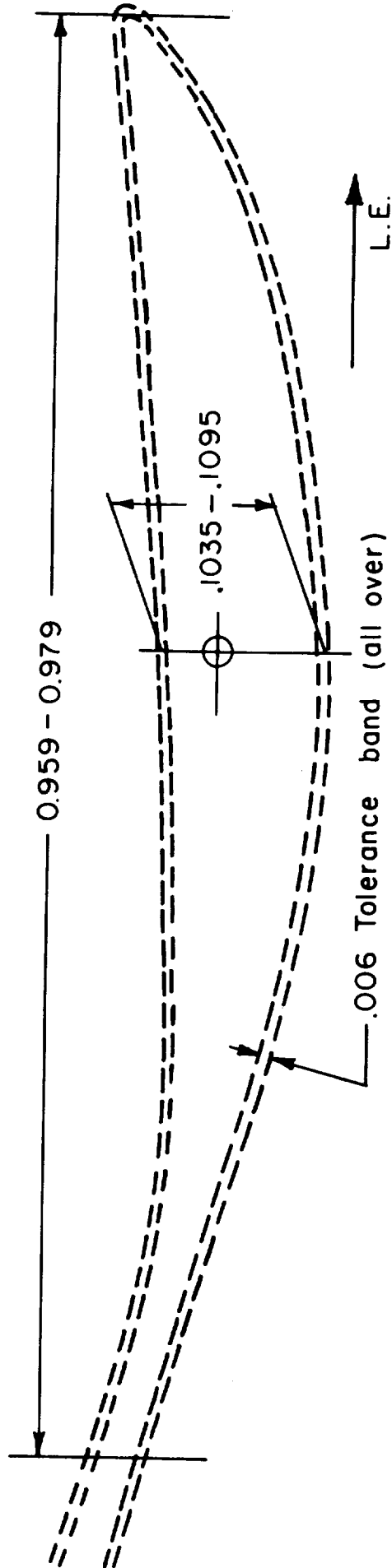
FIGURE 41. THE ENLARGED SKETCH OF THE GE VANE SHAPE, WHICH IS BEING COMMERCIALLY ROLLED FROM INCO 718 BY GE-LYNN (This figure has been reduced down from the original 20X mylar drawing supplied by GE)
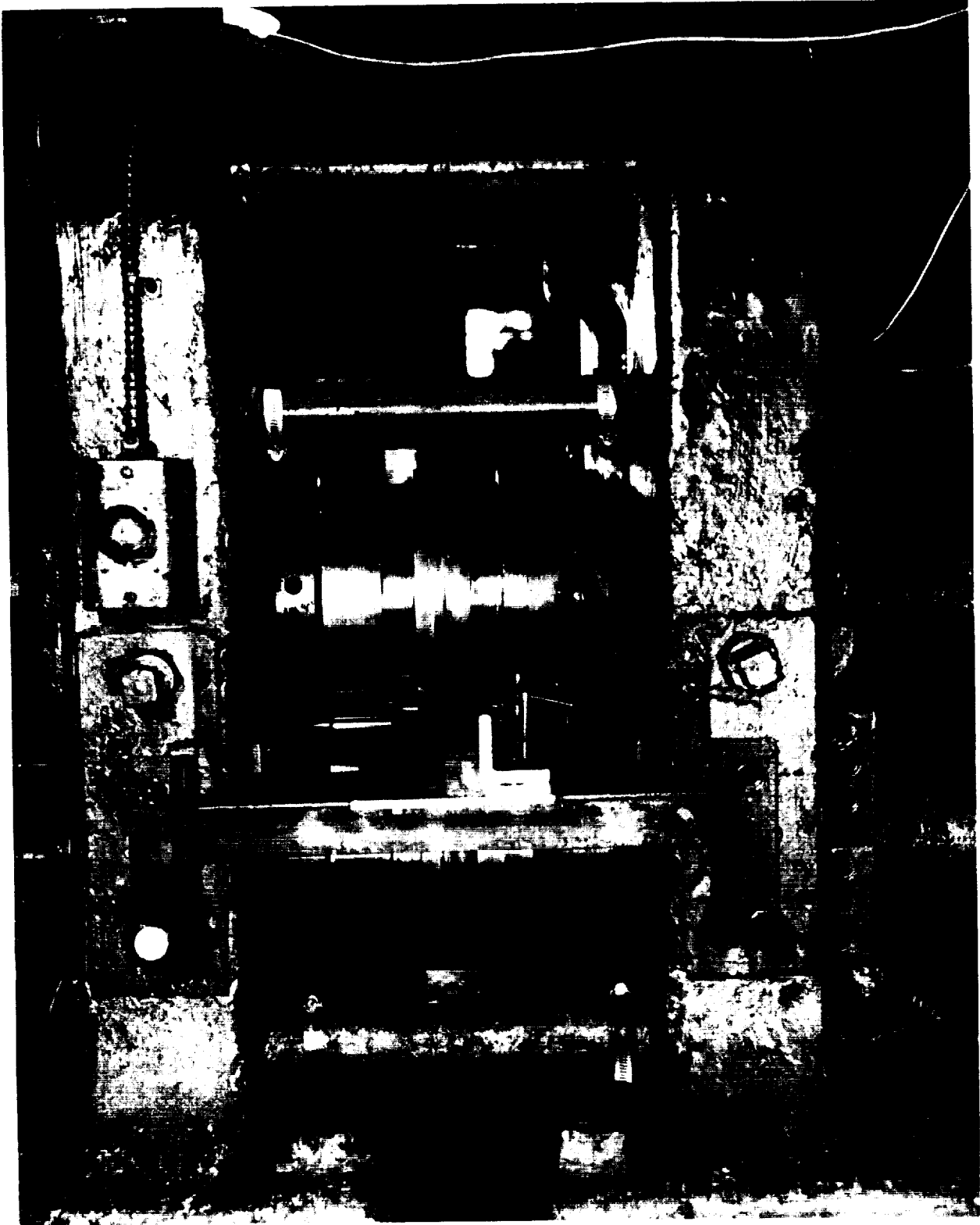
FIGURE 42.   EXIT END OF 2-Hi ROLLING MILL FOR SHAPE-ROLLING TRIALS
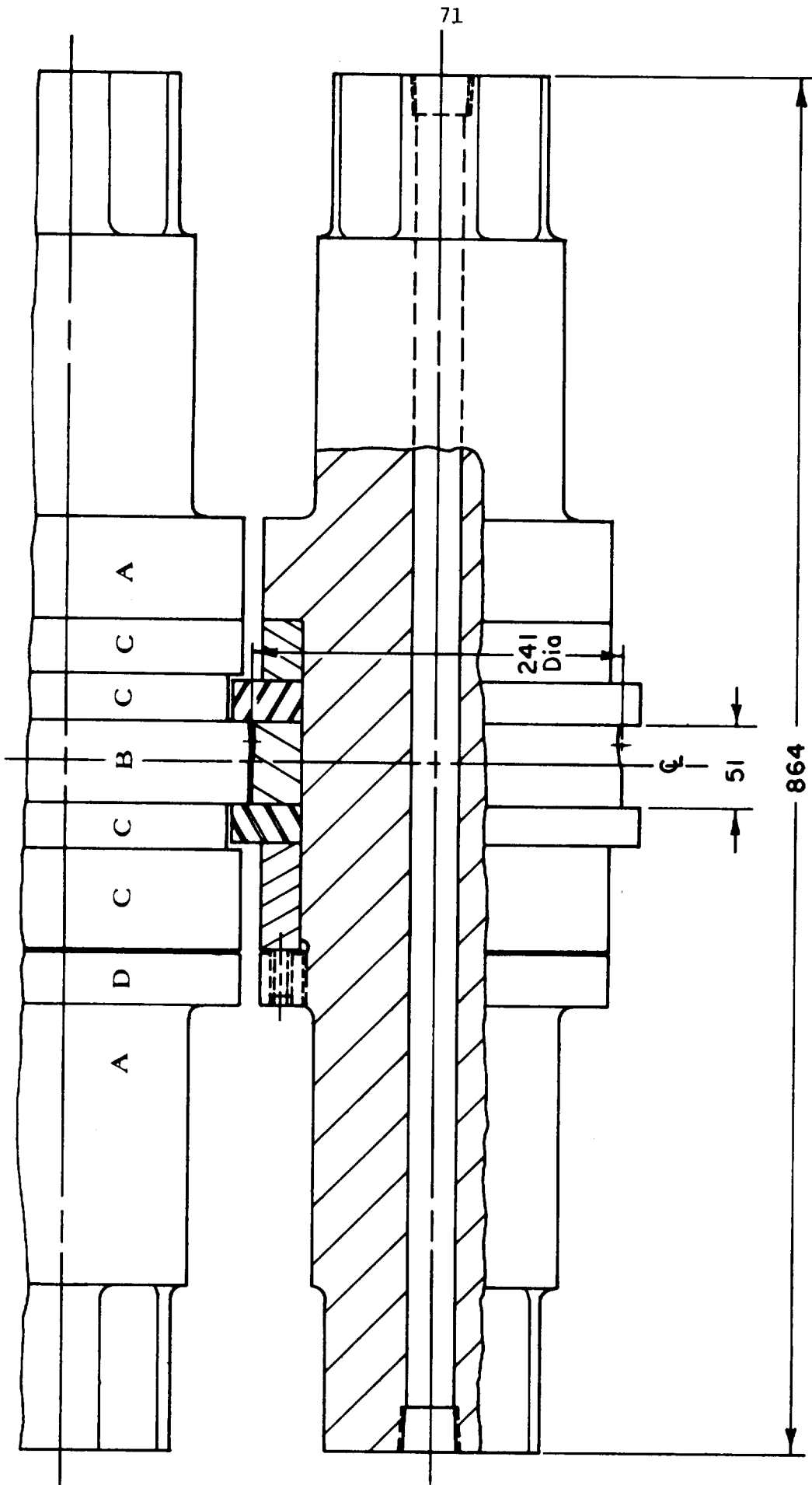
FIGURE 43. ROLL ASSEMBLY FOR ROLLING OF AIRFOIL SHAPES

The pair of sleeves B with the airfoil shape for cold rolling of mild steel shape and the lock nuts D were made from hardened tool steel (R_c 42-44). The sleeves B for hot-isothermal rolling of Ti-6Al-4V alloy shapes were machined from IN 100 cast tubing. All the spacer rings C were machined from Waspaloy. Thus, only the sleeves with the airfoil shape were changed for various shapes for cold (H-13) and hot-isothermal (IN 100) rolling trials. All the sleeves and spacers were ground finished and were fixed on the arbors by three equally-spaced round keys. A single right-angle adjustable guide was made for the entrance side. The rolled piece landed on a flat surface on the exit side. For hot-isothermal rolling trials, the mill was equipped with induction coils to heat the sleeves with the air-foil shape, as shown in Figure 44. The power to the induction coil was sup-plied by an Ajax Magnathermic Corporation's Model 23 HT induction machine. This machine is equipped with a motor generator set. The output voltage of the generator can be adjusted between 0 and 800 volts; and the output power can be adjusted between 0-100 KVA. The output frequency of the generator is fixed to 10 khz. With this set up, temperatures up to 871 C (1600 F) were obtained on the sleeves with the airfoil shape. The temperature of the rolls was monitored with infrared radiation pyrometers.

The mill frame deflects elastically during rolling. In order to set the mill gap prior to rolling, it is necessary to know the mill deflection with respect to applied load. Therefore, the deflection versus load charac-teristic of the mill, with the rolls described in this report, was determined by conducting rolling trials with flat strips. For this purpose, the mill was set to a certain gap and mild steel strips of 50.8 mm width and 3.18 mm thickness were rolled, and the roll separating force was recorded. The dif-ference of the set mill gap and the height of the rolled strip gave the mill deflection for the recorded force. The deflection versus load characteristic of this rolling set up is shown in Figure 45.
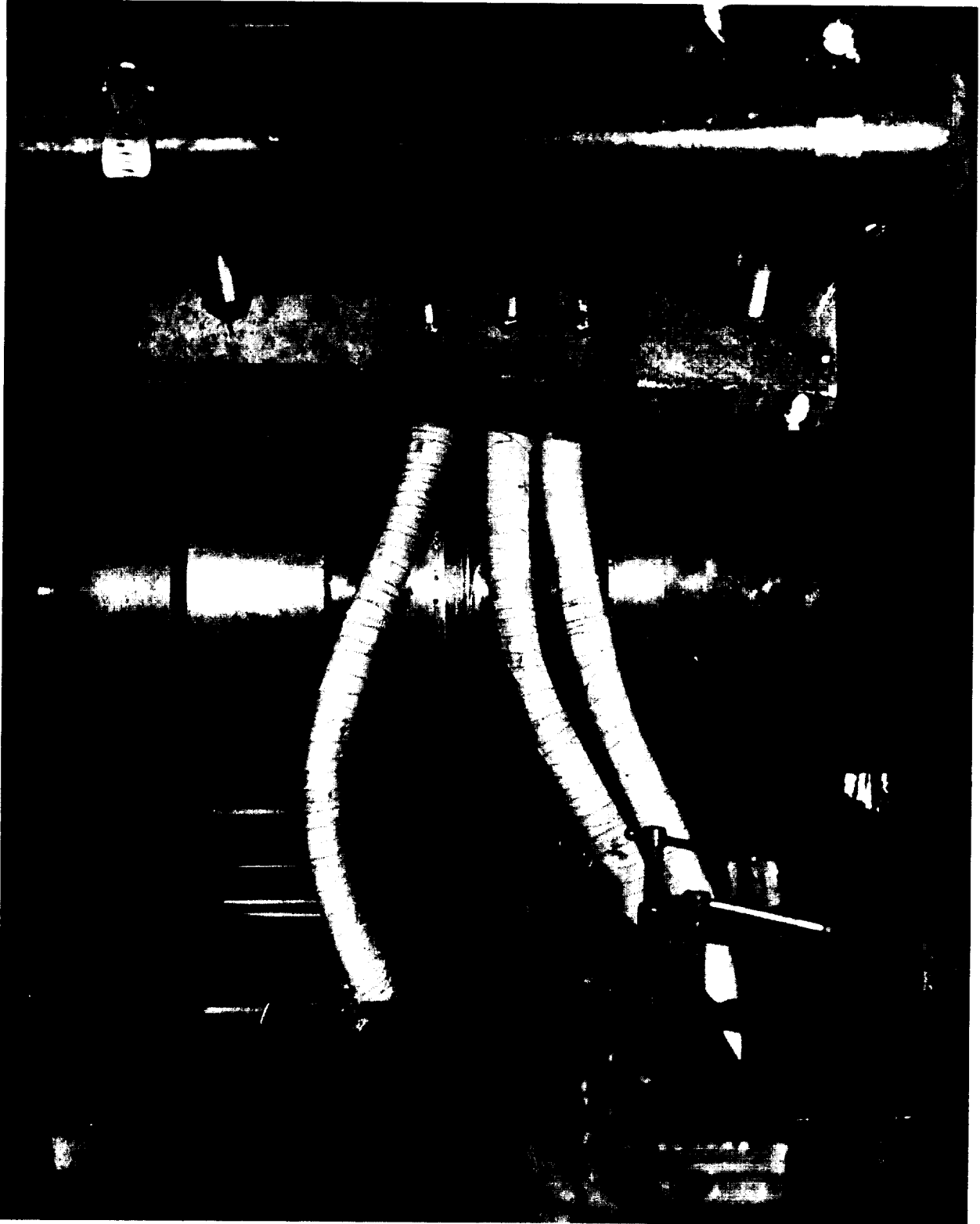
FIGURE 44. INDUCTION COIL FOR HEATING OF IN 100 SLEEVES FOR HOT ISOTHERMAL ROLLING TRIALS
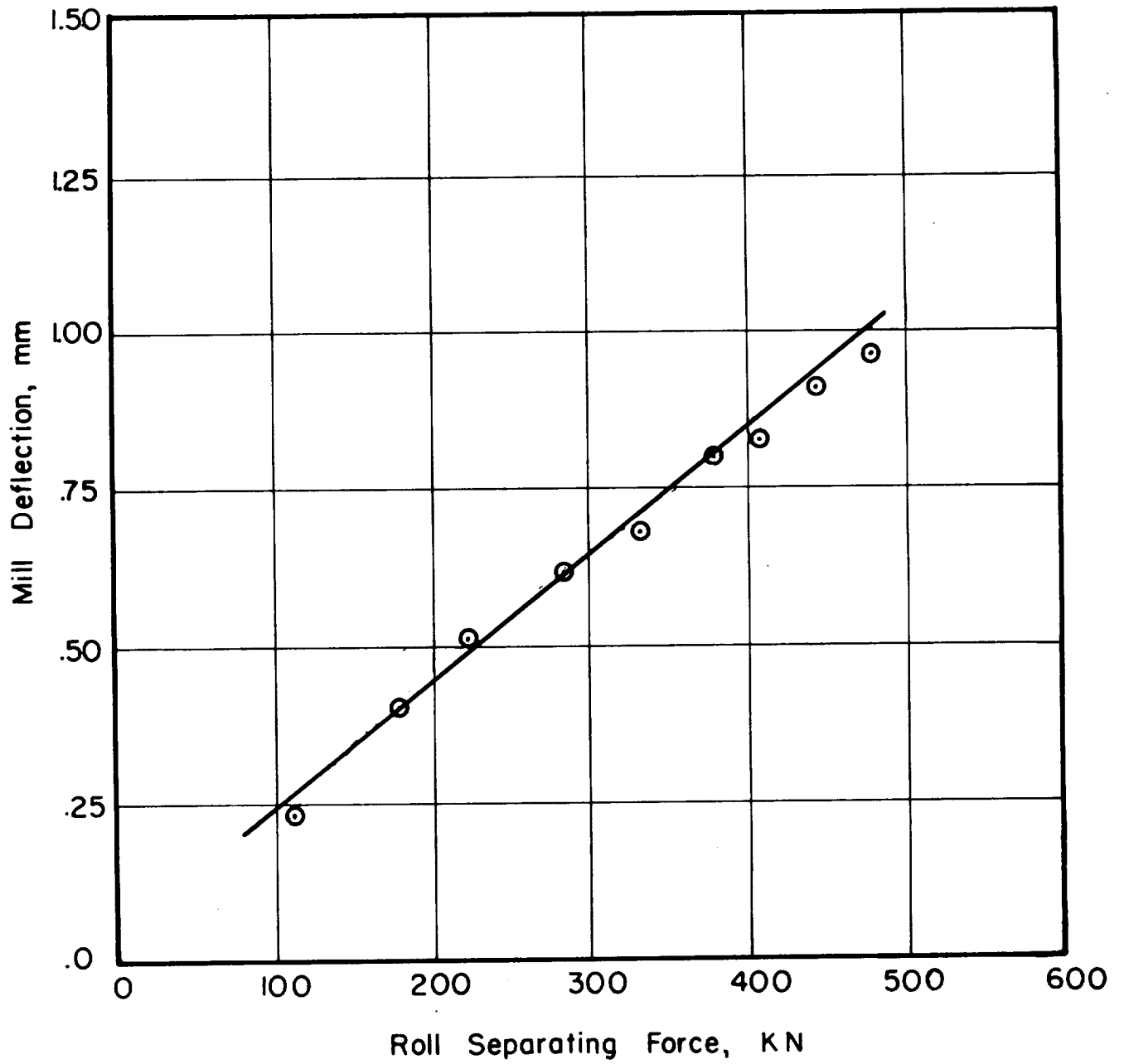
FIGURE 45. DEFLECTION CHARACTERISTICS OF BATTELLE'S 2-HIGH ROLLING MILL WITH
203.2 mm DIAMETER x 304.8 mm WIDE ROLLS

Cold Rolling Experiments

Material: The cold rolling of the airfoil shape shown in Figure 41 was accomplished by using annealed mild steel (AISI 1018) as a model material. Based on preliminary calculations using the computer programs SHPROL and ROLPAS, the initial sheet thickness of 3.18 mm (1/8 in.) was selected. From the as-received (cold-rolled) sheet material, several pieces of 25.4 mm (1.0 in.) width and 305 mm (12.0 in.) length were sheared, keeping the length of the pieces along the rolling direction. These pieces were annealed and the scale was cleaned by shot blasting. The cold rolling specimens were then machined from these pieces to a width of 21.6 mm (0.851 in.) as determined by the computer porgrams SHPROL and ROLPAS.

Tooling: The roll sleeves with airfoil profile were machined from hardened (R_c 42-44) tool steel (H-13). The computer program ROLPAS was used to produce a punched paper tape for the profiles to be machined on the upper and the lower roll sleeves. This tape was then used to machine a pair of templates on Battelle's NC-milling machine. The profiles on the upper and the lower roll sleeves were copy-turned on a lathe using these templates. The rolling surfaces on the sleeves were hand polished by very fine emery cloth. The profile of these roll sleeves was examined by rolling the shape from a soft aluminum strip through the roll assembly in a single pass and comparing the rolled cross section with the desired shape on an optical comparator at 10X magnification.

Initially, the profiles on the roll sleeves were machined on the center of the sleeves, with proper flashing on both the sides. Later, the profiles were machined on one end of the sleeves, thereby eliminating flash on the leading edge of the airfoil section. An additional set of roll sleeves were machined to generate a preform design shown in Figure 46.

Rolling Trials: The specimens rolled through the first set of roll sleeves (centrally-profiled) were numbered beginning with C. Similarly, the specimens rolled through the second (side-profiled) and the third set (preform-profiled) were numbered beginning with S and P, respectively.
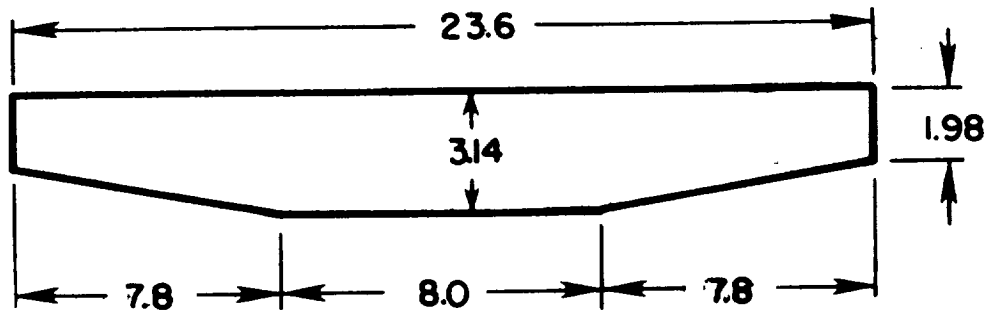
FIGURE 46. PREFORM SHAPE FOR ROLLING OF AIRFOIL SHAPE SHOWN IN FIGURE 41

Based on the computer simulation of the rolling process, it was estimated that the desired shape can be obtained in three passes by closing the roll gap in successive passes. Thus, the various intermediate shapes in this roll-pass schedule are the various cross sections along the rolling direction when the final shape is obtained in a single pass. However, this intermediate cross-section is selected, based on theoretical as well as practical aspects. Hence, apart from theoretically predictable factors such as reduction in area, intermediate anneal, and roll-bite, factors such as straightness, and surface finish of the rolled product are also important. Especially, the straightness of the product in the initial passes is extremely important. It was noticed that if center of the strip is not deformed much in the initial passes, the rolled product remained essentially straight. Therefore, in the initial passes, the maximum height was reduced only slightly and the final shape could still be obtained in a total of three passes.

During cold rolling, the roll speed was kept at approximately 30 rpm. Since the average roll sleeve diameter was approximately 0.241 m (9.5 in.), the roll surface speed was approximately 0.375 m/s. The starting mill gap was set based on required reduction in maximum height and estimated mill deflection for each pass. The workpiece was initially guided through the rolling dies and then it was allowed to feed itself freely. At the end of each pass, the front end of the rolled specimen was cut-off since it was always bent. The small end piece was also used as a record of the intermediate cross section. During each pass, the roll separating force exerted on both the journals was recorded individually on a brush recorder.

Although the rolls, with profiles on the center of the sleeves, produced satisfactory results, as shown in Figure 47, it was found that guiding of the workpiece through the rolls after the first pass was rather difficult. In addition, the control on the flash, especially on the leading edge of the airfoil shape, was not satisfactory. Therefore, the next set of the roll-sleeves, with the profile machined on one end of the sleeves, were used. These rolls produced satisfactory results and much better straightness and uniformity of cross section along the length of the rolled product. It is believed that the absence of flash on the leading edge of the airfoil section facilitated control of straightness and bowing in the lateral plane.

ORIGINAL PAGE IS
OF POOR QUALITY

Pass No.

3rd

2nd

1st
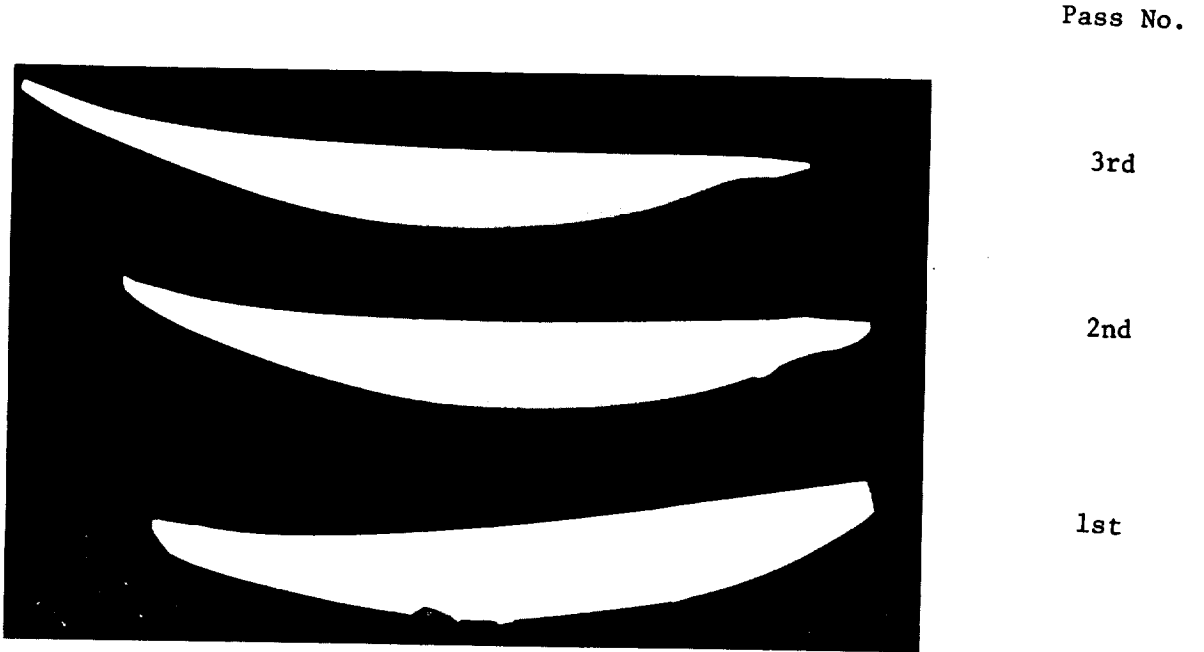
FIGURE 47. CROSS SECTIONS AFTER VARIOUS PASSES THROUGH CENTRALLY-PROFILED ROLL SLEEVES

However, since one end of the roll-die was closed to metal flow, higher rolling loads were seen and four passes were required to achieve the desired shape. Further, the control of the shape at the leading edge was not satisfactory and the leading edge was always thicker than required, as shown in Figure 48. However, since the leading edge is finished by grinding in normal production, this is not a considered a serious drawback.

In order to study the effect of a preform shape other than the shape itself, a preform cross section shown in Figure 46 was rolled using the roll-sleeves designed for this shape. This preform shape was selected based on its simplicity and predictions from the computer program ROLPAS. Since the reduction in the central portion was kept to a minimum, the rolled specimens were extremely straight and uniform along the length. The finished shape could be rolled in two subsequent passes through the side-profiled rolled sleeves. The various cross sections after rolling are shown in Figure 49. It is seen that in this case, better shape control is possible in three passes compared to four pass operation in the previous trials. Thus, preforming has its merits and may be necessary in some cases. Table III summarizes representive results from these cold rolling trials. Some of the cold rolled specimens are shown in Figure 50.

Thin slices (3 mm thick) were cut from the rolled specimens using three types of roll sleeves. The cross sections of these slices were enlarged to 10X magnification on an optical comparator and they were compared with the engineering drawing of the desired airfoil cross section, as shown in Figure 51. The cold rolled cross section with all the three roll-sleeve design produced airfoil shape within the tolerance band, except near the leading edge.

Pass No.

4th

3rd

2nd

1st

FIGURE 48. CROSS SECTIONS AFTER VARIOUS PASSES THROUGH SIDE-PROFILED ROLL SLEEVES

Pass No.

2nd

3rd

1st

FIGURE 49.   CROSS SECTIONS OF THE PREFORM SHAPE AND SUBSEQUENT
PASSES THROUGH SIDE-PROFILED ROLL SLEEVES

TABLE III. REPRESENTATIVE RESULTS FROM COLD ROLLING EXPERIMENTS

Specimen No.	Pass No.	Initial Thickness		Initial Width		Final Max. Thickness		Final Width		Total Load (X 1000)		Lateral Spread Percent
		mm	in.	mm	in.	mm	in.	mm	in.	N	lb.	
C-1	1	3.20	0.126	21.62	0.851	3.124	0.123	24.43	0.962	153.5	34.5	13.0
	2	3.124	0.123	24.43	0.962	3.23	0.127	25.15	0.990	149.0	33.5	3.0
	3	2.972	0.117	25.15	0.990	2.69	0.106	26.36	1.038	180.15	40.5	4.8
C-2	1	3.20	0.126	21.62	0.851	3.175	0.125	24.56	0.967	153.5	34.5	13.6
	2	3.175	0.125	24.56	0.967	2.972	0.117	25.35	0.998	152.13	34.2	3.2
	3	2.972	0.117	25.35	0.998	2.62	0.103	27.05	1.065	200.17	45.0	6.7
S-1	1	3.20	0.126	21.62	0.851	3.15	0.124	23.24	0.915	235.75	53.0	7.5
	2	3.15	0.124	23.24	0.915	3.10	0.122	23.77	0.936	240.20	54.0	2.3
	3	3.10	0.122	23.77	0.936	2.84	0.112	24.38	0.960	293.58	66.0	2.6
	4	2.84	0.112	24.38	0.960	2.62	0.103	25.02	0.985	333.62	75.0	2.6
S-2	1	3.20	0.126	21.62	0.851	3.15	0.124	23.11	0.910	231.31	52.0	6.9
	2	3.15	0.124	23.11	0.910	3.05	0.120	23.67	0.932	244.65	55.0	2.4
	3	3.05	0.120	23.67	0.932	2.87	0.113	24.43	0.962	311.37	70.0	3.2
	4	2.87	0.113	24.43	0.962	2.57	0.101	25.02	0.985	329.17	74.0	2.4
P-1	1	3.20	0.126	21.59	0.850	3.15	0.124	23.62	0.930	117.43	26.4	9.4
	2	3.15	0.124	23.62	0.930	2.997	0.118	25.78	1.015	208.18	46.8	9.1
	3	2.997	0.118	25.78	1.015	2.69	0.106	26.49	1.043	213.51	48.0	2.8
P-2	1	3.20	0.126	21.59	0.850	3.15	0.124	23.65	0.931	117.43	26.4	9.53
	2	3.15	0.124	23.65	0.931	2.997	0.118	25.53	1.005	202.84	45.6	7.95
	3	2.997	0.118	25.53	1.005	2.69	0.106	26.29	1.035	205.51	46.2	2.99
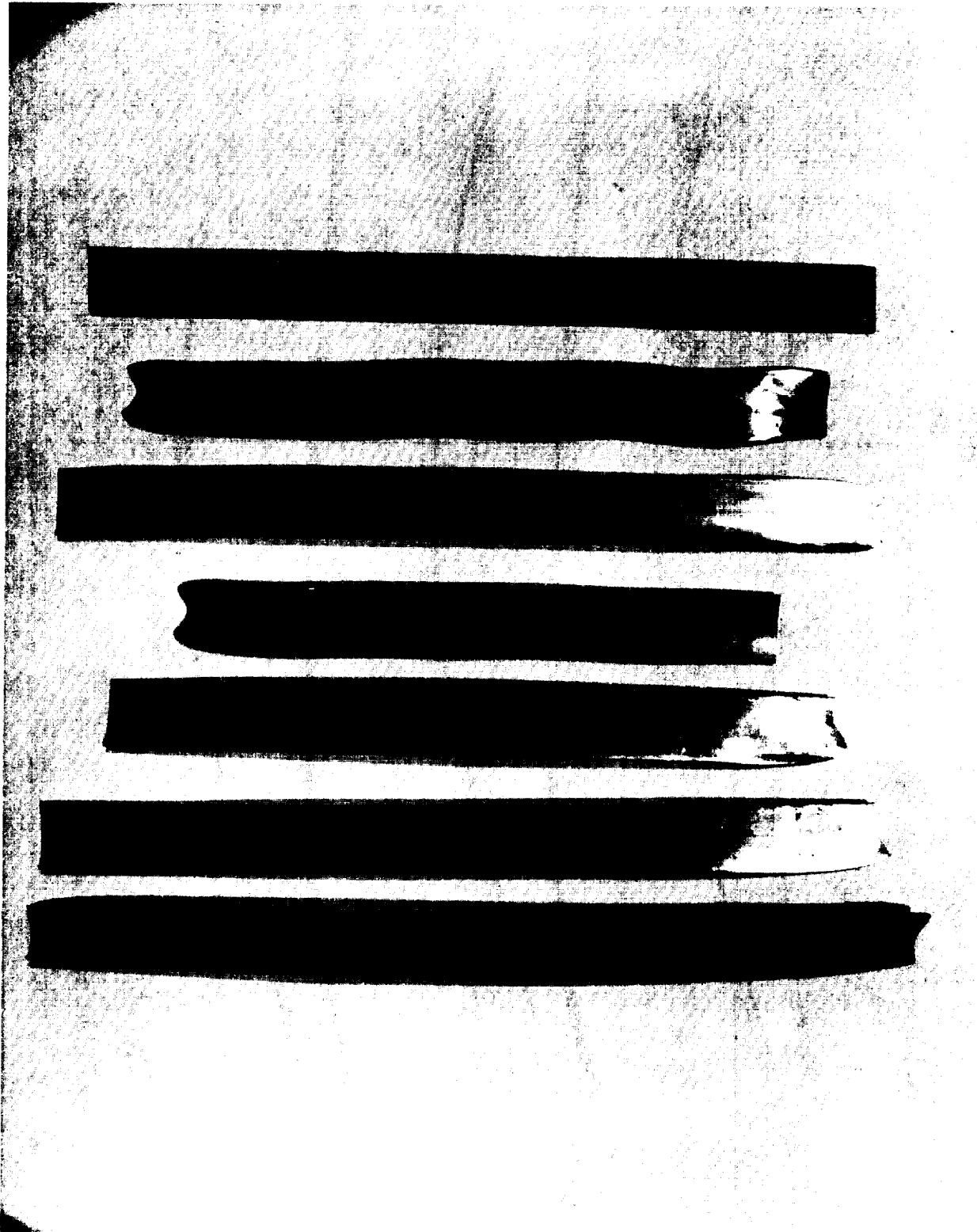
FIGURE 50. COLD ROLLED SPECIMENS FROM VARIOUS TRIALS

(a) Specimen No. C-2

(b) Specimen No. P-2

(c) Specimen No. S-4

——— Product

------- Tolerance Band
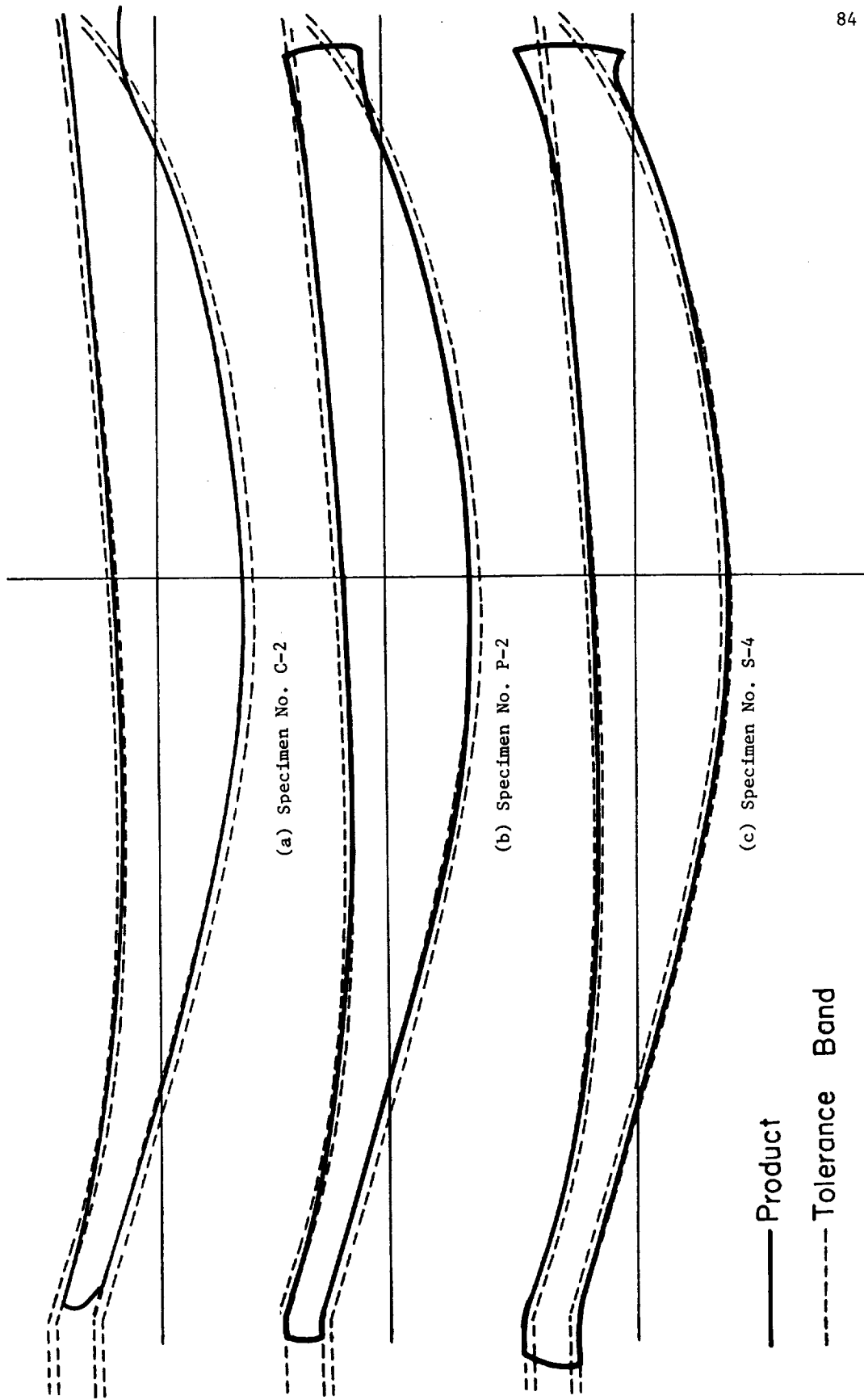
FIGURE 51. COMPARISON OF CROSS SECTIONS OF AS-ROLLED STEEL
SPECIMENS WITH DESIRED CROSS SECTION OF THE AIRFOIL

Hot Rolling Experiments

Material: The hot rolling trials were conducted using Ti-6Al-4V alloy strips of rectangular cross section in as-received conditions. The material was ordered in a sheet of 3.33 mm (0.131 in.) thickness. However, the thickness of the material received varied from 3.33 mm to 3.53 mm. As earlier in the case of cold rolling experiments, several pieces of 24.5 mm (1.0 in.) width and 305 mm(12.0 in.) length were sheared, keeping the length of the pieces along the rolling direction constant. Based on the predictions from the computer program ROLPAS, the rolling specimens were machined to a width of 21.30 mm (0.8385 in.).

Tooling: The roll sleeves with the airfoil profile for hot-isothermal rolling of Ti-6Al-4V alloy shape were machined from a cast IN 100 tube. The templates, produced earlier in the cold rolling trials, were used to copy turn the shape on the sleeves. Based on prior experience, the shape was positioned on the side of the sleeve, thereby eliminating the flash on the leading edge. The rolling surfaces were hand polished using a very fine emery cloth. The sleeves were mounted on the roll arbor and an induction coil, as shown in Figure 44 was wound around the roll sleeves. Several adjustments in the position of the coil were necessary to obtain uniform temperature on the roll-die surface. Temperatures up to 871 C (1600 F) were obtained on the upper die. The temperature on the lower die was always lower than that of the upper die. However, the difference between the temperatures of the upper and lower die reduced to less than 50 C as the heating of the dies continued. The rolls were rotated slowly during heating and the temperature was monitored with a radiation pyrometer.

Rolling Trials: Based on the computer predictions, it was determined that the final airfoil shape can be obtained in single pass under hot-isothermal rolling conditions. Therefore, the rolls were heated to approximately 815 C (1500 F) by induction coils and the Ti-6Al-4V speciment were heated to 955 C (1750 F) in an electric furnace under a protective (Argon) atmosphere. The roll speed was kept at approximately 30 rpm. The

specimen was guided to the roll dies and the airfoil shape was obtained in
a single pass. The roll separating force on both the roll journals was
recorded. The rolled pieces, except for the front end, were fairly straight
and uniform. A few pieces got bowed and twisted due to improper guidance
at the beginning.

Figure 52 shows the initial and final cross section from a typical
hot rolling trial. A few hot-isothermally Ti-6Al-4V specimens are shown in
Figure 53. The results from the hot-isothermal rolling trials are summarized
in Table IV.

A thin slice of 8 mm thickness was cut from a rolled specimen and
its cross-section was compared with the engineering drawing of the airfoil
shape at 10 X magnification, as shown in Figure 54. The rolled section was
within the tolerance band except near the leading and the trailing edges.

Evaluation of Computer Programs SHPROL and ROLPAS

Predictions were made using the computer programs SHPROL and ROLPAS
for selected cases of cold rolling and hot-isothermal rolling trials. In
cold rolling, the predictions of lateral spread, roll separating force, and
roll torque were made for each of the passes, whereas, in hot-isothermal
rolling, predictions were made for single pass rolling to final shape from
a rectangular cross section.

As described earlier, the computer program SHPROL predicts metal
flow during shape rolling. The most important parameter of metal flow in
shape rolling is the lateral spread. Therefore, the lateral spread for var-
ious passes of specimen C-2 (refer to Table III) and the single pass rolling
of specimen T-9 (refer to Table IV) were predicted using the computer pro-
gram SHPROL. The appropriate friction factors and flow stress data were
selected from the material characterization studies conducted earlier. Under
this program. The predicted and measured values of the lateral spread are
compared in Table V.

FIGURE 52. CROSS SECTIONS OF A Ti-6Al-4V ALLOY SPECIMEN BEFORE
AND AFTER HOT-ISOTHERMAL ROLLING
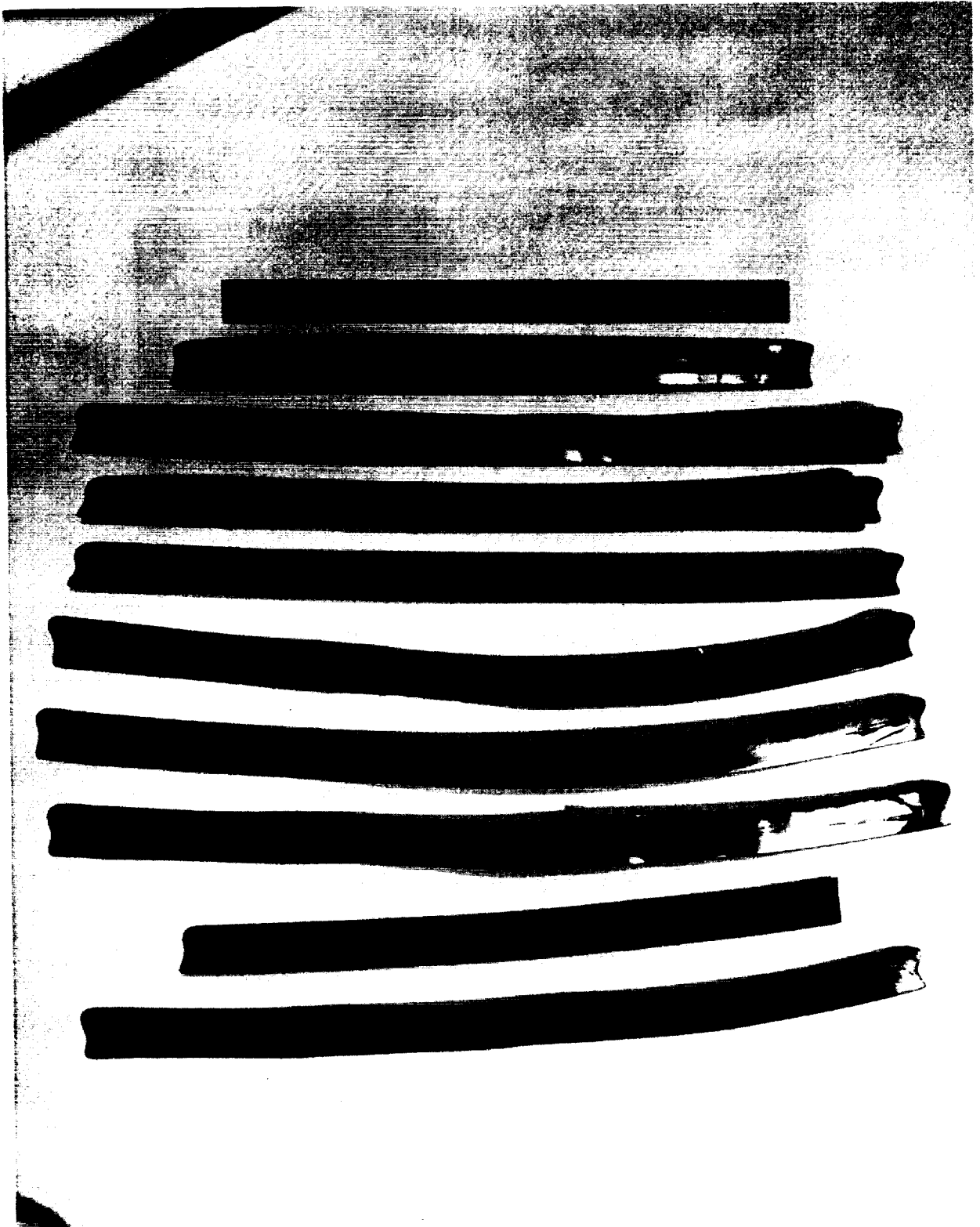
FIGURE 53. HOT-ISOTHERMALLY ROLLED Ti-6Al -4V ALLOY SPECIMENS
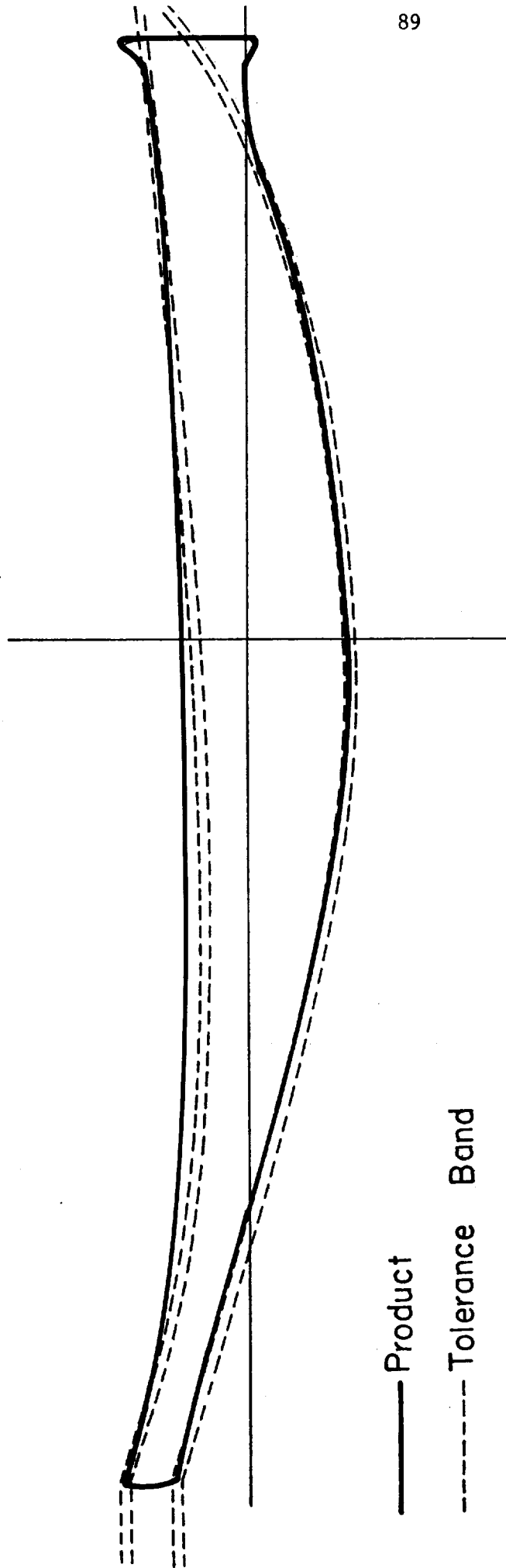
Product

Tolerance Band

SPECIMEN No. T-10

FIGURE 54. COMPARISON OF A CROSS SECTION OF A AS-ROLLED Ti-6Al-4V ALLOY SPECIMEN WITH THE DESIRED CROSS SECTION OF THE AIRFOIL

TABLE IV. RESULTS FROM HOT-ISOTHERMAL ROLLING OF Ti-6Al-4V ALLOY SHAPES

Specimen No.	Initial Thickness mm / in.	Initial Width mm / in.	Final Max. Thickness mm / in.	Final Width mm / in.	Total Load (X 1000) N / lb.	Lateral Spread Percent
T-1	3.53 / 0.139	21.46 / 0.845	3.07 / 0.121	24.51 / 0.965	133.4 / 30.0	14.2
T-2	3.53 / 0.139	21.46 / 0.845	2.87 / 0.113	24.97 / 0.983	146.8 / 33.0	16.3
T-3	3.45 / 0.136	21.46 / 0.845	2.90 / 0.114	24.97 / 0.983	153.5 / 34.5	16.3
T-4	3.48 / 0.137	21.46 / 0.845	3.30 / 0.130	24.13 / 0.950	173.5 / 39.0	12.4
T-5	3.48 / 0.137	21.46 / 0.845	3.02 / 0.119	25.27 / 0.995	155.7 / 35.0	17.8
T-6	3.45 / 0.136	21.44 / 0.844	2.79 / 0.110	24.99 / 1.001	146.8 / 33.0	18.6
T-7	3.28 / 0.129	21.44 / 0.844	2.77 / 0.109	25.78 / 1.015	142.3 / 32.0	20.3
T-8	3.53 / 0.139	21.44 / 0.844	2.77 / 0.109	25.91 / 1.020	142.3 / 32.0	20.9
T-9	3.30 / 0.130	21.31 / 0.839	2.80 / 0.110	24.77 / 0.975	126.8 / 28.5	16.2
T-10	3.43 / 0.135	21.31 / 0.839	2.80 / 0.110	25.15 / 0.990	120.1 / 27.0	18.0
T-11	3.33 / 0.131	21.31 / 0.839	2.80 / 0.110	25.15 / 0.990	122.3 / 27.5	18.0
T-12	3.33 / 0.131	21.31 / 0.839	2.80 / 0.110	25.15 / 0.990	124.6 / 28.0	18.0

TABLE V.   PREDICTED AND MEASURED VALUES OF LATERAL SPREAD

Specimen No.	Pass No.	Predicted Lateral Spread, Percent	Measured Lateral Spread, Percent
C-2	1	22.2	13.6
	2	6.2	3.2
	3	8.6	6.7
T-9	1	13.3	16.2

The discrepency in predictions is the largest in the first pass where a rectangular section is rolled to a shape closer to airfoil section. This results basically from the approximation of the roll-workpiece contact surface made in the analysis. The predictions tend to become more accurate when the initial shape and the final shape during a roll pass are of similar nature.

The values of the roll-separating force as predicted by ROLPAS and as measured during experimental trials are given in Table VI. The first pass of specimen C-1 was simulated with rolls separated by 0.559 mm from their nominal position, since this was the difference observed between the product from first pass and the nominal final product. The flow stress was determined from Figure 9 based on an average value of strain calculated by ROLPAS. As tabulated in Table VI, this resulted in a calculated roll separating force of 172.6kN versus the measured value of 153.5kN.

TABLE VI.   PREDICTED AND MEASURED VALUES OF THE ROLL-SEPARATING FORCE

Specimen No.	Pass No.	Predicted Roll-Separating Force, kN	Measured Roll-Separating Force, kN
C-1	1	172.6	153.5
	3	177.5	180.5
T-11	1	120.5	122.3

Figure 55 shows the outline of the rolling dies used and the stress distribution on the deformation zone of the specimen C-1, in pass 1, as displayed by ROLPAS. Figure 56 shows the intermediate deformation steps as displayed by ROLPAS during simulation of the first pass of the specimen C-1.

The second pass of specimen C-1 as simulated by ROLPAS for a reduction that was equivalent to the sum of the reductions of pass 2 and 3. The calculated and the observed roll-separating forces in this case were higher than those in the first pass, as shown in Table VI. This is primarily due to the increase in the value of the flow stress of the deforming material due to work hardening.

Figure 57 shows selected steps from the simulation of the rolling of the preform shape given in Figure 46 from a rectangular strip of mild steel. The final product shape from this simulation appears somewhat different than the preform shape. This is due to curve smoothing techniques employed in the program ROLPAS.

Similarly, the hot-isothermal rolling of Ti-6Al-4V alloy airfoil shape from a rectangular strip was simulated using ROLPAS. The flow stress and the friction data were selected from Figures 18 and 24, respectively. As seen in Table VI, the predicted values of the roll separating force are in very good agreement with the measured values. The selected simulation steps, as displayed by ROLPAS for hot-isothermal rolling of Ti-6Al-4V alloy shape, are shown in Figure 58. The final shape predicted from the simulation is also in good agreement with the shape obtained from experimental trials.
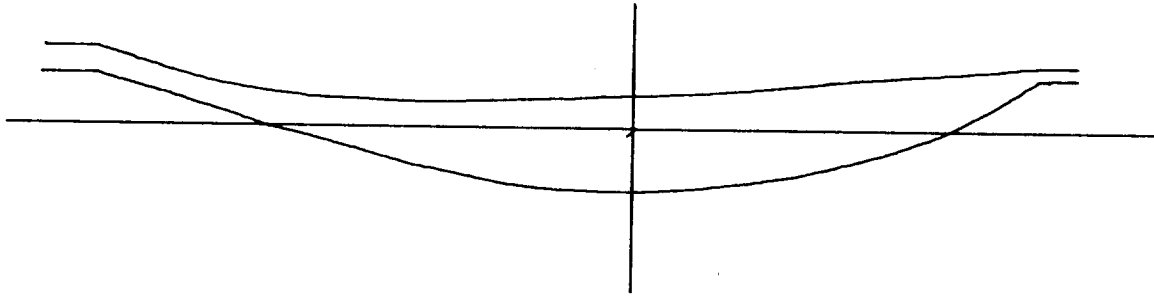
(a) Outline of rolling dies used for C series of rolling experiments
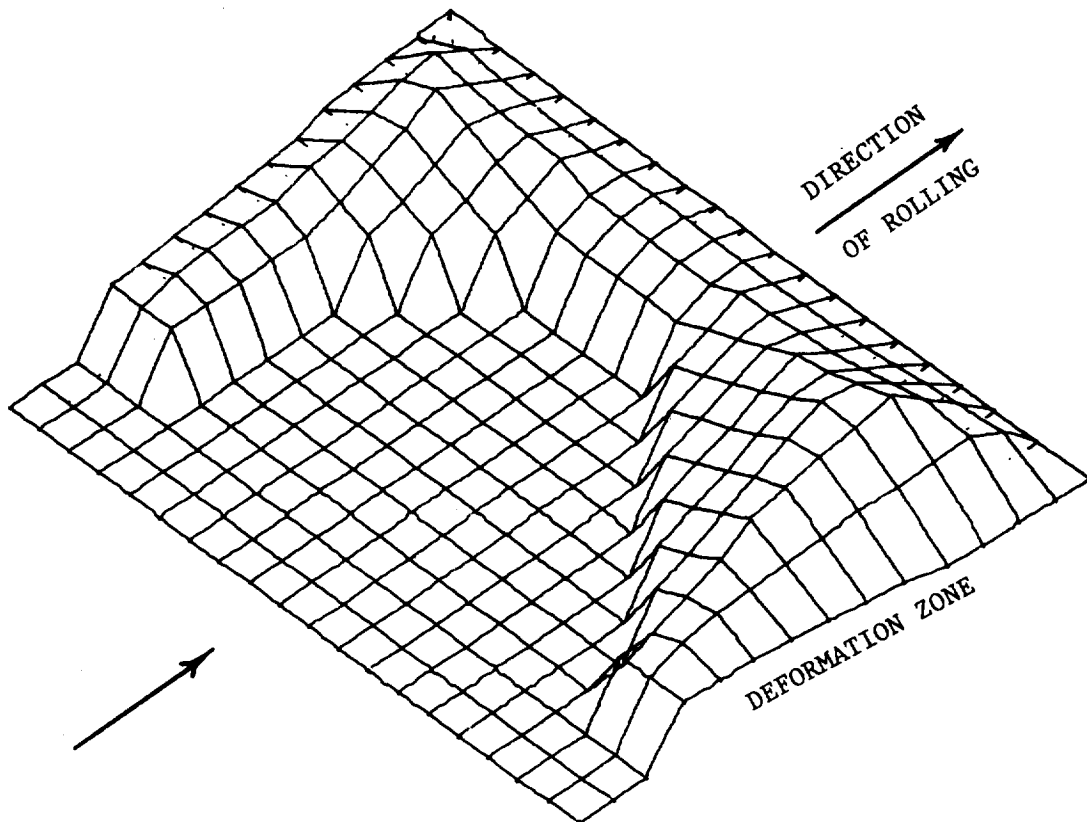
(b) Stress Distribution on the Deformation Zone of Rolling Test C-1 Pass 1, as Displayed by ROLPAS

FIGURE 55. OUTLINE OF ROLLING DIES AND STRESS DISTRIBUTION

C-2

STEP - 1

STEP - 5

STEP - 10

STEP - 15
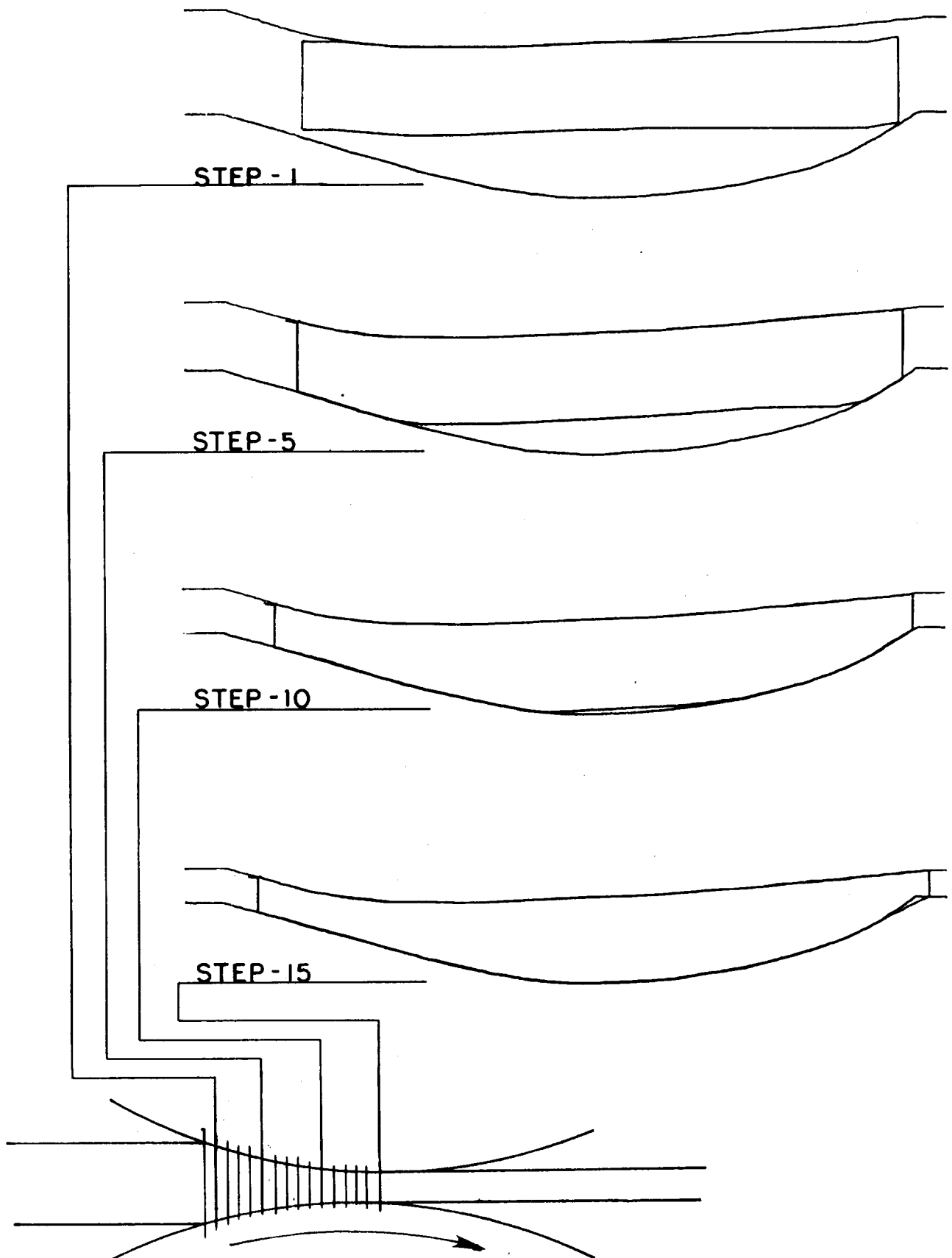
FIGURE 56. SELECTED SIMULATION STEPS AS DISPLAYED BY ROLPAS FOR TEST C-1, FIRST PASS
(COLD ROLLING OF STEEL FROM RECTANGULAR STOCK)

STEP-1

STEP-5

STEP-10

STEP-15
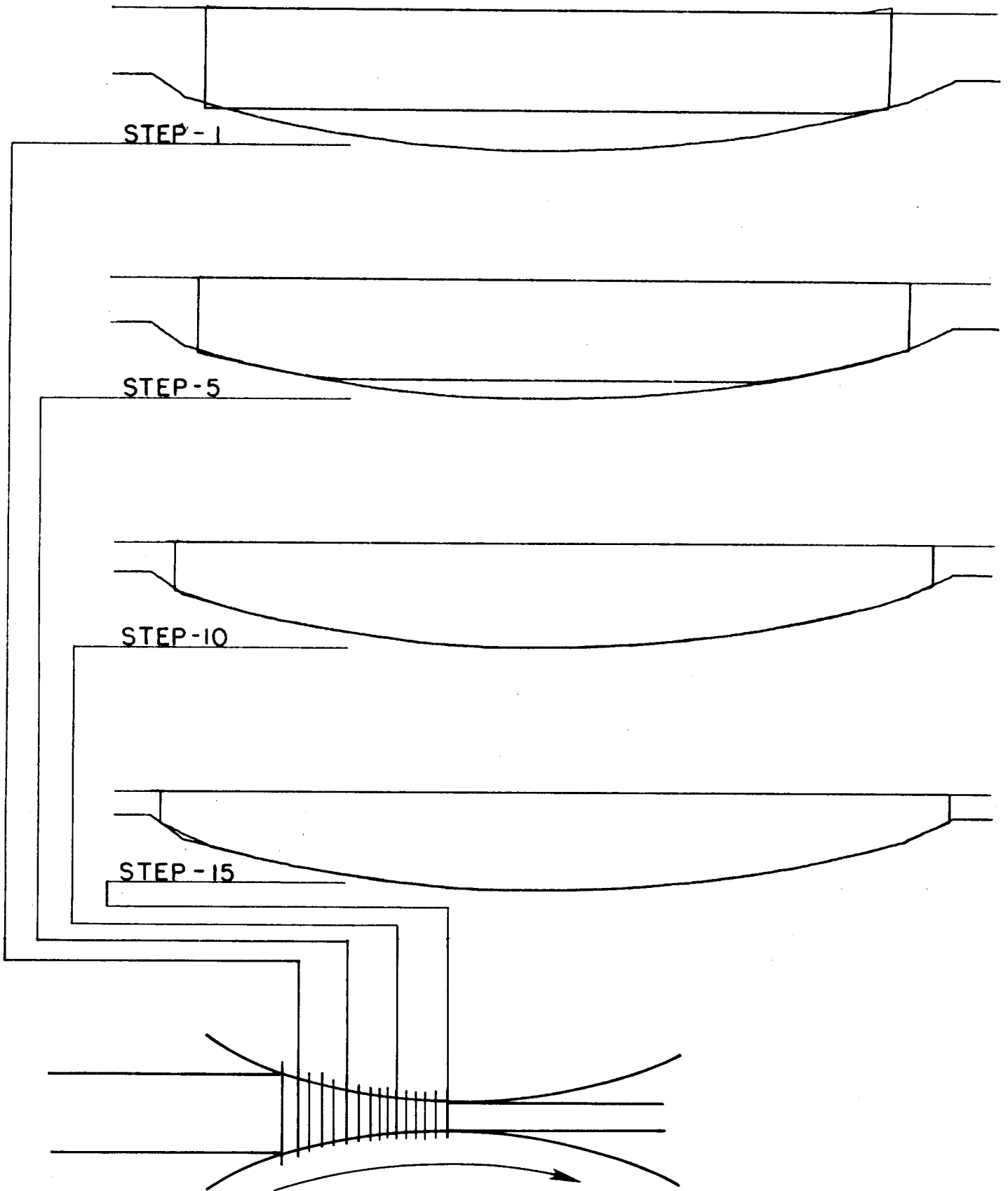
FIGURE 57. SELECTED STEPS FROM THE SIMULATION OF THE ROLLING OF A PREFORM FROM
RECTANGULAR STOCK (COLD ROLLING OF STEEL, COMPUTER DISPLAY)

STEP-1

STEP-5

STEP-10

STEP-15
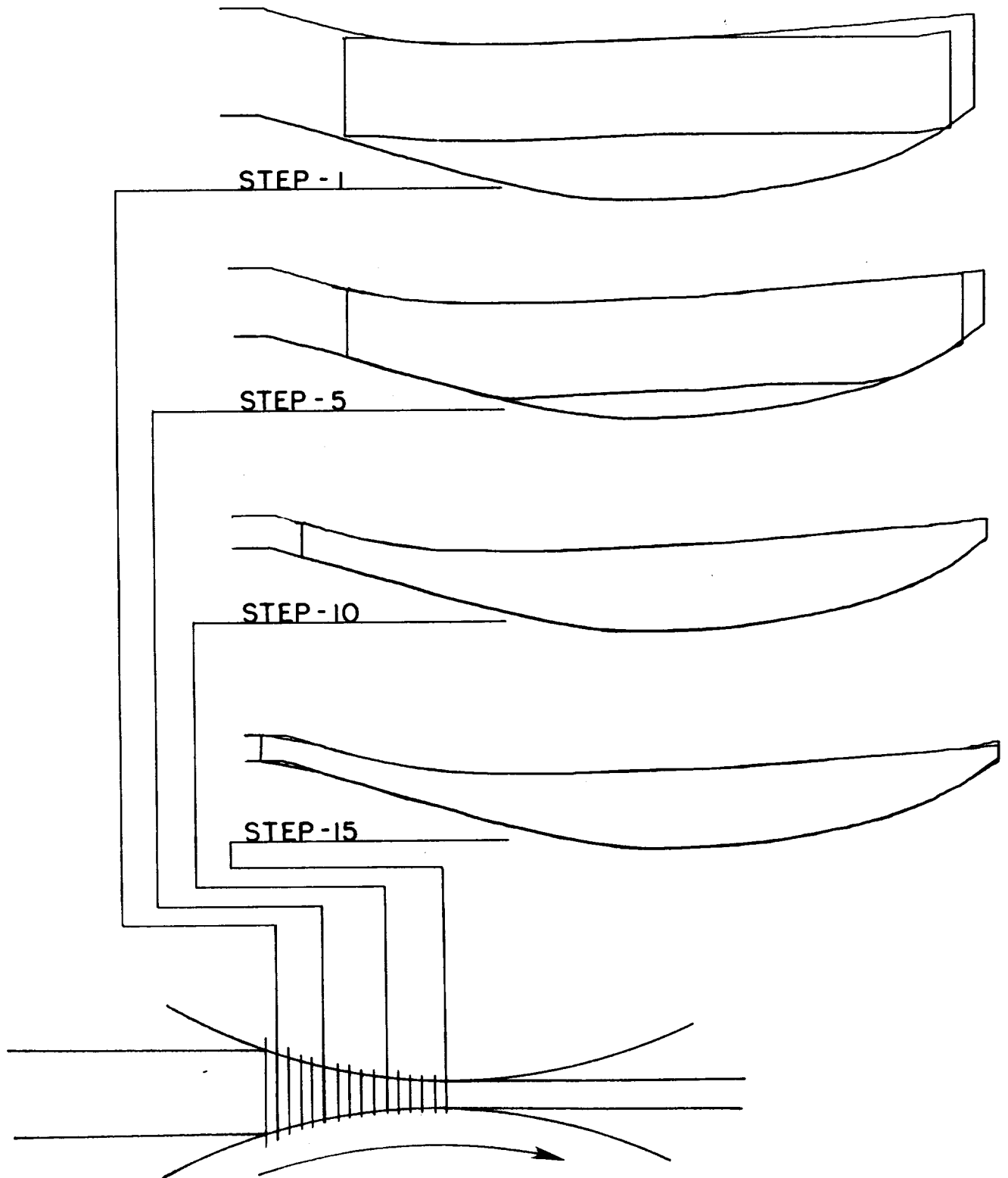
FIGURE 58.   SELECTED SIMULATION STEPS CALCULATED BY ROLPAS FOR TEST T-11
(HOT ROLLING OF Ti-6Al-4V FROM RECTANGULAR STOCK, COMPUTER DISPLAY)

Evaluation of Properties

At the end of experimental rolling trials, both mechanical and metallurgical properties of the rolled material were evaluated. The evaluation of mechanical properties included determination of yield strength, tensile strength, maximum elongation and hardness before and after rolling. For this purpose, tension specimens were machined from both AISI 1018 and Ti-6Al-4V alloy in as-received (as-annealed in case of steel) and as-rolled conditions. Tension tests were conducted on a Baldwin testing machine at room-temperature at cross head speed of .02 mm/s. The mechanical properties of these materials are summarized in Table VII.

TABLE VII. MECHANICAL PROPERTIES OF AS-RECEIVED AND
AS-ROLLED MATERIALS AT ROOM TEMPERATURE

Material	Yield Strength N/mm^2	Tensile Strength N/mm^2	Maximum Elongation Percent	Hardness
As-received AISI 1018 Steel	206.85	349.58	33	$R_B 60$
As-rolled AISI 1018 Steel	508.51	549.53	4.5	$R_B 90$
As-received Ti-6Al-4V alloy	937.72	981.37	13	$R_c 34$
As-rolled Ti-6Al-4V alloy	920.03	994.05	5	$R_c 36$

As seen in Table VII, the tensile properties and the hardness of mild steel improves considerably due to cold rolling, whereas they are virtually unaffected in the case of hot-isothermal rolling of Ti-6Al-4V alloy. However, due to rolling, ductility is greatly reduced in both materials.

In addition to above, a cold-rolled AISI 1018 steel vane and a hot-isothermally rolled Ti-6Al-4V alloy vane was metallographically examined

at NASA-Lewis research center. Metallographic specimens were prepared from
sections taken at various locations shown in Figure 59. All the samples
were etched with a diluted acid mixture (1 part H_2O to 1 part of the follow-
ing: 33cc H_2O, 33 cc acetic acid, 33 cc HNO_3, and 1 cc HF).

Figure 60 shows the surface finish of selected regions of a cross-
section of the AISI 1018 cold rolled steel vane (specimen S-4). The general
smoothness of the surface finish and the thinness of the trailing edge are
the most important features in this Figure. Figure 61 contains photo-
micrographs of a hot rolled Ti-6Al-4V vane (Specimen T-9, taken about 5
inches from the nose of the rolled strip). These photomicrographs reveal
that the hot rolled alloy contains several surface cracks and scrapes. Also,
the region near the surfaces appear to have undergone alloy depletion as the
beta-containing grains disappear near the surface. Comparison of Figures
60 and 61 show that the trailing edge of the hot rolled vane is much thicker
than that of the cold rolled vane.

Commercial Process Evaluation

General Electric Company's H-369 vane, as shown in Figure 62, is
commercially rolled from INCO 718 alloy. This vane is used in stage 4 of
F101 engine. The roll pass schedule for a representive rolling of this
strip is given in the following:

		Length	Width	Maximum Thickness
Starting Stock	G	17	.837,824,825	.105,105,1045
1st Roll Pass	000	17 5/8	.857,848,848	"
Anneal	None			
2nd Roll Pass	.010	18 3/4	.867,861,860	
Anneal	None			
3rd Roll Pass	.010	19 7/8	.877,869,869	.102,102,102
Anneal	1875° 1 hr +			
4th Roll Pass	.005	22		.096,096,096
Anneal	None	cut off 1" fr. lgth.		
5th Roll Pass	Same setting as 4th roll	22 3/8	.887,884,886	.092,092,092
Anneal	1875°			
6th Roll Pass	.010	24 5/8	.917,908,915	.085,085,085
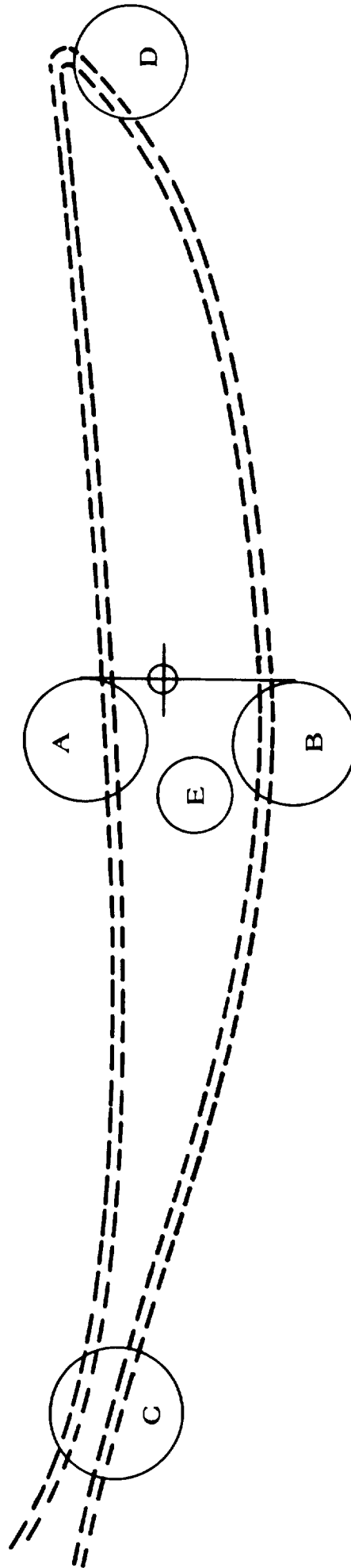
FIGURE 59. VARIOUS LOCATIONS OF METALLOGRAPHIC EXAMINATION
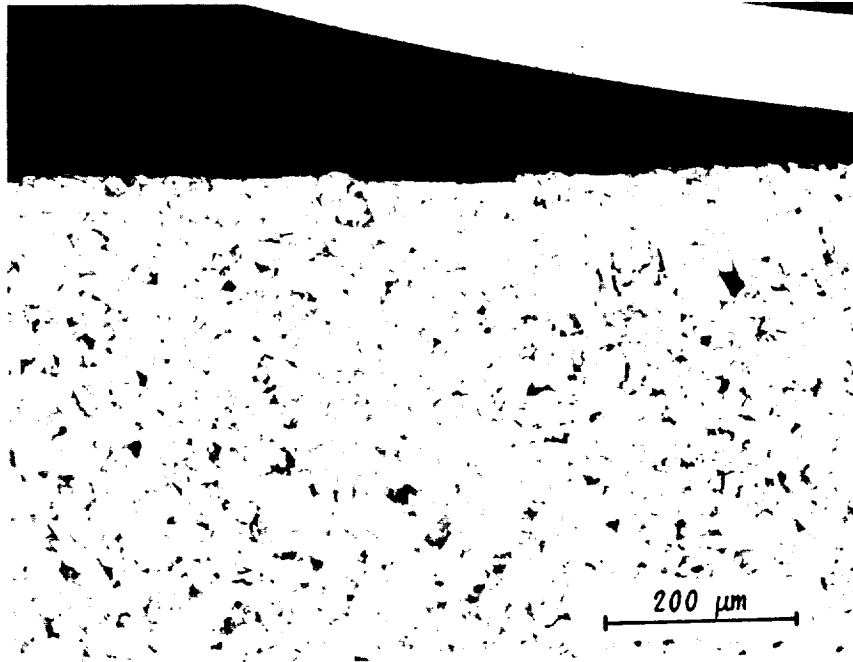
Section A
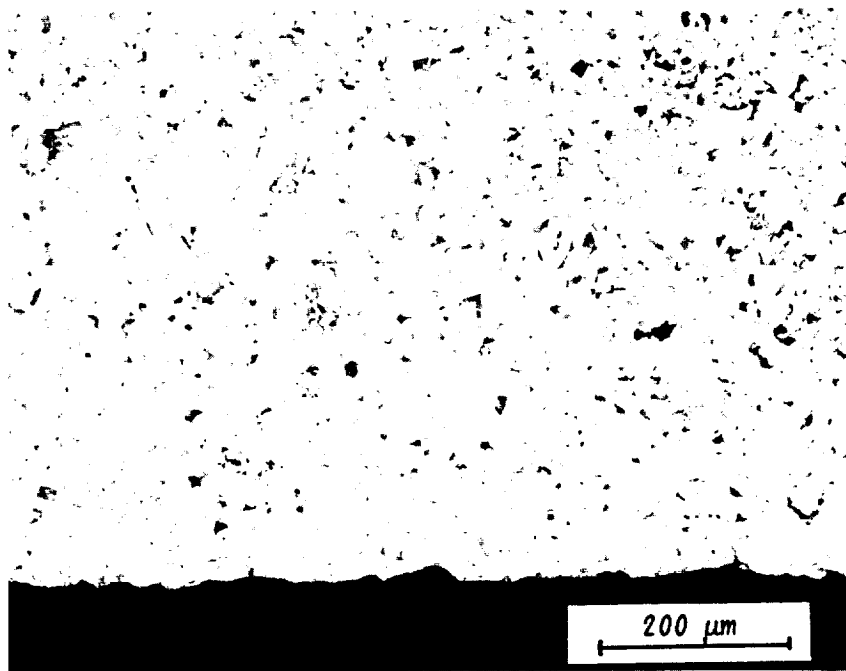
Section B

FIGURE 60. PHOTOMICROGRAPHS OF AS-ROLLED AISI 1018 STEEL VANE

Section C
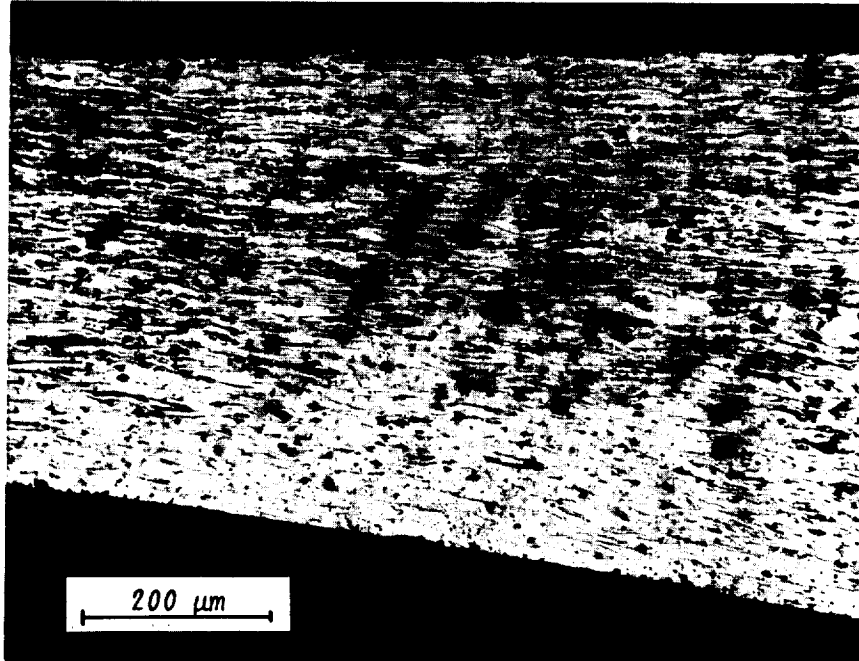
Section D
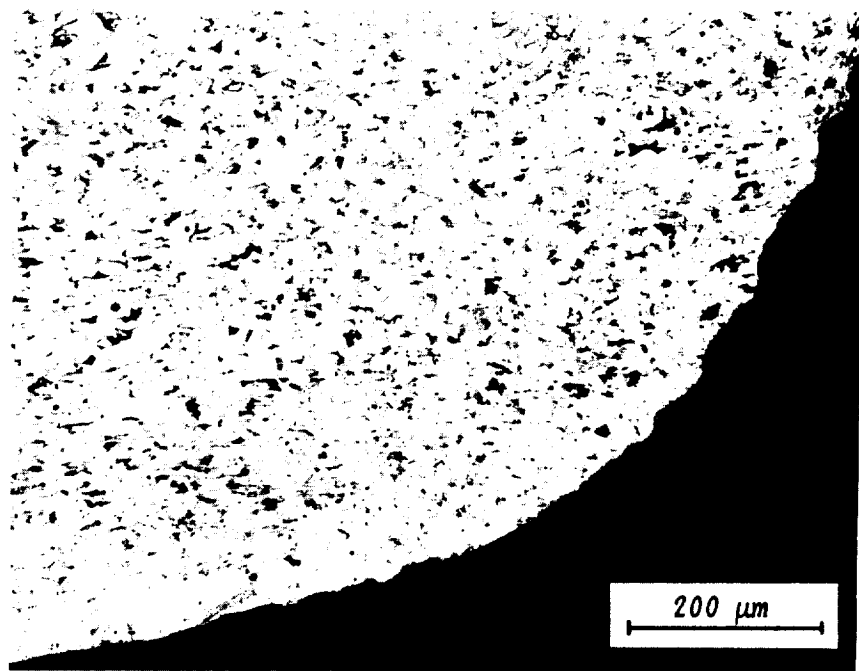
FIGURE 60. CONTINUED
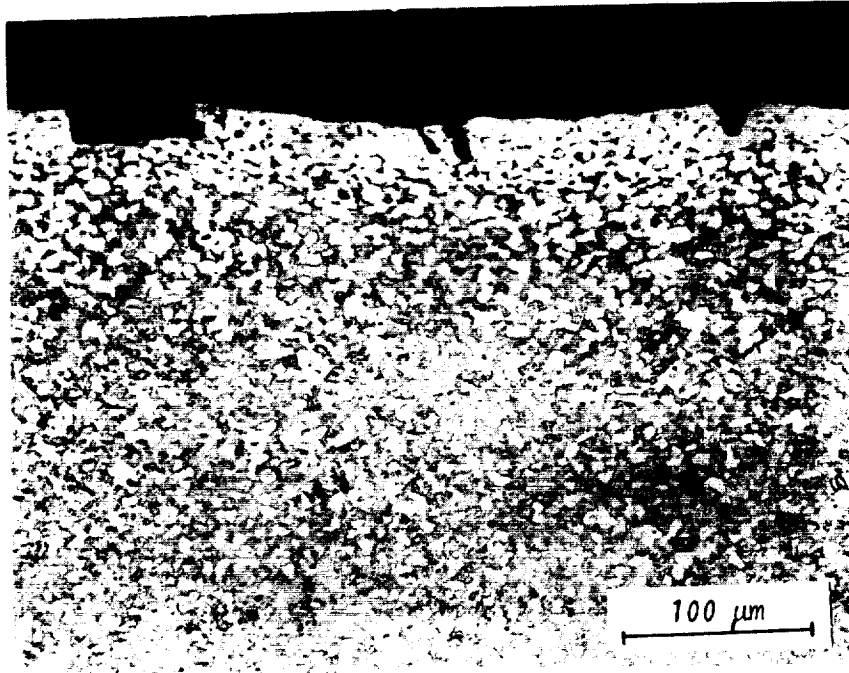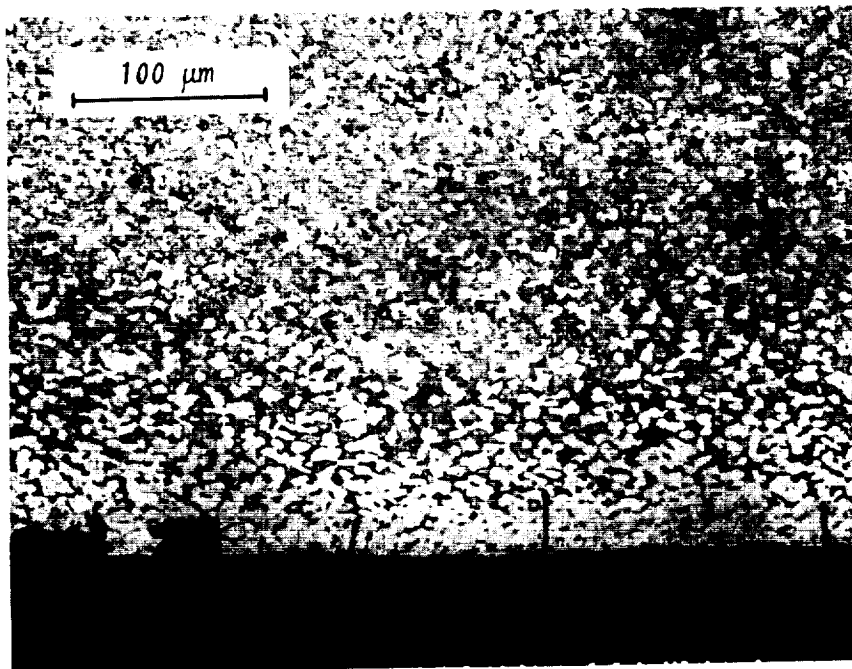
Section A

Section B

FIGURE 61. PHOTOMICROGRAPHS OF AS-ROLLED TI-6Al-4V ALLOY VANE
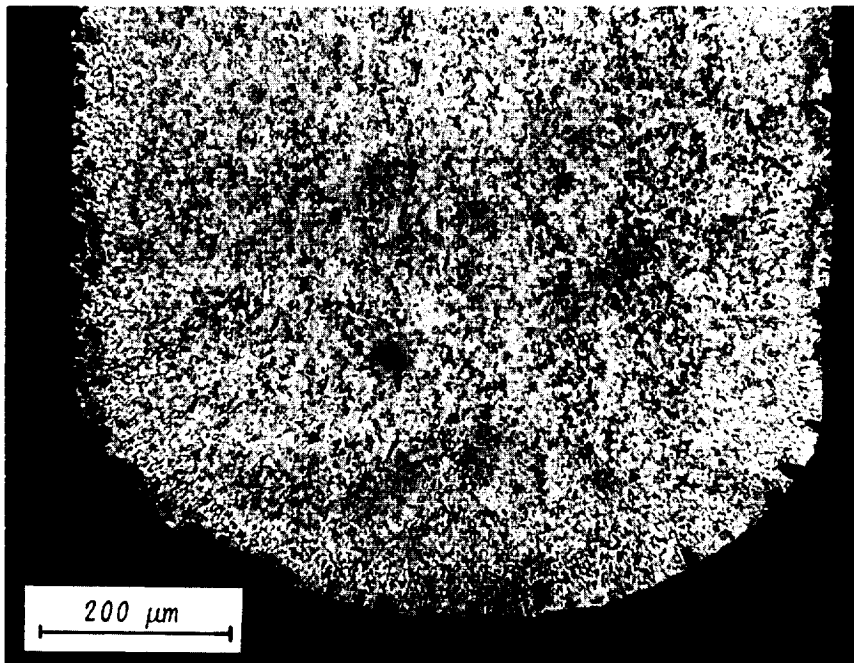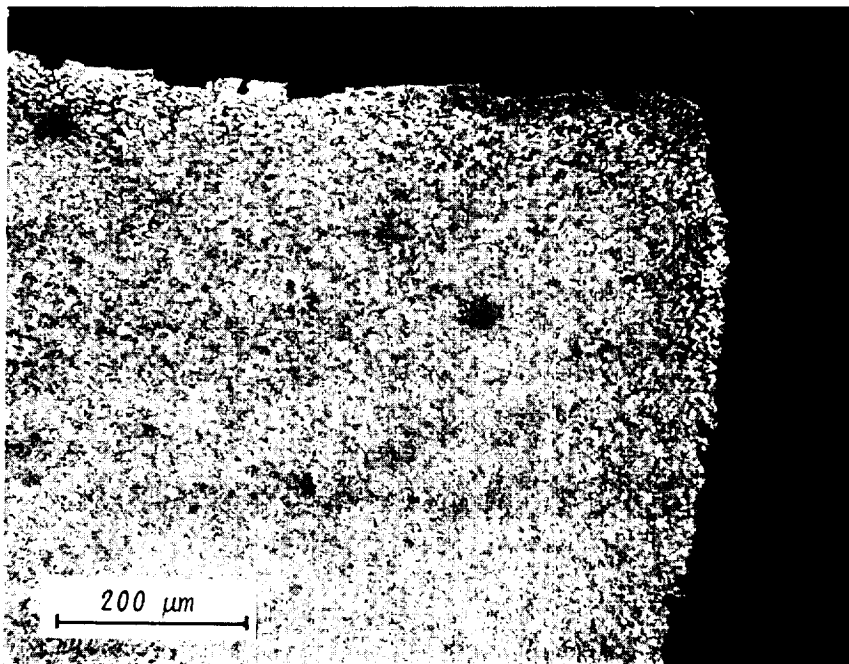
Section C

Section D

FIGURE 61.   CONTINUED
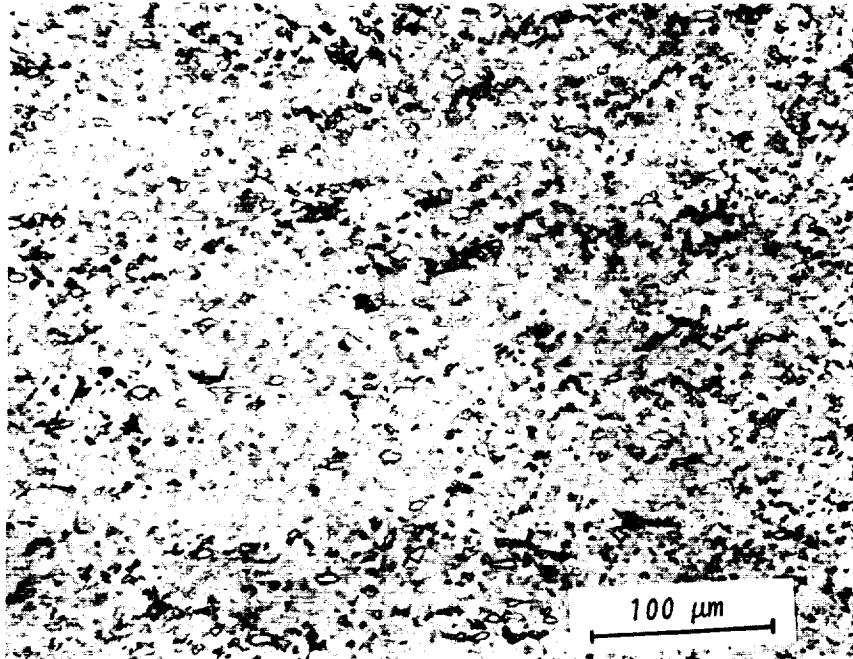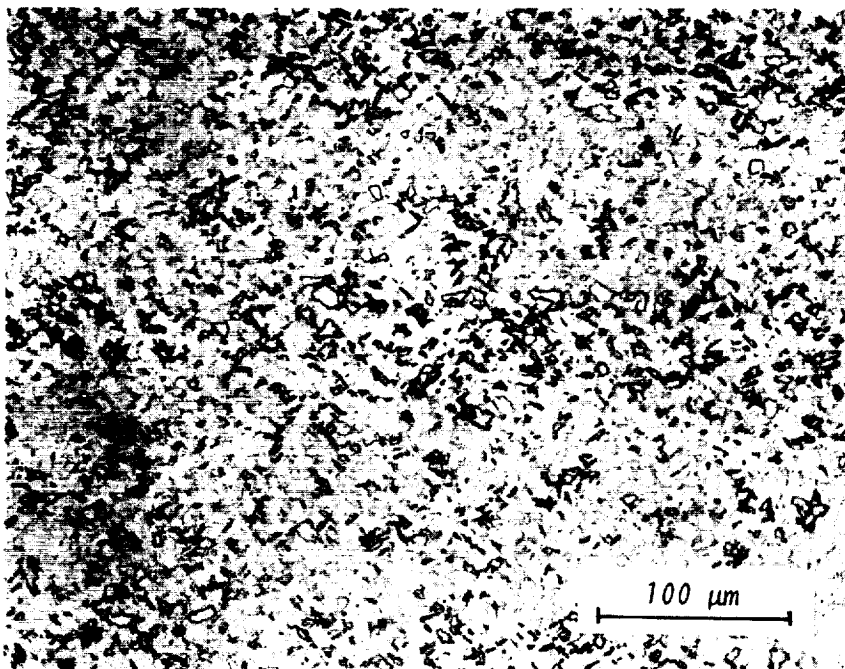
Section C

Section E

FIGURE 61. CONTINUED
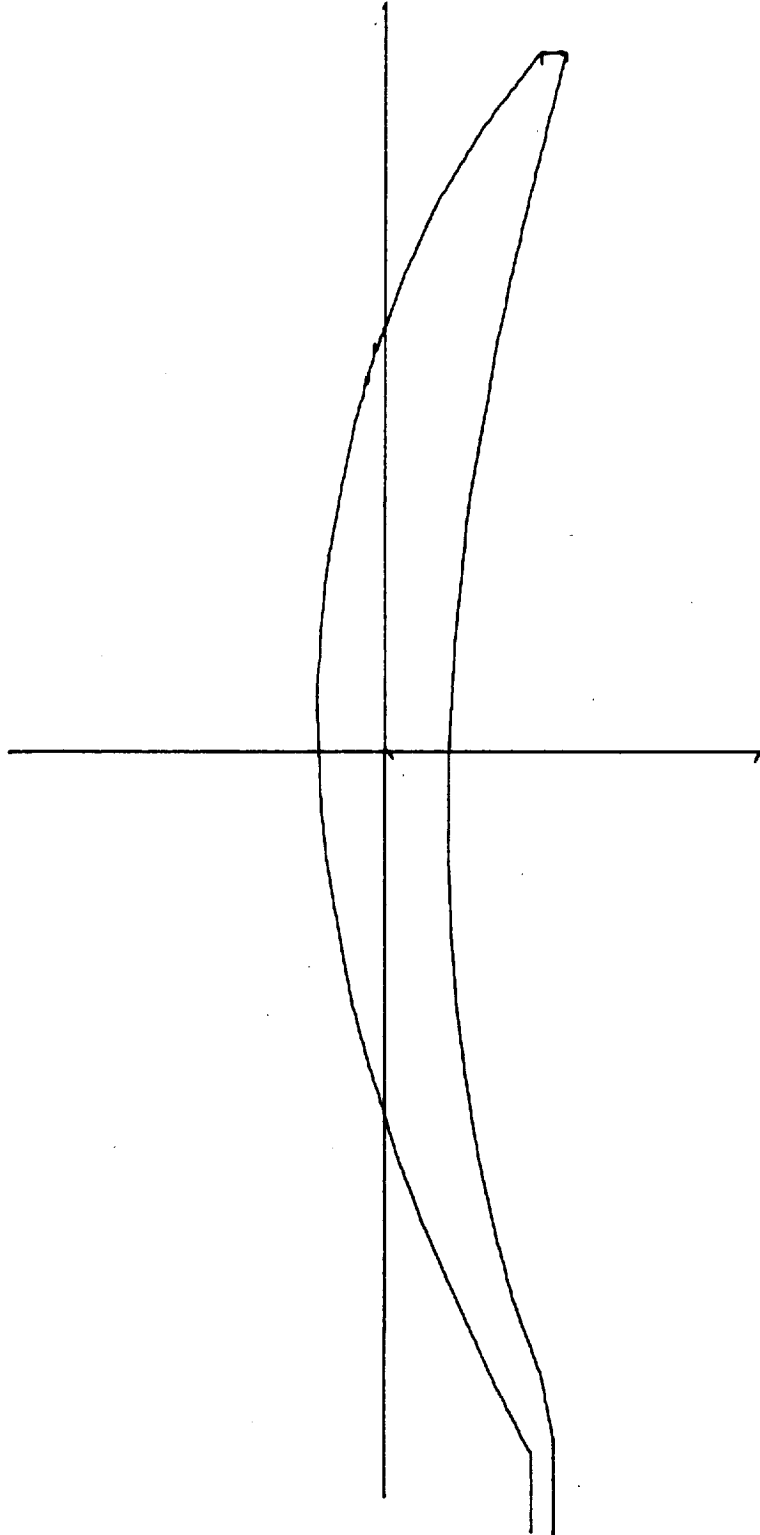
FIGURE 62. GENERAL ELECTRIC'S H-369 VANE (COMPUTER DRAFTED)

It is seen that a total of six passes and two intermediate annealing operation are required for successful rolling of this vane from INCO 718 alloy.

The above roll pass schedule was evaluated using the computer program ROLPAS. Figure 63 shows various intermediate cross sections as if the shape were rolled in a single pass. However, as seen in Figure 64, the maximum reduction in area for this pass schedule is approximately 70 percent, which is well above the limiting reduction of 56 $\pm$ 2 percent INCO 718, as determined earlier under material characterization. Therefore, simulations were carried out in two steps. The first step simulation included the first three passes, just before the first annealing, and the second step simulation included the 4th and 5th passes, just before the second anneal. These results are summarized in Figures 65 and 66, respectively. In both Figures 65 and 66, it is seen that the maximum reduction in area is approximately 30 percent, well below the limiting reduction of 56 $\pm$ 2 percent for INCO 718. Thus, with the aid of ROLPAS it is possible to estimate the number of annealing steps necessary. The number of roll passes taken before each annealing is essentially determined by the load and torque capacities of the rolling mill used. To use a moderate capacity mill, it is possible to take several passes with the same roll design. However, the end effect is the same as using a heavier mill and taking large reductions in reduced number of passes.

In the present evaluation, predicted load and torque values could not be compared with those obtained experimentally since these data were not available. Thus, only the metal flow and required annealing steps were predicted and compared with the actual case.
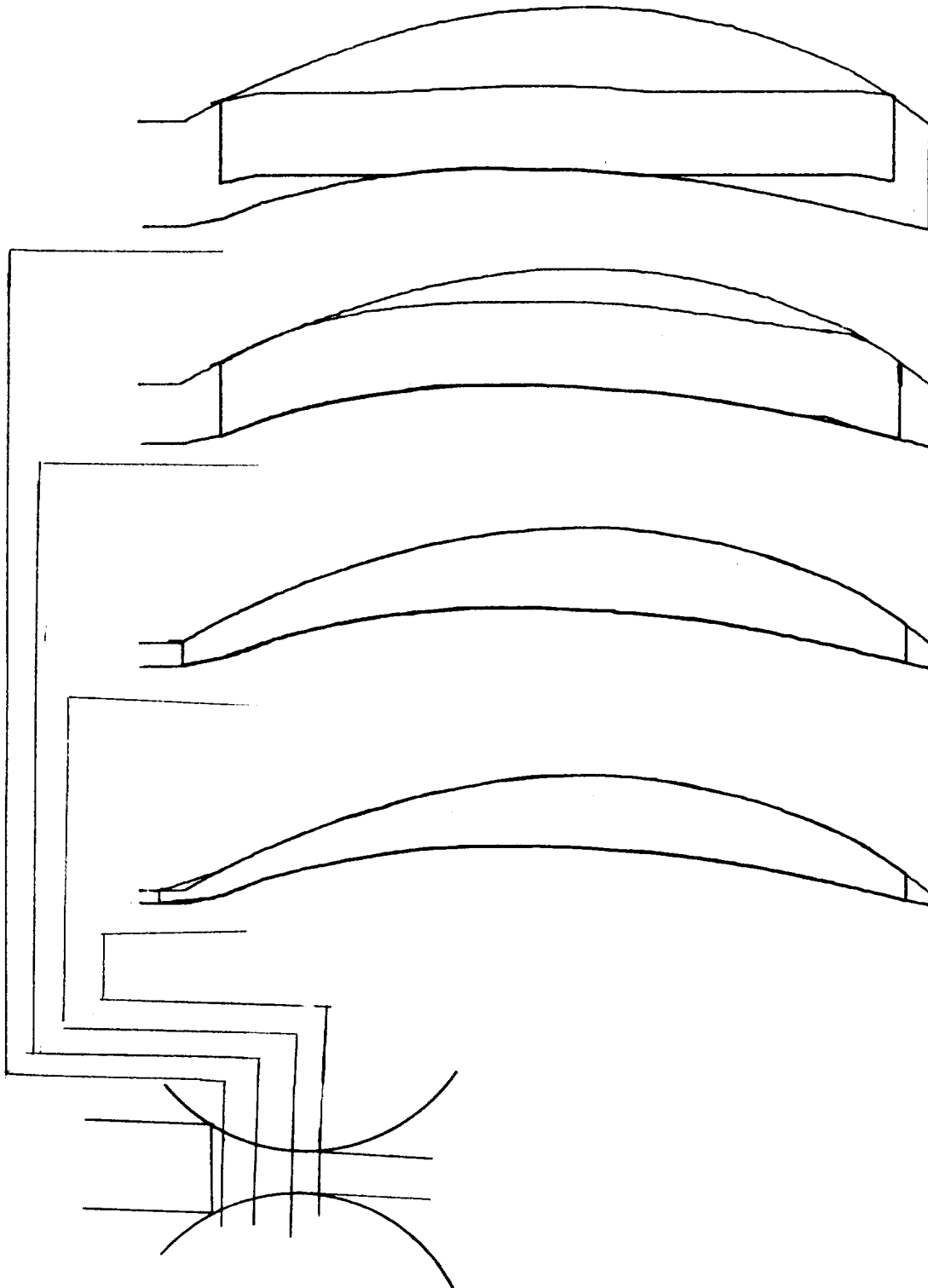
FIGURE 63. INTERMEDIATE SHAPES IN SIMULATION USING ROLPAS (COMPUTER DISPLAYS)
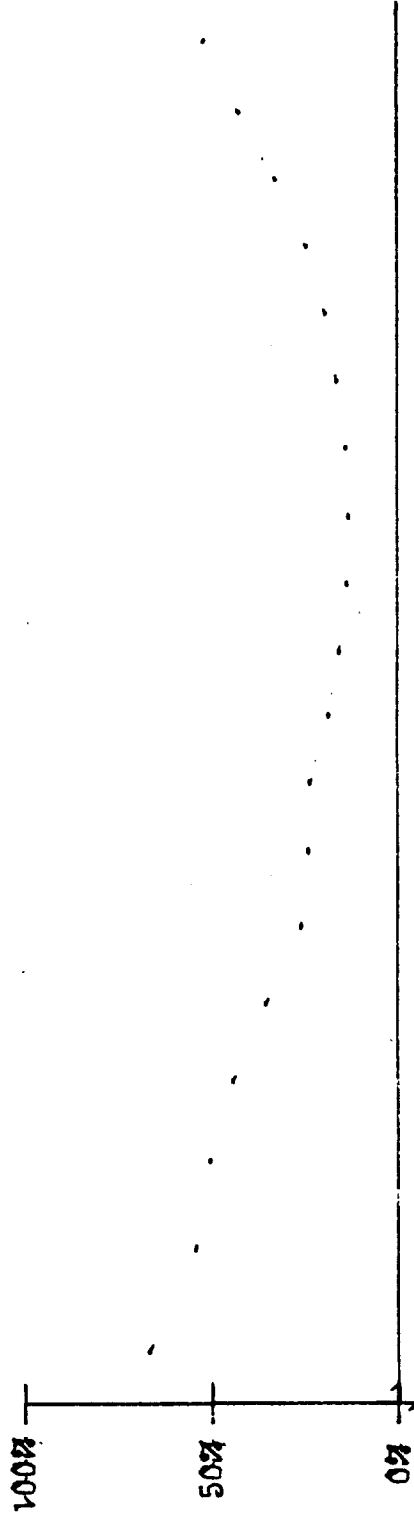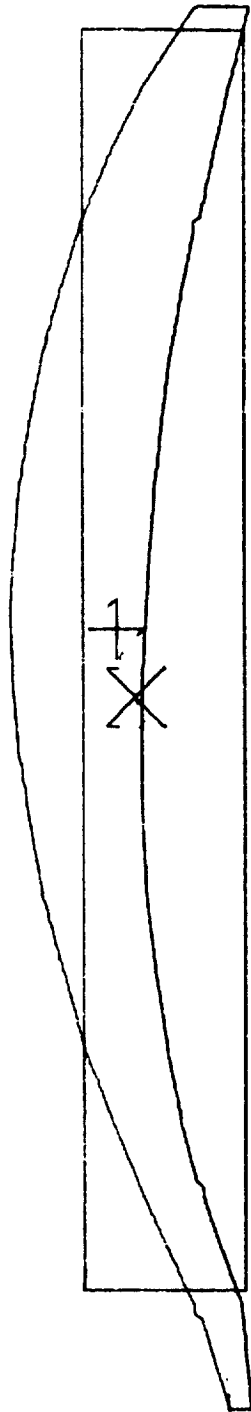
Distribution of % Elongation

FIGURE 64. ESTIMATED ELONGATION ACROSS THE SECTION, OBTAINED FROM THE SIMULATION FOR PASSES 1 THROUGH 6 USING ROLPAS (COMPUTER DISPLAY)

Distribution of % Elongation
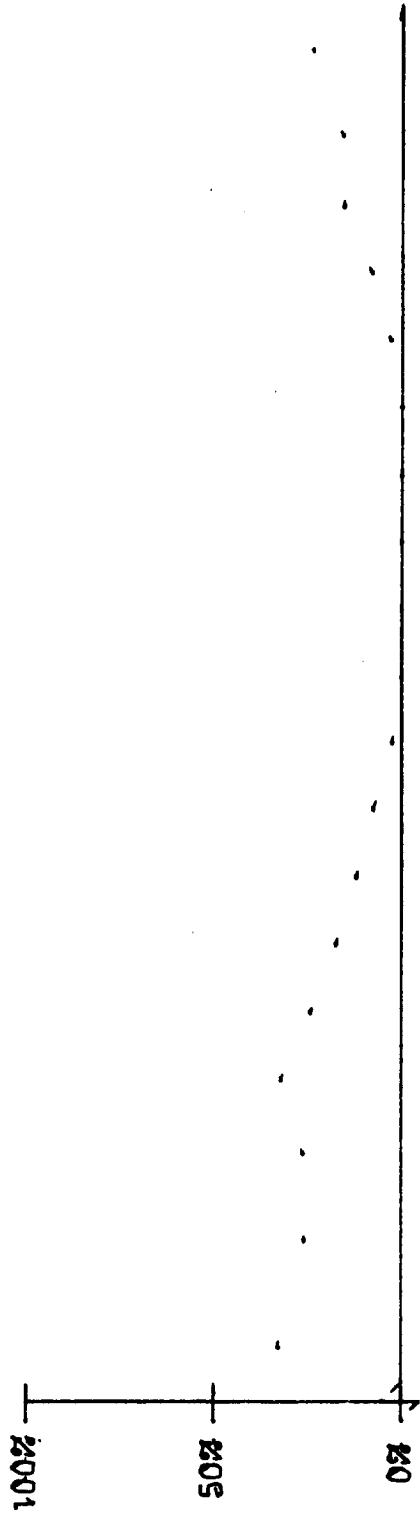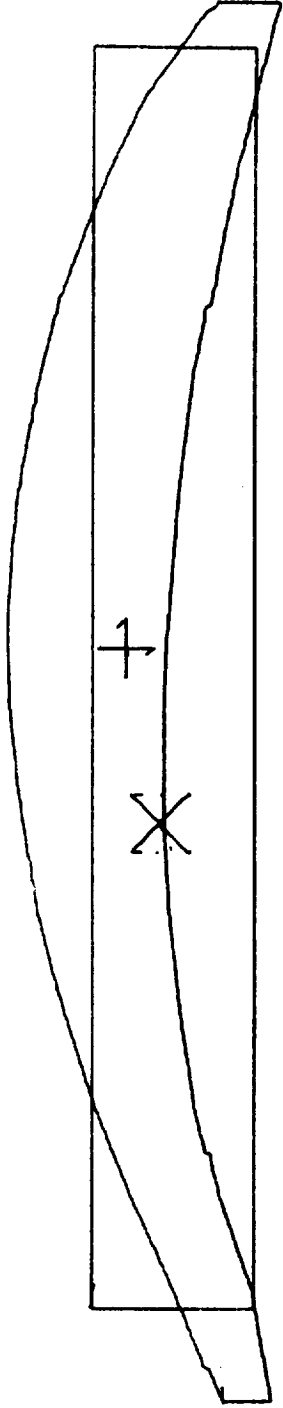
FIGURE 65. DATA OBTAINED FROM SIMULATION FOR PASSES 1 THROUGH 3 USING ROLPAS
(COMPUTER DISPLAY)

Distribution of % Elongation

1001%

50%

0%
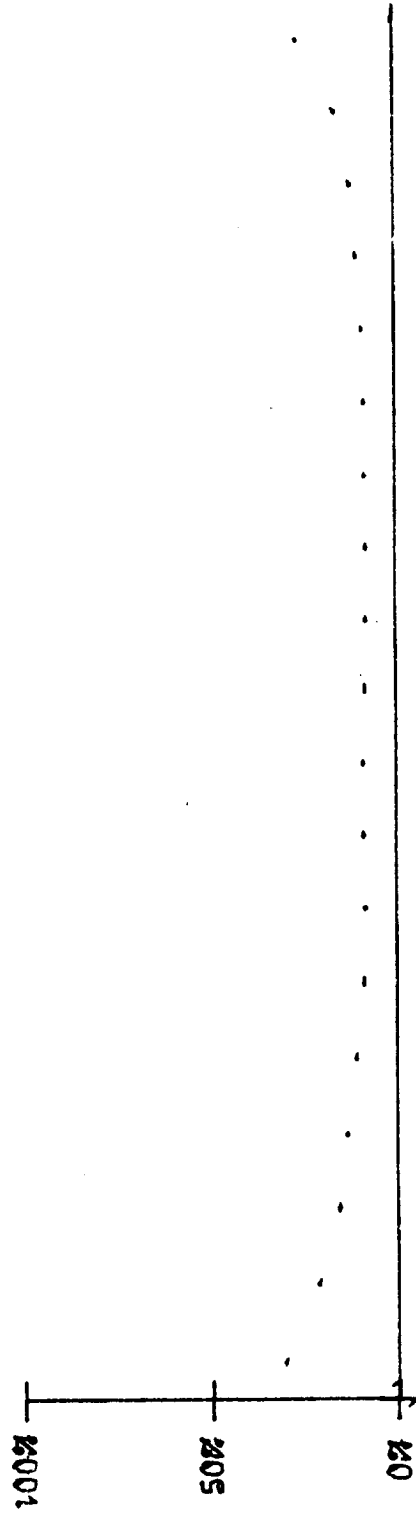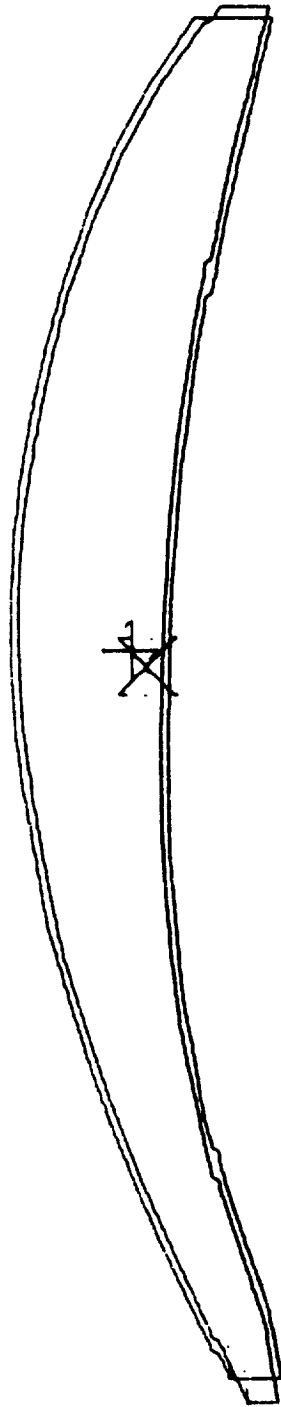
FIGURE 66. DATA OBTAINED FROM SIMULATION FOR PASSES 3 AND 4. USING ROLPAS (COMPUTER DISPLAY)

COST-BENEFIT ANALYSIS

In this task a systematic procedure has been developed for analyzing the cost benefits of applying computer aided analyses in metal forming processes. This procedure involves the following steps.

(1) Consider the forming process to which computer-aided techniques will be applied.

(2) List all the operations involved in this process, and estimate the costs associated with each operation, in actual figures or in percentage of total product cost.

(3) Determine the operations affected by the use of computer-aided techniques.

(4) Make best estimates of cost reductions expected in these operations.

(5) Using the information obtained in Step 4, estimate the total cost reduction expected by applying computer techniques to the process.

The economics of any metal forming process will include the following cost factors:

(a) Cost of estimating and planning, before and after an order is received.

(b) Cost of incoming stock weight (including final part weight, scrap, and rejects)

(c) Cost of energy (for heating in hot forming, and heat treating).

(d) Die costs (design, material, manufacturing, and quality control).

(e) Machine costs (depreciation, maintenance, and energy).

(f) Costs of post-forming treatment (cleaning, stretching, bending, and others).

(g) Quality control costs.

(h) Process development costs (die tryout, debugging of a new process, proving out or acceptance of a new process).

The last item, process development costs, can be considerable (as much as 20 to 50 percent of the total cost of an entire production batch) in aerospace-related metal-forming processes because these processes are inherently difficult and the production lot is relatively small. The application of computer-aided analyses is expected to reduce the costs in all the above listed items to various degrees. The most significant effects of computer-aided analyses can be expected to be in Items (a), (b), (c), (d), and (h), listed above.

In order to illustrate the cost - benefits of utilizing Computer Aided Design and Manufacturing (CAD/CAM) techniques in metal forming, two processes (precision forging and shape extrusion) have been considered, in addition to shape rolling investigated in the present program. Battelle has developed CAD/CAM technique for all these processes. Therefore, they were selected.

Extrusion of Structural Shapes

Battelle recently completed a program for the Army on the CAD/CAM application to extrusion of shapes. The results given below were developed to a large extent under that Army program.

The application of the CAD/CAM extrusion system is expected to reduce manufacturing costs and delivery schedules of extrusions and to increase the productivity of extrusion operations. In order to evaluate these potential benefits, it is necessary to review the details of the present extrusion practice.

Present Extrusion Practice. The various steps involved in producing extruded products can be summarized as follows:

1.0 Estimating

    1.1 Receive customer inquiry (section drawing, material specifications, quantity, delivery date).

    1.2 Prepare quotation.

        1.2.1 Determine the circumscribing circle, the area, and the perimeter of the cross section.

        1.2.2 Estimate die costs, including backup tooling.

        1.2.3 Estimate press costs, including auxiliary equipment and handling.

        1.2.4 Estimate material costs, including scrap losses.

2.0 Die Design and Manufacture

It is assumed that the order is received and results of calculations, made in Step 1.2.1 above, are available. At this stage, a precise cost estimating and control is necessary.

    2.1 Determine the optimum number of orifices in the die, estimate the extrusion load and select the appropriate extrusion press.

    2.2 Locate and orient the orifices relative to billet axis for uniform metal flow and select the backup tooling, if it is available.

    2.3 Correct the dimensions of the die orifices to account for thermal shrinkage and local die deflection.

    2.4 Design die bearings to assure appropriate shape definition and straightness.

    2.5 Prepare a die drawing.

    2.6 Manufacture the die either by tracer copymilling or by EDM (wire or conventional).

3.0 <u>Determination of Process Conditions</u>

    3.1 For the given press and number of die orifices, select optimum billet and butt lengths to give maximum yield.

    3.2 Select billet temperature, uniform or variable in axial direction.

    3.3 Select press speed for the given alloy to result in maximum production rate without extrusion defects (hot shortness in hard alloys).

4.0 <u>Extrusion, Straightening, Stretching</u>

    4.1 Perform die trials and corrections to ensure straightness and die fill.

    4.2 Extrude and saw.

    4.3 Stretch, straighten and saw to appropriate lengths.

    4.4 Package and ship.

<u>Potential Non-Tangible Benefits of the CAD/CAM Extrusion System</u>. The CAD/CAM system for extrusion, available at this time, is only applicable to solid shape dies, and cannot entirely handle porthole, bridge and feeder-plate type dies. Nevertheless, in the extrusion of solid shapes, especially those from hard alloys and for aerospace applications, this system would assist companies in a variety of ways in improving the efficiency of current operation practices. The CAD/CAM system would be helpful in virtually all the various operational steps, discussed above. The major non-tangible benefits, which could be provided by the present CAD/CAM system, are:

- More Precise Estimating
- Reduction in Delivery Schedules
- Less Dependence upon Skilled Die Makers
- Reduction in the Number of Die Failures
- Improved Utilization of Existing Press Capacity
- Continuous Improvement of Die and Process Technology

Potential Tangible Benefits of the CAD/CAM Extrusion System. In order to identify and estimate the cost benefits which may result from the application of the CAD/CAM Extrusion system, it is helpful to consider (a) the common problem areas in extrusion which may be affected by the introduction of the CAD/CAM system, and (b) a hypothetical extrusion plant where the system may be introduced.

An extensive evaluation of extrusion plant operations and costs is reviewed by Ferguson from Alcoa[19] and Waugh[20] of Kaiser. Based on this information, the common problem areas which can be affected by CAD/CAM application are:

(1) **Extrusion Conditions and Operations**

- Extruding at a slower speed than necessary reduces productivity.

- Using too short billets reduces yield and productivity.

- Excessive breakthrough pressures, because the press capacity is barely sufficient for the job, requires slowing down the ram and lowering productivity.

(2) **Dies**

- Inadequate die bearing design causes excessive twist in the extrusion. As a result, scrap losses increase and/or handling requirements for stretching and twisting increase.

- In multiple-hole dies, inadequate die design causes variable runout lengths. If one or more sections are too short or too long, scrap losses increase.

- Unnecessarily long bearings and excessively large reduction ratio slows down production.

- New dies requiring more than one trial waste valuable press time and increase scrap losses.

- Dies designed to give an extrusion within tolerances, but having dimensions on the heavier side, result in loss of material and reduce yield.

For the purpose of illustrating the potential cost benefits of CAD/CAM application, we consider an extrusion plant as follows:

- Equipment: Four extrusion presses, 1000 to 5000 ton capacity.

- Plant Capacity Per Year: 48 million pounds gross (this value is estimated by considering that a 2500-ton press can process 12 million pounds of billets when operating five days/week and two 8-hour shifts/day[19]).

- Cost Per Press Per Hour: $100 to $200, average $150.

- Equipment Utilization Rate: 60 percent (50 to 60 percent is considered average in the industry[19]).

- Material Utilization: Shipped product weight versus incoming billet weight is 75 percent. (This value varies between 70 to 85 percent[19]; 15 to 30 percent scrap is due to (a) butt length, (b) lengths of extrusion on both ends, used for stretching and twisting, and (c) scrap due to high twist, unequal runout length in multiple-hole dies, or insufficient die fill).

- New Dies Per Year: 1000 (reasonable for a four press plant).

- Estimates Made Per Year: 6000 (considering that only 15 to 20 percent of quoted inquiries become firm orders).

- Time and Cost Per Estimate: 1/4 to 1 hour, an average $15 per estimate (considering that 1 man-hour costs about $30).

- Time and Cost for One Die Design: 1 to 8 hours[21,22], about $30 to $240, average $150.

- Manufacturing Cost Per Die: $150 to $1000 or more, average $300.

- Extrusion Tolerances: Average (the dimensions of the extrusion are not close to lower tolerance range, the dimensions of orifices of the same shape in the same die are not exactly identical).

● Average Number and Cost of Trials Per New Die: Two;
$10 to $30 per trial, average $20 per trial.

For the example plant, considered above, the application of CAD/CAM
may result in the following cost savings:

(1) Estimating: An average of 50 percent reduction in
estimating time is quite realistic. It is reported
that for standard structurals shapes, this time has
been reduced to one-fifth of conventional estimating
time [21,23]. This would result in annual savings of
$7.5 x 6000 = $45,000 per year.

(2) Die Design: Savings of 20 to 50 percent can be
expected [21,23], so that about 33 percent time cost
savings in average is a reasonable assumption. This
would result in $50 x 1000 = $50,000 per year.

(3) Die and Template Manufacturing: Considering that most
modern die shops use EDM and even wire EDM by optical
copying, the advantages of CAD/CAM here would be more
in quality and reproducibility and delivery date than
in cost reduction. Nevertheless, average cost reductions
may be in the order of 10 percent. This would result in
$30 x 1000 = $30,000 per year.

(4) Die Trials: Dies designed by CAD will reduce die trials
from two to one trial per die. This would save about
$20 x 1000 = $20,000 per year.

(5) Material Yield: The use of CAD/CAM will increase material
yield in three ways:

● For a given press, the billet length will be more
accurately optimized, so butt length losses will
be reduced.

● In multiple-hole dies, the runout lengths will be
more even than before, so scrap losses will be
reduced.

- The dies will be manufactured to the lower limit of
  thickness and width tolerances; thus, the extrusions
  delivered to customers will be lighter in weight,
  while satisfying tolerance requirements.

As a result, the material yield will increase. It is
difficult to estimate how much this increase could be.
A probable one percent increase in yield would mean, in our
example, 480,000 pounds. With an average cost of $0.75
per pound, this would result in a savings of $360,000.
If we assume a 1/2 percent increase in material yield,
the savings would be $180,000 per year.

(6) Press Time: The use of optimized billet length and
reduction of die trials will also increase press
productivity and provide additional press time.
Provided this additional press time is used for increased
production, additional savings would result. However,
These are difficult to estimate and may be ignored in
the present cost-benefit study.

In summarizing, for the illustrative example plant of 48 million
pounds gross (billet weight) capacity, the total potential savings per year
would be in the order of:

$45,000	Estimating
$50,000	Die Design
$30,000	Die manufacture
$20,000	Die trials
$180,000	Assuming 1/2 percent increase in material utilization
$325,000	TOTAL.

These figures assume that the CAD/CAM system is fully operational
and staff has been trained to utilize the system to its full potential.
Obviously, for smaller plants, the savings would be correspondingly smaller
and the amount of savings for various operational steps would also vary from
plant to plant. However, the example reviewed above illustrates that for
extrusion plants with large capacity, CAD/CAM system would offer advantages
in the medium and long-range.

Precision Forging of Turbine and Compressor Blades

A typical sequence of forging titanium blades is given in Table VIII. This sequence is for a forging process, which has been entirely debugged and made operational. In establishing this process sequence, several "interactions" or die try-outs are necessary as indicated by step 16. Using the general procedure for cost-benefit analysis, discussed earlier, the major operations which are affected by computer applications are given in Table IX. (Values of estimated percentage costs before and after CAD/CAM application are for a production lot are also given, as well as a brief reason for cost reduction).

The estimated figures given in Table IX will vary with material, size of blade and the specific capabilities of a given forge stop. However, experience in blade forging technology indicates that these figures are realistic. In this example savings of approximately 20 percent are estimated. By considering on one hand the number of blade types, lot sizes and total production, and on the other hand the cost of CAD/CAM hardware and software; it will be possible to make a final economic analysis. This analysis will then allow one to decide whether CAD/CAM is an economically attractive alternative in a specific forge shop.

Rolling of Airfoil Shapes

A cost estimate comparison between conventional rolling practice and one that uses CAD/CAM techniques, is given in Table X. It is based on the relative contributions of various major manufacturing activities to the overall product cost. The estimates in Table X will vary with material, product size mix as well as established practices. However in any case, savings of 10% to 20% would be expected.

The savings factor would be larger for smaller lots and smaller for larger lots. In a given shape rolling plant, the justification should be based on actual dollar figures. However, usual cost accounting practice makes it very difficult to assess actual costs of individual manufacturing activities.

TABLE VIII. A TYPICAL SEQUENCE OF OPERATIONS IN PRECISION FORGING OF TITANIUM FAN BLADES
(Variations exist depending on installation and blade geometry)

Operation	Equipment	Major Input (Material, Labor, Energy)

1. Quality Control on Stock
   Composition
   Dimensions
   Surface Finish
	-
	-
	Visual
		
		Labor

2. Billet Separation	Saw	Energy/Labor
3. Billet Coating	Spray or Dipping Machine	Energy/Labor/Coating
4. Billet Heating	Furnace/Induction Heater	Energy (Electric, Gas)
5. Preforming (Extrusion/Upsetting)	Preform Machine (Extrusion Press/Upsetter)	Labor
6. Quality Control	Visual	Labor
7. Surface Treatment (Sand Blast/ Chem Mill)	Sand Blaster/Tumbler Chem Mill Tank	Energy
8. Preform Coating	Spray or Dipping Machine	Energy/Labor/Coating
9. Preform Heating	Furnace	Energy (Electric, Gas)
10. Die Forging (Blocker)	Forging Press/Dies	Labor/Die Lubricant Energy (Die Heating)
11. Trimming	Trim Press/Dies (Trim Saw)	Labor
12. Surface Treatment (Sand Blast/ Chem Mill)	Sand Blaster/Tumbler Chem Mill Tank	Energy
13. Blocker Coating	Spray or Dipping Machine	Energy/Labor/Coating
14. Blocker Heating	Furnace	Energy (Electric, Gas)
15. Die Forging (Finish)	Forging Press/Dies	Labor/Die Lubricant Energy (Die Heating)
16. Inspect dimensions, return to step 1, make changes in 2,5,10,15 and repeat steps 1 thru 15, iterate until desired tolerances are obtained		
17. Trimming	Trim Press/Dies (Trim Saw)	Labor

TABLE VIII. (Continued)

Operation	Equipment	Major Input (Material, Labor, Energy)
18. Surface Treatment (Sand Blast/ Chem Mill)	Sand Blaster/Tumbler Chem Mill Tank	Energy
19. Quality Control		
Dimensions	Gages	Labor
Surface Cracks	Dye Penetrant	Labor
20. Heat Treatment	Furnace	Energy
21. Straightening	Straightening Fixture	Labor
22. Surface Polishing	Polishing Machine	Energy
23. Final Inspection		
Dimensions	Gages	Labor
Surface Finish	Visual	Labor
Mechanical Properties	Mechanical Testing Machine	Labor

TABLE IX. ESTIMATED COSTS IN BLADE FORGING BEFORE AND AFTER
APPLICATION OF CAD/CAM (IN PERCENT OF COSTS IN
CONVENTIONAL FORGING PROCEDURE, WITHOUT CAD/CAM)

Costs for Major Activity	Before	After	Brief Reason
Estimating/Planning	3	3	Computerization reduces some of the costs but increases the effort for initial data preparation and handling
Material	50	45	Improved process control and die design reduces scrap and flash losses
Energy	3	3	No appreciable difference
Die (Design, Manu-facture and Modi-fication)	8	4	Numerical drafting and NC machining reduce design and manufacture costs drastically
Machine Utilization	5	5	No appreciable difference
Post Forging Operations	12	10	Dies with reproducible dimensions provide consistency and reduce need for straightening
Quality Control	4	4	No appreciable difference, unless QC is automated
Process Development/Die Try-Outs	15	7	CAD makes predictions for preform design and for finish die design, as a result trial and error are minimized
TOTAL	100	84	

TABLE X.   ESTIMATED COSTS IN ROLLING OF AIRFOILS.   COMPARISON
BETWEEN CONVENTIONAL PRACTICE AND THE APPLICATION OF
CAD/CAM TECHNIQUES

Major Activity	% Cost Conventional	% Cost CAD/CAM	Remarks
Estimating/Planning	4	3	Though routine calculations are automated, input data requirements are more stringent.
Material	45	40	Improved process and die design would reduce scrap and flash losses.
Energy	3	3	No appreciable difference.
Die Design and Manufacture	9	5	Design chores are automated, tryouts are minimized. NC machining provides repeatability. Designs are more consistent.
Machine Utilization	5	5	No appreciable difference.
Post Rolling Operations	15	12	Somewhat less costly due to improved product definition in as rolled condition.
Process Development	15	10	Tryouts minimized due to computer simulation.
Quality Control	4	4	No difference unless also computer automated.
TOTAL	100%	82%	

REFERENCES

(1) Trinks, W., Roll-Pass Design, Volumes I and II, The Penton Publishing Company, 1941.

(2) Beynon, R. E., Roll Design and Mill Layout, Association of Iron and Steel Engineers, Pittsburgh, Pennsylvania, 1956.

(3) Hoff, E. H., and Dahl, T., Rolling and Roll-Shape Design, (in German) Verlag Stahleisen, Dusseldorf, 1954.

(4) Neumann, H., Shape Design of Rolls, (in German) VEB Deutscher Verlag, Leibzig, 1969.

(5) Kruger, C. M., Considerations on the Theory and Practice of Roll-Pass Design, (in German) Stahl und Eisen, 81, 1961, p 858.

(6) Schutza, A., Comparison of Practical Roll-Pass Designs for Angles, (in German) Stahlund Eisen 90, 1970, p 796.

(7) Rheinhausen, H. K., and Menne, H., Different Roll-Pass Designs for U Profiles, (in German) Stahl und Eisen, 90, 1970, p 801.

(8) Wusatowski, Z., The Average Elongation in Shape Rolling, (in German) Neue Hutte, 2, 1957, p 24.

(9) Neumann, H., Division of a Profile Into Components in Rolling of Steel I-Beams, (in German) Neue Hutte, I, 1962, p 480.

(10) Douglas, J. R., Altan, T., and Fiorentino, R. J., "Isothermal Uniform Compression Test for Determining Flow Stress of Metals at Forging Temperature", Chapter 3, A Study of Mechanics of Closed-Die Forging, Phase II, Final Report, (1972) AMMRC-CTR 72-25, Contract No. DAAG46-71-C0095.

(11) Kobayashi, S., Lee, C. H., and Oh, S. I., "Workability Theory of Materials in Plastic Deformation Processes", USAF Technical Report AFML-TR-73-192, May 1973.

(12) Burgdoff, N., "Investigation of Friction Values for Metal-Forming Processes by Ring Compression Method", (in German), Industrie-Anzeiger, Vol. 89, 1967, p 799.

(13) Lee, C. H., and Altan, T., "Influence of Flow Stress and Friction Upon Metal Flow in Upset Forging of Rings and Cylinders", ASME Transactions, J. Engr. Ind., Vol. 94, No. 3, August 1972, p 775.

(14) Metals Handbook, Vol. 7, Eighth Edition, American Society for Metals, Metals Park, Ohio 44073, 1973.

(15) Luton, M. J., and Sellows, C. M., "Dynamic Recrystallization in Nickel and Nickel-Iron Alloys During High Temperature Deformation", Acta. Met., Vol. 17, 1969, pp 1033-43.

(16) Lahoti, G. D., Clauer, A. H., Rosenfield, A. R. and Altan, T., "Application of Process Modeling to Hot-Isothermal Rolling of Titanium Alloy Strips," presented at the TMS-AIME Symposium on "Formability, Analysis, Modeling and Experimentation," October 24-27, 1977, Chicago, Illinois, to be published in proceedings.

(17) Whittenberger, J. D., and Moore, T. J., "Elevated-Temperature Flow Strength, Creep Resistance and Diffusion Welding Characteristics of Ti-6Al-2Nb-1Ta-0.8Mo," NASA Technical Memorandum, NASA TM-73854, December 1977.

(18) Thomsen, E. G., Yang, C. T., and Kobayashi, Mechanics of Plastic Deformation in Metal Processing, The McMillan Company, New York, 1964.

(19) Ferguson, R. T., "Evaluating Extrusion Plant Operations", Light Metal Age, April, 1969, p 6.

(20) Waugh, T. L., "Controlling Extrusion Plant Costs", Proceedings of Second International Symposium on Extrusion Technology, November, 1977, Atlanta, Georgia, p 107.

(21) Post, C. T., "The Strong Link that Ties CAD to CAM", Iron Age, August 22, 1977, p 29.

(22) Watts, G. A., and Veenman, P., "Computer-Aided Design in the Non-Ferrous Metals Industry", Computer-Aided Design, Vol. 8, No. 1, January 1976, p 13.

(23) Private Communication with Mr. Mel Henley, Manager, Computer-Aided Die Design and Manufacturing, Martin Marietta Aluminum, Torrance, California.

APPENDIX A

DETERMINATION OF FLOW STRESS, WORKABILITY AND FRICTION FACTOR

APPENDIX A

DETERMINATION OF FLOW STRESS, WORKABILITY AND FRICTION FACTOR

The two basic material characteristics that greatly influence the rolling process are the flow stress and the workability of the material being rolled. The flow stress represents the resistance of a material to plastic deformation, and the workability represents its ability to deform without failure, regardless of the magnitude of the local stress and strain rate required for deformation. In shape rolling process, relatively moderate strains and strain rates are encountered in the deforming material. Consequently, the response of the alloys of interest must be determined in the practical range of temperatures, strains, and strain rates. Another important variable to be characterized is the friction factor (ratio of frictional shear stress to shear flow stress) at the tool-material interface.

The mild steel (AISI 1018 in the present case) and the superalloy (Inco 718) can be cold worked. The typical hot-working temperature for Ti-6Al-4V alloy is 927 C (1700 F). Therefore, it is appropriate to determine the flow stress and workability of AISI 1018 steel and Inco 718 at room temperature, and those of Ti-6Al-4V alloy at 927 C (1700 F). The experimental set-up is shown in Figure A-1.

UNIFORM COMPRESSION TESTS

Specimens were machined to a nominal diameter of 12.7 mm (0.500 inch), a nominal height of 19.1 mm (0.750 inch), and sharp corners were broken. They were cleaned with acetone and placed on teflon sheets in between hardened steel platens (65 Rockwell C). The test conditions are summarized in Table 1.

The AISI 1018 tests were conducted in a Baldwin universal testing machine of 267 kN (60,000 lb) capacity. More load was required for INCO 718, hence, a 445 kN (100,000 lb) capacity machine was used. The teflon sheets were replaced at every 10% reduction in order to ensure adequate lubrication and prevent bulging. Three specimens of each material were tested.
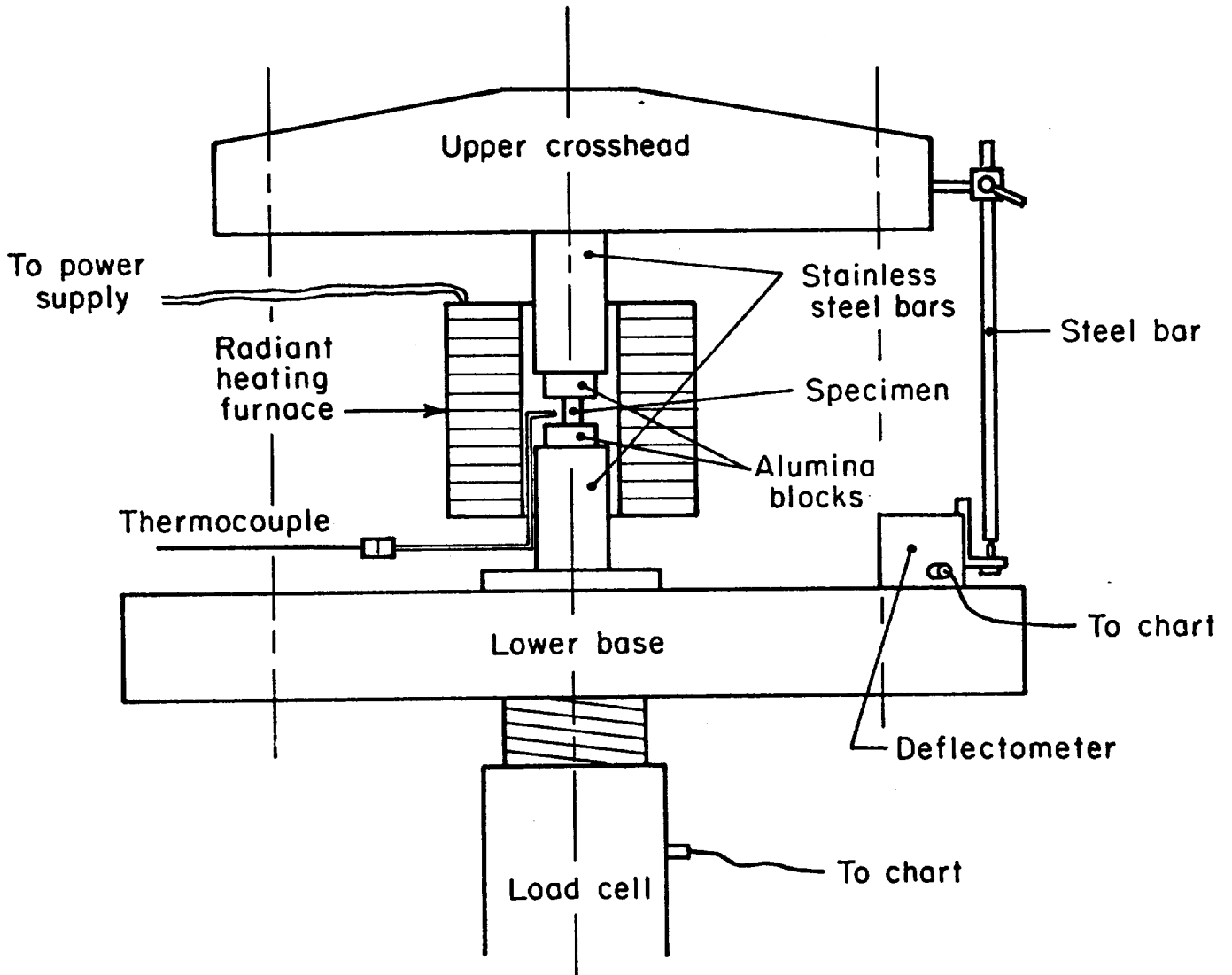
FIGURE A-1.   EXPERIMENTAL SET UP ON A UNIVERSAL TESTING
MACHINE FOR HOT UPSET TESTS

The Ti-6Al-4V tests were conducted under isothermal conditions at 927 C (1700 F) using powdered window glass as lubricant. The experimental set up is illustrated in Figure A-1. A spiral groove was machined at the ends of each specimen to enhance lubricant retainment and ensure uniform upset conditions. Three specimens were tested. A summary of uniform upset test results is given in Table 2.

A typical load-displacement curve, obtained during upsetting of an AISI 1018 steel specimen, is illustrated in Figure A-2. From the load-displacement curves, the necessary calculations to obtain the flow stress versus strain curves, given in Figures A-3 through A-5, were made using a simple computer program and a PDP-11 minicomputer. Figure A-6 shows specimens from the three materials before and after deformation in uniform upset tests.

WORKABILITY TESTS

Workability tests were conducted for AISI 1018 and INCO 718 at room temperature. 12.7 mm (0.5-inch) diameter, 19.1 mm (0.750-inch) long nonlubricated cylindrical specimens were compressed in a universal testing machine until cracks appeared. AISI 1018 specimens were compressed 70 percent without any cracks, at which point the test was stopped. INCO 718 specimens showed classical 45 degree cracks at approximately 56 percent ± 2 percent reduction consistently. Figure A-7 shows an INCO 718 specimen which cracked at 56 percent reduction in height and an uncracked AISI 1018 steel specimen which was compressed to 70 percent reduction in height.

RING UPSET TESTS

Ring tests with AISI 1018 and INCO 718 samples were conducted at room temperature using essentially the same experimental set up as that used for uniform compression and workability tests. Ring specimens were machined to have 19.1 mm (0.750-inch) OD x 9.52 mm (0.375-inch) ID x 6.35 mm (0.250-inch) height. Rings were upset between flat hardened platens to approximately 15, 30 and 40 percent reduction in height. In order to approximate the friction conditions, which are present during

TABLE 1. UNIFORM COMPRESSION TEST CONDITIONS

MATERIAL	CONDITION	TEST TEMP.	TEST MACHINE	CROSSHEAD SP.	LUBRICANT
AISI 1018	Annealed at 871 C (1600 F) for 1 hr Furnace Cooled	Room Temperature	Baldwin Capacity 267 kN (60.000 lb)	0.5 mm/min (0.02 inch/min)	Teflon Sheet 0.010 inch (.254 mm)
INCO 718	Annealed at 982 C (1800 F) for 1 hr. Air Cooled	Room Temperature	Baldwin Capacity 445 kN (100.00 lb)	0.5 mm/min (0.02 inch/min)	Teflon Sheet 0.010 inch (.254 mm)
Ti-6Aℓ-4V	As Received	927 C (1700 F)	Baldwin Capacity 267 kN (60.000 lb)	25.4 mm/min (1 inch/min)	Window Glass

NOTES: 1) Nominal dimensions of all samples were 12.7 mm (0.500-inch) diameter x 19.1 mm (0.750-inch) high.

2) During the tests that were conducted at room temperature, the lubricant (teflon sheet) was replaced at every 10 percent reduction.

TABLE 2. SUMMARY OF UNIFORM COMPRESSION TEST RESULTS

Specimen Number	Material/ Temperature	Lubricant	Initial Diameter, mm (inch)	Initial Height, mm (inch)	Final Diameter, mm (inch)	Final Height, mm (inch)	Reduction in Height, Percent	Maximum Load kN (lb x 10^3)
AC1	AISI 1018 (ROOM TEMPERATURE)	TEFLON	12.72 (0.501)	19.05 (0.750)	16.18 (0.637)	11.76 (0.463)	38	127.6 (28.7)
AC2			12.82 (0.505)	19.05 (0.750)	16.58 (0.653)	11.17 (0.440)	41	124.1 (27.9)
AC3			12.75 (0.502)	19.05 (0.750)	16.45 (0.648)	11.40 (0.449)	40	121.8 (27.4)
IC1	INCO 718 (ROOM TEMPERATURE)	TEFLON	12.72 (0.501)	19.07 (0.751)	16.15 (0.636)	11.81 (0.465)	38	315.8 (71.0)
IC2			12.82 (0.505)	19.05 (0.750)	16.45 (0.648)	11.40 (0.449)	40	329.6 (74.1)
IC3			12.72 (0.501)	19.05 (0.750)	16.43 (0.647)	11.40 (0.449)	40	329.2 (74.0)
TC1	Ti-6Aℓ-4V (927 ± 5 C)	WINDOW GLASS	12.82 (0.505)	18.39 (0.724)	15.31 (0.603)	13.20 (0.520)	28	9.2 (2.07)
TC2			12.70 (0.500)	18.99 (0.748)	15.59 (0.614)	13.15 (0.518)	31	9.3 (2.10)
TC3			12.72 (0.501)	19.06 (0.7505)	16.89 (0.665)	11.45 (0.451)	40	10.1 (2.28)
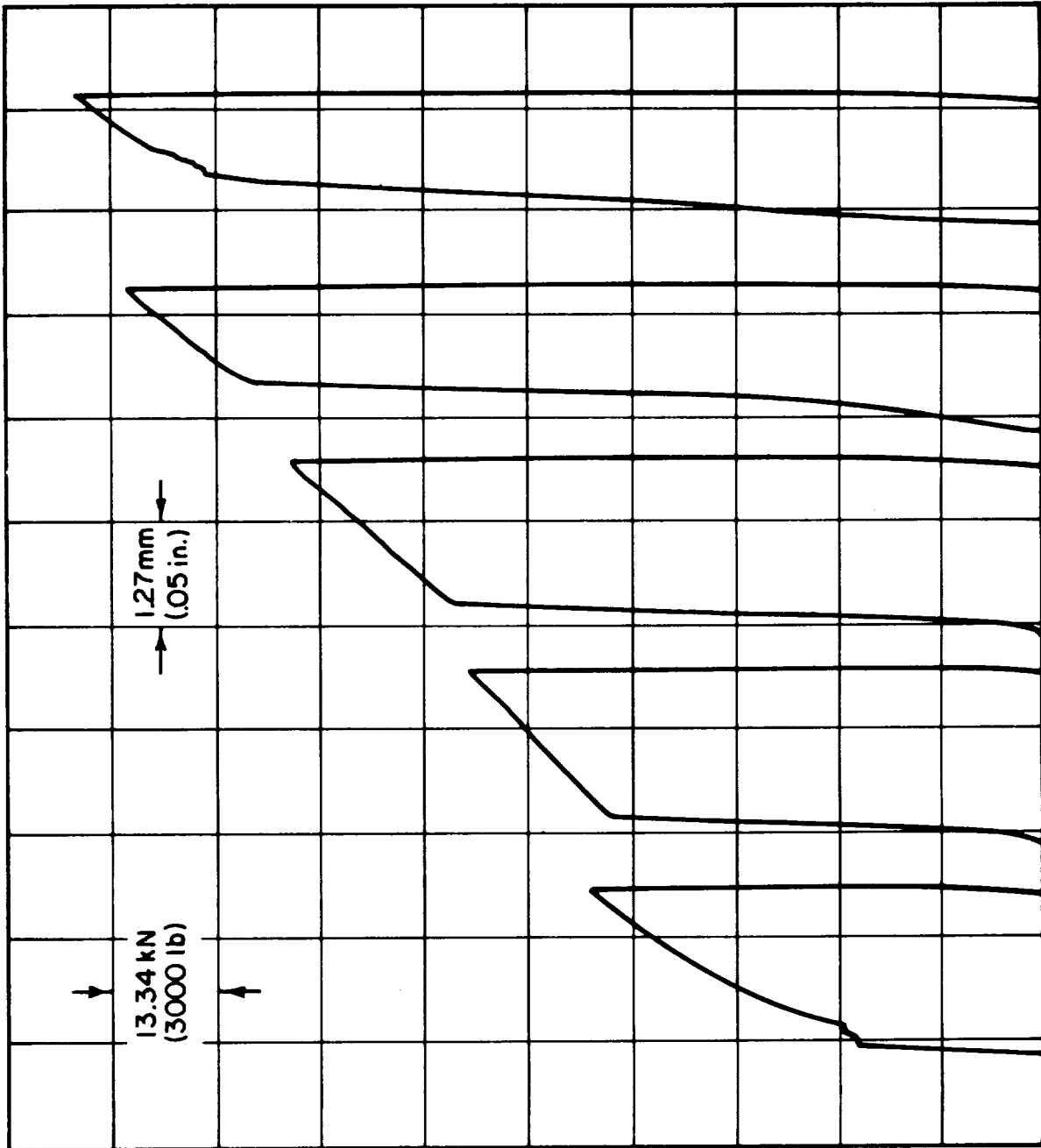
FIGURE A-2. LOAD VERSUS DISPLACEMENT CURVE IN UNIFORM COMPRESSION OF AISI 1018 STEEL CYLINDER AT ROOM TEMPERATURES (The test was conducted in five steps and the Teflon sheets were replaced at the beginning of each step)
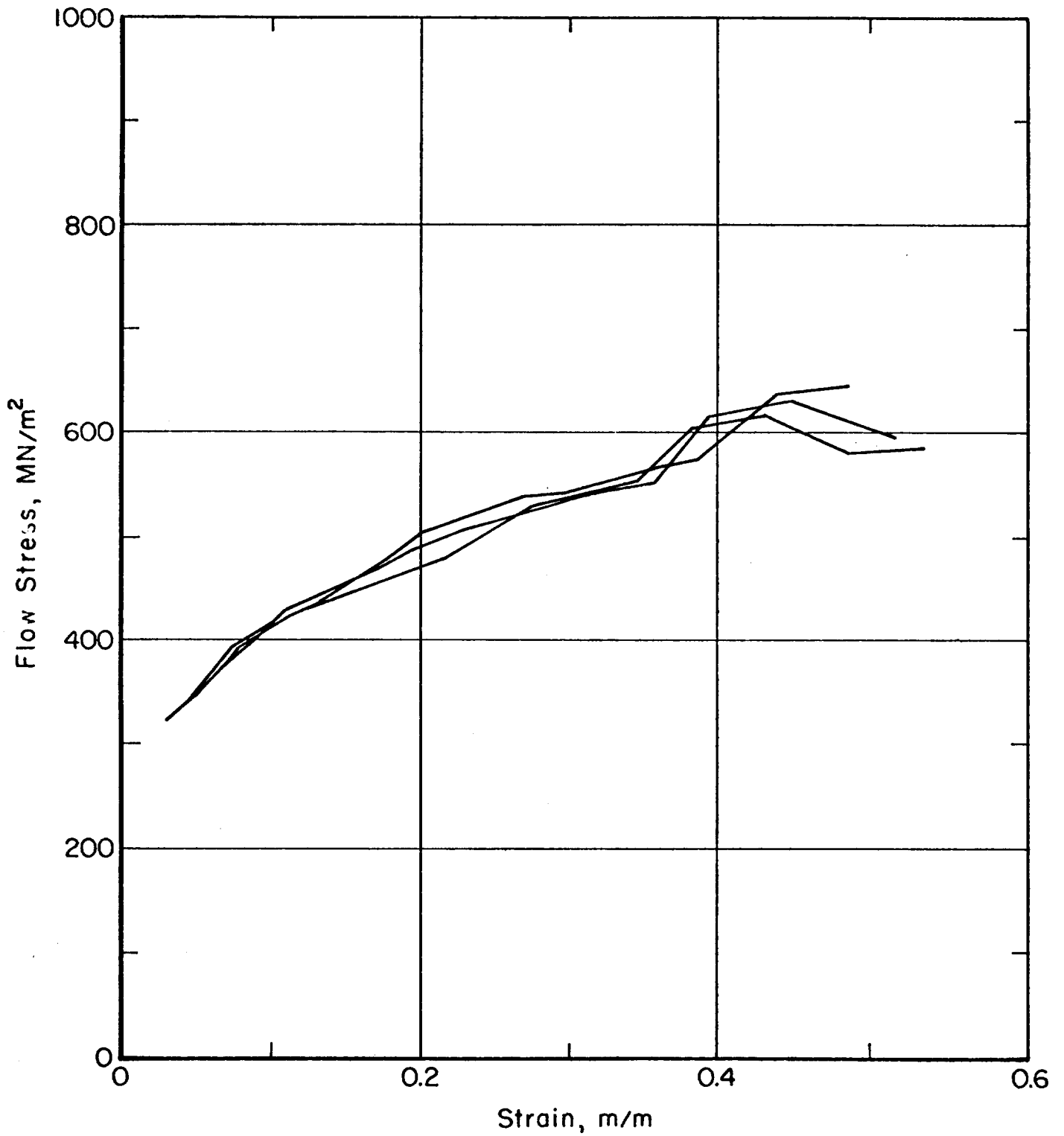
FIGURE A-3. UNIFORM COMPRESSION TEST RESULTS FOR AISI 1018 AT ROOM TEMPERATURE
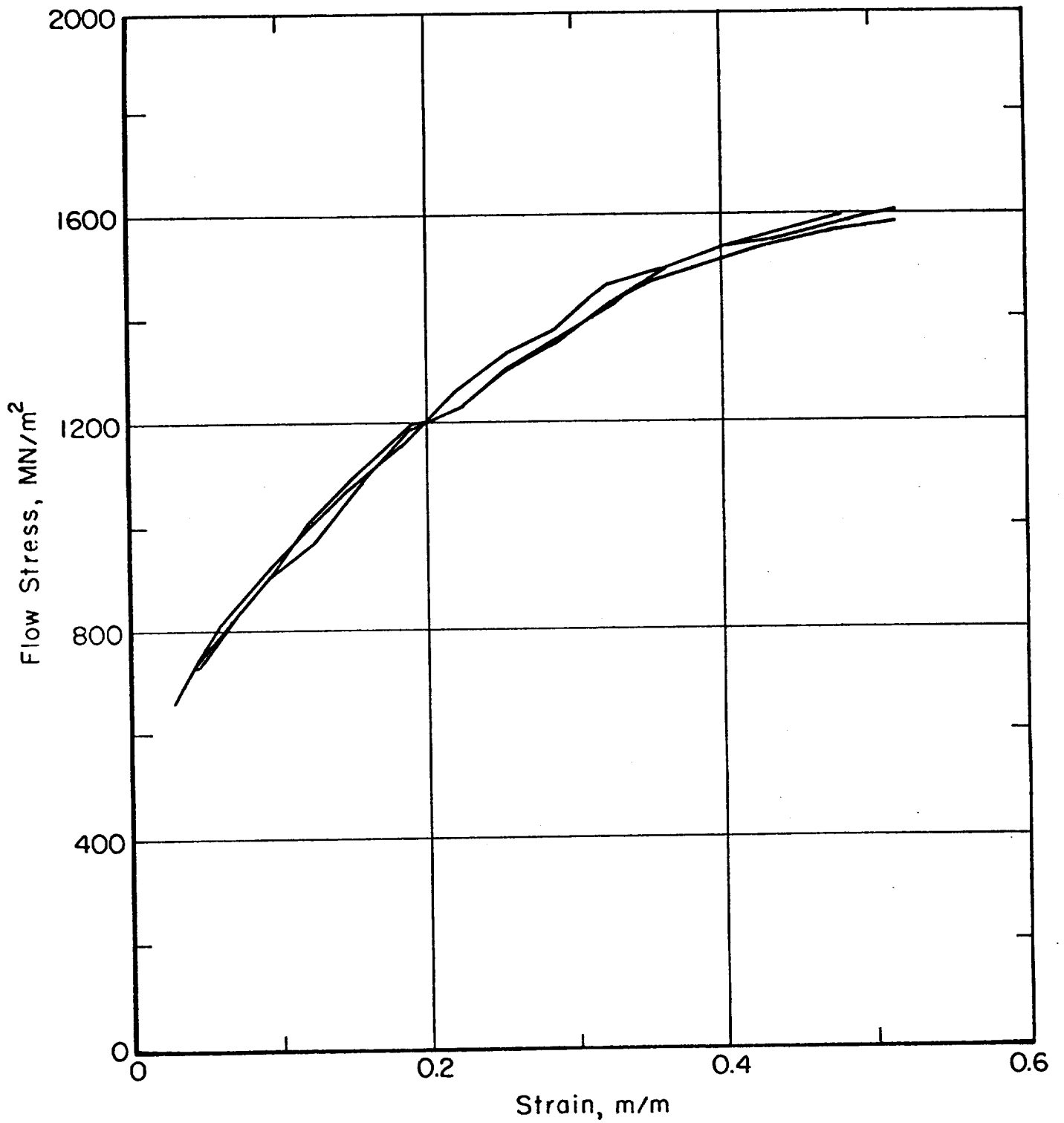
FIGURE A-4. UNIFORM COMPRESSION TEST RESULTS FOR INCO 718 AT ROOM TEMPERATURE
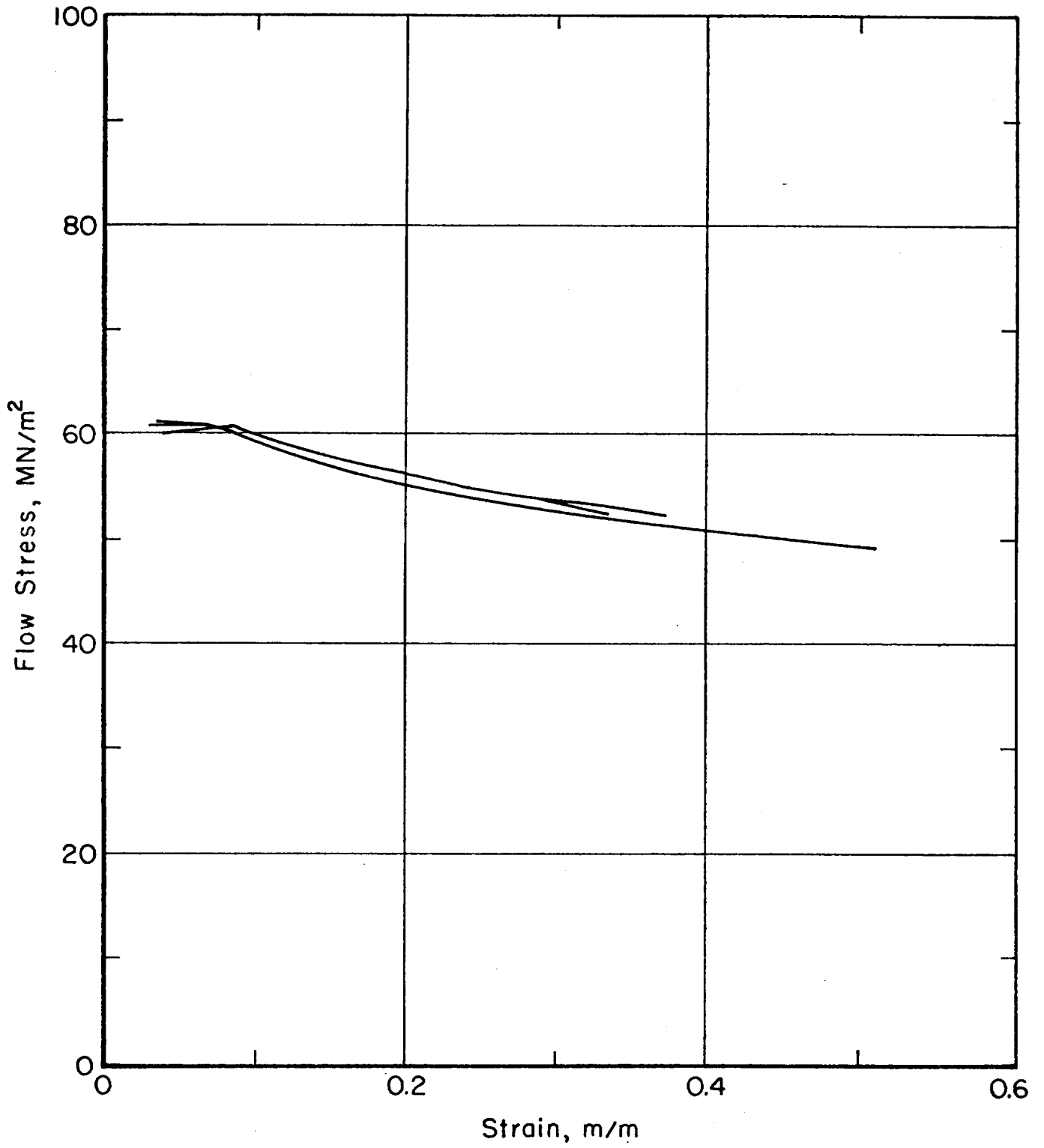
FIGURE A-5.   UNIFORM COMPRESSION TEST RESULTS FOR Ti-6Aℓ-4V AT 927 C (1700 F)

FIGURE A-6.   UNIFORM COMPRESSION SAMPLES BEFORE AND AFTER DEFORMATION
(Left to Right: AISI 1018 Steel, INCO 718, Ti-6Al-4V Alloy)

(a)   (b)

FIGURE A-7. DEFORMED SAMPLES FROM NONUNIFORM COMPRESSION
             TESTS FOR DETERMINING WORKABILITY (Left to
             Right: INCO 718 Specimen after 56 Percent
             Reduction; AISI 1018 Steel Specimen after 70
             Percent Reduction)

cold shape rolling in practice, the rings were dipped into a drawing lubricant (Turco Draw 300) prior to upsetting. After the tests, the dimensions of the rings were measured. A summary of the ring test results is given in Table 3. The friction shear factor m was determined from the variation of the internal ring diameter by using the theoretical calibration curves given in Figure A-8. The results show that the friction factor m is approximately 0.3 for INCO 718 and 0.25 for AISI 1018. Figure A-9 shows AISI 1018 steel rings before deformation and after 20, 30 and 40 percent reduction in height. Figure A-8 also shows the ring test results for Ti-6Al-4V alloy under hot-isothermal conditions.

TABLE 3. SUMMARY OF RING TEST RESULTS AT ROOM TEMPERATURE (LUBRICANT: TURCO DRAW 300, CROSSHEAD SPEED = 0.42 mm/sec (1.0 inch/min))

Specimen No.	Material	Initial OD, mm (inch)	Initial ID, mm (inch)	Initial Height, mm (inch)	Final ID, mm (inch)	Final Height, mm (inch)	Reduction in Height, Percent	Decrease in Minimum Bore Dia. Percent
IR1	INCO 718	9.52 (0.375)	19.05 (0.750)	6.37 (0.251)	9.39 (0.370)	5.38 (0.212)	15.6	1.33
IR2	INCO 718	9.52 (0.375)	19.15 (0.754)	6.35 (0.250)	9.09 (0.358)	4.01 (0.158)	36.8	4.50
IR3	INCO 718	9.47 (0.373)	19.07 (0.751)	6.35 (0.250)	8.89 (0.350)	3.83 (0.151)	39.6	6.10
AR1	AISI 1015	9.50 (0.374)	19.05 (0.750)	6.35 (0.250)	9.16 (0.361)	5.05 (0.199)	20.4	3.48
AR2	AISI 1015	9.47 (0.373)	49.07 (0.751)	6.32 (0.249)	9.29 (0.366)	4.47 (0.176)	29.3	2.4
AR3	AISI 1015	9.52 (0.375)	19.07 (0.751)	6.32 (0.249)	9.37 (0.369)	3.83 (0.151)	39.3	1.6
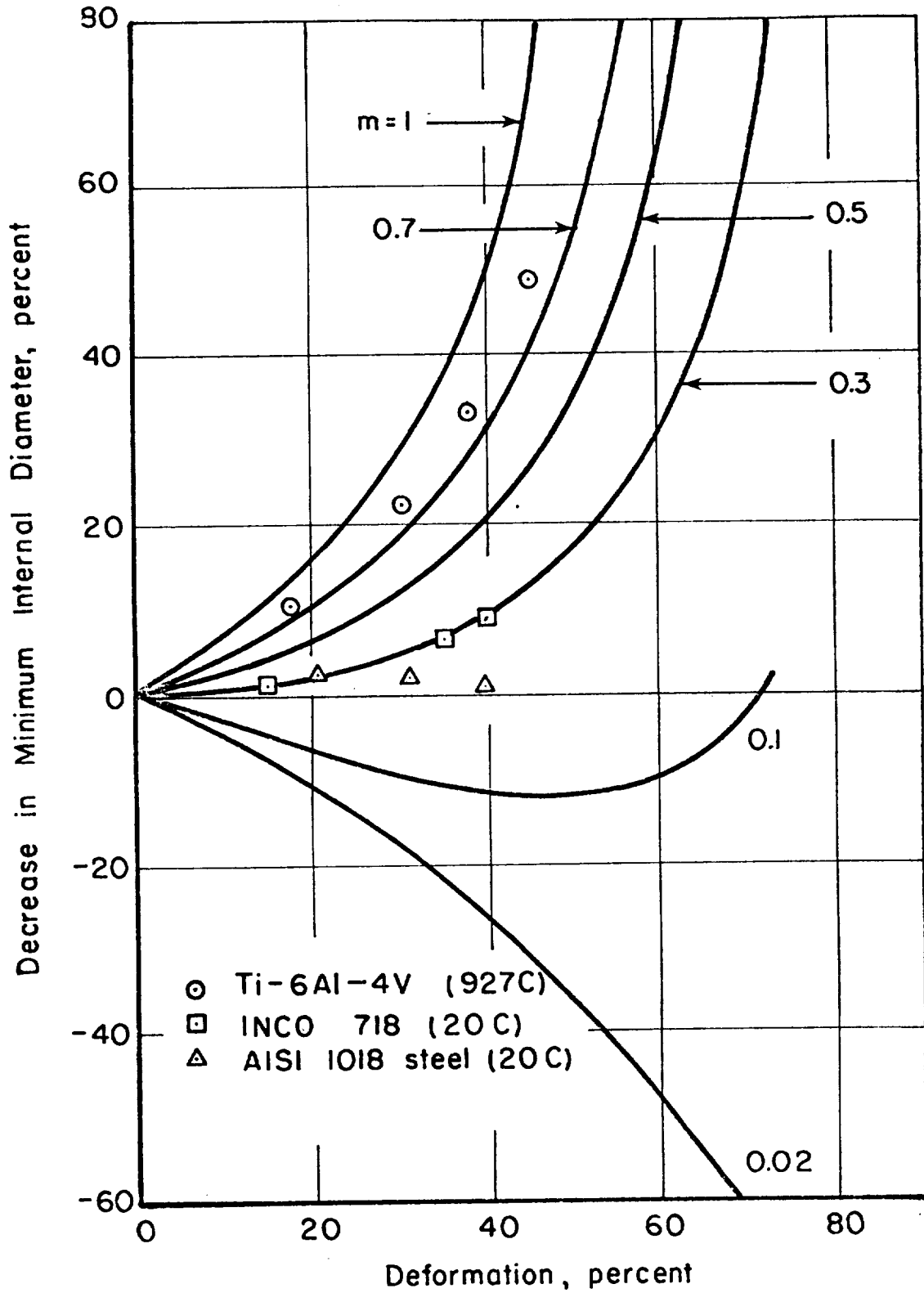
FIGURE A-8. THEORETICAL CALIBRATION AND EXPERIMENTAL POINTS
FOR DETERMINING FRICTION FROM UPSETTING 6:3:2
RINGS

FIGURE A-9. AISI 1018 RINGS BEFORE AND AFTER DEFORMATION
(Left to Right: Reduction in Height 0, 20,
30 and 40 Percent, Respectively)

APPENDIX B

ANALYSIS OF METAL FLOW IN ROLLING OF AIRFOIL SHAPES

APPENDIX B

ANALYSIS OF METAL FLOW IN ROLLING OF AIRFOIL SHAPES

In rolling of shapes, the material elongates in the rolling direction as
well as it spreads in the transverse direction. Thus, an analysis of deformation
in rolling of airfoil shapes includes not only the determination of roll torque and
the location of the neutral plane, but also the determination of spread in the trans-
verse direction. The purpose of the present analysis is to determine the distribution
of metal flow during rolling of a bar with an initial arbitrary section through a pair
of rolls with airfoil-like contours.

Assumptions

The present analysis employs the upper-bound type theory to predict the
distribution of metal within the deformation zone between the rolls. One essential
feature of applying the upper-bound technique to the present uncontained steady-state
metal flow problem is to find a kinematically admissible velocity field which does
not change the volume shape, and satisfies the volume constancy and the velocity
boundary conditions. It is usually very difficult to find an admissible velocity
field for problems involving general configurations even under nonsteady-state
conditions. The condition of steady-state makes the problem of determining an
admissible velocity field even more difficult. Therefore, a modular approach,
somewhat similar to the finite-element method, is developed here and the following
simplifying assumptions are made in performing the present analysis:

(1) An airfoil shape can be considered as an aggregate of slabs,
     as shown in Figure B-1.
(2) Plane sections perpendicular to the rolling direction remain
     plane during rolling. Thus, the axial velocity (i.e.,
     velocity in rolling x-direction) at any section perpendicular
     to the rolling direction is uniform over the cross section.
(3) The velocity components in the transverse y, and the thickness
     z directions are functions of x and linear in y and z coordi-
     nates, respectively. (See Figure B-1).
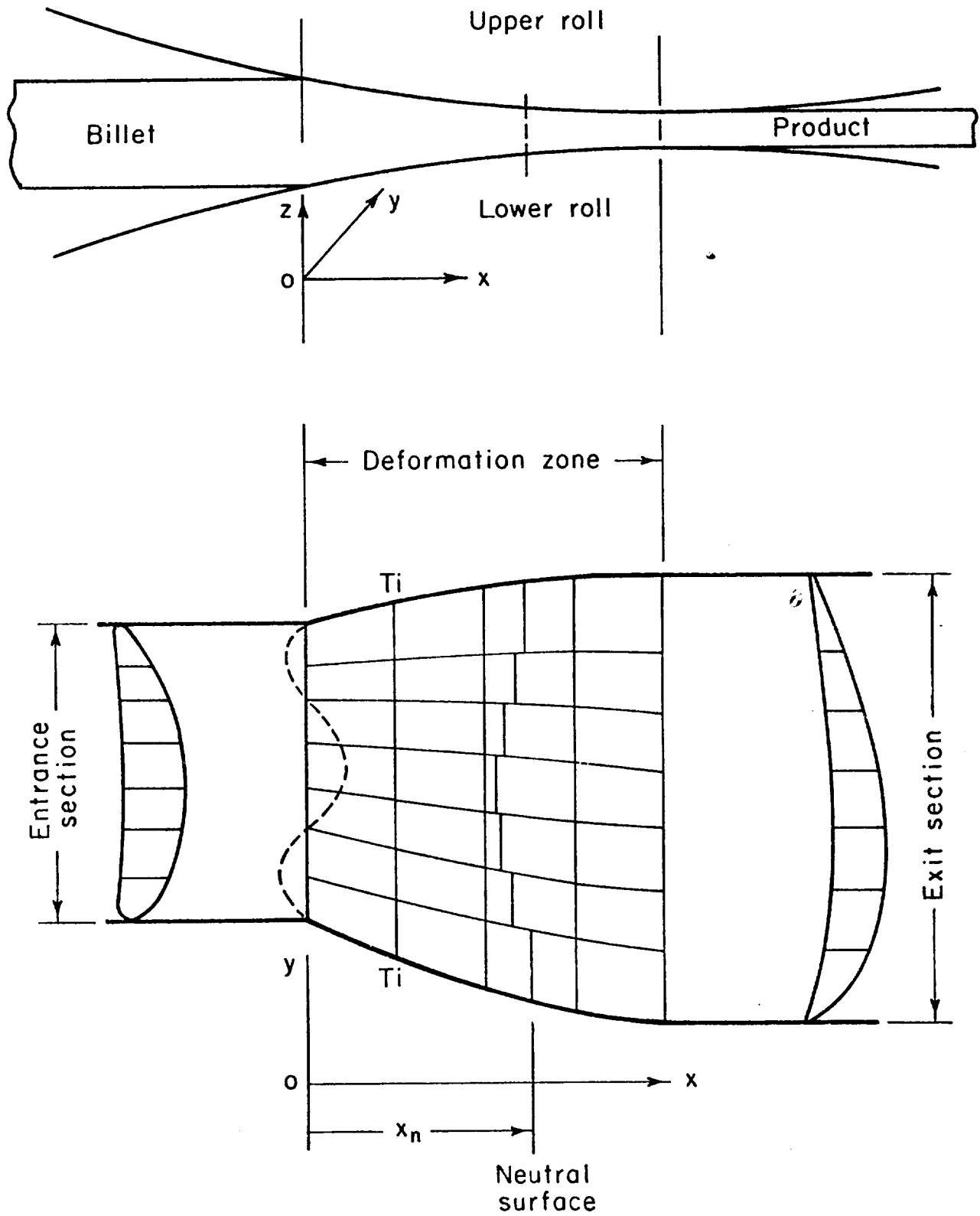
FIGURE B-1. CONFIGURATION OF DEFORMATION ZONE IN ROLLING OF AIRFOIL SHAPES

The above assumptions correspond approximately to actual metal flow conditions and have been shown to yield good predictions of metal flow in rolling of plates.

Coordinate Systems

In design of turbine engine airfoils, normally the cartesian coordinate (x,y,z) system is used. The x-, y- and the z- axes are defined along the width, length and the thickness of the airfoil, respectively. The coordinate system A, Figure B-2, in rolling of airfoil sections, is based on this accepted practice and will be used in the stress analysis and the calculation of the roll-separating force.

However, the coordinate system B, as shown in Figure B-2, is normally used in analyzing metal flow in rolling of plates and sheets. Here, the rolling direction is taken as the x- axis, and the y- and the z- axes are defined along the width and the thickness directions, respectively. Therefore, for the sake of convenience in developing the velocity field in rolling of airfoil shapes, the coordinate system B of Figure B-2 will be used in the following analysis.

Analysis

The method used in solving the present problem is somewhat similar to the finite-element method in the sense that the deformation zone is divided into quadrilateral elements on the x-y plane, as shown in Figure B-1. The divisions in the transverse (y-) direction are made such that the velocities normal to the dividing lines are zero. Thus, these lines represent streamlines of metal flow. However, a finite number of velocity discontinuities occur across the planes perpendicular to x-y plane and passing through these streamlines. The divisions along the longitudinal (x) direction, lines T_i-T_i, are made arbitrarily. Similarly, a finite number of velocity discontinuities occur across the y-z planes passing through these transverse lines, T_i-T_i, dividing the deformation zone.

It is assumed that the top and bottom surfaces of each element can be approximated by tapered planes, and the cross section of each element by a rectangle, as shown in Figure B-3, where the area under a rectangle with broken lines is equal to the area of the original element. With this assumption, it is possible to treat each element as a plate for which it is possible to derive a kinematically admissible
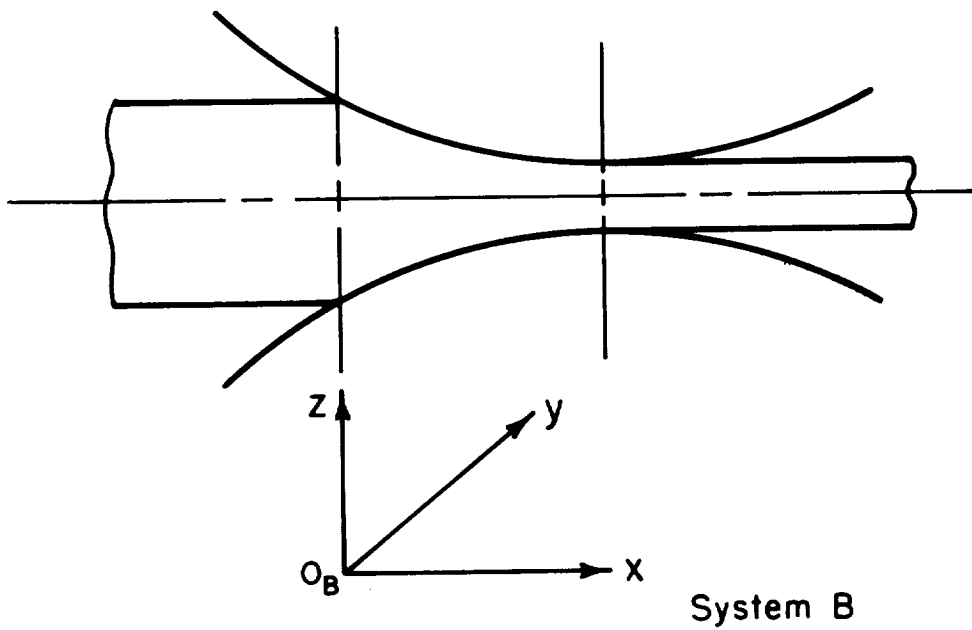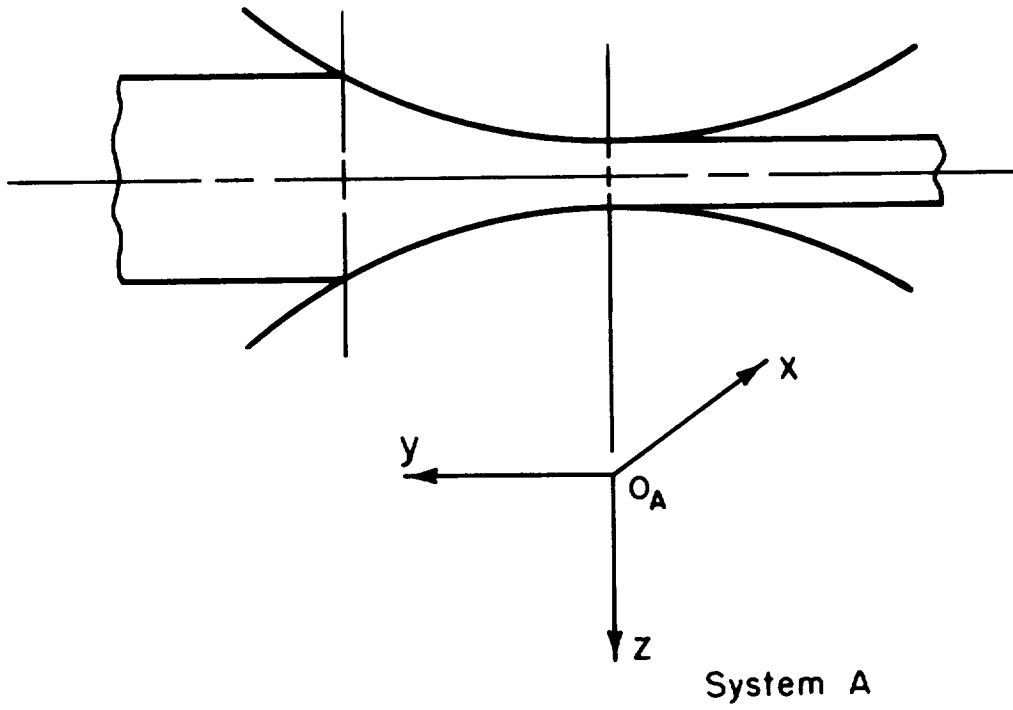
FIGURE B-2. COORDINATE SYSTEMS USED IN ANALYZING THE ROLLING OF AIRFOIL SHAPES
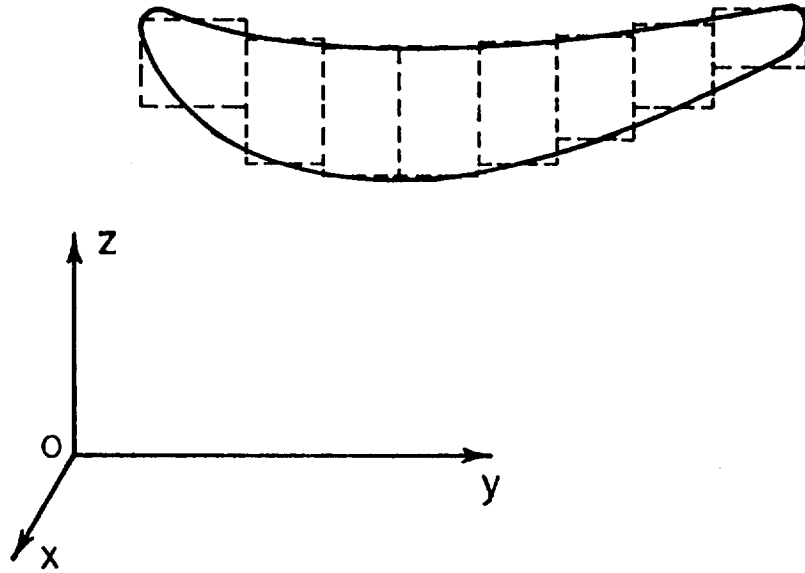
FIGURE B-3. DIVISION OF AN AIRFOIL SECTION INTO RECTANGULAR ELEMENTS

velocity field.

　　　Once the outer boundaries in the transverse (y) direction, namely, $y = w_1(x)$ and $y = w_2(x)$, are known, the location of longitudinal lines in the deformation zone, Figure B-4, can be computed from assumption (2), given above. In order to keep the number of unknown variables to a minimum, the curves $y = w_1(x)$ and $y = w_2(x)$ are considered as a third order polynomials, each with two unknowns. The location of the neutral plane, $x = x_n$, Figures B-1 and B-4, is an additional unknown. Thus, a total of five independent variables, which are determined by minimization of the total energy rate, are sufficient for the formulation of the problem.

Admissible Velocity Field

　　　Consider an element in the x-y plane, as shown in Figure B-5. A local coordinate system (ζ, ξ, η) is defined for an individual element. The coordinate of the origin of this system with respect to the global system (x,y,z) is designated by (X_1, Y) in the x-y plane and by (X_2, Z) in the x-z plane, and it is determined by finding the intersection of Lines I and II, as shown in Figure B-5. If (x_1, y_4) and (x_2, y_3) are the coordinates of Points 4 and 3, respectively, then the equation of Line I is given by:

$$y = f_1(x) = \frac{y_3 - y_4}{x_2 - x_1} (x - x_1) + y_4 \quad . \tag{B-1}$$

Similarly, if (x_1, y_1) and (x_2, y_2) are the coordinates of Points 1 and 2, respectively, the equation of Line II is given by:

$$y = f_2(x) - \frac{y_2 - y_1}{x_2 - x_1} (x - x_1) + y_1 \quad . \tag{B-2}$$

The coordinate (X_1, Y) are determined by solving Equations (B-1) and (B-2) as follows:

$$\left. \begin{aligned} X_1 &= \frac{(x_2 - x_1)(y_1 - y_4)}{(y_1 - y_2 + y_3 - y_4)} + x_1 \\[2em] Y &= \frac{(y_3 - y_4)(y_1 - y_4)}{(y_1 - y_2 + y_3 - y_4)} + y_4 \quad . \end{aligned} \right\} \tag{B-3}$$
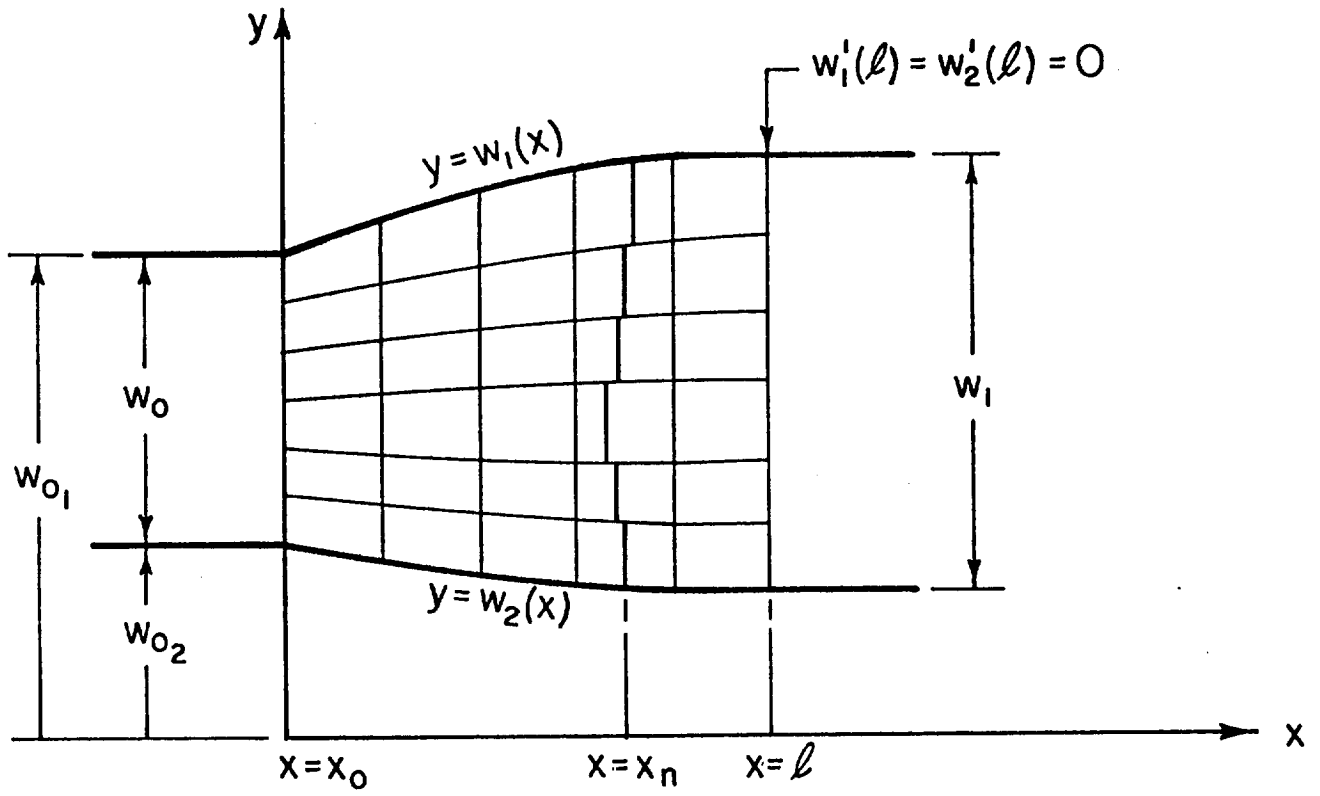
FIGURE B-4.   BOUNDARIES OF THE DEFORMATION ZONE
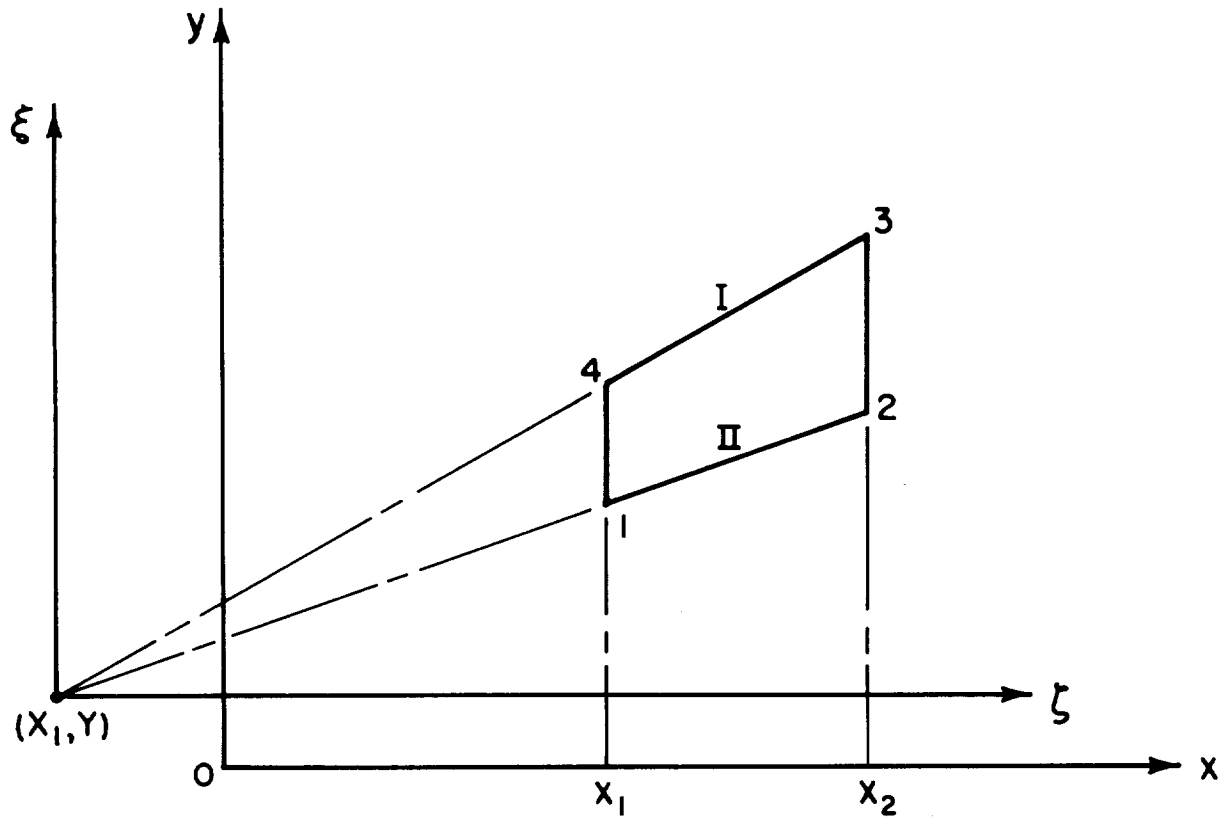
FIGURE B-5. CONFIGURATION OF AN ELEMENT IN THE x-y PLANE

Similarly, referring to Figure B-6, if (x_1, H_1), (x_2, H_2), (x_2, H_3) and (x_1, H_4) are the coordinates of Points 1, 2, 3 and 4, respectively, the equations of Lines III and IV are given by:

$$z = h_1(x) = \frac{H_3 - H_4}{x_2 - x_1} (x - x_1) + H_4 \tag{B-4}$$

$$z = h_2(x) = \frac{H_2 - H_1}{x_2 - x_1} (x - x_1) + H_1 \quad . \tag{B-5}$$

Then, the coordinate (X_2, Z) are given as:

$$X_2 = \frac{(x_2 - x_1)(H_1 - H_4)}{(H_1 - H_2 + H_3 - H_4)} + x_1 \tag{B-6}$$

$$Z = \frac{(H_3 - H_4)(H_1 - H_4)}{(H_1 - H_2 + H_3 - H_4)} + H_4 \quad .$$

For unit velocity of the incoming strip, if v_x, v_y, and v_z are the components of velocity in the x-, y- and z- directions, respectively, the steady-state admissibility condition requires that

$$\left. \frac{v_y}{v_x} \right|_{y = f_1} = f_1'(x) \quad , \quad \text{and} \quad \left. \frac{v_y}{v_x} \right|_{y = f_2} = f_2'(x) \quad ,$$

where prime represents derivative with respect to x. The above condition is satisfied if we select:

$$\frac{v_y}{v_x} = \frac{f_1'(x)(y - Y)}{f_1(x) - Y} = \frac{f_2'(x)(y - Y)}{f_2(x) - Y} \quad . \tag{B-7}$$

Similarly, in order that the deforming material remains in contact with the rolls, it is required that:
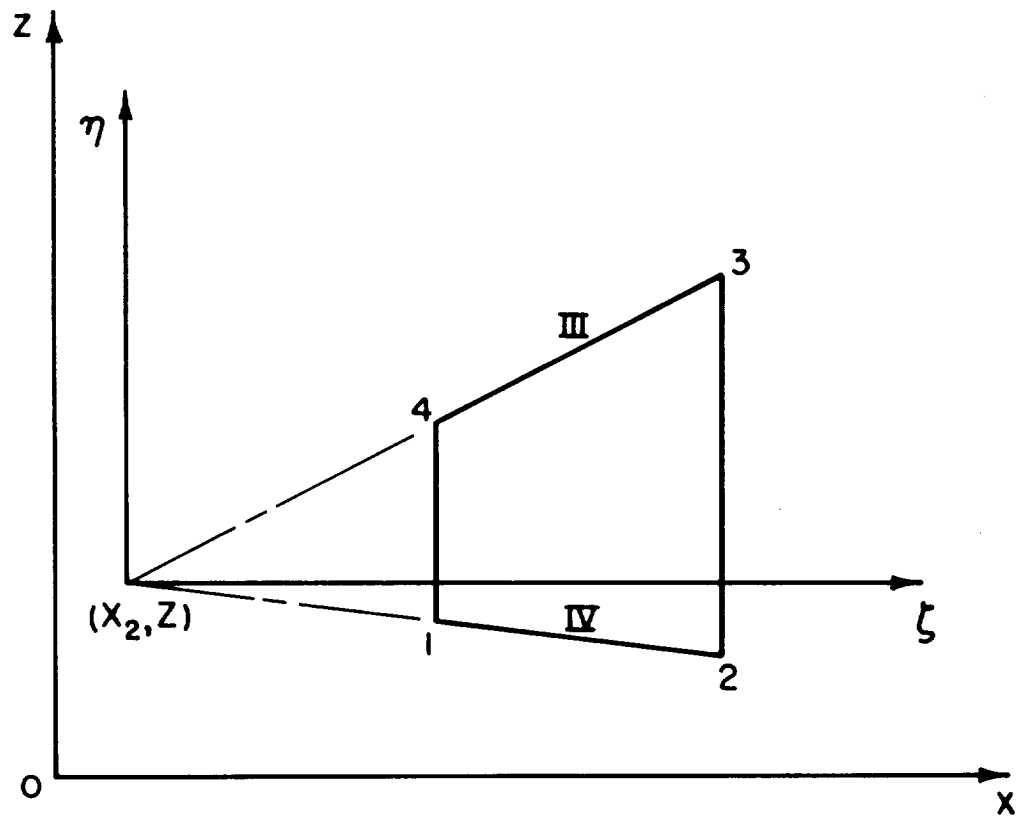
FIGURE B-6.   CONFIGURATION OF AN ELEMENT IN THE x-z PLANE

$$\frac{v_z}{v_x}\bigg|_{z \,=\, h_1} = h_1^{'}(x) \quad , \quad \text{and} \quad \frac{v_z}{v_x}\bigg|_{z \,=\, h_2} = h_2^{'}(x) \quad .$$

The above condition is satisfied if we select:

$$\frac{v_z}{v_x} = \frac{h_1^{'}(x)(z-Z)}{h_1(x)-Z} = \frac{h_2^{'}(x)(z-Z)}{h_2(x)-Z} \quad . \tag{B-8}$$

If the velocity in the rolling direction (x-direction) is taken as the ratio of incoming area of cross section to the current area of cross section (according to assumption 2), then for an element i, we have:

$$v_x = \frac{A_i(x_o)}{A_i(x)} \quad , \tag{B-9}$$

where $A(x) = (f_1 - f_2) \cdot (h_1 - h_2)$, area of cross section of an element i at a given x. If actual velocity of the incoming strip is U, then it is defined by:

$$V_{tx}(x_n) - U \, v_x(x_n) = 0 \quad , \tag{B-10}$$

where V_{tx} is the x-component of roll surface velocity and x_n is the location of the neutral plane. (See Figure B-4).

The kinematically admissible velocity in the deformation zone for an element i is then given by:

$$\left. \begin{aligned} V_x &= U \, v_x = U \, \frac{A_i(x_o)}{A_i(x)} \\[2ex] V_y &= U \, v_y = U \, v_x \, \frac{f_1^{'}(y-Y)}{f_1 - Y} \\[2ex] V_z &= U \, v_z = U \, v_x \, \frac{h_1^{'}(z-Z)}{h_1 - Z} \quad . \end{aligned} \right\} \tag{B-11}$$

Let us define $\phi = f - y$ and $\psi = h - z$. Also, now onward, we will use local coordinate system (ζ, ξ, η) which is related to the global coordinate system (x, y, z) as follows:

$$\zeta = x, \quad \xi = y - Y, \text{ and } \eta = z - Z \quad .$$

However, since x and ζ are identical, x will be used instead of ζ.

Strain-Rate Field

The components of the strain-rate field can be derived from Equations (B-11). If $\dot{\epsilon}_x$, $\dot{\epsilon}_y$, and $\dot{\epsilon}_z$ represent the normal strain-rate components and $\dot{\gamma}_{xy}$ and $\dot{\gamma}_{xz}$ are the shear strain rates, then

$$
\left.
\begin{aligned}
\dot{\epsilon}_x &= U\,\frac{\partial v_x}{\partial x} = -\,U\,v_x\,\frac{A'(x)}{A(x)} = -\,U\,v_x\left(\frac{\phi'}{\phi} + \frac{\psi'}{\psi}\right) \\[2ex]
\dot{\epsilon}_y &= U\,\frac{\partial v_y}{\partial y} = U\,v_x\,\frac{\phi'}{\phi} \\[2ex]
\dot{\epsilon}_z &= U\,\frac{\partial v_z}{\partial z} = U\,v_x\,\frac{\psi'}{\psi} \\[2ex]
\dot{\gamma}_{xy} &= U\left(\frac{\partial v_x}{\partial y} + \frac{\partial v_y}{\partial x}\right) = -\,U\,v_x\left(2\,\frac{\phi'}{\phi} + \frac{\psi'}{\psi}\right)\frac{\phi'}{\phi}\,\xi \\[2ex]
\dot{\gamma}_{xz} &= U\left(\frac{\partial v_x}{\partial z} + \frac{\partial v_z}{\partial x}\right) = -\,U\,v_x\left(\frac{\phi'}{\phi} + 2\,\frac{\psi'}{\psi}\right)\frac{\psi'}{\psi}\,\eta \quad .
\end{aligned}
\right\} \quad \text{(B-12)}
$$

Deformation Energy Rate

The energy rate of plastic deformation, $\dot{E}_p$, for an element, is given as follows:

$$\dot{E}_p = \int_V \bar{\sigma}\,\dot{\epsilon}\,dV \quad , \tag{B-13}$$

where $\bar{\sigma}$ is the flow stress of the deforming material, V is the volume of the element, and $\dot{\epsilon}$ is the effective strain rate given by:

$$\dot{\varepsilon} = \sqrt{\frac{2}{3} \left(\dot{\varepsilon}_x^2 + \dot{\varepsilon}_y^2 + \dot{\varepsilon}_z^2 + \frac{1}{2} \dot{\gamma}_{xy}^2 + \frac{1}{2} \dot{\gamma}_{xz}^2 \right)} \quad . \tag{B-14}$$

Using Equations (B-13) and (B-14), we obtain:

$$\dot{E}_p = \int_{x_1}^{x_2} \int_{\phi_2}^{\phi_1} \int_{\psi_2}^{\psi_1} \sqrt{\frac{2}{3}} \ U\bar{\sigma} \ v_x \ \sqrt{P^2 + Q^2 \xi^2 + R^2 \eta^2} \ d\eta d\xi dx \quad , \tag{B-15}$$

where

$$P^2 = 2 \left\{ \left(\frac{\phi'}{\phi} \right)^2 + \left(\frac{\psi'}{\psi} \right)^2 + \frac{\phi'}{\phi} \cdot \frac{\psi'}{\psi} \right\}$$

$$Q^2 = \frac{1}{2} \left\{ 2 \left(\frac{\phi'}{\phi} \right)^2 + \frac{\phi'}{\phi} \cdot \frac{\psi'}{\psi} \right\}^2$$

$$R^2 = \frac{1}{2} \left\{ \frac{\phi'}{\phi} \cdot \frac{\psi'}{\psi} + 2 \left(\frac{\psi'}{\psi} \right)^2 \right\}^2 \quad .$$

It is possible to carry out the integration on the right-hand side of Equation (B-15) with respect to η and ξ. The result is as follows:

$$\frac{\dot{E}_p}{kU} = \frac{1}{\sqrt{2}} \int_{x_1}^{x_2} \left[\frac{\phi\psi}{2} \sqrt{P^2 + Q^2 \phi^2 + R^2 \psi^2} + \frac{\phi(P^2 + Q^2 \phi^2)}{2|R|} \right.$$

$$\cdot \ln \left(\frac{|R|\psi + \sqrt{P^2 + Q^2 \phi^2 + R^2 \psi^2}}{\sqrt{P^2 + Q^2 \phi^2}} \right)$$

$$+ \frac{P^2}{|QR|} \left\{ I_1 \left[\sqrt{P^2 + Q^2 \phi^2} , \ |Q|\phi, |R|\psi \right] - I_1 \left[|P|, 0, |R|\psi \right] \right\}$$

$$+ \frac{1}{|QR|} \left\{ I_2 \left[\sqrt{P^2 + Q^2 \phi^2} , \ |Q|\phi, |R|\psi \right] - I_2 \left[|P|, 0, |R|\psi \right] \right\} \right] dx \tag{B-16}$$

where $\quad k = \bar{\sigma}/\sqrt{3}$

$$I_1(a,b,c) = \int_0^c \ln\left(b + \sqrt{x^2 + a^2}\right) dx$$

$$= c \ln\left(b + \sqrt{a^2 + c^2}\right) - c + b \ln\left(\frac{\sqrt{a^2 + c^2} + c}{a}\right)$$

$$+ 2\sqrt{a^2 - b^2} \cdot \tan^{-1}\left[\sqrt{\frac{a-b}{a+b}} \cdot \frac{\sqrt{a^2 + c^2} - a}{c}\right] \quad , \quad a > b$$

$$= c \ln\left(b + \sqrt{a^2 + c^2}\right) - c + b \ln\left(\frac{\sqrt{a^2 + c^2} + c}{a}\right)$$

$$+ \frac{1}{b-a}\sqrt{\frac{b-a}{b+a}} \cdot \ln\left\{\frac{\sqrt{\frac{b+a}{b-a}} + \frac{c}{a + \sqrt{a^2 + c^2}}}{\sqrt{\frac{b+a}{b-a}} - \frac{c}{a + \sqrt{a^2 + c^2}}}\right\} \quad , \quad a < b \quad .$$

For a special case:

$$I_1(o,b,c) = (b + c)\left\{\ln(b + c) - 1\right\} - b(\ln b - 1)$$

and $\quad I_2(a,b,c) = \int_0^c x^2 \ln\left(b + \sqrt{x^2 + a^2}\right) dx$

$$= \frac{1}{3}\left\{c^3 \ln\left(b + \sqrt{a^2 + c^2}\right) + (a^2 - b^2)c - \frac{1}{3}c^3\right.$$

$$+ \frac{bc}{2}\sqrt{a^2 + c^2} - \frac{b}{2}(3a^2 - 2b^2)\ln\left(\frac{\sqrt{a^2 + c^2} + c}{a}\right)$$

$$\left. - 2(a^2 - b^2)\sqrt{a^2 - b^2} \cdot \tan^{-1}\left[\sqrt{\frac{a-b}{a+b}} \cdot \frac{\sqrt{a^2 + c^2} - a}{c}\right]\right\}, a > b$$

$$= \frac{1}{3}\left\{c^3 \ln\left(b + \sqrt{a^2 + c^2}\right) + (a^2 - b^2)c - \frac{1}{3}c^3\right.$$

$$+ \frac{bc}{2} \sqrt{a^2 + c^2} - \frac{b}{2} (3a^2 - 2b^2) \ln \left(\frac{\sqrt{a^2 + c^2} + c}{a} \right)$$

$$- (b^2 - a^2)\sqrt{b^2 - a^2} \ln \left[\frac{\sqrt{\frac{b+a}{b-a}} + \frac{c}{a + \sqrt{a^2 + c^2}}}{\sqrt{\frac{b+a}{b-a}} - \frac{c}{a + \sqrt{a^2 + c^2}}} \right] \right\} , a < b .$$

For special case:

$$I_2(o.b,c) = \left\{ \frac{1}{3} (b + c)^3 - b(b + c)^2 + b^2(b + c) \right\} \ln (b + c)$$

$$- \frac{b^3}{3} \ln (b) - \left\{ \frac{1}{a} (b + c)^3 - \frac{b}{2} (b + c)^2 \right.$$

$$\left. + b^2 (b + c) \right\} + \frac{11}{18} b^3 .$$

Energy Rate of Velocity Discontinuities Along the Transverse Sections

Across the transverse sections, velocity discontinuities occur along the y- and the z- directions. The energy rate, associated with shearing along these sections, represents a portion of the total energy rate. Consider two elements, 'ℓ' and 'r', as shown in Figure B-7. The mismatch in the y- and the z- components of the velocity across the Plane 2-3 or 1'-4' causes shear across this plane. The velocity differentials along the y- and z- directions across this plane is given by:

$$\frac{\Delta V_y}{V_x} = \frac{f_r'(y - Y_r)}{f_r - Y_r} - \frac{f_\ell'(y - y_\ell)}{f_\ell - Y_\ell} = Ay + B$$

$$\frac{\Delta V_z}{V_x} = \frac{h_r'(z - Z_r)}{h_r - Z_r} - \frac{h_\ell'(z - Z_\ell)}{h_\ell - Z_\ell} = C z + D \qquad \text{(B-17)}$$
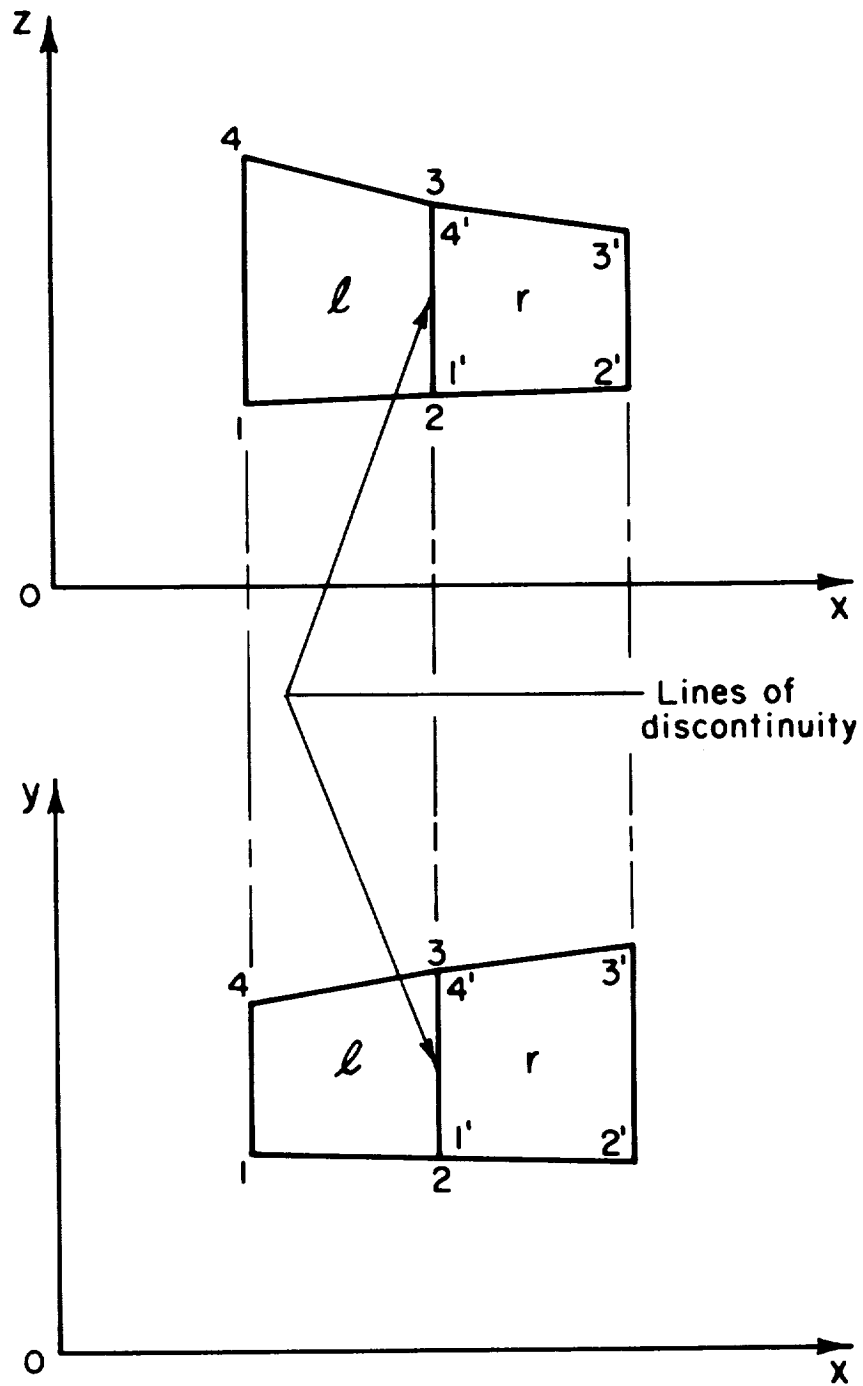
FIGURE B-7. VELOCITY DISCONTINUITY ALONG THE TRANSVERSE SECTIONS

where

$$A = \frac{f'_r}{f_r - Y_r} - \frac{f'_\ell}{f_\ell - Y_\ell}$$

$$B = \frac{f'_r \, Y_r}{f_r - Y_r} - \frac{f'_\ell \, Y_\ell}{f_\ell - Y_\ell}$$

$$C = \frac{h'_r}{h_r - Z_r} - \frac{h'_\ell}{h_\ell - Z_\ell}$$

and

$$D = \frac{h'_r \, Z_r}{h_r - Z_r} - \frac{h'_\ell \, Z_\ell}{h_\ell - Z_\ell}$$

The energy rate due to velocity discontinuity on the transverse section between element 'ℓ' and 'r' is given by:

$$\dot{E}_{dt} = \int_A k \, |\Delta V| \, dA$$

$$= \int_A k \, \sqrt{\Delta V_y^2 + \Delta V_z^2} \, d_z d_x$$

$$= k \, V_x \int_{f_r}^{f_\ell} \int_{h_r}^{h_\ell} \sqrt{(Ay + B)^2 + (Cz + D)^2} \, dz \, dy \qquad . \qquad \text{(B-18)}$$

Substituting

$$S = Ay + B$$

$$T = Cz + D$$

$$\dot{E}_{dt} = \frac{kUv_x}{AC} \int_{S_2}^{S_1} \int_{T_2}^{T_1} \sqrt{S^2 + T^2} \, dT \, dS$$

$$= \dot{E}_{dt} (S_1, T_1) + \dot{E}_{dt} (S_2, T_2) - \dot{E}_{dt} (S_1, T_2) - \dot{E}_{dt} (S_2, T_1)$$

where

$$\dot{E}_{dt}(S,T) = \frac{kUv_x}{AC} \int_o^S \int_o^T \sqrt{S^2 + T^2} \, dT \, dS$$

$$= \frac{kUv_x}{AC} \left\{ \frac{ST}{4} \sqrt{S^2 + T^2} + \frac{T^3}{4} \ln \left(S + \frac{\sqrt{S^2 + T^2}}{T} \right) \right.$$

$$\left. + \frac{1}{2} I_2 (T,T,S) - S^3 \left(\frac{1}{6} \ln S - \frac{1}{18} \right) \right\}$$

Energy Rate of Velocity Discontinuities Along the Longitudinal Sections

Across the longitudinal sections, velocity discontinuities occur along the longitudinal (s-) direction and along the (z-) direction. The energy rate associated with shearing along these sections represent a portion of the total energy rate. Consider two elements, 'i' and 'j', as shown in Figure B-8. The shearing occurs across the shaded area due to mismatch between elements 'i' and 'j'. This mismatch may also look like, as shown in Figure B-9. The velocity differentials along the s- and the z- directions are given by:

$$\Delta V_z = \frac{V_{xi} h_i' (z - Z_i)}{h_i - Z_i} - \frac{V_{xj} h_j' (z - Z_j)}{h_j - Z_j} = \alpha(x) \cdot z + \beta(x)$$

$$\Delta V_s = \Delta V_x \cdot \sqrt{1 + (f')^2} = \sqrt{\gamma(x)} \quad , \tag{B-19}$$

where

$$\alpha(x) = \frac{V_{xi} h_i'}{h_i - Z_i} - \frac{V_{xj} h_j'}{h_j - Z_j}$$

$$\beta(x) = - \frac{V_{xi} h_i' Z_i}{h_i - Z_i} - \frac{V_{xj} h_j' Z_j}{h_j - Z_j}$$

The energy rate due to velocity discontinuity on the longitudinal section between elements 'i' and 'j' is then:

$$\dot{E}_{ds} = k \int_A |\Delta V| \, dA$$

$$= kU \sqrt{1 + (f')^2} \int_{x_1}^{x_2} \int_{h_2}^{h_1} \sqrt{[\alpha(x) z + \beta(x)]^2 + \gamma^2(x)} \, d_z \, d_x$$
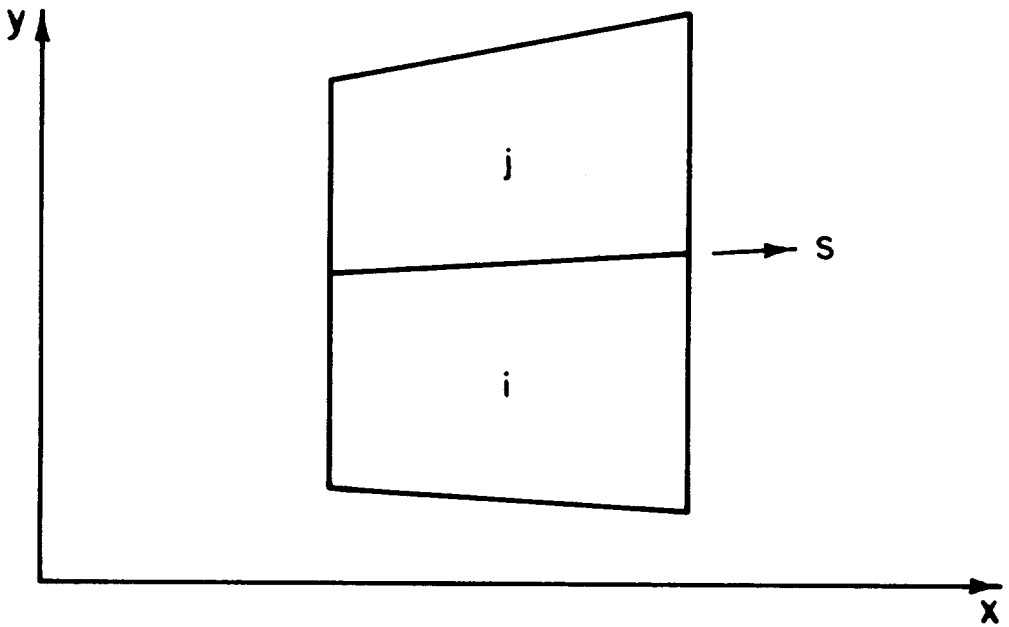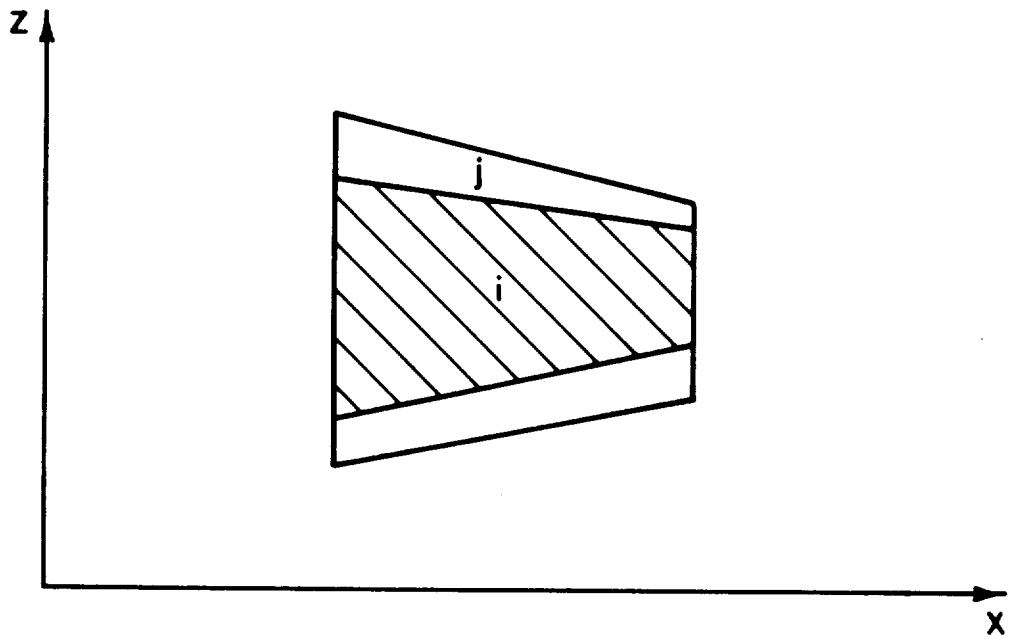
FIGURE B-8. VELOCITY DISCONTINUITIES ALONG THE LONGITUDINAL SECTIONS
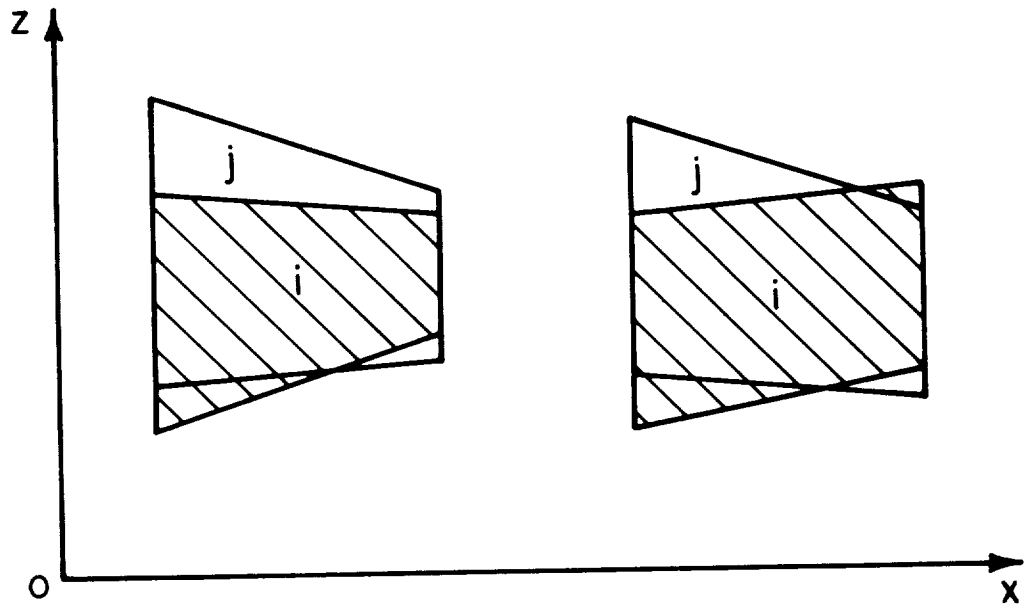
(a)
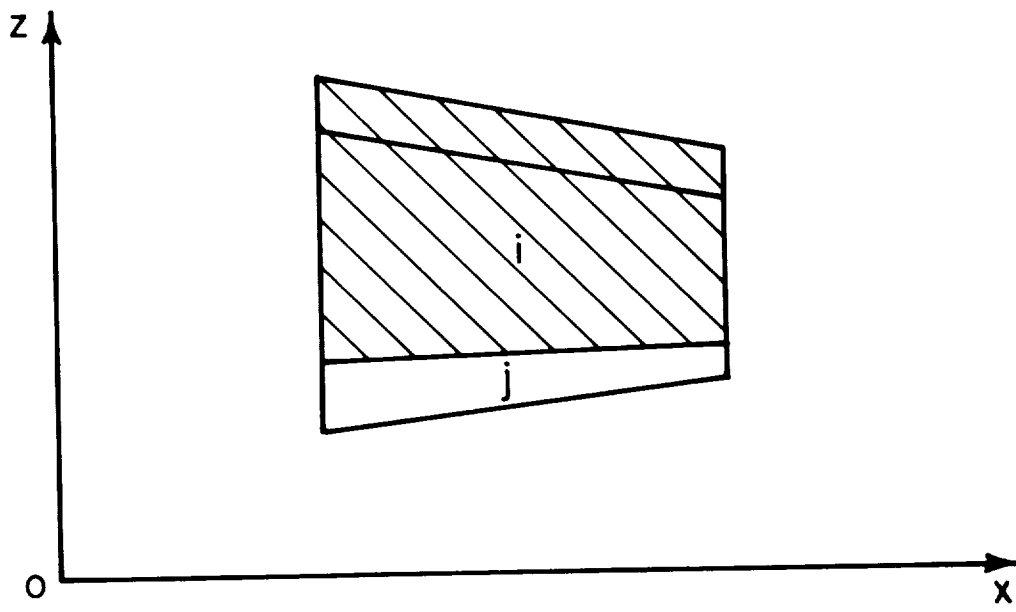
(b)

FIGURE B-9. POSSIBLE MISMATCH OF ELEMENTS ALONG THE LONGITUDINAL DIRECTION

$$= kU \sqrt{1 + (f')^2} \int_{x_1}^{x_2} \left\{ \left(\frac{h_1 + \frac{\beta}{\alpha}}{2} \right) \sqrt{(\alpha h_1 + \beta)^2 + \gamma^2} \right.$$

$$- \frac{h_2 + \frac{\beta}{\alpha}}{2} \sqrt{(\alpha h_2 + \beta)^2 + \gamma^2}$$

$$\left. + \frac{\gamma^2}{2|\alpha|} \ln \left[\frac{\alpha h_1 + \beta + \sqrt{(\alpha h_1 + \beta)^2 + \gamma^2}}{\alpha h_2 + \beta + \sqrt{(\alpha h_2 + \beta)^2 + \gamma^2}} \right] \right\} dx \qquad . \qquad \text{(B-20)}$$

The integration with respect to x is carried numerically. To $\dot{E}_{ds}$, given above, an additional term for energy of the free surface (unshaded area) is added. This is given by $\dot{E}_{dj} = k \int_A |V_j| dA$, where V_j is the resultant velocity on the unshaded area.

Friction Energy Rate

Energy is dissipated in overcoming the friction at the roll workpiece interfaces. If ω is the angular velocity of the upper roll with radius vector of R_1, then the roll surface velocity is $\omega_1 R_1$. However, since the circular segments are approximated by straight-lines, this surface velocity does not lie in a plane surface. Instead, it may be assumed that the axial component V_{Rx} is given as:

$$V_{Rx} = \omega_1 R_1 \cos\theta = \omega_1 (z_{r1} - h_1) \quad .$$

Now, in order that the tool remains in contact with the material, the vertical component of surface velocity is given by:

$$V_{Rz} = h_1' \cdot V_{Rx} = \omega(z_{r1} - h_1) \cdot h_1' \quad .$$

The velocity differentials along the roll workpiece contact are then given by:
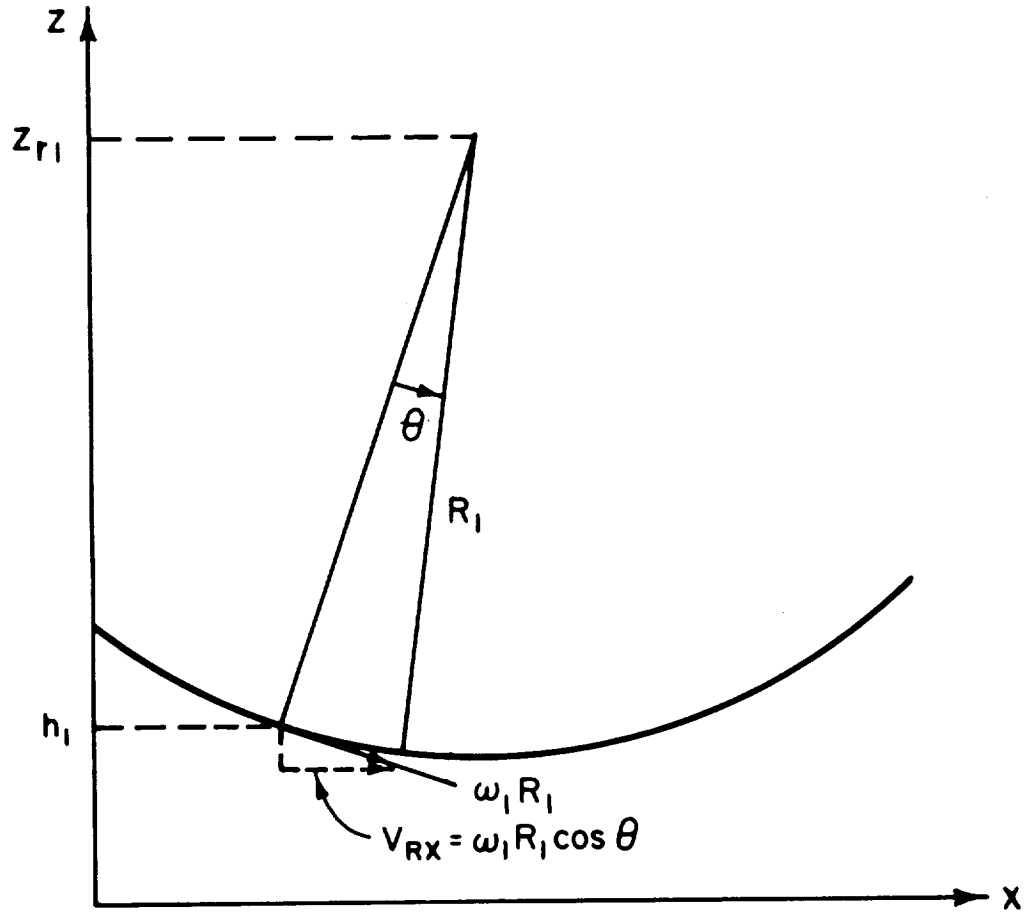
FIGURE B-10. TANGENTIAL VELOCITY AT THE ROLL-WORKPIECE INTERFACE

$$\Delta V_x = V_{Rx} - V_x = U \left\{ \frac{\omega(Z_r - h)}{U} - v_x \right\}$$

$$\Delta V_y = V_x \frac{f'(y - Y)}{f - Y} = U v_x \frac{f'(y - Y)}{f - Y}$$

$$\Delta V_z = V_{RZ} - V_z = U h' \left\{ \frac{\omega(Z_r - h)}{U} - v_x \right\} .$$

The energy dissipation rate due to friction $\dot{E}_f$ is given as below:

$$\dot{E}_f = mk \int_A |\Delta V| \, dA \quad , \tag{B-21}$$

where m is the friction shear factor and can have a value between 0 to 1.

Substituting for $|\Delta V|$ in Equation (B-21) and integrating with respect to ξ, we have:

$$\dot{E}_f = mkU \int_{x_1}^{x_2} \sqrt{1 + (h')^2} \left[\frac{\xi}{2} \sqrt{\left(\frac{\phi' v_x}{\phi} \right)^2 \xi^2 + \left\{ 1 + (h')^2 \right\} \left\{ \frac{\omega(Z_r - h)}{U} - v_x \right\}^2} \right.$$

$$+ \frac{1}{2} \left| \frac{\phi}{\phi' v_x} \right| \left\{ 1 + (h')^2 \right\} \left\{ \frac{\omega(Z_r - h)}{U} - v_x \right\}^2 \tag{B-22}$$

$$\left. \cdot \ln \left\{ \xi \left| \frac{\phi' v_x}{\phi} \right| + \sqrt{\left(\frac{\phi' v_x}{\phi} \right)^2 \xi^2 + \left\{ 1 + (h')^2 \right\} \left\{ \frac{\omega(Z_r - h)}{U} - v_x \right\}^2} \right\} \right]_{\xi_2}^{\xi_1} d_x$$

Subscripts 1 and 2 can be used for the upper and lower rolls.

Total Energy Rate

The total energy dissipation rate is the sum of the deformation energy rate, the energy rates due to velocity discontinuities and the friction energy rate. It is a function of unknown spread profiles w_1 and w_2, and the location of the neutral plane x_n. The unknown coefficients of w_1 and w_2 and x_n are determined by minimizing the total energy rate, $\dot{E}$, which is given as:

$$\dot{E} = \dot{E}_p + \dot{E}_{dt} + \dot{E}_{ds} + \dot{E}_f \quad ; \tag{B-23}$$

The minimization of $\dot{E}$ with respect to unknown parameters is done by using numerical techniques. The whole procedure has been computerized. The details of this computer program are given in Appendix C.

Calculation of Roll Torque

The roll torque is given as:

$$T = \int R \times dF \quad , \tag{B-24}$$

where R is the radius vector and F is the force vector in the rolling direction, tangential to roll surfaces. If i and k are the unit vectors along the x- and the z- directions, then the radius vector and the force vector are given as:

$$R = (x - \ell) \, i + (Z_r - h) \, k$$

$$dF = \frac{m(i + h'\,k)\left\{\frac{\omega}{U}(Z_r - h) - v_x\right\}\sqrt{1 + (h')^2}\ d_x\, d_y}{\left[\sqrt{1 + (h')^2}\ \left\{\frac{\omega(Z_r - h)}{U} - v_x\right\}^2 + v_x^{\,2}\left\{\frac{f'(y - Y)}{f - Y}\right\}^2\right]^{1/2}} \quad .$$

After substituting for R and dF in Equation (B-24), the integration with respect to y can be carried out analytically. Integration with respect to x is best carried numerically. The calculation of the torque is also included in the computer program, a description of which is given in Appendix C.

APPENDIX C

DESCRIPTION OF THE COMPUTER PROGRAMS SHPROL

APPENDIX C

DESCRIPTION OF THE COMPUTER PROGRAMS SHPROL

A system of computer programs, named SHPROL, was developed at Battelle-Columbus to analyze the metal flow in rolling of airfoil shapes. The analysis utilizes a modular upper-bound approach to determine a kinematically-admissible velocity field, the associated lateral spread, and the torque required under steady-state rolling conditions. The details of the method and the mathematical derivations are given in Appendix B, "Analysis of Metal Flow in Rolling of Airfoil Shapes".

SHPROL is coded in FORTRAN IV and requires approximately $60,000_8$ words of memory space in a CDC Cyber 70 computer. The properties of the material being deformed are provided through a subroutine named MATERL and the other input variables are read in through data cards. Figure C-1 shows a schematic representation of the various subroutines and subprograms in the programs SHPROL. At any level, the calling sequence is from left to right and then top to bottom. Thus, SHPROL calls subroutines HITIP, SPLINE, COEFF, in that order, before it calls subroutine ARRANGE. (Note: subroutines with a star(*) represent utility subroutines for performing operations such as integration, interpolation, minimization, and other standard mathematical operations).

Input to and Output from SHPROL

All the input data to the computer programs SHPROL are transferred through READ statements. This includes variables defining the number of elements in the deformation zone, shape and location of the preform section, shape and location of the upper and lower roll profiles, angular velocities of rolls, friction factor at the roll-workpiece interface, temperature of workpiece, and some controlling variables for selecting proper options. A detailed description of these variables will be given in the input preparation. The flow stress of the deforming material, as a function of strain, strain rate and temperature, is furnished through a subroutine named MATERL, and it needs to be inserted in the program deck for the material under consideration.

FIGURE C-1. STRUCTURE OF THE SYSTEM OF COMPUTER PROGRAMS SHPROL

(* Utility Subroutine)

The output from the program prints coordinates of the grid points, spread profiles as functions of axial distance (in rolling direction) from roll entry, the total energy dissipation rate and its various components, the location of the neutral plane, the extension rate as a function of axial distance, and the strain, strain rate and flow stress distribution in the deforming material. The output corresponds to a minimum total energy rate, which is minimized by a simplex method with respect to various unknown parameters. At the end of the execution, the output from the minimization routine is written on TAPE7. If further calculations are required, for example, to reduce the error of minimization, the contents of TAPE7 are read into TAPE8 and calculations are restarted from the point where they were left rather than from the beginning.

Details of the Computer Program SHPROL

The basic functions of the main program and the various subroutines and subprograms in the system of computer programs SHPROL are briefly described in the following.

Main Program SHPROL

This main program provides the storage area by determining the starting location of each variable in the blank common and the size of the blank common array. If the necessary size of the blank common array is larger than the prescribed value, it prints directions for appropriate changes and terminates the program. It also reads the information from the following data card:

1st Data Card: NUMPX,NUMPY,NCAL,NDATAT,NDATAB,NWDAT,NWDAB,NPRINT*

---

* Refer to list of Important Variables at the end of this appendix for definition of the variable names used here.

Subroutine HITIP

Purpose: This subroutine reads the workpiece geometry, and the roll surface geometries in independent coordinate systems, and then converts all the information to global coordinate system with the help of other geometrical inputs. As shown in Figure C-2, coordinate system (x,y,z) is the global system and it defines the geometries of the top and bottom roll contour, the workpiece contour, and their relative positions during rolling. The systems (x,y',z') and (x,y'',z'') are used to read the geometries of the top and the bottom roll surfaces, and the system (x,y''',z''') is used to read the geometry of the incoming workpiece. These coordinate systems can be totally arbitrary. The geometries of the roll surfaces and the workpiece are assembled on the global system by properly defining the coordinates of the origin of the individual system, namely (OY1, OZ1), (OY2, OZ2) and (OY3, OZ3). It then calculates roll gap and workpiece section at various locations along the rolling direction. This routine also approximates the contact arc at the entrance with a straight-line such that the actual contact area between the rolls and the material is equal to the approximate contact area, as shown in Figure C-3. This subroutine also reads the following data cards:

  2nd Data Card: OY1,OZ1,OY2,OZ2,OY3,OZ3,ZR(1),ZR(2)
  3rd Data Card: (YDATAT(I),HDATAT(I), I = 1, NDATAT)
  4th Data Card: (YDATAB(I),HDATAB(I), I = 1, NDATAB)
  5th Data Card: (YWDAT(I),HWDAT(I), I = 1, NWDAT)
  6th Data Card: (YWDAB(I),HWDAB(I), I = 1, NWDAB)
  7th Data Card: (WO(I), I = 1,2), (SPL(I), I = 1,2)

Calling Sequence: CALL HITIP (YCAL,HCALT,HCALB,HWCAT,HWCAB,YDATAT,HDATAT, YDATAB,HDATAB,YWDAT,HWDAT,YWDAB,HWDAB,NUMPX,NCAL,NDATAT, NDATAB,NWDAT,NWDAB)
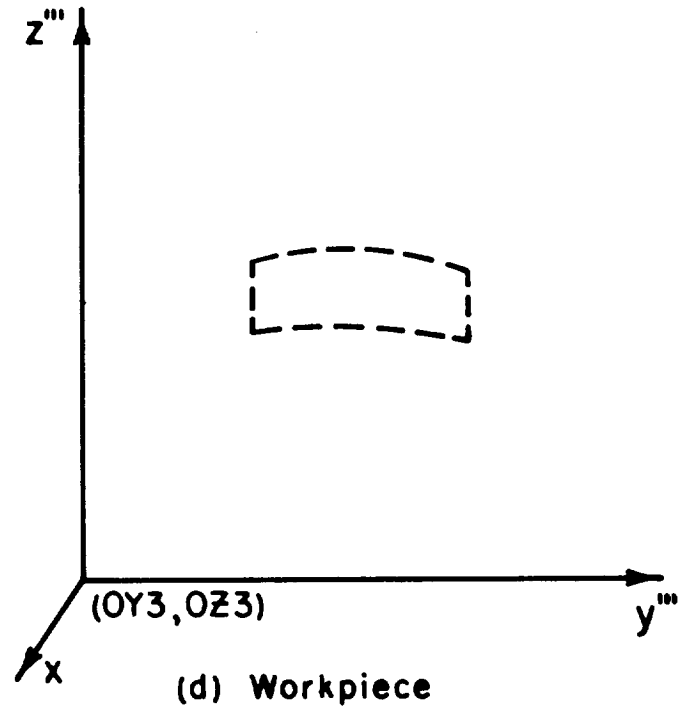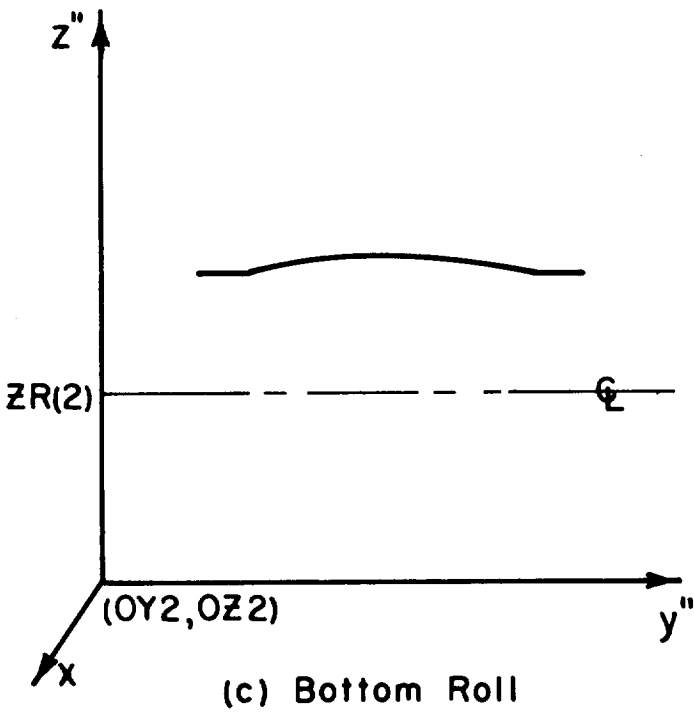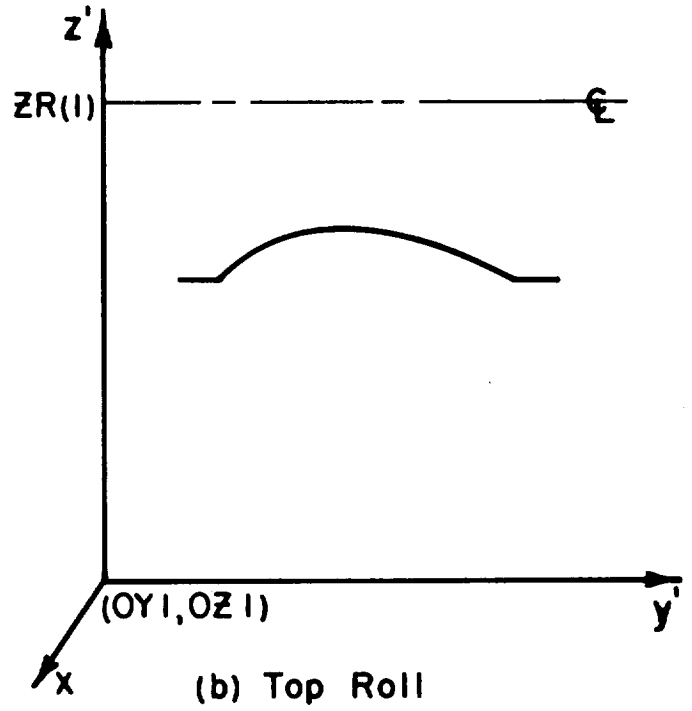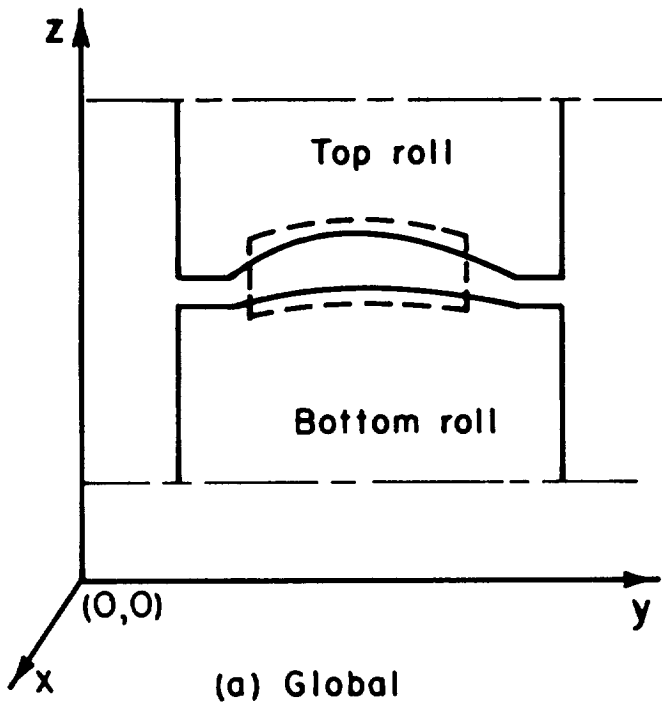
FIGURE C-2. COORDINATE SYSTEMS FOR ROLL SURFACES AND WORKPIECE
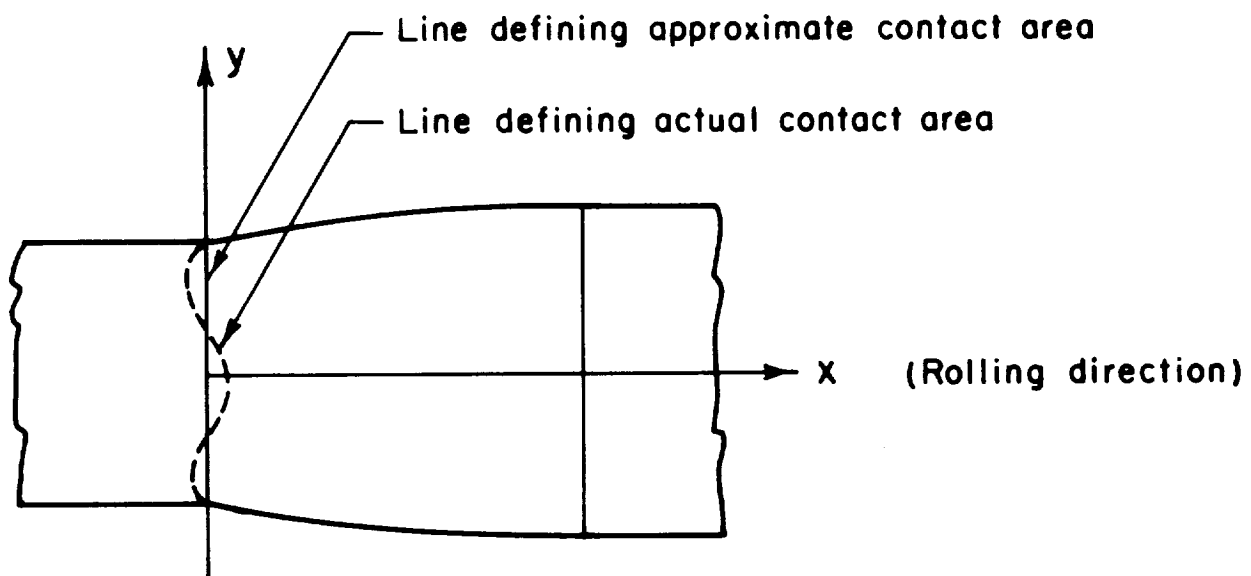
FIGURE C-3. ACTUAL AND APPROXIMATE ARC OF CONTACTS AT ROLL ENTRANCE

Input: YDATAT,HDATAT,YDATAB,HDATAB,YWDAT,HWDAT,YWDAB,HWDAB,NUMPX,

NCAL,NDATAT,NDATAB,NWDAT,NWDAB

Output: YCAL,HCALT,HCALB,HWCAT,HWCAB

Subroutine SPLINE

Purpose: This subroutine is used for interpolation by spline fit[1].
A smooth curve is drawn through the points in such a way
that its slope and its curvature, both are continuous
functions. Interpolation is done by merely reading points
off the smooth curve thus generated.

Calling Sequence: CALL SPLINE (X,Y,NXY,XTR,YTR,NXYTR)

Input: X = Array of independent variable

Y = Array of   dependent variable at X

NXY = Number of elements in X and Y

XTR = Array of dependent variable at X
interpolation is required

NXYTR = Number of elements in XTR

Output: YTR = Array of interpolated values at XTR values.

Subroutine COEFF

Purpose: This subroutine is used by the subroutine SPLINE to
determine the constants by solving linear simultaneous
equations.

Calling Sequence: CALL COEFF (X,Y,M,C)

Input: X = Array of independent variable

Y = Array of dependent variable

M = Number of elements in X and Y

Output: C = Coefficients of spline curve

---

(1)   R. H. Pennington, Introductory Computer Methods and Numerical Analysis, 2nd
Edition, McMillan, 1971.

Subroutine ARRANGE

Purpose: This subroutine develops a numbering system for the nodal points, elements, and the discontinuity surfaces and their interrelationship. Each element is defined by four nodal points and each discontinuity surface is defined by two element numbers.

Calling Sequence: CALL ARRANGE (MPEL,MST,MSL,NUMPX,NUMPY,NUMNP,NUMEL,NUMST, NUMSL)

Input: NUMPX,NUMPY,NUMNP,NUMEL,NUMST,NUMSL

Output: MPEL,MST,MSL

Subroutine ROLLING

Purpose: This is the main subroutine in the program. It reads most of the input data (other than geometries of the rolls and the workpiece), calls other major subroutines and governs printing of results through subroutine OUTP. The input variables read in this routine include the several control variables providing various options, such as shape of the spread profiles (parabolic or third order polynomial), the boundary conditions at the edges (free or fixed), symmetry in the thickness direction (yes or no) and the limiting number of iterations during energy minimization. Also, in order to reduce the number of iterations during energy minimization, this routine reads an array of numbers CONST(I) which, when multiplied by the guess values of various input variables, yield approximately the same quantity. This information is, however, not always essential and a user may leave blank spaces on the input card, if so desired. This subroutine also reads the following data cards:

    8th Data Card: Heading, up to 80 characters
    9th Data Card: OGA(1),OGA(2),FRIC,TEMP
   10th Data Card: NCURVE,NFIX,NSYM,NCOUNT,ITER,ERIT,ERITE
   11th Data Card: (CONST(I), I = 1,5)

Calling Sequence: CALL ROLLING (YCAL,HCALT,HCALB,HWCAT,HWCAB,MPEL,X,Y,H,AY,BY,

AZ,BZ,YY,ZZ,VO,XN,ISLOP,MST,EJUMP,MSL,GRA,NCAL,NUMPX,NUMPY,

NUMNP,NUMEL,NUMST,NUMSL)

Input: YCAL,HCALT,HCALB,HWCAT,HWCAB,MPEL,X,Y,H,AY,BY,AZ,BZ,YY,ZZ,VO,

XN,ISLOP,MST,EJUMP,MSL,GRA,NCAL,NUMPX,NUMPY,NUMNP,NUMEL,

NUMST,NUMSL

Subroutine MINI

Purpose: This is a function minimization routine based on the Simplex
Method[2] and is used for minimization of the total energy
rate with respect to various parameters. Figure C-4 shows
the flow chart of this simplex method. The numbers on the
chart indicate the statement numbers in the program. When
the input is just a single point, this program creates an
initial simplex in such a way that the initial guess point
is located at the centroid of the simplex and the apexes are
at an equal distance equal to "STEP".

The termination of the minimization procedure is done in two
ways. In the first way, the minimization procedure is ter-
minated when the minimum condition is satisfied. The minimum
condition can be reached either when the maximum distance
between the simplex points becomes less than a small quantity
"ERIT" or when the maximum directional derivative of the
simplex hyperplane becomes less than a small quantity "ERITE".
In the second way, the minimization procedure is terminated
when the maximum number of iteration exceeds a specified
number "ITER".

This subroutine also reads the following data card:
    12th Data Card: (PB(I), I = NUMVA), STEP

---

(2) J. A. Nelder and R. Mead, "A Simplex Method for Function Minimization", Computer
Journal, Vol. 7, No. 4, 1965, p 308.

ENTER

Calculate initial P_i and y_i

Determine h, calculate $\bar{P}$

Form $P = (1 + a)\bar{P} - a P_h$

Calculate y

[350] is $y^* < y_1$?

[300] Yes

Form $P** = (1 + \gamma)P* - \gamma\bar{P}$

Calculate y**

[450] is $y*** < y_1$?   No

[320] Yes

Replace P_h by P**

[360]Yes   is $y* > y_i$, $i \neq h$?

[450] No

[370]No   is $y* > y_h$?

[390] Yes

Replace P_h by P*

Form $P** = \beta P_h + (1 - \beta)\bar{P}$

Calculate y**

[410] is $y** > y_h$?

No [320]

Yes   Replace all P_i's by $(P_i + P_1)/2$

Replace P_h by P**

Replace P_h by P*

[800] Has minimum been reached?

Yes ——→ EXIT

No
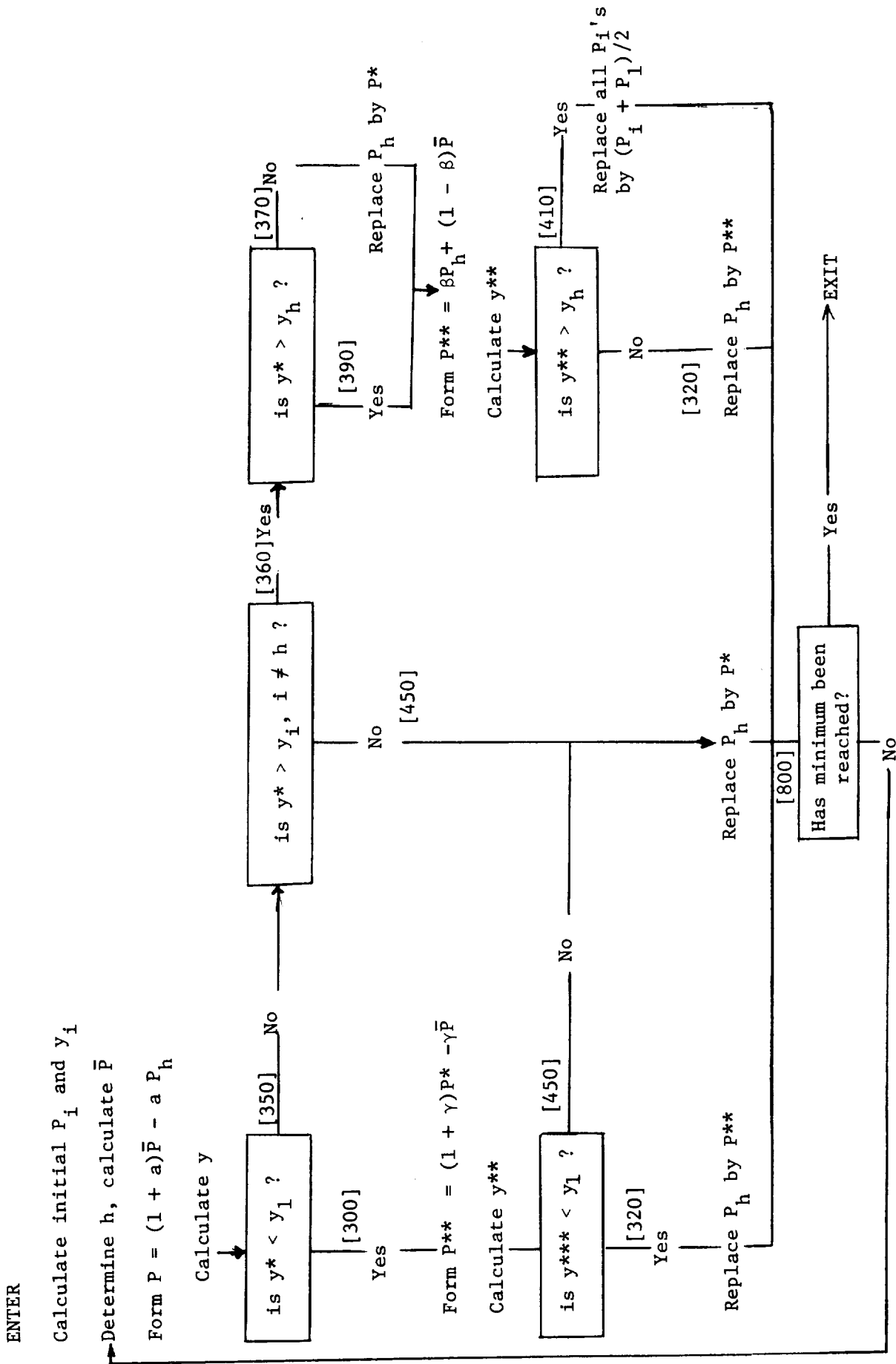
FIGURE C-4.   FLOW CHART OF SUBROUTINE MINI (Corresponding Variables in the Program: P_i XS(J,I), J = 1,2 . . ., NUMVA, y_i = YS(I), $\bar{P}$ = PB, P* = PA, y* = YA, P** = PA2, y** = YA2)

Calling Sequence: CALL MINI (YCAL,HCALT,HCALB,MPEL,X,Y,H,AY,BY,AZ,BZ,YY,ZZ,VO,
XN,ISLOP,MST,EJUMP,MSL,GRA,XS,YS,PB,ITER,ERIT,NCAL,NUMPX,
NUMPY,NUMNP,NUMEL,NUMST,NUMSL,NUMUA)

Input: PB(I), Initial guess values of various parameters, and all the variables in the call statement.

Output: D(I), Values of various parameters corresponding to minimum energy rate.

Subroutine ETOTAL

Purpose: This subroutine evaluates the total energy-dissipation rate for given values of parameters and process conditions. The total energy rate is the sum of the energy rate associated with plastic deformation, friction, and the discontinuities along the transverse and the longitudinal directions.

Calling Sequence: CALL ETOTAL (ENERGY,P,X,Y,H,AY,BY,AZ,BZ,YY,ZZ,ISLOP,MST,MSL,
GRA,EJUMP,MPEL,VO,XN,YCAL,HCALT,HCALB,NCAL,NUMP,NUMEL,NUMST,
NUMSL,NUMPX,NUMPY,NUMUA).

Input: All the variables in the call statement except ENERGY

Output: ENERGY

Subroutine PROCESS

Purpose: This subroutine calculates D(J), the coefficients of the polynomials describing the spread profiles from the guess values PB(I), where the assumed spread profiles are given by:

$$w_1(x) = w_{o1} + d_1 x + \left(\frac{3w_o d_2}{\ell^2} - \frac{2d_1}{\ell} \right) x^2 + \left(\frac{d_1}{\ell^2} - \frac{2w_o d_2}{\ell^3} \right) x^3$$

$$w_2 x = w_{o2} + d_3 x + \left(\frac{3w_o d_4}{\ell^2} - \frac{2d_3}{\ell} \right) x^2 + \left(\frac{d_3}{\ell^2} - \frac{2w_o d_2}{\ell^3} \right) x^3$$

where w_{o1}, w_{o2} and w_o are as shown in Figure C-5. The relationship between D(J) and P(I) are given in Table C-1.
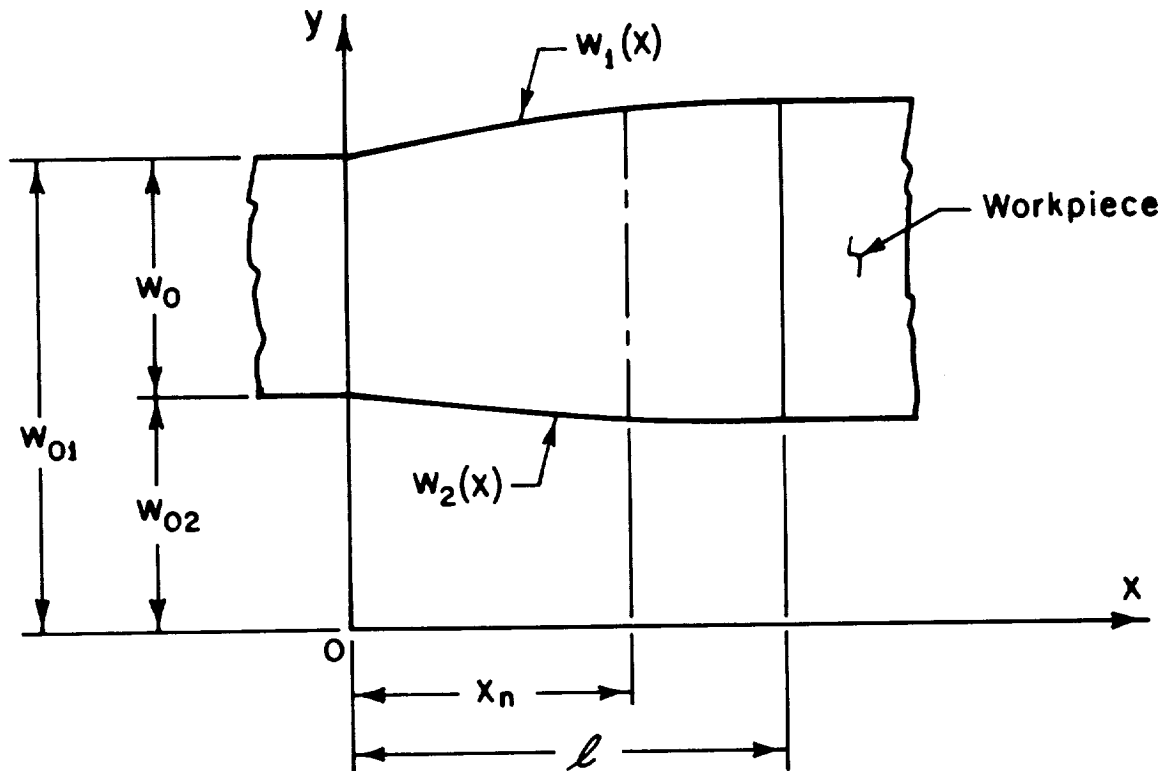
FIGURE C-5. CONFIGURATION OF THE APPROXIMATE PLASTIC REGION IN
ROLLING SHAPES (Plan View; x is rolling direction
and y is width or transverse direction)

TABLE C-1. RELATIONSHIP BETWEEN d_j AND p_i

	FOR NCURVE = 1 (Parabolic Spread)			FOR NCURVE = 2 (Third Order Polynomial Spread)		
	Case I NFIX = 0	Case II NFIX = 1	Case III NFIX = 2	Case IV NFIX = 0	Case V NFIX = 1	Case VI NFIX = 2
d_1	$2w_o p_1/\ell$	0	$2w_o p_1/\ell$	p_1	0	p_1
d_2	p_1	0	p_1	p_2	0	p_2
d_3	$2w_o p_2/\ell$	$2w_o p_1 \ell$	0	p_3	p_1	0
d_4	p_2	p_1	0	p_4	p_2	0
d_5	$p_3 \ell$	$p_2 \ell$	$p_2 \ell$	$p_5 \ell$	$p_3 \ell$	$p_3 \ell$

Calling Sequence: CALL PROCESS (P,NUMVA)

    Input: P(I), I = 1, NUMVA

    Output: D(J), J = 1,5

Subroutine DISCRIT

Purpose: This subroutine divides the sections along the transverse and the rolling direction in rectangular elements, as described in Appendix B. For each element, the locations of the nodal points, area of surfaces, volume and other properties are determined.

Calling Sequence: CALL DISCRIT (MPEL,X,Y,H,AY,BY,AZ,BZ,YY,ZZ,ISLOP,MST,MSL, XN,VO,GRA,YCAL,HCALT,HCALB,NCAL,NUMNP,NUMEL,NUMST,NUMSL, NUMPX,NUMPY)

    Input: YCAL,HCALT,HCALB,NCAL,NUMNP,NUMEL,NUMST,NUMSL,NUMPX,NUMPY, MPEL,MST,MSL

    Output: X,Y,H,AY,BY,AZ,BZ,YY,ZZ,ISLOP,XN,VO,GRA

Subroutine AREA

Purpose: This subroutine calculates the areas of cross sections and average heights at each cross section.

Calling Sequence: CALL AREA (Y1,Y2,A,P,HG1,HG2,N,YCAL,HCALT,HCALB,NCAL)

    Input: Y1,Y2,N,YCAL,HCALT,HCALB,NCAL

    Output: A = Area, HG1 = Average upper height, HG2 = Average lower height

Subroutine EDIST

Purpose: This subroutine calculates the energy rate due to velocity discontinuities along the transverse sections. This energy rate for each section is then stored in an array EJUMP.

Calling Sequence: CALL EDIST (EDT,X,Y,Z,AY,BY,AZ,BZ,YY,ZZ,MST,ISLOP,VO,EJUMP, NUMEL,NUMST,NUMPX,NUMPY)

    Input: All the variables in the call statement except EDT

    Output: EDT, the energy rate due to velocity discontinuities along the transverse sections.

Subroutine INTEG

Purpose: This subroutine provides the value of the integral in computing energy rate due to velocity discontinuities along the transverse sections. It is called by subroutine EDIST.

Calling Sequence: CALL INTEG (FTN1, FTN2, A,B,X)

Input: X = Independent variable, A = Lower limit, B = Upper limit

Output: FTN1,FTN2 = Values of two integrals, respectively.

Subroutine EDEFM

Purpose: This subroutine calculates the energy rate due to plastic deformation under the rolls. The integration in the energy term is carried out numerically by the Newton-Cotes five-point scheme, where the maximum number of iterations are fixed to ten. (See description of Subroutine QUAD for details).

Calling Sequence: CALL EDEFM (ED,X,AY,BY,AZ,BZ,YY,ZZ,VO,ISLOP,EJUMP,NUMPX, NUMPY,NUMEL)

Input: All the variables in the call statement except ED

Output: ED, the energy rate due to plastic deformation

Subroutine DUMMY

Purpose: This subroutine defines arrays A,B,II and JJ.

Calling Sequence: CALL DUMMY (AY,BY,AZ,BZ,YY,ZZ,VO,ISLOP,NC,N,M)

Input: All the variables in the call statement

Output: A,B,II,JJ

Subroutine QUAD

Purpose: This subroutine numerically approximates the value of an integral by using the Newton-Cotes five-point formula[3]. In this method, the interval is divided into four equal length subintervals and the Newton-Cotes five-point approximation is used. If the error is larger than the specified error bound, the number of intervals is doubled and the Newton-Cotes formula is again applied. The procedure of doubling the number of intervals and applying the Newton-Cotes formula is continued until the real error is within the specified error bounds.

Calling Sequence: CALL QUAD (A,B,AREA1,AREA2,RELERR,N,NAME)

Input: A = Lower limit of the integral

B = Upper limit of the integral

NAME = Name of the REAL FUNCTION type subroutine which computes the integrand, must appear in an EXTERNAL statement.

Output: AREA1 = Integrated value by $(N-1)^{th}$ iteration

AREA2 = Integrated value by N'th iteration

RELERR = Calculated value of the relative error

N = Number of iterations conducted.

Function POWP

Purpose: This function subprogram provides the integrand of the deformation energy integration for a given element at a given distance along the rolling direction.

Function Reference: VALUE = POWP(X)

Input: X, distance along the rolling direction

Output: VALUE

---

(3) D. D. McCracken and W. S. Dorn, Numerical Methods and Fortran Programming, John Wiley, 1964.

Subroutine FLOW

Purpose: This subroutine provides the material flow stress for given strain value under cold rolling condition*. Under hot rolling conditions, since material does not work harden, a constant value of flow stress is adequate. The value of flow stress provided by this routine is used for determining metal flow only.

Calling Sequence: CALL FLOW (EPS,SIG)

Input: EPS, strain

Output: SIG, flow stress

Subroutine EDISS

Purpose: This subroutine calculates the energy rate due to velocity discontinuities along the longitudinal sections. This energy rate for each section is then stored in array EJUMP.

Calling Sequence: CALL EDISS (ED,X,AY,BY,AZ,BZ,YY,ZZ,VO,ISLOP,MSL,EJUMP,NUMPX, NUMPY,NUMEL,NUMSL)

Input: All the variables in the call statement except EJUMP

Output: ED, the energy rate due to velocity discontinuities along the longitudinal sections

Function PODS

Purpose: This function subprogram provides the value of the integrand in the expression for energy rate due to velocity discontinuities along the longitudinal sections at a given distance along the rolling direction.

Function Reference: VALUE = PODS(X)

Input: X, the distance along the rolling direction

Output: VALUE

---

* Metal flow is not significantly influenced by work-hardening characteristics. Therefore, a constant value of flow stress SIG is sufficient for metal flow analysis. However, in order to calculate the torque, the exact flow stress value must be used and obtained from Subroutine MATERL, as described later.

Function SQF

Purpose: This function gives the value of an integral given in the following form:

$$SQF = \int_A^B \left\{ (Px + Q)^2 + T^2 \right\} dx$$

Function Reference: VALUE = SQF (P,Q,T,A,B)

Input: P,Q,T,A,B

Output: VALUE

Function WA

Purpose: This function provides the third order polynomial for the spread function $w_1(x)$. Through ENTRY WB, it provides the polynomial for the spread function $w_2(x)$.

Function Reference: w_1 = WA(X)

w_2 = WB(X)

Subroutine EDIFS

Purpose: This subroutine calculates the energy rate associated with overcoming the frictional constraints at the roll-workpiece interfaces. The friction shear stress is defined as equal to $m\bar{\sigma}/\sqrt{3}$, where m is a constant ($0 \leq m \leq 1$) and $\bar{\sigma}$ is the material flow stress. The resultant velocity of the interface is calculated and the friction energy rate is computed based on this velocity.

Calling Sequence: CALL EDIFS (ED,X,AY,BY,AZ,BZ,YY,ZZ,VO,ISLOP,XN,EJUMP,NUMEL, NUMPX,NUMPY)

Input: All the variables in the call statement, except ED

Output: Ed, the energy rate required to overcome friction between the rolls and the workpiece.

Function Reference: VALUE = POWF(X)

    Input: X

    Output: VALUE

Subroutine LIN2

  Purpose: This subroutine solves the matrix equation $\underline{A}\ \underline{X} + \underline{B} = 0$.
    The matrix $\underline{B}$ is replaced by the solution matrix $\underline{X}$. $\underline{A}$ must
    be square and non-singular. $\underline{B}$ must have the same number
    of rows as $\underline{A}$. This routine is used here for solution of
    simultaneous linear equations. The method consists of
    Gaussian elimination followed by back substitution[4].

  Calling Sequence: CALL LIN2 (A,N,NN,EPS,B,M,MM,LTEMP,IERR,DET,HPIV,PIV,LPR,
    LPC)

    Input: A = The coefficient matrix

     N = The order of A

     NN = The number of words of storage provided for each
      column of A in the calling program

    EPS = Error bound, customarily zero

     B = The constant term matrix

     M = The number of columns of B

     MM = The number of words of storage provided for each
      column of B in the calling program

    LTEMP = A block of at least N words of temporary integer
      storage

    Output: X = The solution matrix

     IERR = 2 if no columns of X are found

      = 0 if all columns of X are found

     DET = plus or minus the product of the current and all
      preceding pivots

     NPIV = The number of current pivot

     PIV = The current pivot

     LPR = The first NPIV positions in the row

     LPC = The first NPIV positions in the column

---

(4) D. D. McCracken and W. S. Dorn, Numerical Methods and Fortran Programming, John Wiley, 1964.

Subroutine TORQUE

Purpose: This subroutine calculates the roll torque on the top and bottom surfaces by direct integration. The total torque is calculated this way should be approximately equal to the total energy rate, ETOTAL, for properly converged solution.

Calling Sequence: CALL TORQUE (TQ,X,AY,BY,AZ,BZ,YY,ZZ,XN,ISLOP,VO,EJUMP, NUMEL,NUMPX,NUMPY)

Input: All the variables in the call statement except TQ

Output: TQ, the torque values for the upper and the lower rolls.

Function YFT

Purpose: This function provides the value of the integrand in calculation of torque. The flow stress of the material is taken as a function of strain, strain rate and temperature here by calling subroutine MATERL instead of subroutine FLOW.

Function Reference: VALUE = YFT(X)

Input: X

Output: VALUE

Subroutine MATERL

Purpose: This subroutine furnishes the tabulated flow stress data for a range of strains, strain rates, and temperatures. It also calculates the flow stress for given values of strain, strain rate, and temperature.

Calling Sequence: CALL MATERL (STRAIN,STRRAT,TEMP,FSTRES)

Input: STRAIN = strain, STRRAT = strain rate, TEMP = temperature

Output: FSTRES = flow stress

Function FSTRS

Purpose: Using the flow-stress data available from the subroutine MATERL, this subprogram performs the interpolation for determining the flow stress for given values of strain, strain rate, and temperature, which are also supplied by the subroutine MATERL.

Function Reference: FSTRES = FSTRS (MSTRN,MTEMP,T,ASTR,AC,AM,TEMP,STR,STRRAT)

Input: TEMP = temperature, STR = strain, STRRAT = strain rate. The other variables MSTRN, MTEMP, T, ASTR, AC, and AM are internally defined within the subroutine MATERL.

Subroutine AITKN

Purpose: This subroutine performs polynomial interpolation of a table of values Y versus X.

Calling Sequence: CALL AITKN (X,Y,N,K,XB,YB,T,IEX)

Input: X = a one-dimensional array of monotonous independent variables

Y = a one-dimensional array of dependent variables

N = the number of X-Y pairs

K = the degree of interpolating polynomial, $K \leq N - 1$

XB = the value of the independent variable to be used

Output: YB = the interpolated value of the dependent variable

IEX = integer for error check, 1 if extrapolation was performed, 0 otherwise.

The variable name T represents a one-dimensional array of at least 2 (K + 1) words used for temporary storage.

Subroutine OUTP

Purpose: This subroutine prints all the output in a systematic form.

Calling Sequence: CALL OUTP (X,Y,H,FLOW,XN,GRA,TQ,HED,NUMPX,NUMPY,NUMEL,NUMNP)

Input: All the variables in the call statement.

Output: The printed results.

Preparation of Input Data

The preparation of the input data for the program SHPROL is given in the following. The quantities in parentheses at the end of each description represent an example case.

1. First Set of Data Card, Format (8I5)

Columns 1-10: NUMPX, Number of nodal points in the x-direction (See Figure C-6) (5)

11-20: NUMPY, Number of nodal points in the y-direction (See Figure C-6) (7)

21-30: NCAL, Number of points where extra values on the upper and lower contours of the roll and the workpiece are interpolated. This helps to define the contours more accurately at intermediate points (51)

31-40: NDATAT, Number of points supplied to define the top roll contour (design data) (28)

41-50: NDATAB, Number of points supplied to define the bottom roll contour (design data) (27)

51-60: NWDAT, Number of points supplied to define the top contour of workpiece (design data) (26)

61-70: NWDAB, Number of points supplied to define the bottom contour of workpiece (design data) (25)

71-80: NPRINT, Printing option (1). If NPRINT = 0, interpolated values of contact surface are printed. If NPRINT $\neq$ 0, interpolated values of contact surface are not printed.
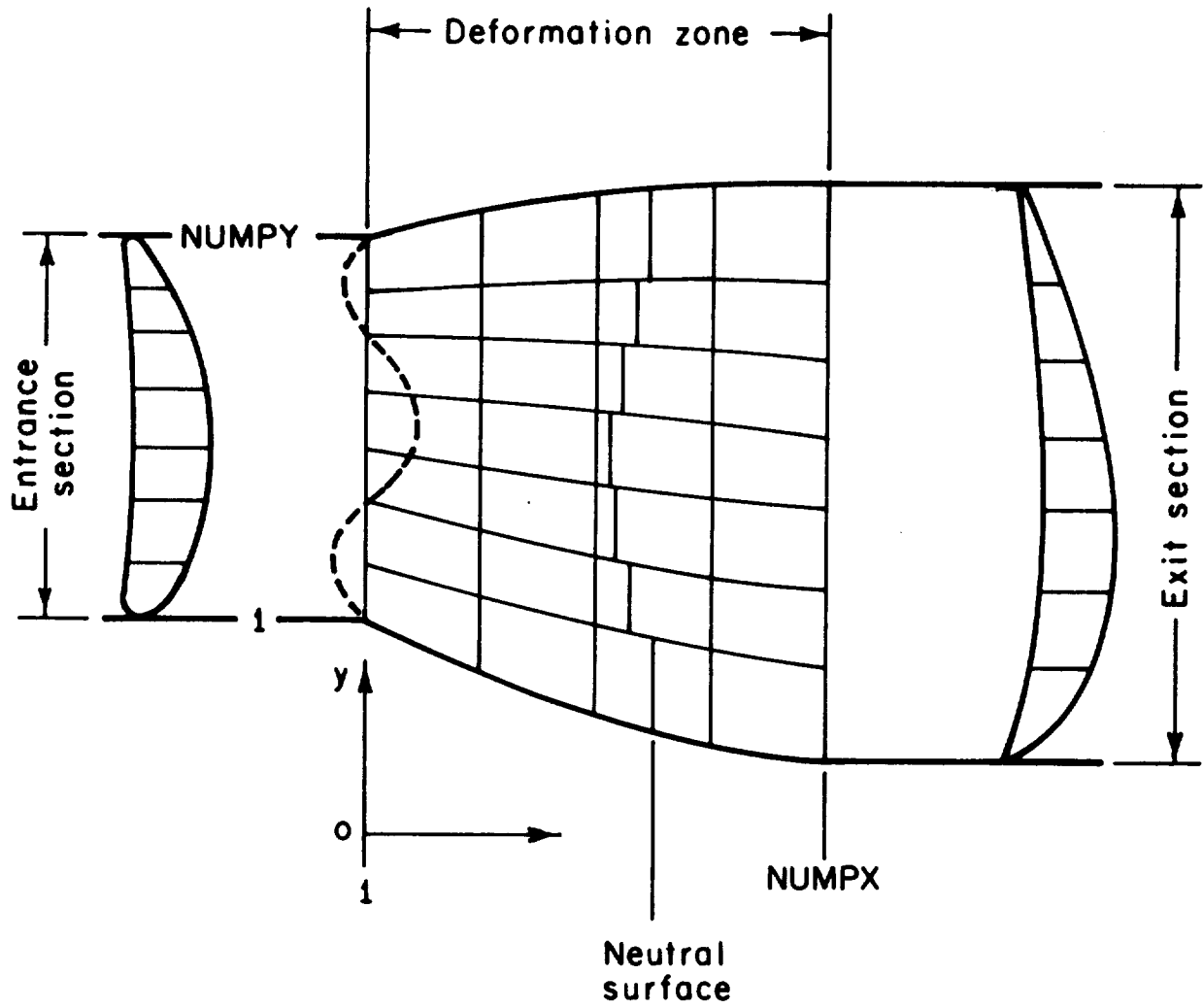
FIGURE C-6. CONFIGURATION OF DEFORMATION ZONE IN ROLLING OF AIRFOIL SHAPES

2. Second Set of Data Card, Format (8F10.0)

  (See Figure C-2)

  Columns 1-10: OY1, y-coordinate of the origin of the coordinate

       system for the upper roll contour (0.)

     11-20: OZ1, z-coordinate of the origin of the coordinate system

       for the upper roll contour (0.)

     21-30: OY2, y-coordinate of the origin of the coordinate system

       for the lower roll contour (0.)

     31-40: OZ2, z-coordinate of the origin of the coordinate system

       for the lower roll contour (0.)

     41-50: OY3, y-coordinate of the origin of the coordinate system

       for the workpiece contour (0.)

     51-60: OZ3, y-coordinate of the origin of the coordinate system

       for the workpiece contour (0.)

     61-70: ZR(1), z-coordinate of the upper roll axis in its own

       coordinate system (4.0)

     71-80: ZR(2), z-coordinate of the lower roll axis in its own

       coordinate system (-4.0).

3. Third Set of Data Card, Format (8F10.0)

  Columns 1-10: YDATA(1), y-coordinate of the upper roll contour in its own

       coordinate system

     11-20: ZDATA(1), z-coordinate of the upper roll contour in its

       coordinate system

     21-30: YDATA(2)

     31-40: ZDATA(2)

     41-50: YDATA(3)

     51-60: ZDATA(3)

     61-70: YDATA(4)

     71-80: ZDATA(4)

Continue on additional cards in the similar manner up to NDATAT pairs
of coordinates. Example: -0.4570, -0.0939, -0.4232, -0.0764, -0.3911,
-0.0608, -0.3634, -0.0477, etc.

4. Fourth Set of Data Card, Format (8F10.0)

Columns 1-10: YDATAB(1), y-coordinate of the lower roll contour
in its own coordinate system

11-20: ZDATAB(1), z-coordinate of the lower roll contour
in its own coordinate system

21-30: YDATAB(2)

31-40: ZDATAB(2)

41-50: YDATAB(3)

51-60: ZDATAB(3)

61-70: YDATAB(4)

71-80: ZDATAB(4)

Continue on additional cards in the similar manner up to NDATAB pairs
of coordinates. Example: -0.4570, -0.1248, -0.4277, -0.1089, -0.39112,
-0.0940, -0.3533, -0.0817, etc.

5. Fifth Set of Data Card, Format (8F10.0)

Columns 1-10: YWDAT(1), y-coordinate of the workpiece top contour in
its own coordinate system

11-20: ZWDAT(1), z-coordinate of the workpiece top surface in
its own coordinate system

21-30: YWDAT(2)

31-40: ZWDAT(2)

41-50: YWDAT(3)

51-60: ZWDAT(3)

61-70: YWDAT(4)

71-80: ZWDAT(4)

Continue on additional cards in the similar manner up to NWDAT pairs
of coordinates. Example: -0.4570, -0.0877, -0.4232, -0.0702, -0.3911,
-0.0546, -0.3634, -0.0415, etc.

6. Sixth Set of Data Card, Format (8F10.0)

Columns 1-10: YWDAB(1), y-coordinate of the workpiece bottom contour in its own coordinate system

11-20: ZWDAB(1), z-coordinate of the workpiece bottom contour in its own coordinate system

21-30: YWDAB(2)

31-40: ZWDAB(2)

41-50: YWDAB(3)

51-60: ZWDAB(3)

61-70: YWDAB(4)

71-80: ZWDAB(4)

Continue on additional cards in the similar manner up to NWDAB pairs of coordinates. Example: -0.4570, -0.1311, -0.4277, -0.1152, -0.3912, -0.1003, -0.3533, -0.0880, etc.

7. Seventh Set of Data Card, Format (4F10.0)

Column 1-10: WO(1), y-coordinate of the far end* of the undeformed workpiece in its own coordinate system (See Figure C-5) (0.4)

11-20: WO(2), y-coordinate of the near end* of the undeformed workpiece in its own coordinate system (-0.4)

21-30: SPL(1), y-coordinate of the far end* of the roll gap in the workpiece coordinate system (0.)

31-40: SPL(2), y-coordinate of the near end* of the roll gap in the workpiece coordinate system (-0.457)

Note: If SPL(1) = 0, the far end is free. If SPL(2) = 0, the near end is free. If Columns 21 through 40 are left blank, width of the roll gap is taken as infinity (open ends) as a default value.

---

* Near end = low y-value, far end = high y-value.

8. Eithth Data Card, Format (8A10)

Columns 1-80: Heading of up to 80 characters, which the user wants to print on the output for identification purpose.
Example: ROLLING OF H369 AIRFOIL

9. Ninth Data Card, Format (4F10.0)

Columns 1-10: OGA(1), Angular velocity of top roll, rad/sec (1.0)
11-20: OGA(2), Angular velocity of bottom roll, rad/sec (-1.0)
21-30: FRIC, Friction shear factor m (0.5)
31-40: TEMP, Temperature of the billet, C (800.)

10. Tenth Data Card, Format (5I5,5X,2E10.3)

Columns 1-5: NCURVE, a code number to select the type of lateral spread profile (1)
If NCURVE = 1, a parabolic profile is assumed
If NCURVE = 2, a third order polynomial profile is assumed
6-10: NFIX, a code number to specify the end conditions in the width direction (0)
If NFIX = 0, both ends of the workpiece are free to move
If NFIX = 1, far end of the workpiece is fixed
If NFIX = 2, near end of the workpiece is fixed.
11-15: NSYM, a code for symmetry of workpiece (0)
If NSYM = 0, no symmetry in the thickness direction
If NSYM = 1, workpiece symmetric in the thickness direction

16-20: NCOUNT, the number of previous iterations* (0)

If NCOUNT = 0, no previous iterations

If NCOUNT ≠ 0, the results of last iterations
available on Tape 8 are used as starting
values

21-25: ITER, maximum number of iterations allowed in the run (10)

26-30: Blank

31-40: ERIT, error limit on the simplex size during minimization
(1.0E-03)

41-50: ERITE, error limit on the maximum directional derivative
during the minimization (1.0E-03)

11. Eleventh Data Card, Format (8F10.0)

Columns 1-10: CONST(1), (10.)

11-20: CONST(2), (10.)

21-30: CONST(3), (0.)

31-40: CONST(4), (0.)

41-50: CONST(5), (0.)

The values of CONST(I) are selected in such a way that when multiplied
by the corresponding guess values PB(I) of the unknown parameters for
energy minimization, they yield approximately the same quantity. (PB(I)'s
are discussed in Subroutine PROCESS). This way, the minimization of the
energy rate is accelerated. However, if the user cannot come up with
reasonable values of these constants, a blank card should be inserted
here. This will ensure that the default values of 1 is used in the
computations.

12. Twelfth Data Card, Format (8F10.0)

Read (PB(I), I = NUMVA), STEP, where NUMVA has a value between 2 to 5,
depending upon the boundary conditions, explained later. Each quantity
is punched within ten columns, beginning with Column 1. STEP represents

---

* This control is useful when solution does not converge in the first run. In the
next run, the results from the last iteration of the previous run are used as
starting values.

a small displacement from the guessed values. The values of
PB(I), the guess values of the various unknown parameters, are
selected according to the guidelines given in Table C-2.

Example: 0.01, -0.01, 0.65, 0.05

TABLE C-2. GUIDELINES FOR ESTIMATING GUESS VALUES PB(I) (See Figure C-5)

(i) Case I: When NCURVE = 1, and NFIX = 0

Columns 1-10: $PB(1) = \dfrac{w_1(\ell) - w_1(0)}{w_1(0) - w_2(0)}$,

11-20: $PB(2) = \dfrac{w_2(\ell) - w_2(0)}{w_1(0) - w_2(0)}$,

21-30: $PB(3) = x_n/\ell$ (Usually equal to 0.65)

31-40: STEP

(ii) Case II: When NCURVE = 1, NFIX = 1

Columns 1-10: $PB(1) = \dfrac{w_2(\ell) - w_2(0)}{w_1(0) - w_2(0)}$

11-20: $PB(2) = x_n/\ell$ (Usually equal to 0.65)

21-30: STEP

(iii) Case III: When NCURVE = 1, NFIX = 2

Columns 1-10: $PB(1) = \dfrac{w_1(\ell) - w_1(0)}{w_1(0) - w_2(0)}$

11-20: $PB(2) = x_n/\ell$ (Usually equal to 0.65)

21-30: STEP

TABLE C-2. (Continued)

(iv)   Case IV: When NCURVE = 2, NFIX = 0

Columns 1-10: $PB(1) = \left.\dfrac{dw_1(x)}{dx}\right|_{x=0}$

11-20: $PB(2) = \dfrac{w_1(\ell) - w_1(0)}{w_1(0) - w_2(0)}$

21-30: $PB(3) = \left.\dfrac{dw_2(x)}{dx}\right|_{x=0}$

31-40: $PB(4) = \dfrac{w_2(\ell) - w_2(0)}{w_1(0) - w_2(0)}$

41-50: $PB(5) = x_n/\ell$ (Usually equal to 0.65)

51-60:   STEP

(v)   Case V: When NCURVE = 2, NFIX = 1

Columns 1-10: $PB(1) = \left.\dfrac{dw_2(x)}{dx}\right|_{x=0}$

11-20: $PB(2) = \dfrac{w_2(\ell) - w_2(0)}{w_1(0) - w_2(0)}$

21-30: $PB(3) = x_n/\ell$ (Usually equal to 0.65)

31-40:   STEP

(vi)   Case VI: When NCURVE = 2, NFIX = 2

Columns 1-10: $PB(1) = \left.\dfrac{dw_1(x)}{dx}\right|_{x=0}$

11-20: $PB(2) = \dfrac{w_1(\ell) - w_1(0)}{w_1(0) - w_2(0)}$

21-30: $PB(3) = x_n/\ell$ (Usually equal to 0.65)

31-40:   STEP

List of Important Variables

ALFA	Reflection coefficient, recommended value = 1.0
AY	Slope of grid lines in the x-direction
AZ	Slope of grid lines in the z-direction
BETA	Contraction coefficient, recommended value = 0.5
BY	y-intercept of grid lines
BZ	z-intercept of grid lines
CONST	This array adjusts the sensitivity of energy function with respect to unknown parameters. Has default value of 1.0

D(1) $\quad w_1(0)$

D(2) $\quad \left[w_1(\ell) - w_1(0)\right]/w_1(0)$

D(3) $\quad w_2'(0)$

D(4) $\quad \left[w_2(\ell) - w_2(0)\right]/w_2(0)$

D(5) $\quad x_n/\ell$

(See Figure C-5)

EJUMP	Amount of strain jumps on the transverse sections
FRIC	Constant friction shear factor ($0 \le$ FRIC ≤ 1)
GAMA	Expansion coefficient, recommended value = 2.0
H	Array of z-coordinates of grid points
HCALB	Interpolated values of height of bottom-roll contour
HCALT	Interpolated values of height to top-roll contour
HDATAB	Array of z-coordinates of points during the bottom-roll contour in local coordinate system

HDATAT	Array of z-coordinates of points defining the top roll contour in local coordinate system
HWCAB	Interpolated values of height of bottom-workpiece contour
HWCAT	Interpolated values of height of top-workpiece contour
HWDAB	Array of z-coordinates of points defining the bottom contour of the workpiece in local coordinate system
HWDAT	Array of z-coordinates of points defining the top contour of the workpiece in local coordinate system
ISLOP	Logical variable to check the slopes of grid lines
MPEL	Array to describe the elements surrounding a given element, counter-clockwise
MSL	Array to describe the elements on both sides of a longitudinal section of discontinuity
MST	Array to describe the elements on both sides of a transverse section of discontinuity
NCAL	Number of points where interpolated heights of roll and workpiece contours are required
NCOUNT	Number of energy value evaluations
NCURVE	A variable for selection option of spread profile. If NCURVE = 1, parabolic spread profile is assumed. If NCURVE = 2, third order polynomial spread profile is assumed.
NDATAB	Number of data points to be supplied for bottom roll contour
NDATAT	Number of data points to be supplied for top roll contour
NEUTAL	Number of stream duct where location of the neutral plane is specified (guess value)

NFIX	A variable for selecting option for end condition
	If NFIX = 0, both ends are free to move
	If NFIX = 1, far end of the strip is fixed
	If NFIX = 2, near end of the strip is fixed
NSYM	A variable for selecting option for symmetry
	If NSYM = 0, no symmetry in thickness direction
	If NSYM = 1, symmetry in thickness direction
NUMEL	Total number of elements
NUMNP	Total number of nodal points
NUMPX	Number of nodal points in the rolling direction
NUMPY	Number of nodal points in the transverse direction
NUMSL	Total number of longitudinal sections
NUMST	Total number of transverse sections
NUMVA	Number of spread parameters for minimizing energy rate
NWDAB	Number of data points to be supplied for workpiece bottom contour
NWDAT	Number of data points to be supplied for workpiece top contour
OY1	y-coordinate of the origin of the coordinate system for the top roll contour
OY2	y-coordinate of the origin of the coordinate system for the bottom roll contour
OY3	y-coordinate of the origin of the coordinate system for the workpiece contour
OZ1	z-coordinate of the origin of the coordinate system for the top roll contour

OZ2	z-coordinate of the origin of the coordinate system for the bottom roll contour
OZ3	z-coordinates of the origin of the coordinate system for the workpiece contours
PB	Initially, this array contains guess values of the unknown parameters of the spread function for minimization energy. Later, it contains coordinates of the centroid of current simplex, excluding the point which gives the maximum value of the function.
STEP	Value of an increment to determine initial simplex polygon
TQ	Real array for torque values, TQ(1) for top roll, TQ(2) for bottom roll
U	x-velocity at the entrance plane
VO	Material flow rate ratio through an element
WO(1)	y-coordinate of the far end of the workpiece at entrance (Large y-coordinate)
WO(2)	y-coordinate of the near end of the workpiece at entrance (Small y-coordinate)
X	Array of x-coordinates of grid points
XLNTH	Contact length under the rolls
XN	x-coordinate of the neutral line, XN(N,1) for the top surface, XN(N,2) for the bottom surface
XS	Real array constituting the simplex for minimization
Y	Array of y-coordinates of grid points
YCAL	y-coordinates of points where heights of workpiece and roll contours are interpolated
YDATAB	Array of y-coordinates of points defining the bottom roll contour in local coordinate system

YDATAT   Array of y-coordinates of points defining top roll contour in local coordinate system

YWDAB   Array of y-coordinates of points defining the bottom contour of the workpiece in local coordinate system

YWDAT   Array of y-coordinates of points defining the top contour of the workpiece in local coordinate system

YY   y-coordinate of the point of intersection of two grid lines on the x-y plane

YS   Array of energy value for the simplex points

ZR(1)   z-coordinates of the top roll axis

ZR(2)   z-coordinates of the bottom roll axis

ZZ   z-coordinate of the point of intersection of two grid lines on the x-z plane

APPENDIX D

COMPUTER SYSTEM REQUIREMENTS

FOR ROLPAS

APPENDIX D

COMPUTER SYSTEM REQUIREMENTS

The ROLPAS system was developed on a PDP-11/40 minicomputer using RT-11 operating system. In order to run ROLPAS with no (or minor) modifications, the following hardware and software components are required:

(1) A PDP-11 series computer (except LSI-11) with a minimum of 28K words of memory operating under RT-11.

(2) A random access external storage device such as a disk cartridge drive or a dual floppy disk drive.

(3) A computer terminal (keyboard/printer) such as a teletype or DEC-writer.

(4) VT-11 display processor with a graphics CRT and light pen.

(5) An x-y plotter interfaced to the PDP-11. Needed only if hard copies of the CRT graphics is desired.

The graphics related modules of ROLPAS are designed and coded to use the VT-11 display processor and its extensive interactive capabilities. Since all the graphics related routines are physically separate entities, with moderate effort, they can be recoded for another graphical input/output device, such as a Tektronix direct view storage tube.

All program modules, other than low level graphic routines, are written in standard FORTRAN-IV; thus, conversion to a different operating environment should be relatively straight forward.

DESCRIPTION OF COMMON DATA STORAGE AREAS

The following describes the contents of COMMON blocks. These areas are used as a means of communication between various program modules.

<u>COMMON/SYSPR/:</u> System parameters reside in this area.

    INPT: FORTRAN logical unit for input of the geometry of the shape to be rolled.

    LIST: FORTRAN logical unit for listing of intermediate and final results.

    INTI: FORTRAN logical unit for interactive input.

    INTO: FORTRAN logical unit for interactive output.

    ZERO: Floating point zero.

<u>COMMON/SURFG/:</u> Roll and material surface geometry reside in this area.

    NA: Number of points in the x-direction on the exit section. Does not include the points defining flash.

    NX: Number of points defining the material surface in the x-direction. I = 1,2, . . . NX

    NY: Number of points defining the material surface in the y-direction. J = 1,2, . . . NY

    NZ: Number of points defining the material surface in the z-direction. K = 1, NZ. K = 1 for the upper surface and K = 2 for the lower surface.

    XM(I,J): x-coordinates of the deforming material surface, Figure D-1.

    YM(J): y-coordinates of the deforming material surface, Figure D-1.

    ZM(I,J,K): z-coordinates of the deforming material surface, Figure D-1.

    XE(I,N): Matrices containing the x and z coordinates defining the entrance (preform) and

    ZE(I,N): exit (roll) geometries.

    N = 1 for upper surface of entrance section

    N = 2 for lower surface of entrance section

    N = 3 for upper surface of exit section

    N = 4 for lower surface of exit section.

    NE(N): Contains the number of elements in each column of XE and ZE.
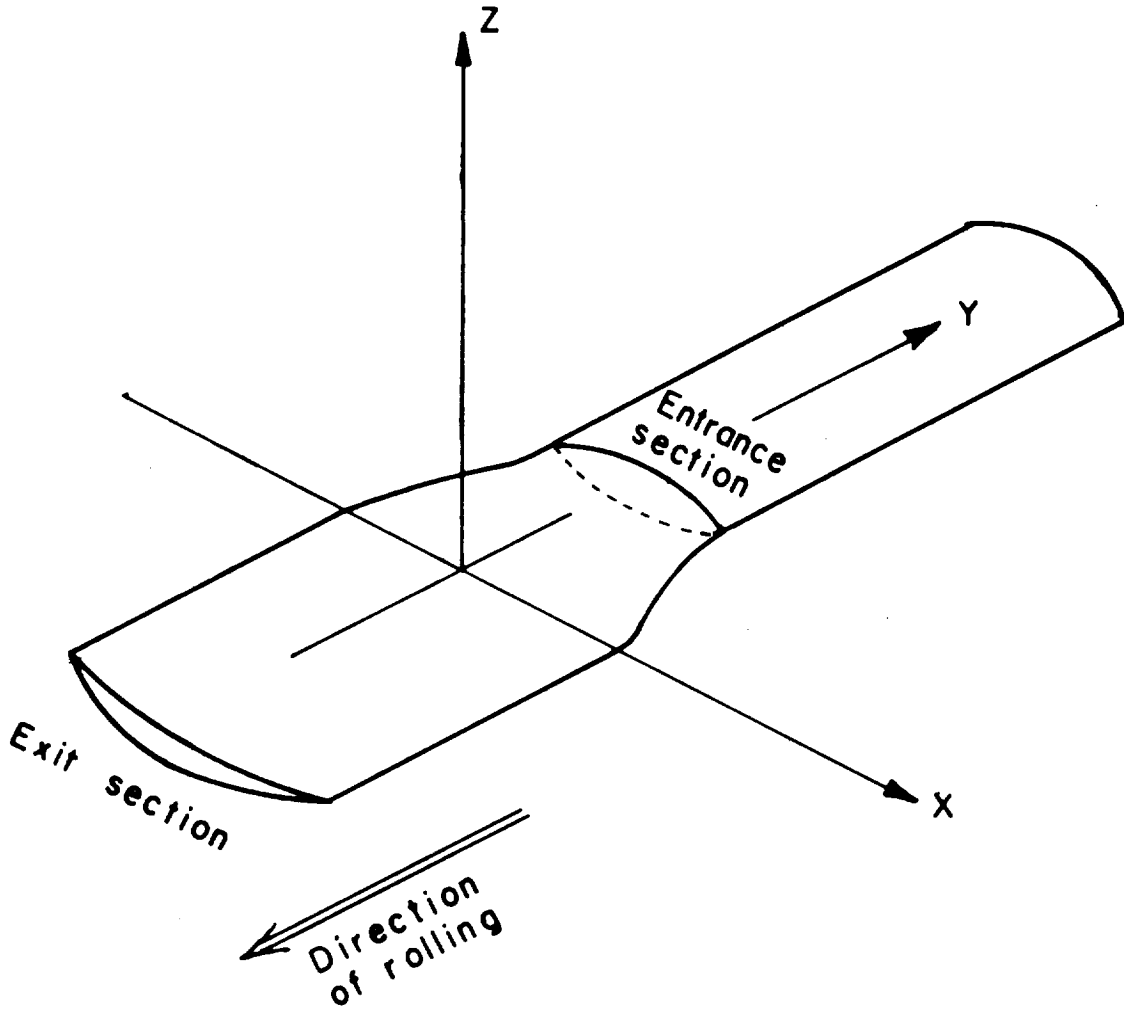
FIGURE D-1.   COORDINATE SYSTEM OF ROLPAS

XP(I):   Points describing the preform surface, normally interpolated
ZP(I,K):   from the input section described in XE and ZE.

NP: Number of points in XP and ZP.

XR(I):   Points describing the roll surface at the exit section,
ZR(I,K):   includes flashlands, if any. Interpolated from XE and ZE.

NR(N):   Points to elements of XR and ZR as illustrated in Figure D-2.

ZRL(I,K):   z-coordinates of the roll surface at YM(J) and XR(I)

ZRLM(I,K):   z-coordinates of the roll surface at YM(J) and XM(I,J)

IDFP(N,K):   Indices to the points of intersection of roll and material

cross section

NDFP(K):   Number of indices in IDFP

IDFA(N):   Indices of the deforming region

NEUTRL(N):   Indices of the neutral surfaces

NDE: Number of indices in IDFA

COMMON/PRMTR/:   Process and input data related parameters

FS: Flow stress

FF: Friction factor

ID: An array containing the identification of the input data

LH: Number of characters in ID

ROLDIA: Roll diameter

PEMX: Overall percent elongation

EFCTR: Elongation factor calculated by subroutine EPRMTR

COMMON/SCRAC/:   Consists of four arrays used as a scratch pad area by various

subroutines.

COMMON/RSLTS/:   Storage area for results of simulation and analysis.

SZ(I,J):   Vertical component of stress at XM(I,J)

FORCEY: Component of roll-separating force in the y-direction

FORCEZ: Component of roll-separating force in the z-direction

XCG: x-coordinate of the centroid of the exit section

ZCG: z-coordinate of the centroid of the exit section

ZRC(K):   z-coordinates of the upper and lower roll axis

ZRPLN: z-coordinate of the plane of rolling

FIGURE D-2. DEFINITIONS OF THE ELEMENTS OF THE POINTER ARRAY NR
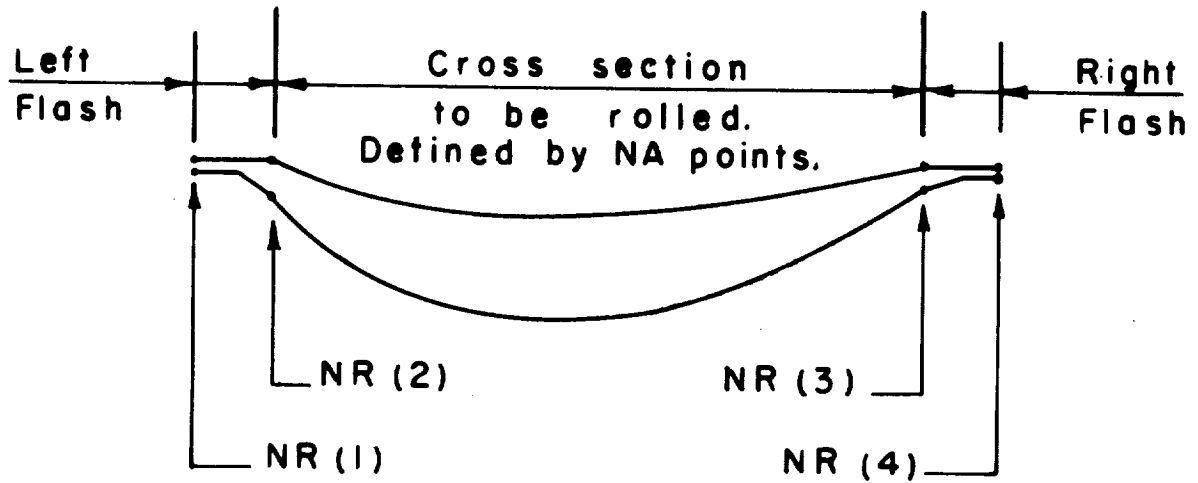
NR(1) = 1

NR(2) = NR(1) + 2 if there is flash on the left
NR(1) when there is no flash on the left

NR(3) = NR(2) + NA - 1

NR(4) = NR(3) + 2 if there is flash on the right
NR(3) when there is no flash on the right

FIGURE D-2. DEFINITIONS OF THE ELEMENTS OF THE POINTER ARRAY NR

COMMON/GRAPH/: Storage area for graphics related parameters

IXTRNS: x-coordinate of the center of the screen in screen (object space) units

IYTRNS: y-coordinate of the center of the screen

LSTAG: Identification tag of the last "item" displayed

SF: Scale factor

IDSPBF: Display file area

LDSPBF: Length of IDSPBF

IXYFLG: Status word used by the x-y plotter package

DESCRIPTION OF PROGRAM MODULES

PROGRAM ROLPAS

Purpose: Main program module of the ROLPAS system. It provides control and sequencing of the operating subroutines.

Method: User interface is via a menu of operations displayed on the left side of the screen. Menu elements are selected, "picked", with the light pen. At any given stage of the program, only those operations that are logically acceptable are displayed on the menu. This prevents execution of illogical sequence of operations by the user.

SUBROUTINE STMENU

Purpose: To set up the "operations" menu on the left side of the screen.

Call Sequence: CALL STMENU

Method: It is called by the main program to construct the operations menu on the left side of the screen. The graphics system is initiatilized, then the menu is set up via calls to LEGNDG.

SUBROUTINE PRMTRS

Purpose: To interact with the user in order to obtain rolling parameters.

Call Sequence: CALL PRMTRS

Method: Together with an appropriate question, the present value of the parameter is displayed to the operator. If only a carriage return is entered, the existing value is left unchanged. This routine is used to input the following variables: (1) scale factor, (2) roll diameter, (3) flow stress, and (4) friction factor.

SUBROUTINE DSPLY1

Purpose: Display the entrance and exit cross sections to enable visual checkout of input geometry.

Call Sequence: CALL DSPLY1

Method: Using routines IXIY and LINESG, the input arrays XE and ZE are displayed. The entrance and exit sections are super-imposed as input. Tracking cross is enabled to facilitate separation of the various input components for easier visual checkout.

SUBROUTINE DSPLY2

Purpose: Display the interpolated exit section together with flash.

Call Sequence: CALL DSPLY2 (IANS)

On exit IANS = $\emptyset$ if flash design is satisfactory.

IANS = 1 if flash design is unsatisfactory.

Method: The interpolated exit section in arrays XR and ZR are displayed using display routines IXIY and LINESG. The flash is displayed as blinking elements. Then the user is asked to decide on the acceptability of the flash. After the answer (Yes or No) is received, the display is removed and the routine exits.

SUBROUTINE DSPLY3

    Purpose: To display the entrance and exit sections (XP, ZP and
                XR, ZR, respectively) together with the plane of rolling
                and allow the modification of relative positions.

Call Sequence: CALL DSPLY3

    Method: The entrance section is displayed as a dashed curve, the
                exit section as a solid curve with a cross at its centroid.
                The plane of rolling is displayed as a dot-dash line
                initially passing through the centroid of the exit section.
                The tracking cross is enabled so that the user can modify
                the relative positions of the entrance and exit sections
                and the roll plane dynamically via the light pen. Upon
                return from the tracking cross controller, the new positions
                of the entrance section and the plane of rolling are obtained
                from the display file and the geometric data base is updated
                as appropriate.

SUBROUTINE DSPSM1

    Purpose: To display the material and the roll cross section at j'th
                simulation step.

Call Sequence: CALL DSPSM1(J), where $1 \leq J \leq NY$.

    Method: The upper and lower roll surface (stored in XR, ZRL) are
                displayed as solid curves. The input material cross section
                is superimposed as a dashed line curve.

SUBROUTINE DSPSM2

    Purpose: To replace the input material section displayed by DSPSM1
                with the output geometry.

Call Sequence: CALL DSPSM2(J), where $1 \leq J \leq NY$.

Method: The input material geometry as displayed by DSPSM1 is replaced by the output material geometry; thus, the deformation of the material at the J'th step is visually simulated. Optionally, the user is provided with a hard copy plot of the J'th simulation step via the x-y plotter.

SUBROUTINE DSPLYS

Purpose: To provide an orthographic projection of the stress surface in three dimensions.

Call Sequence: CALL DSPLYS

Method: Each cross section and each flowline is displayed, thus presenting a mesh that represents the stress surface. The user is asked to enter the desired angles of rotation around the three axis. Direction cosines are calculated by a call to DCOSIN and the companion routine ROTVEC is used to perform the rotation for each surface point (vector). The user is also given the option to obtain a hard copy of the display on the x-y plotter.

SUBROUTINE IXIYM

Purpose: To transform J'th material section points to display coordinates.

Call Sequence: CALL IXIYM (J,IX,IY,N)

 J: Index to J'th material section, $1 \le J \le NY$

 IX: On exit contains the x-coordinates for display

 IY: On exit contains the y-coordinates for display

 N: On exit contains the number of elements in IX, IY.

Method: The points on the upper surface of the J'th material section are transformed and stored in IX, IY. The order is from left to right. This is followed by the transformation of the points on the lower surface. These are stored in IX, IY in the order right to left. The first point in IX, IY is duplicated as the last point so that a closed figure is formed when IX, IY are displayed.

SUBROUTINE IXIY2D

Purpose:	To transform the interpolated entrance or exit section array to display coordinates.
Call Sequence:	CALL IXIY2D (X,Z,NXZ,IX,IY,N)
	X,Z: X and Z coordinates of the entrance or exit section
	NXZ: Number of elements in X and Z
	IX,IY: Display coordinates
	N: Number of elements in IX and IY.
Method:	The points on the top surface are transformed and stored in IX,IY. The order is from left to right (-x to +x). Then the lower surface points are transformed. The order is from right to left (+x to -x). The first point is copied as the last point so that a closed curve results when displayed.

SUBROUTINE IXIY

Purpose:	To scale and translate a point (vector) into display coordinates.
Call Sequence:	CALL IXIY (X,Y,IX,IY)
	X,Y: Input coordinates (subject space)
	IX,IY: Output in display coordinates (object space).
Method:	Uses the function ISCALE to perform the scaling and translates the points to display coordinates. The result is checked for limits of the screen and truncated, if required.

FUNCTION ISCALE

Purpose:	To scale a value (x or y coordinate) for the GT4Ø screen.
Call Sequence:	IV = ISCALE (VALUE, SCLFAC)
	VALUE: input coordinate in inches
	SCLFAC: Scale factor.

Method: Nine inches on the GT40 screen is equal to 1024 units
(rasters). Therefore, there are 113.78 units/inch.
VALUE is multiplied by the scale factor and 113.78.
Then check for error is performed (very large
magnitude) before being truncated into an integer.

FUNCTION UNSCAL

Purpose: To transform screen coordinates to user coordinates.

Call Sequence: V = UNSCAL (IVALUE,SCLFAC)

IVALUE: Display coordinate

SCLFAC: Scale factor

Method: IVALUE is floated and divided by the scale factor and by
113.78 which is the conversion factor between screen
coordinates and inches. That is 1 inch = 113.78 units on
the GT4$\emptyset$ screen.

SUBROUTINE CROSS

Purpose: To append a cross to the last display item.

Call Sequence: CALL CROSS (IDX,IDY)

IDX: The length of the x-component of the cross in screen
units. IDX is measured from the center.

IDY: The length of the y-component of the cross in screen
units as measured from the center.

Method: The starting and ending point of the display is the center
of the cross. Five calls are issued to VECTOR to add
vectors to the last display item so as to form a cross on
the screen. The shape of the cross resembles a + sign.

SUBROUTINE XCROSS

Purpose: To append an x-shaped cross to the last display item.

Call Sequence: CALL XCROSS (IDX,IDY)

IDX: The length of the x-component of the cross in screen
units as measured from the center of the cross

IDY: The length of the y-component.

Method: Five successive calls to VECTOR are issued to add five vectors to the last item so as to display a cross. The beam starts and ends at the center of the cross.

SUBROUTINE DCOSIN

Purpose: To calculate the direction cosines and form the 3-D rotation matrix.

Call Sequence: CALL DCOSIN (AXY,AYZ,AZX)

AXY: Rotation angle around z-axis

AYZ: Rotation angle around x-axis

AZX: Rotation angle around y-axis

Method: Cosines and sines of the three angles are calculated and the 3x3 rotation matrix is formed. The rotation matrix resides in labeled common DCSNMX. The companion routine ROTVEC accesses the same common area.

SUBROUTINE ROTVEC

Purpose: Rotate a vector in 3-D space.

Call Sequence: CALL ROTVEC (XI,YI,ZI,X,Y,Z)

XI,YI,ZI: The components of the vector to be rotated

X,Y,Z: The components of the rotated vector.

Method: Uses the direction cosine matrix prepared by DCOSIN and residing in common area DCSNMX. The input vector represented by XI,YI,ZI is multiplied by the rotation matrix. The resultant vector is returned in X, Y and Z.

SUBROUTINE READIN

Purpose: To read and interpret the input data file containing the cross sections of the entrance and exit geometries. Additionally, scale factor, flow stress, friction factor and roll diameter are input in an interactive mode via this routine.

Call Sequence: READIN -- Parameters are passed via common areas.

Method: The input data file is organized as follows:

Header identifying the data, up to 80 characters

Entrance plane geometry, upper half

XE(1,1),ZE(1,1)

XE(2,1),ZE(2,1)

"   "   Ordered from -x to +x in format 2F10.0

End of record signalled by x = 9999.

or greater

"   "   NE(1) = N

XE(N,1),ZE(N,1)

9999.,9999.

Entrance plane geometry, lower half

XE(1,2),ZE(1,2)

XE(2,2),ZE(2,2)

"   "

"   "

XE(N,2),ZE(N,2)

9999.,9999.   NE(2) = N

Exit plane geometry, upper half

XE(1,3),ZE(1,3)

XE(2,3),ZE(2,3)

"   "

"   "

XE(N,3),ZE(N,3)

9999.,9999.   NE(3) = N

Exit plane geometry, lower half

XE(1,4),ZE(1,4)

XE(2,4),ZE(2,4)

"   "

"   "

XE(N,4),ZE(N,4)

9999.,9999.   NE(4) = N

Thus, the set of points (x,z pairs) describing the upper
and lower surfaces of the entrance and exit sections are
of variable length. The rest of the variables are entered
from the keyboard in answer to questions displayed by the
computer program.

FUNCTION AREA

Purpose: Calculates the area of any polygon given the coordinates of
its vertices.

Call Sequence: A = AREA(N,X,Z) where

X = X-coordinates of the vertices

Z = Z-coordinates of the vertices

N = Number of vertices.

Method: Uses the following summation, which is based on calculation
of successive triangular areas.

$$\text{Area} = \frac{1}{2} \sum_{i=2}^{n} (X_i Z_{i-1} - X_{i-1} Z_i) + \frac{1}{2} (X_1 Z_n - X_n Z_1)$$

SUBROUTINE XCGZCG

Purpose: Calculates the coordinates of the centroid of any polygon
given the coordinates of its vertices.

Call Sequence: CALL XCGZCG (N,X,Z,XCG,ZCG)

where X = X-coordinates of the vertices

Z = Z-coordinates of the vertices

N = Number of vertices

XCG = X-coordinate of the centroid

ZCG = Z-coordinate of the centroid

Method: Uses the following summation, which is based on the calculation of centroids of successive triangular areas:

$$X_{cg} = \frac{1}{4.A} [\sum_{i=2}^{n} (X_i^2 \cdot Z_{i-1} - X_{i-1}^2 \cdot Z_i) + (X_1^2 1 Z_n - X_n^2 Z_1)]$$

(D-2)

Similarly:

$$Z_{cg} = \frac{1}{4.A} [\sum_{i=2}^{n} (X_i \cdot Z_{i-1}^2 - X_{i-1} Z_i^2) + (X_1 \cdot Z_n^2 - X_n \cdot Z_1^2)]$$

(D-3)

where A = area of the polygon which is calculated by a call to Function AREA.

FUNCTION AREAM

Purpose: Calculates the area of the portion of J'th material cross section between I1 and I2.

Call Sequence: AM = AREAM (I1,I2,J)

where

I1 = starting index of XM(I,J) and ZM(I,J,K)

I2 = ending index of XM(I,J) and ZM(I,J,K)

 J = index in the y-direction

Method: The effected elements of XM and ZM are organized into a one-dimensional array and Function AREA is called to perform the actual area calculation.

FUNCTION AREAR

Purpose: Calculates the partial cross-sectional area of roll geometry between indices I1 and I2.

Call Sequence: AR = AREAR (I1,I2,XX,ZZ,NZ)

where

I1 = index of starting point in XX and ZZ

I2 = index of ending point in XX and ZZ

XX = input vector containing the x-coordinates

ZZ = input matrix containing the upper and lower z-coordinates

NZ = total length of ZZ. Note that XX and ZZ are assumed to be dimensional XX(NZ), ZZ(NZ,2).

Method: The effected elements of XX and ZZ are organized into a one-dimensional array and Function AREA is called to perform the actual area calculation.

SUBROUTINE XZCG2D

Purpose: Calculates the X and Z coordinates of the centroid of entrance and exit cross sections.

Call Sequence: CALL XZCG2D (X,Z,N1,N2,XCG,ZCG)

where

X = a vector containing the x-coordinates

Z = a matrix composed of two vectors, z-coordinates of upper and lower surfaces

N1 = index of starting point in X and Z

N2 = index of ending point in X and Z

XCG = X-coordinate of the centroid

ZCG = Z-coordinates of the centroid.

Method: The effected elements of X and Z are organized into a one-dimensional array and subroutine XCGZCG is called to perform the actual calculations.

FUNCTION ZLINE

Purpose: Calculates the z-value given x using the general form of the equation of a line.

Call Sequence: ZVAL = ZLINE(COEF,X)

where

COEF = an array containing the coefficients of the equation of a line in the form $Ax + Cz = D$

COEF(1) = A

COEF(2) = C

COEF(3) = D

X = X-value.

Method: Z = (D − A.X)/C, if C is zero and error message is output
and execution is terminated.

SUBROUTINE LINEQ

Purpose: Determines the coefficients of the equation of a line
defined by two points.

Call Sequence: CALL LINEQ (X1,Y1,X2,Y2,COEF)

where

X1,Y1 = X and Y coordinates of the first point

X2,Y2 = X and Y coordinates of the second point

 COEF = On exit contains the coefficients of the
line equation Ax + By = C

COEF(1) = A

COEF(2) = B

COEF(3) = C

Method: Matrix algebra is used to determine the coefficients. The
values are normalized such that A and B are the components
of a unit vector normal to the line and C is the distance
from the origin to the line. C is always positive. When
coincident points are detected, an error condition results.

SUBROUTINE INT2LN

Purpose: To find the intersection of two lines given the coefficients
of both equations.

Call Sequence: CALL INT2LN (COEF1,COEF2,X,Y)

where

COEFF1 = an array containing the coefficients of the first
equation as described above

COEFF2 = an array containing the coefficients of the
second equation

 X,Y = coordinates of the point of intersection.

Method: Matrix algebra is used to determine the point of inter-
           section. The determinant of the system is calculated.
           A zero determinant signifies parallel lines and causes
           an error condition.

SUBROUTINE STRSZX

Purpose: Determines σ_z on planes parallel to the zx-plane. Neutral
            planes are also located.

Call Sequence: CALL STRSZX(J)
            where
            J = index to the J'th material cross section.

Method: Portions of the J'th material cross section that are indicated
           as deforming (via IDFA in labeled common SURFG) are manipulated
           so as to form deformation units. These are submitted to
           subroutine SLAB which performs the actual stress analysis.

           IDFA is assumed to contain pairs of indices pointing to the
           starting and ending points of the deforming regions as shown
           in Figure D-3. Analysis starts at both ends of the deforming
           region, for example, at IDFA(1) and IDFA(2), and progresses
           towards the center of the region. It progresses to the
           right from IDFA(1) and to the left from IDFA(2). The point
           at which the two stress curves intersect is termed the
           neutral plane. Metal on the left side of the neutral plane
           flows left and metal on the right side flows right.

           The various cases of no-flashland conditions, as summarized
           in Figure D-4 are also checked for and appropriate action is
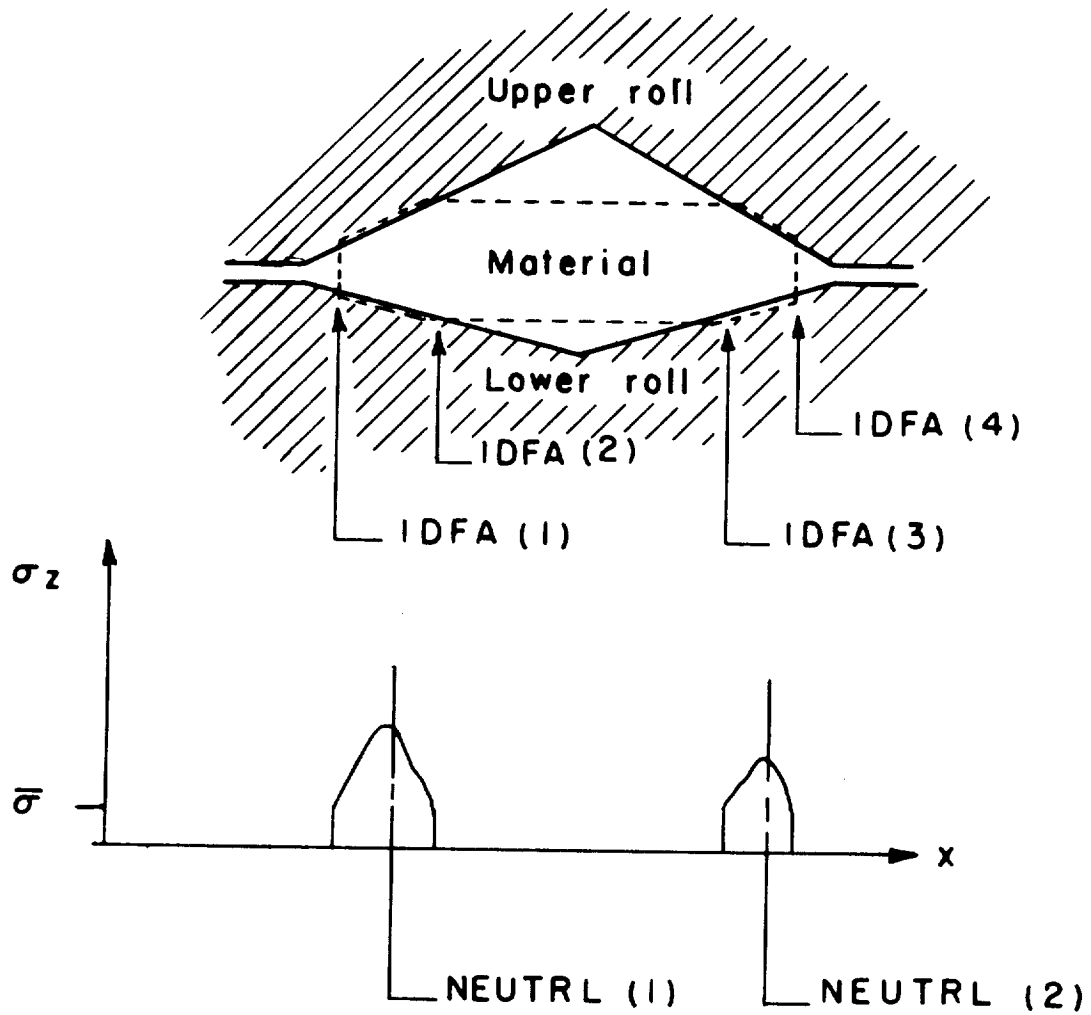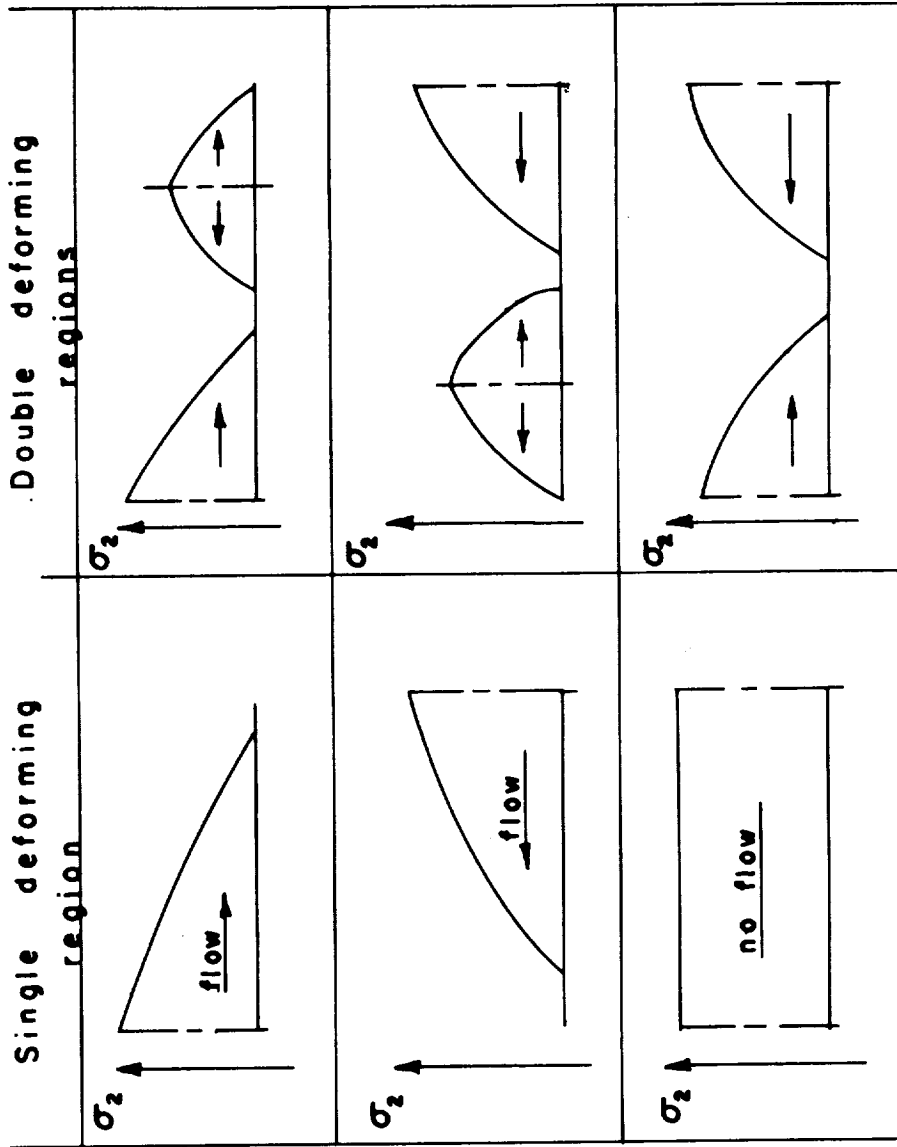   taken.

FIGURE D-3. DEFINITION OF THE POINTER ARRAY IDFA AND CONCEPTUAL STRESS
DISTRIBUTION DURING ROLLING OF A RECTANGLE THROUGH
DIAMOND LIKE ROLLS

FIGURE D-4. VARIOUS POSSIBLE CASES OF NO-FLASH SHOWING THE DIRECTION OF METAL FLOW AND THE POSITION OF THE NEUTRAL PLANES

SUBROUTINE STRSUZ

Purpose: Calculates the vertical stresses along the streamlines.

Call Sequence: CALL STRSUZ

Method: The streamlines of Figure D-5 are expanded into a fictitious dimension U. Analysis is started at both ends of the stream-line; from -U towards +U and from +U towards -U. Actual stress analysis is performed via subroutine SLAB. The stress value in SZ(I,J) as calculated by STRSZX is compared to the value just calculated. The lower value is accepted as the valid σ_z for the node in question.

SUBROUTINE SLAB

Purpose: Calculates the stress distribution in plane-strain upsetting of metals between inclined platens using the "slab" method of analysis.

Call Sequence: CALL SLAB (XU,ZU,FS,FF,SZE,SZB)

where

XU,ZU = coordinates of the corners of the deformation element as illustrated in Figure D-6

FS = flow stress

FF = friction factor

SZE = vertical stress at the known boundary σ_{ze}

SZB = vertical stress at the unknown boundary σ_{zb}

Method: Given the corner coordinates XU (1 to 4) and ZU (1 to 4), flow stress, friction factor and the vertical stress at the known boundary, the vertical stress at the unknown boundary, σ_{zb}, is calculated. Before exit from the routine, boundary geometry is updated in preparation for a possible subsequent call to evaluate the adjacent deformation element.
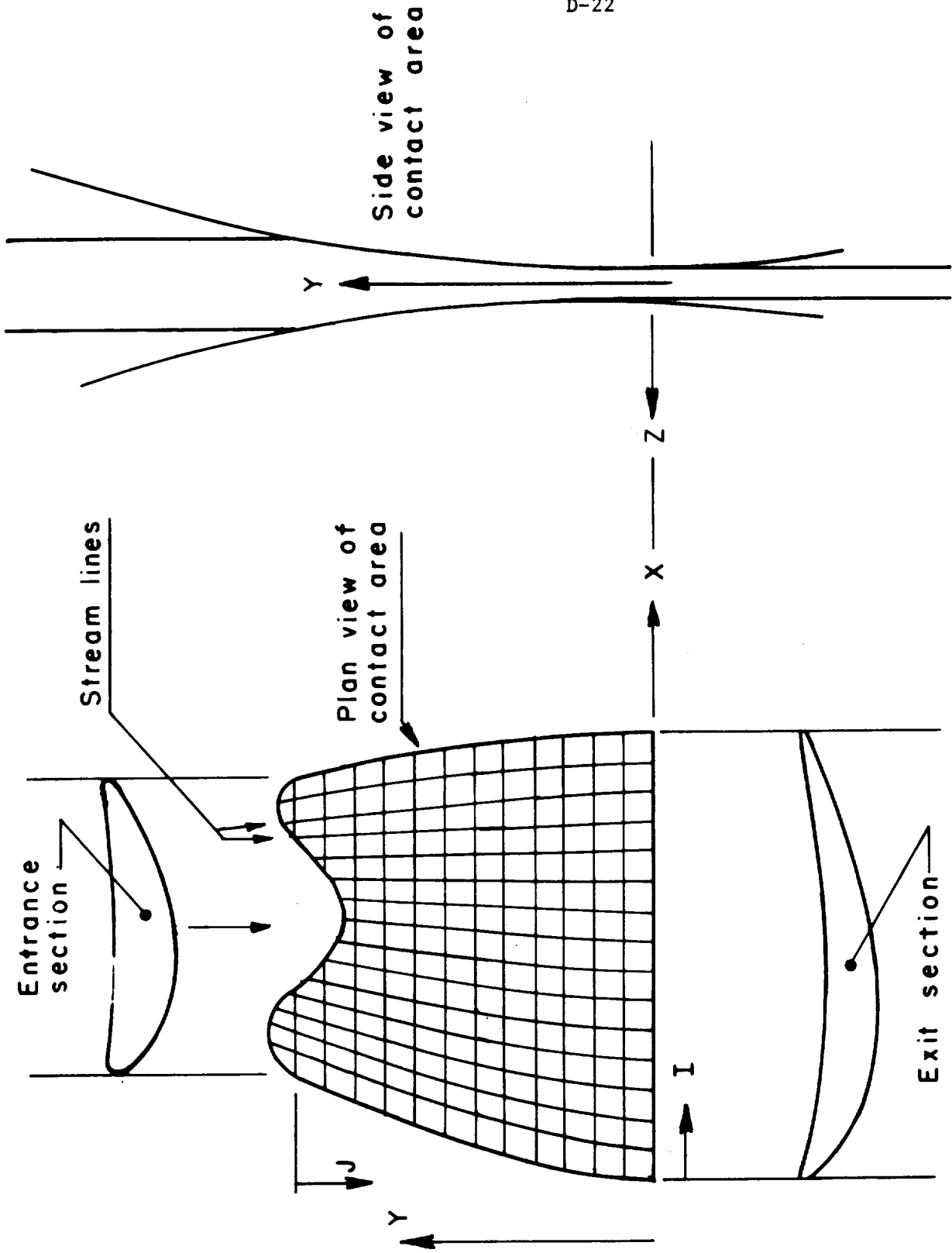
FIGURE D-5.   PLAN AND SIDE VIEWS OF THEORETICAL CONTACT AREA OF ROLLS AND
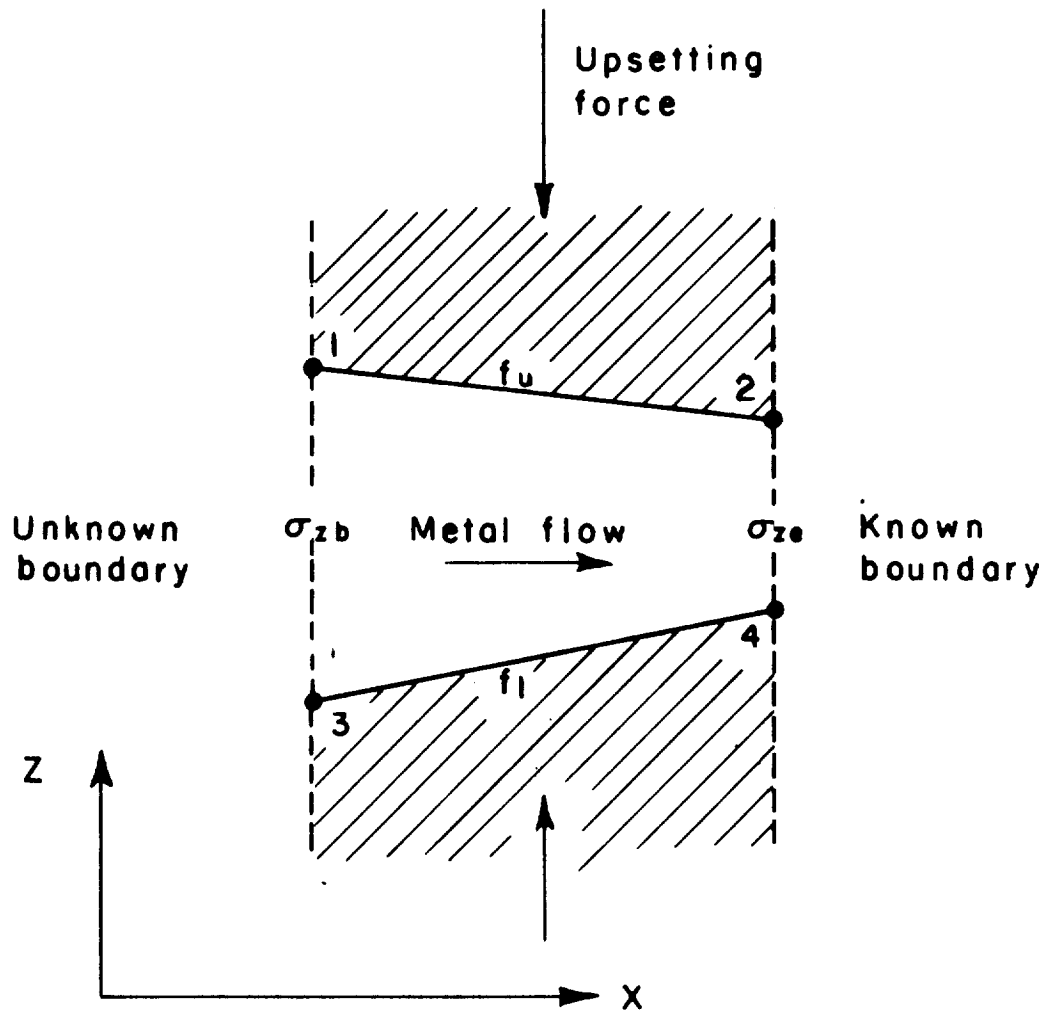MATERIAL DURING ROLLING OF AIRFOILS

FIGURE D-6. DEFINITION OF DEFORMATION ELEMENT PARAMETERS
AS USED IN SUBROUTINE SLAB

Various possible configurations of inclined platens for lateral upset of metals is shown in Figure D-7. The vertical stress σ_z is given by:

$$\sigma_{zb} = \frac{K_2}{K_1} \ln \left(\frac{h_e}{h_b + K_1 X} \right) + \sigma_{ze} \qquad (D-4)$$

where $K_1 = \tan\alpha + \tan\beta$

$$K_2 = \bar{\sigma} \left[\frac{2K_1}{\sqrt{3}} + f_u (1 + \tan^2\alpha) + f_\ell (1 + \tan^2\beta) \right] \qquad (D-5)$$

α and β = angles as defined in Figure D-7

$\bar{\sigma}$ = flow stress of the material

f_u and f_ℓ = friction factor on the upper and lower surfaces

When the surfaces are parallel, Equation (D-5) reduces to:

$$\sigma_{zb} = (f_u + f_\ell) \bar{\sigma} \frac{X}{h_b} + \sigma_{ze} \qquad (D-6)$$

Theoretical considerations limit the absolute value of K_1 to 2. That is, if the surfaces are inclined at more than 45 degrees, metal flows by internal shear rather than sliding on the platen surface. When this condition is detected, the friction factor for the shearing side is set to equal shear friction factor (0.577) and the boundary geometry is updated correspondingly.

Another limitation concerns very tall, but slender elements. In this case, the calculated value of σ_{zb} is less than the known boundary value of σ_{ze}. The element is modified into a parallel deformation unit and σ_{ze} is recalculated. Metal flow in the same direction requires increasing σ_{ze} values.
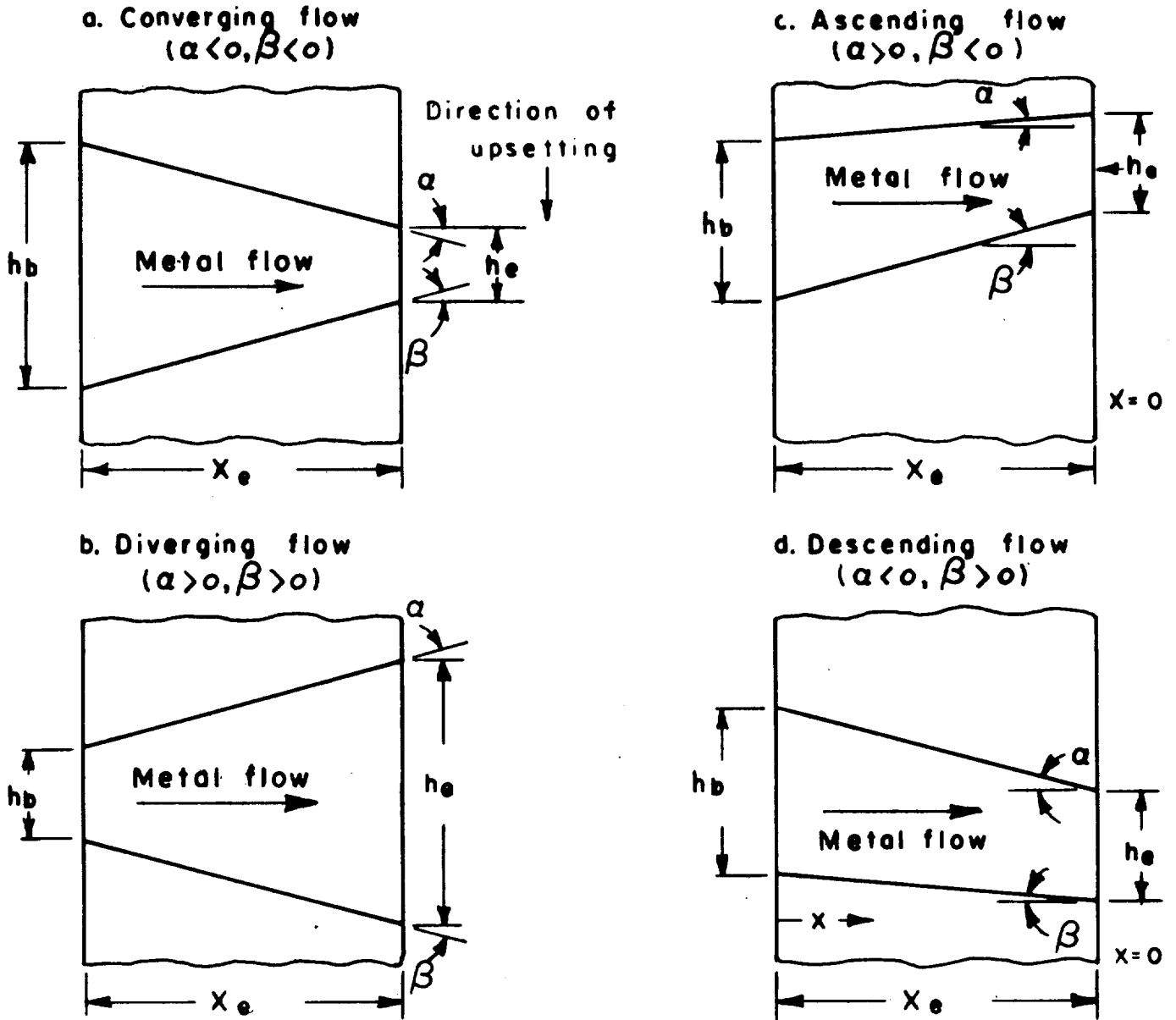
FIGURE D-7. VARIOUS POSSIBLE CONFIGURATIONS OF INCLINED PLATENS ENCOUNTERED DURING PLANE-STRAIN UPSETTING

Subroutine INTPLT

Purpose: Performs various types of interpolation as required by input data.

Call Sequence: CALL INTPLT (INTYP, XIN, ZIN, NIN, XOUT, ZOUT, NOUT)

Where:

INTYP = Interpolation type specifier.
INTYP = 0 for spline interpolation
= 1 for linear interpolation
= 2 for 2nd order polynomial interpolation
= N for N'th order polynomial interpolation.

XIN, ZIN = X and Z coordinates of points describing the input curve on which interpolation will be performed. X must be monotonic.

NIN = Number of point in XIN and ZIN.

XOUT = The x-values at which new z-values are desired.

ZOUT = The interpolated z-values.

NOUT = Number of elements in XOUT and ZOUT.

Method: When spline interpolation is requested, it is only performed within the roll cavity. Any extrapolation is based on linear interpolation.

Linear and n'th order polynomial interpolation is performed using AITKN, a library routine. Spline interpolation is performed by SPLINE and COEFF another couple of library routines. Spline interpolation needs a minimum of four input points. If the input curve has less than four elements, linear interpolation is performed.

Subroutine INTRPE

Purpose: Performs the interpolation of the entrance section using INTPLT.

Call Sequence: CALL INTRPE

Method: The interpolation interval is determined as being from the minimum of the upper and lower surfaces to the maximum of upper and lower surfaces. The interval is divided into an equal number of points (X-values) and INTPLT is called to perform spline interpolation.

Subroutine INTRPX

Purpose: Performs the interpolation of the exit section using INTPLT.

Call Sequence: CALL INTRPX

Method: The interpolation interval is determined as being from the minimum x-coordinate of the upper and lower surfaces to the maximum x-coordinate of the upper and lower surfaces. The interval is divided into equidistant x-values. INTPLT is used to perform spline interpolation and calculate z-values.

Subroutine ADDFLS

Purpose: To add flash to the exit section.

Call Sequence: CALL ADDFLS

Method: When the routine is entered, default values for flash thickness, flash width and flash extension are calculated for both the left and the right sides of the exit shape. Then the user is asked to enter the flash thickness, width and extension (flash extension is the distance between the roll cavity and the flashland proper). As in other routines that request user input, a carriage return is all that is required to select the default values.

Depending on the flash geometry parameters input and the part geometry, two kinds of flash land is generated.

1. Tangent flash extension. The airfoil surface is extended till the distance between the extension is equal to the specified flash thickness. Then the flash land is added.

2. Non-tangent flash. If the flash extension thus calculated is greater than the specified distance, than non tangent flash is constructed.

Subroutine SUMARY

Purpose: To prepare a summary of the results of a roll pass design session.

Call Sequence: CALL SUMARY

Method: The following are calculated within this routine:

1. Actual percent elongation from entrance to exit, based on cross sectional areas.

2. The average reduction in height.

3. Load, by integrating the stress distribution over the deformation zone.

4. Average pressure.

5. Maximum pressure.

6. Coordinates of the centers of force and torque.

Subroutine REDUCE

Purpose: To display the distribution of percent elongation along the width (x-axis) of the exit shape.

Call Sequence: CALL REDUCE

Method: The cross sectional area of each of the elements of the input shape (preform) and the output shape are calculated.

$$\frac{Ai(input) - Ai(output)}{Ai(input)} = \text{percent elongation of the element.}$$

In the process, the x and z coordinates of the center of elongation is also calculated. The resultant display includes the variation of elongation along the exit shape; as well as, the entrance and exit shapes together with the centroid of the exit shape (marked with a +) and the center of elongation (marked with an x). The displayed distance between the centroid and the center of elongation is a measure of the bending (sideways as well as up or down) that would be observed as the product exits the rolls.

Subroutine MOVRLS

Purpose: To move the rolls so as to increase of decrease the separation between the two.

Call Sequence: CALL MOVRLS

Method: The user is asked to enter the desired roll movement. The upper and lower roll surface coordinates are updated as required and the routine exits.

Subroutine RLBITE

Purpose: Determines if the rolls would bite the incoming stock.

Call Sequence: CALL RLBITE (IFLG)

IFLG is returned to the calling program.

IFLG = 1 if the incoming stock will slide freely through the rolls.

IFLG = 0 if conditions are satisfactory.

IFLG =-1 if the rolls won't bite the incoming stock.

Method: The maximum roll opening and the maximum bite are determined. The condition of excessive roll opening is checked for. Then the minimum acceptable roll opening is calculated by:

$$(H_{roll})^{min} = (H_{preform})^{max} - (roll\ diameter) \cdot [(1.0 - COS(tan^{-1}(f))]$$

where f = friction factor.

These calculations are based on the element at which maximum roll bite was determined. This would be the element at which initial contact between the incoming stock and the rolls would occur.

A final comparison between (H_{roll})min and the actual roll opening indicates the suitability of the present roll opening for successful bite.

Subroutine REXIT

Purpose: To rotate the exit shape on the z-x plane according to user input.

Call Sequence: CALL REXIT

Method: The exit section is displayed. The rotation angle is obtained from the user. The exit section is rotated as requested using DCOSIN and ROTVEC. The rotated image is displayed superimposed on the original. If the specified angle of rotation is zero, the routine exits without modifying the data base.

Subroutine RDYSIM

Purpose: To initialize the system for simulation of a roll pass.

Call Sequence: CALL RDYSIM
This routine is called just before entry into the simulation loop.

Method: The roll section is interpolated at the same x-values as the preform section. The maximum roll opening and interference is determined. These are used to find the points at which the preform touches the roll surface. The preform is centered so as to simulate the position at which it would enter the rolls. The stress array is zeroed, % spread related variables are initialized and control returns to the calling module.

Subroutine ROLSRF

Purpose: To calculate the z-coordinates of the roll surface at the j'th simulation step.

Call Sequence: CALL ROLSRF (J)
where: J is the simulation index.

Method: The left and right side indexes are determined based on the position of the material with respect to the flashlands. The roll contour at YM(J) is generated. The z-coordinates of the roll surface at the x-coordinates of the material surface is also determined by interpolation.

The material cross section and the interpolated roll section are scanned from left to right to determine the points or intersection. Indeces of deforming and nondeforming regions are found and index arrays, IDFA, IDFP and NDFP are set for use by stress and area matching routines.

Subroutine MATCHA

Purpose: Performs material distribution according to stress analysis results and within the constraints of the deforming region.

Call Sequence: CALL MATCHA(J)
Where J is the simulation index.

Method: Cross sectional areas of the deforming zones on both sides of each neutral surface is calculated. These are reduced according to percent spread; where, a parabolic spread distribution is assumed.

If there are two neutral surfaces; (two separate deforming zone) then, the central area is distributed first, with the excess divided between the end portions of the section. Then left and right side areas are distributed and the new material cross sectional geometry is determined. Finally, the present material geometry is copied into the next section so as to proceed with the next simulation step.

APPENDIX E

SIMULATION OF SHAPE ROLLING

APPENDIX E

SIMULATION OF SHAPE ROLLING

INTRODUCTION

A simulation approach is required in order to determine roll separating forces and at the same time obtain an idea of metal flow during rolling. A numerical model was developed for calculating the stress distribution and for determining the geometry of the deformation zone during rolling of airfoil like shapes. The resulting computer program, ROLPAS, is capable of processing rounds, slabs, diamonds, airfoils, but not T, H or U or other such shapes with a protrusion.

DESCRIPTION OF METHOD

The deformation zone is divided into NY cross sections parallel to the roll axis , as shown in Figure E-1. The following steps take place while operating on the J'th cross section.

1. The material cross section at J-1'st section is input to the J'th roll section.

2. The intersections of the material and the roll cross sections are found and the boundaries of the deformation zones are determined.

3. Stress analysis is performed on the deformation zones to determine the location of the neutral surfaces as well as the stress distribution.

4. Cross sectional area is distributed as a function of the neutral surfaces as well as the expected percent elongation.

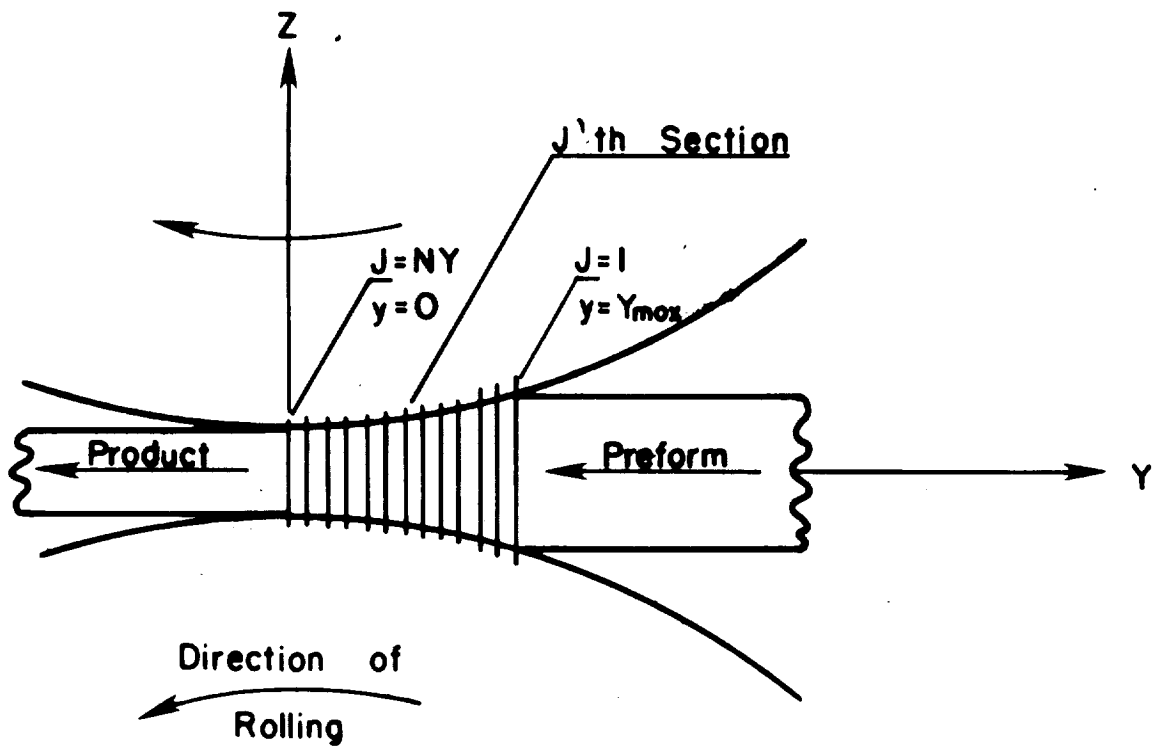5. J is incremented and simulation continues with step 1 till the last cross section is processed.

FIGURE E-1. POSITION OF CROSS SECTIONS USED FOR SIMULATION

Coordinate System

The same coordinate system is used in all derivations, interpolations and calculations related to simulation of roll passes. This unified approach minimizes ambiguity, and potential confusion as well as simplifying computer programming. As shown in Figure E-2, the x-axis is parallel to the roll axis, the y-axis is parallel to the rolling direction and the z-axis is perpendicular to the roll axis and the direction of rolling.

Determination of Initial Contact Points Between the Preform and the Rolls

The initial contact between rolls and preform of arbitrary geometry could consist of two or more points. In this simulation only contacts of two and three points are considered. These are illustrated in Figure E-3. The solutions for both conditions are the same and follow the sequence below.

1. The roll geometry (exit section) is interpolated at the same x-values as the preform geometry (entrance section).

2. The difference in heights is calculated for each x-value. That is: $H_{\Delta,i} = H_{e,i} - H_{x,i}$

   Maximum of $H_{\Delta,i}$ is determined. A negative value signifies that the preform will not intersect the rolls and that the perform is thinner than the roll gap.

3. The maximum interference of the rolls and the preform are calculated as depicted in Figure E-4. The interferences on both sides are summed to yield: $\Delta H_{max} = \Delta H_{top} + \Delta H_{bottom}$

4. The y-coordinate at which the initial contact occurs, Y_{max}, is than calculated by:

$$Y_{max} = \frac{D - H_{x,max}}{2} - \frac{D - H_{x,max} - \Delta H_{max}}{}$$

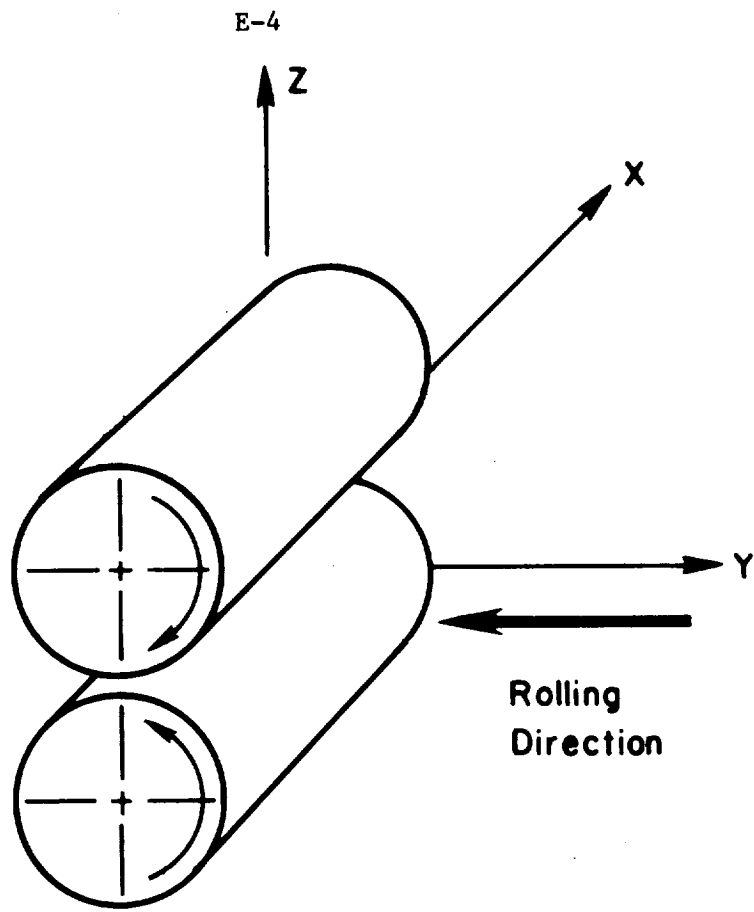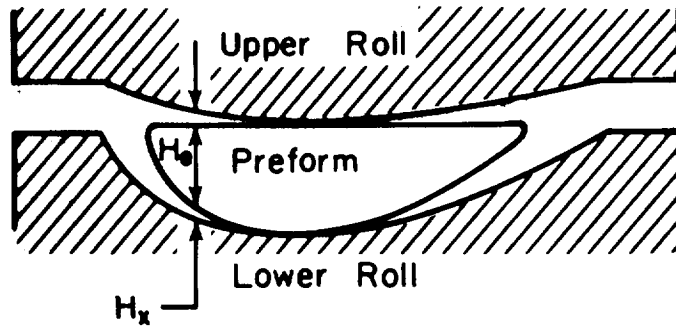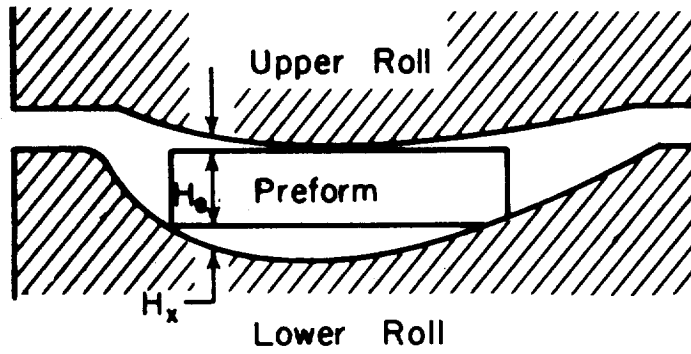   where: D : Roll diameter, measured from axis of rotation to centroid of exit shape.

FIGURE E-2. COORDINATE SYSTEM AND ROLLING DIRECTION
USED IN MODELLING OF ROLL PASS SIMULATION

(a)

(b)

FIGURE E-3. (a) TWO POINT AND (b) THREE
POINT INITIAL CONTACT

: $H_{x,max}$: Maximum opening of the exit cross section

: ΔH_{max} : Maximum interference as defined in step 3.

The solution just outlined is applicable to rolls and preforms of arbitrary shape. It does not take into account the possibility of the incoming strip twisting (rotation of the section) as it enters the rolls.

5. Once Y_{max} is determined, the roll contour at the first and subsequent steps can be determined. The preform outline is mathematically jiggled up and down and centered in the roll section at $y = Y_{max}$. The preform data set is translated to coincide with this centering action.

Determination of Deformation Zones

The determination of deformation zones at any step of the simulation is accomplished as follows:

1. The points defining the material outline are tested against the points defining the extremes of the roll cavity. If material is extruding outside the flashland, indices are set such that subsequent analysis is carried within the roll cavity.

2. The regions of deformation are found by determining the portions of the input material outline that is above the roll cavity upper surface outline and below the roll cavity lower surface outline. Since both outlines are defined by a set of points, the most straight forward solution is to interpolate z-coordinates of the roll section at the same x-coordinates as the material points. Then corresponding z-ccordinates can be compared to determine deformation zones. Figure E-5 illustrates two different kinds of deformation zones, single zone and two separated zones.
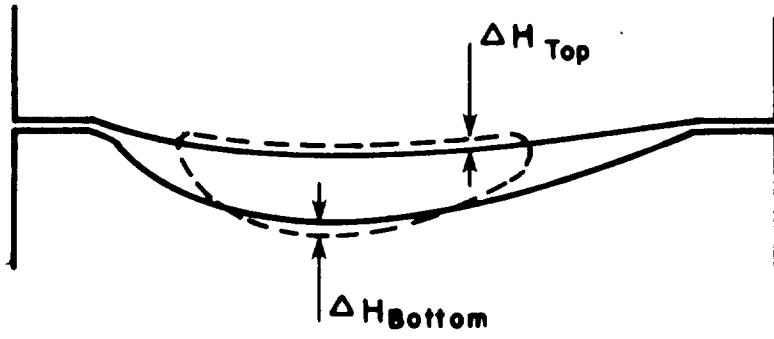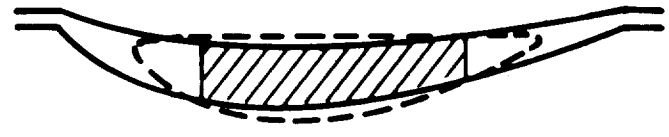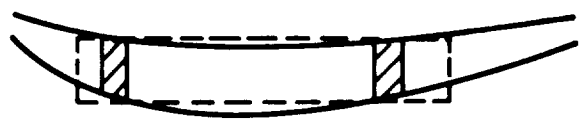
FIGURE E-4. MAXIMUM INTERFERENCE OF THE
ROLLS AND THE PREFORM

a) Single Deformation Zone

a) Dual Deformation Zones

FIGURE E-5. SINGLE AND DUAL DEFORMATION ZONES

3. The indexes obtained during the intersection scan above are
    analyzed to determine the boundaries of the deformation zones.
    Regions beyond the deformation zones, as in figure E-5b, are
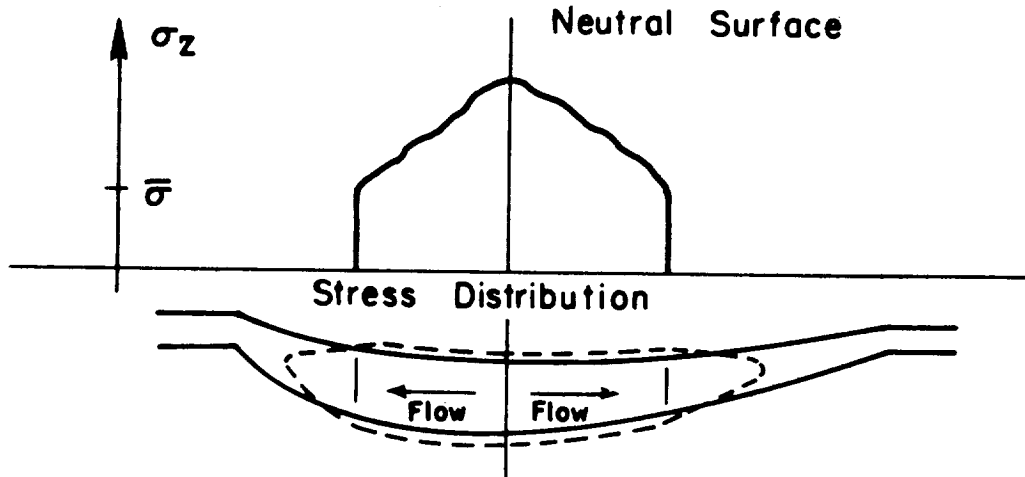   assumed to bend.

Stress Analysis

Stress analysis is performed on the deformation zones. "Slab
Method" is used. The technique is outlined in Appendix D under subroutine
SLAB. As shown in Figure E-6, stress distribution and the positions of
the neutral surfaces are the two important outputs from the stress analysis
module.

Stress analysis during simulation is performed along the sections,
parallel to the zx-plane. The resulting stress surface will not truly
reflect the corner effects or the entry, exit boundary conditions. After
the simulation is completed, as a last step, stress analysis is performed
along the flow lines. Thus the stress at a given point is calculated twice
once in each direction. The lower stress value is selected as being more
correctly representative of the expected stress at that point. This
approach is justified by the minimum energy theorem. This stress distri-
bution is integrated to obtain roll separating force.

Material Distribution

Once the number and position of the neutral surfaces are known,
the cross sectional areas of the deformation zones can be distributed. This
is the final step of the simulation where actual metal movement is considered.
The direction of metal flow is indicated by the neutral surfaces. That is,
metal on the left flows left and metal on the right side of a neutral surface
flows right. Due to the nature of the process, elongation (reduction in
cross sectional area, flow in -y direction) is also taking place. The deform-
ing material not only spreads left and right (flow parallel to x-axis) but
elongates in the direction of rolling just as in extrusion. The spread pheno-

a) Single Deformation Zone, One Neutral Surface
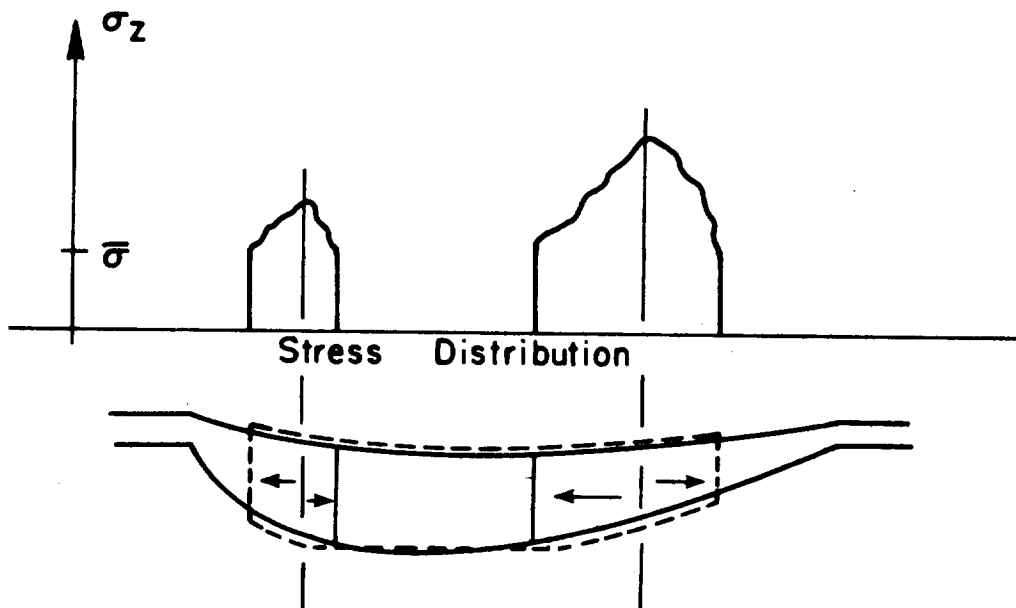
b) Two Deformation Zones, Two Neutral Surfaces

FIGURE E-6.   REPRESENTATIVE STRESS DISTRIBUTIONS AND
METAL FLOW DIRECTIONS FOR CASES OF
SINGLE AND DUAL DEFORMATION ZONES

menon is emulated as a parabolic function. This selection is consistent
with experimental observations. The coefficients of the parabolic spread
distribution is calculated based on roll and preform geometry and expected
maximum spread. The value for the maximum expected spread can be obtained
by the computer program SHPROL or estimated based on similiar rolling con-
ditions.

To perform the actual material distribution, the cross sectional
areas on the left, in between and on the right of the neutral surfaces,
figure E-6b, are calculated. The portions of these areas that are due to
the deformation zones are reduced by the amount lost to elongation. The
rest are distributed as follows:

1. If two neutral surfaces exist, than the area in between the
two is distributed so as to simulate a uniform increase in
thickness while staying within the roll cavity constraints.
Any extra area (material) is added to the left and right
side areas.

2. If only one neutral surface exists as in Figure E-6a, or,
after the completion of central area distribution, the
areas on the left and right hand sides are distributed.
The material is assumed to move left (or right) a delta
amount. Points that were in contact with the rolls, re-
main in contact. Points that exceed the roll surface are
forced to conform to the roll contour. This is an iter-
ative procedure that calculates a ΔX based on the Δ area
and the distance from the neutral surface to the extreme
point on the section.
The area distribution logic and arithmetic is implemented
by subroutine MATCHA in ROLPAS.

DISTRIBUTION LIST

Air Force Materials Laboratory
Attn: AFML/LLM (A. M. Adair)
Wright-Patterson AFB
OH 45433

Air Force Materials Laboratory
Attn: AFML/LLM (H. Gegel)
Wright-Patterson AFB
OH 45433

Air Force Materials Laboratory
Attn: AFML/LTM (N. E. Klarquist)
Wright-Patterson AFB
OH 45433

Air Force Materials Laboratory
Attn: AFML/LTM (Dennis Wisnosky)
Wright-Patterson AFB
OH 45433

Air Force Materials Laboratory
Attn: AFML/LT (Gerald C. Shumaker)
Wright-Patterson AFB
OH 45433

Air Force Materials Laboratory
Attn: Robert Ondercin, AFML/LTM
Wright-Patterson AFB
OH 45433

Rock Island Arsenal
Attn: Joseph D. DiBenedetto
General Thomas J. Rodman Lab
Rock Island, IL 61201

U.S. Army Aviation Systems Command
Attn: G. Gorline, AMSAV/PUEB
Manufacturing Methods & Technology
Mart Building
12th and Spruce Streets
St. Louis, MO 63201

U.S. Army Materials & Mechanics
  Research Center
Attn: Roger Gagne, AMXMR/ER
Watertown MA 02172

NASA Langley Research Center
Attn: E. Hoffman
Manufacturing Technology Section
Mail Stop 188A
Hampton, VA 23365

NASA-Lewis
Attn: Charles Blankenship
Mail Stop 105-1
21000 Brookpark Road
Cleveland, OH 44135

NASA-Lewis (5 Copies)
Attn: Dan Whittenberger
Mail Stop 105-1
21000 Brookpark Road
Cleveland OH 44135

Allegheny Ludlum Steel Corp
Attn R. A. Lula
Assistant to VP Tech Director
Advanced Technology Planning
Research Center
Alabama & Pacific Avenues
Brackenridge PA 15014

Aluminum Company of America
Attn: Walter L. Crawford
Assistant Director
Alcoa Technical Center
Alcoa Center PA 15069

Avco Lycoming
Attn: L. J. Fiedler
556 Main Street
Stratford CT 06497

Babcock & Wilcox
Attn: Henry A. Domian
Research Center
P.O. Box 835
Alliance OH 44601

Bethlehem Steel corp
Attn: Dr. H. Darlington
Section Manager
Forming & Mech Evaluation
Homer Research Labs
Bethlehem PA 18016

Bethlehem Steel Corp
Attn: Roger Whiteley
Homer Research Labs
Bethlehem   PA   18016

Caterpillar Tractor Company
Attn: John A. McDonald
600 W. Washington St, Bldg. W
E. Peoria,   IL   61630

Crucible, Inc.
Materials Research Center
Attn: E. J. Dulis
P.O. Box 88
Parkway West & Route 60
Pittsburgh PA   15230

FMC Corp
Attn: Johan Hendriks
Central Engrg Laboratories
1185 Coleman Avenue
Santa Clair   CA   95052

General Electric Corporation
Aircraft Engine Group
Attn: Mr. Roger Peebles
Cincinnati OH   45215

General Electric Company
Aircraft Engine Group
Attn: W. Hanson
Mail Drop 26802
1000 Western Ave
W. Lynn   MA   01905

Gulf & Western Energy Prod Co
Attn: Dan Sheppel
Works Manager
Bonney Forge Division
Cedar & Meadow Streets
Allentown, PA   18105

Inland Steel Company
Attn: Bernard S. Levy
Inland Steel Research Lab
East Chicago IN   46312

International Harvester Company
Attn: F. J. Hussey
Solar Division
2200 Pacific Highway
P.O. Box 80966
San Diego   CA   92138

LaSalle Steel Company
Attn: John Frasz
Manager Marketing
P.O. Box 6800A
Chicago IL   60680

Northrop Corporation
Attn: Donald Stansbarger
Mngr, Mfg Res & Tech Dept
3901 W Broadway
Hawthorne   CA   90250

Ontario Corporation
Attn: Mr. Hal Glass
1200 W Jackson Street
Muncie IN   47302

Pratt & Whitney Aircraft Group
Commercial Products Division
Attn: Mr. Manfred Adler
400 E. Main St
East Hartford   CT   06108

Pratt & Whitney Aircraft Group
Commercial Products Division
Attn: Ray Slack
400 E Main Street
East Hartford CT   06108

Pratt & Whitney Aircraft Group
Government Products Division
Attn: E. E. Barton, Jr.
P.O. Box 2691
West Palm Beach FL   33402

Solar
Attn: Arthur G. Metcalfe
Associate Director of Research
Mail Zone R-1
2200 Pacific Highway
P.O. Box 80966
San Diego   CA   92138

Teledyne-Allvac
Frank Elliott
P.O. Box 759
Monroe   NC   28110

U.S. Steel Corporation
Attn: Donald W Derber
General Manager Marketing
Machinery & Allied Ind
600 Grant Street
Pittsburgh PA   15230

Westinghouse Electric Corp
Central Research Laboratories
Dr. Alan T. Male
Manager, Materials Processing Res
Beulah Road, Churchill Borough
Pittsburgh   PA   15235

Universal-Cyclops Specialty Steel Div
Attn: Mr. H. L. Black
Mayer Street
Bridgeville   PA   15017

Rathbone Corporation
Attn: Mr. Leonard S. Dorsett, President
Palmer   MA   01069

General Electric Company
Attn: Mr. Don E. Nulk, Manager
Metal-Forming Research
Mail Drop 26802
1000 Western Avenue
Lynn   MA   01910

Caterpillar Tractor Company
Attn: Mr. Kenneth L. Blair
Process Control Manager
100 N East Adams Street
Peoria   ILL   61602

Armco Steel Corporation
Attn: Dr. Rollin E. Hook
Low Carbon Steel Section
Research Center
Middletown   OH   45043

Air Force Office of Scientific
   Research
Attn: Dr. Alan H. Rosenstein
         Program Manager
Directorate of Electronic & Solid
   State Sciences
Bolling Air Force Base, Bldg 410
Washington   DC   20332

Air Force Materials Laboratory
Attn: AFML/LTM (Mr. Robert Ondercin)
Wright-Patterson AFB, OH   45433

Picatinny Arsenal
Attn: Dr. K. R. Iyer
DRDAR/SCM/E, Bldg 3409
U.S. Army Armament Research
   & Development Command
Dover NJ   07801

NASA Headquarters
600 Independence Avenue, SW
Washington, DC   20546
Attn: RWM/J. Gangler

NASA-Lewis Research Center
Attn: Library (2 Copies)
MS 60-3
21000 Brookpark Road
Cleveland, OH   44135

NASA-Lewis Research Center
Attn: New Technology
MS 7-3
21000 Brookpark Road
Cleveland, OH   44135

NASA-Lewis Research Center
Attn: J. Liwosz, MS 500-313
21000 Brookpark Road
Cleveland OH   44135

Aluminum Company of America
Attn: J. H. Dudas
Alcoa Technical Center
Alcoa Center, PA   15069

The American Welding & Mfg Company
Attn: Mr. Gary R. Coupland
Dietz Road, NE
Warren, OH   44482

Bell Helicopter Co.
Attn: W. B. Bond
P. O. Box 482
Ft. Worth, TX   76101

Boeing Commercial Airplane Company
Attn: George L. Petoff
Orgn B-7661 M/S 77-48
P. O. Box 3707
Seattle, Washington   98124

Boeing Vertol Company
Attn: Mr. Robert L. Mayer
MS P32-27
P. O. Box 16858
Philadelphia, PA 19142

Caterpillar Tractor Company
Attn: John A. McDonald
600 W. Washington St., Bldg W.
E. Peoria, IL 61630

Curtiss-Wright Corporation
Attn: Cleve Speer
Senior Operations Analyst (Corporate)
One Passaic Street
Wood-Ridge, NJ 07075

Douglas Aircraft Company
Attn: Dr. T. L. MacKay
Branch Manager, Metals Research
3855 Lakewood Blvd
Long Beach, CA 90801

Eaton Corporation
Attn: Mr. A. M. Sabroff, Mgr.
Manufacturing Services Center
32500 Chardon Road
Willoughby Hills, OH 44094

Fairchild Republic Company
Attn: Mr. W. Travis
Republic Aviation Division
Bldg 29W, Dept. 485
Farmingdale, LI, NY 17735

Garrett Corporation
Attn: M. J. Duffy
Airesearch Manufacturing Co.
402 So. 36th Street
Phoenix, AZ 85034

General Dynamics - Ft. Worth Div.
Attn: E. E. Kaminski
P. O. Box 748
Ft. Worth, TX 76101

General Motors Technical Center
Attn: Kenneth E. Ruff
Dept. Head, Mfg. Dev
Computer-Aided Processing &
 Machine Controls
Environmental Activities Bldg
Warren, MI 48090

Grumman Aerospace Corporation
Attn: C. Micillo Manager
Advanced Materials & Process Div
Bethpage, LI, NY 11714

Hughes Aircraft Company
Attn: Mr. William I. Green
Assistant Division Manager
P. O. Box 11337
Tucson, AZ 85734

Kelsey-Hayes Company
Attn: Gary Hoffman
Utica Division
Utica, NY 13503

Lockheed Aircraft Corporation
Attn: Dr. Morris A. Steinberg
Director of Tech Applications
P. O. Box 551
Burbank, CA 91520

Martin Marietta Aerospace
Attn: Richard V. Robertson
Chief, Structural Mfg Engrg.
Orlando Division
Mail Point 248, P. O. Box 5837
Orlando, FL 32805

McDonnell Douglas Aircraft Co.
Attn: William T. Richards
P. O. Box 516
St. Louis, MO 63166

Pratt & Whitney Aircraft
Government Products Division
Attn: Ralph E. Anderson, Mail Stop B08
P. O. Box 2691
West Palm Beach, FL 33402

Reisner Metals Inc.
Attn: Chief Metallurgist
5421 East Firestone Place
South Gage, CA 90280

RMI Inc.
Attn: Dr. H. Bomberger
Niles, OH 44446

Rockwell International Science Center
Attn: Mr. C. H. Hamilton
1049 Camino Dos Rios
Thousand Oaks, CA 91360

Sandia Corporation
Sandia Laboratories
Attn: Henry J. Rack
Mechanical Metallurgy
Division 5532
Albuquerque, NM 87115

Sikorsky Aircraft
Manufacturing Engineering Dept.
Attn: Stanley Silverstein
N. Main Street
Stratford, CN 06602

TIMET INC
Attn: H. Rosenberg
400 Rouser Road
P. O. Box 2824
Pittsburgh, Pennsylvania 15230

TRW, Inc.
Attn: Mr. Wm Spiegelberg
23555 Euclid Ave.
Cleveland, Oh 44117

Watervliet Arsenal
Attn: Mr. L. Liuzzi
DRDAR-LCB-SE
Watervliet, NY 12189

NASA-Scientific and Technical Information
  Facility
Attn: Accessing Department
P. O. Box 8757
Baltimore/Washington International Airport
MD 21240

Defense Documentation Center
Cameron Station
5010 Duke Street
Alexandria, VA 22314

Kelsey Hayes, Inc.
Attn: T. Miles
7250 Whitmore Lake Road
Brighton, MI 48116

IIT Research Institute
Attn: K. Kulkarni
10 West 35th Street
Chicago, IL 60616

MCIC
Battelle Columbus
505 King Avenue
Columbus, Ohio 43201

Special Metals, Inc.
Attn: S. Reichman
New Hartford, NY 13413

Cartech, Inc.
Attn: D. Muzyka
P. O. Box 662
Reading, PA 19603

AiResearch Manufacturing Co.
Attn: R. Kirby
P. O. Box 5217
Phoenix, AZ 85010